



University of **Strathclyde** **Glasgow**

An investigation into silk fibroin for diverse wound healing applications

Gemma Egan, BEng (Hons)

Department of Biomedical Engineering

University of Strathclyde

Glasgow

A thesis submitted in fulfilment of the requirements for the degree of Doctor of

Engineering

2023

Declaration

This thesis is the result of the author's original research. It has been composed by the author and has not been previously submitted for examination which has led to the award of a degree.

The copyright of this thesis belongs to the author under the terms of the United Kingdom Copyright Acts as qualified by University of Strathclyde Regulation 3.50.

Due acknowledgement must always be made of the use of any material contained in, or derived from, this thesis.

A handwritten signature in black ink, consisting of a large, stylized initial 'B' followed by a series of connected loops and a long horizontal tail.

Signed:

Date: 19/6/23

Abstract

Wound healing is typically defined by a cascade of events which include haemostasis, inflammation, proliferation, and remodelling. Several factors can influence these stages of wound healing, potentially prolonging them and causing the wound to become a chronic wound. Inflammation can be prolonged by the presence of microbial pathogens. Silk is a versatile biomaterial that has been used in healthcare in various formats such as sutures and meshes but has recently gained FDA approval for the first regenerated silk material for use as an injectable medical therapy. Therefore, the aim of this thesis was to investigate the potential further uses of silk fibroin in a wound care setting in the format of hydrogels, aqueous solution, and films. First, silk hydrogels were made by two methods to tune the crystallinity and the subsequent release in PBS was monitored over 72 hours. Significantly more silk fibroin leached from hydrogels with an amorphous silk fibroin structure than with a beta sheet-rich silk fibroin structure, although all hydrogels leached silk fibroin. The leached silk was biologically active, as it induced vitro chemokinesis and faster scratch assay wound healing by activating receptor tyrosine kinases (Chapter 2). Next, the antimicrobial activity of silk fibroin was investigated with two wound pathogens. Silk fibroin solutions containing $\geq 4\%$ w/v silk fibroin did not support the growth of two common wound pathogens, *Staphylococcus aureus* (*S. aureus*) and *Pseudomonas aeruginosa* (*P. aeruginosa*). When liquid silk was added to a wound pad and placed on inoculated culture plates mimicking wound fluid, silk was bacteriostatic. Viability tests of the bacterial cells in the presence of liquid silk showed that cells remained intact within the silk but could not be cultured (Chapter 3). Finally, the ability of silk

films to be used as a versatile sensor was investigated. Silk films and hydrogels could adapt a micropatterned surface after casting on PDMS and this was retained after crystallisation of the films. Films could also be loaded with natural dyes, folded into origami canoes and were able to sense and react to a change in the environmental pH and contaminants in water (Chapter 4). Overall, this thesis explores the impact silk fibroin could have on the key elements of wound healing and the future work needed to validate this further (Chapter 5).

Research Outputs

Publications:

1. **The biologically active biopolymer silk: The antibacterial effects of solubilised *Bombyx mori* silk fibroin with common wound pathogens**

Gemma Egan, Aiden J Hannah, Patricia Connolly, F. Philipp Seib, *Submitted and under editorial review as of May 2023*

Chapter 3

2. **Smart Silk Origami as Eco-sensors for Environmental Pollution**

Saphia A. L. Matthew, **Gemma Egan**, Kimia Witte, Jirada Kaewchuchuen, Suttinee Phuagkhaopong, John D. Totten, and F. Philipp Seib, *ACS Applied Bio Materials* (2022) 5 (8), 3658-3666 DOI: 10.1021/acsabm.2c00023

Chapter 4

3. **Impact of silk hydrogel secondary structure on hydrogel formation, silk leaching and in vitro response.**

Gemma Egan, Suttinee Phuagkhaopong, Saphia A. L. Matthew, Patricia Connolly, and F. Philipp Seib, *Scientific Reports* (2022), 12, 3729. DOI: 10.1038/s41598-022-07437-4

Chapter 2

Conference contributions

1. **BioMedEng19**, Imperial College London, 5-6 September 2019. *Poster Presentation*
2. **11th World Biomaterial Congress 2020**, SECC Glasgow, 11-15 December 2020. *Poster Presentation*
3. **Doctoral School Multidisciplinary Symposium 2020**, University of Strathclyde, 26-28 May 2020, *Twitter Online Poster Presentation*
4. **SIPBS Research Day**, University of Strathclyde, 13 January 2021, *Poster Presentation (winner)*
5. **Woundcare, Tissue Repair and Regenerative Medicine**, Dubai, UAE, 5-6 December 2022, *Oral Presentation*

Acknowledgements

I would like to express my deepest gratitude to my supervisors, Dr Philipp Seib and Professor Patricia Connolly, for their patience, guidance, support, and encouragement throughout the project and beyond. The time invested in my development has been invaluable and I am incredibly grateful to them both.

My thanks also go to those I worked with in the lab; in the Seib lab- John and Tar for helping with initial training, to Maria and Refaya who provided interesting discussions during their time in the lab, and to Kimia, Jaa, June and Saphia for their support, feedback, and company; and in TIC to Brian and Aiden for their training in microbiology and help in supporting my work. I would also like to thank Carol, Sean, and Louise, for their reassurance and advice throughout my write up. Special thanks must go to Caitlin, for her support throughout my studies at Strathclyde and her encouragement with this thesis.

I would like to acknowledge the support and funding offered by the EPSRC for the CDT, offering an invaluable extension after the effects of covid-19 on the project.

Finally, I would like to thank those closest to me. My parents, for their continuous encouragement, comfort and guidance, Deryk and Christina, for their companionship and reassurance, and to Rhona, for keeping me going.

Last, but certainly not least, I would like to thank David for his love, patience and understanding. I would also like to thank my cat, Ben, for his company during the late evenings of work.

List of Figures

FIGURE 1-1. LAYERS OF THE SKIN. IMAGE FROM FREEPIK.COM AVAILABLE AT HTTPS://WWW.FREEPIK.COM/PREMIUM-VECTOR/HUMAN-SKIN-LAYERS-ANATOMY-DERMIS-EPIDERMIS-HYPODERMIS-TISSUE-SKIN-STRUCTURE-VEINS-SWEAT-PORES-HAIR-FOLLICLES-VECTOR-INFOGRAPHIC_23859333.HTM	3
FIGURE 1-2. CUTANEOUS WOUND REPAIR PROCESS. THE 4 STAGES OF WOUND HEALING ARE DESCRIBED BY HAEMOSTASIS, INFLAMMATION, PROLIFERATION, AND REMODELLING. IMAGE FROM (ANDRADE, ET AL., 2022).....	6
FIGURE 1-3. SILK THREAD COMPOSITION. IMAGE FROM (WU, ET AL., 2022)	27
FIGURE 2-1. ELECTROGELATION OF SILK FIBROIN SOLUTION. A) SHOWS TIN FOIL ELECTRODES IN SILK SOLUTION WITH CLOUDINESS OBSERVED AROUND THE ANODE INDICATING THE FORMATION OF HYDROGEL. B) LEFT SHOWS THE SILK SOLUTION AFTER IT HAS UNDERGONE ELECTROGELATION. CLOUDINESS WAS OBSERVED IN THE SILK SOLUTION WHEN COMPARED THE RIGHT, CONTROL SILK SOLUTION BEFORE ELECTROGELATION. C) SHOWS AN ELECTROGEL FORMED ON A WIRE ELECTRODE. D) SHOWS ELECTROGEL ON A PETRI DISH ONCE REMOVED FROM THE ELECTRODE.	56
FIGURE 2-2. STANDARD GROWTH CURVE OBSERVED WHEN CELLS ARE SEEDED AT TWO DIFFERENT DENSITIES. THE ABSORBANCE OF 570NM LIGHT INDICATES THE METABOLIC ACTIVITY OF THE CELLS OVER 12 DAYS.	62
FIGURE 2-3. CELL MIGRATION ASSAY DIAGRAM. CHEMOTX DISPOSABLE CHEMOTAXIS PLATES CONSISTING OF A PCTE MEMBRANE OVER A 96 WELL PLATE. IMAGE DISPLAYS THE PLACEMENT OF SPIKED MEDIUM AND CELLS. CELLS CAN TRAVEL THROUGH THE PORES AND WILL ADHERE TO THE FIBRONECTIN COATED MEMBRANE FOR COUNTING.	65
FIGURE 2-4. A) PROCESSING OF SILK SOLUTION INTO HYDROGELS BY SONICATION OR ELECTRO GELATION. GRAPHIC DEPICTS THE EXPECTED ALIGNMENT OF THE SECONDARY STRUCTURES OF THE HYDROGELS. B) THE EFFICIENCY OF THE GELATION PROCESS, C) THE SILK CONTENT OF EACH HYDROGEL. DATA ANALYSIS EVALUATED BY UNPAIRED T-TEST (N = 4, ± SD). ASTERISKS DENOTE STATISTICAL SIGNIFICANCE AS FOLLOWS: *P < 0.05, **P < 0.01, ***P < 0.001, ****P < 0.0001.	70
FIGURE 2-5. PH TESTING OF SONICATED HYDROGEL WITH PHENOL RED AND PH PAPER. NO COLOUR CHANGE FROM THE PINK PHENOL RED IS SEEN WHEN UNDERGOING SONICATION. PH PAPER INDICATES THAT THE PH REMAINS NEUTRAL WHEN UNDERGOING SONICATION.	72
FIGURE 2-6. PH TESTING ELECTRO GEL WITH PH PAPER. TOP PH OF SILK SOLUTION BEFORE ELECTRO GELATION. BELOW ELECTRO-GEL PLACED ON THE PH PAPER. A COLOUR CHANGE TO YELLOW CAN BE SEEN ON THE PH PAPER INDICATING A DROP IN PH.	73
FIGURE 2-7. PH TESTING ELECTRO-GEL WITH PHENOL RED. SILK SOLUTION IS PINK WHEN PHENOL RED IS ADDED INDICATING A NEUTRAL-BASIC PH. ONCE ELECTRO-GELATION OCCURS, ONLY A LOCAL COLOUR CHANGE TO YELLOW IS SEEN AS THE ELECTRO GEL FORMS.	74
FIGURE 2-8. PROTEIN RELEASE AND CHARACTERISATION FROM SILK HYDROGELS MEASURED BY PROTEIN QUANTIFICATION AND GEL ELECTROPHORESIS. (A) ELECTRO-GEL PROTEIN RELEASE IN WATER AND PBS OVER 72 HOURS. (B) SONICATED HYDROGEL PROTEIN RELEASE IN WATER AND PBS OVER 72 HOURS.....	76
FIGURE 2-9. SONICATED SILK HYDROGELS WERE MORE CRYSTALLINE THAN E-GELS WHILE THE LEACHED SILK FROM BOTH HYDROGEL TYPES DISPLAYED A SILK I-LIKE THERMAL SIGNATURE. THE VARIATION IN (A) ONSET OF DESORPTION (T _{0,DES}), (B) ISO GLASS TRANSITION TEMPERATURE (T _G), (C) ISO CHANGE IN HEAT CAPACITY (ΔC _P), (D) ONSET OF CRYSTALLIZATION (T _{0,C}), AND (E) ENTHALPY OF COLD CRYSTALLIZATION (ΔH _C) FROM FIRST-CYCLE DSC AND (F) THE EXTRAPOLATED ONSET OF DECOMPOSITION FROM FIRST-CYCLE TGA. ERROR BARS ARE HIDDEN IN THE BARS AND PLOT SYMBOLS WHEN NOT VISIBLE (N = 3, ± SD).	83
FIGURE 2-10. FTIR ABSORBANCE SPECTRA OF THE AMIDE I REGION OF ELECTRO-GELS AND SONICATED GELS. CONTROLS INCLUDED WERE UNTREATED AIR-DRIED SILK FILM (UT), ETHANOL TREATED SILK FILMS (EtOH) AND THE CURRENT TREATED SOLUTION REMAINING AFTER REMOVAL OF THE ELECTRO-GEL (CT). LEACHED SAMPLES IN WATER OF BOTH ELECTRO-GEL AND SONICATED GEL AFTER 72 HOURS ARE INCLUDED HERE. LINES AT 1640 AND 1621 INDICATE THE AMORPHOUS AND CRYSTALLINE REGION, RESPECTIVELY (N = 3). (A) 2 ND DERIVATIVE METHOD RESULT (B) HU ET AL. METHOD. DATA ANALYSIS EVALUATED BY TWO-WAY ANOVA FOLLOWED BY TUKEY'S MULTIPLE COMPARISONS TEST. (N = 4, ± SD). ASTERISKS DENOTE STATISTICAL SIGNIFICANCE DETERMINED USING POST-HOC TESTS AS FOLLOWS: *P < 0.05, **P < 0.01, ***P < 0.001, ****P < 0.0001.	86

FIGURE 2-11. SEM IMAGES OF SONICATED HYDROGELS, ELECTRO-GELS, AND THE LEACHED SILK FROM BOTH. SILK SOLUTION IS INCLUDED AS A REFERENCE. SCALE BAR 5 μM	90
FIGURE 2-12. SDS PAGE OF PROTEIN RELEASED FROM ELECTRO-GELS AND SONICATED GELS. STANDARDS INCLUDED ARE SILK SOLUTION AND FREEZE-DRIED SILK SOLUTION RECONSTITUTED IN WATER. (B) DENSITOMETRY ANALYSIS OF SDS PAGE.	92
FIGURE 2-13. IN VITRO STUDIES WITH SILK FIBROIN. NIH 3T3 MOUSE FIBROBLASTS WERE USED THROUGHOUT. (A) CELL PROLIFERATION OF NIH3T3 FIBROBLASTS INCUBATED WITH SILK SOLUTION FOR 72 HOURS AND CELL VIABILITY MEASURED WITH AN MTT ASSAY (N = 3). (B) CELL PROLIFERATION OF NIH3T3 FIBROBLASTS INCUBATED WITH LEACHED SAMPLES OF SILK FROM ELECTRO-GELS, SONICATED GELS, OR SILK SOLUTION AFTER 72 HOURS (N = 3). DATA ANALYSIS EVALUATED BY TWO-WAY ANOVA FOLLOWED BY TUKEY'S MULTIPLE COMPARISONS TEST. (N = 3, \pm SD). ASTERISKS DENOTE STATISTICAL SIGNIFICANCE DETERMINED USING POST-HOC TESTS AS FOLLOWS: * $p < 0.05$, ** $p < 0.01$, *** $p < 0.001$, **** $p < 0.0001$	94
FIGURE 2-14. (A) CELL MIGRATION ACROSS A PERMEABLE MEMBRANE AFTER EXPOSURE TO SILK SOLUTION FOR 3.5 HOURS (N = 4). (B) CELL MIGRATION AT 1600 $\mu\text{G}/\text{ML}$ SILK SOLUTION AND CONTROLS WITH THE PRESENCE OF FBS AS A POSITIVE CONTROL AND WATER AS THE NEGATIVE CONTROL. DATA ANALYSIS EVALUATED BY TWO-WAY ANOVA FOLLOWED BY TUKEY'S MULTIPLE COMPARISONS TEST. (N = 4, \pm SD). ASTERISKS DENOTE STATISTICAL SIGNIFICANCE DETERMINED USING POST-HOC TESTS AS FOLLOWS: * $p < 0.05$, ** $p < 0.01$, *** $p < 0.001$, **** $p < 0.0001$	96
FIGURE 2-15. WOUND CLOSURE ASSAY WITH NIH3T3 FIBROBLASTS AT 1 AND 7 HOURS. BROKEN LINES INDICATE THE BORDER OF CELL GROWTH. SCALE BAR 400 μM	98
FIGURE 2-16. WOUND CLOSURE ASSAY WIDTH OVER 4 AND 7 HOURS IN THE PRESENCE OF SILK SOLUTION, WATER OR FBS. DATA ANALYSIS EVALUATED BY TWO-WAY ANOVA FOLLOWED BY ŠIDÁK'S MULTIPLE COMPARISONS TEST (N = 4, \pm SD). ASTERISKS DENOTE STATISTICAL SIGNIFICANCE DETERMINED USING POST-HOC TESTS AS FOLLOWS: * $p < 0.05$, ** $p < 0.01$, *** $p < 0.001$, **** $p < 0.0001$	99
FIGURE 2-17. PHOSPHORYLATION ARRAY IN THE PRESENCE OF SILK SOLUTION, WATER OR FBS.....	101
FIGURE 3-1. STERILITY TESTING OF SILK FIBROIN SOLUTION (5% W/V) IN TRYPTIC SOYA BROTH (TSB) BEFORE AND AFTER STORAGE AT 4 °C, ROOM TEMPERATURE (RT) AND 37 °C FOR 14 DAYS. (A) TSB WAS INCUBATED AT BOTH ROOM TEMPERATURE AND AT 37 °C FOR 14 DAYS AND THEN EXAMINED FOR GROWTH (I.E., TURBIDITY).	120
FIGURE 3-2. MINIMUM BACTERICIDAL AND INHIBITORY CONCENTRATIONS OF SILK FIBROIN TESTING STRATEGY. OVERNIGHT CULTURES OF <i>S. AUREUS</i> AND <i>P. AERUGINOSA</i> WERE INCUBATED IN LB MEDIA BEFORE BEING CENTRIFUGED AT 12,100 X G FOR 5 MINUTES AND THE SUPERNATANT REMOVED. THIS WAS REPEATED WITH WATER TO WASH THE CELLS. THE CELLS WERE THEN RESUSPENDED IN LB MEDIA, WATER OR AQUEOUS SILK SOLUTION AND INCUBATED AT 37°C, 150 RPM IN AN ORBITAL INCUBATOR OVERNIGHT. THE CELLS WERE AGAIN WASHED THROUGH CENTRIFUGATION AND WITH WATER, AS BEFORE. COLONY COUNTING WAS PERFORMED BEFORE THE CELLS WERE SUSPENDED IN THE SOLUTION AND AFTER THE FINAL WASH TO DETERMINE VIABILITY.	123
FIGURE 3-3. WOUNDPAD DRESSING PROCEDURE. WOUNDPAD WAS REMOVED FROM A STANDARD PLASTER DRESSING BEFORE BEING SOAKED IN SILK SOLUTION OR ETHANOL AND PLACED ON EITHER <i>S AUREUS</i> OR <i>P AERUGINOSA</i> ON AGAR PLATES. GROWTH WAS THEN OBSERVED AFTER INCUBATION OVERNIGHT.	125
FIGURE 3-4. CONDUCTIVITY MEASUREMENTS OF THE DIALYSATE OVER 72 H RESULTING IN AN AQUEOUS SILK FIBROIN SOLUTION.....	129
FIGURE 3-5. CONCENTRATION OF SODIUM CARBONATE IN WATER BEFORE AND AFTER SILK DEGUMMING, SILK RINSING AND IN THE FINAL SILK SOLUTION. DATA ANALYSIS EVALUATED BY ONE-WAY ANOVA FOLLOWED BY TUKEY'S MULTIPLE COMPARISONS TEST (N = 3, \pm SD) ASTERISKS DENOTE STATISTICAL SIGNIFICANCE DETERMINED USING POST-HOC TESTS AS FOLLOWS: * $p < 0.05$, ** $p < 0.01$, *** $p < 0.001$, **** $p < 0.0001$	131
FIGURE 3-6. MINIMUM BACTERICIDAL CONCENTRATION OF SODIUM CARBONATE IN WATER OVER 24-HOUR INCUBATION WITH <i>STAPHYLOCOCCUS AUREUS</i> AND <i>PSEUDOMONAS AERUGINOSA</i> DATA ANALYSIS EVALUATED BY TWO-WAY ANOVA FOLLOWED BY TUKEY'S MULTIPLE COMPARISONS TEST. (N = 4, \pm SD). ASTERISKS DENOTE STATISTICAL SIGNIFICANCE DETERMINED USING POST-HOC TESTS AS FOLLOWS: * $p < 0.05$, ** $p < 0.01$, *** $p < 0.001$, **** $p < 0.0001$	133

FIGURE 3-7. FTIR SPECTRA AND (C) FTIR ANALYSIS OF SILK FIBROIN SOLUTION INCUBATED IN THE ORBITAL INCUBATOR AT 37 °C 150 RPM FOR 24 H. SILK WAS AIR DRIED INTO FILMS FOR ANALYSIS. AIR-DRIED AMORPHOUS CONTROL AND ETHANOL (EtOH) TREATED CRYSTALLINE SILK FILM CONTROLS (DATA FROM CHAPTER 2). DATA ANALYSIS EVALUATED BY ONE-WAY ANOVA FOLLOWED BY TUKEY'S MULTIPLE COMPARISONS TEST. ASTERISKS DENOTE STATISTICAL SIGNIFICANCE DETERMINED USING POST-HOC TESTS AS FOLLOWS: *p < 0.05, **p < 0.01, ***p < 0.001, ****p < 0.0001. (N = 3, ± SD)	135
FIGURE 3-8. STERILITY TESTING OF SILK SOLUTION WITH TSB. GREEN AND YELLOW COLOUR CODING INDICATES NO GROWTH AND GROWTH, RESPECTIVELY. (N = 3)	137
FIGURE 3-9. TRYPTIC SOYA BROTH (TSB) CONTROL TESTING. SPIKED TSB WITH STAPHYLOCOCCUS AUREUS AND PSEUDOMONAS AERUGINOSA AT CONCENTRATIONS 10 ¹ - 10 ⁷ CFU/ML AFTER 24 INCUBATIONS. COLONIES WERE COUNTED AT TIME 0 AND TIME 24, AND SOLUTIONS WERE IMAGED AND VISUALLY ASSESSED FOR TURBIDITY, INDICATING CONTAMINATION. EXPERIMENT RUN IN TRIPPLICATE, N = 1 SHOWN WITH CORRESPONDING IMAGES FOR COUNTED COLONIES IN GRAPHS BELOW. DATA ANALYSIS EVALUATED BY TWO-WAY ANOVA FOLLOWED BY TUKEY'S MULTIPLE COMPARISONS TEST. ASTERISKS DENOTE STATISTICAL SIGNIFICANCE DETERMINED USING POST-HOC TESTS AS FOLLOWS: *p < 0.05, **p < 0.01, ***p < 0.001, ****p < 0.0001.	138
FIGURE 3-10. STERILITY TESTING OF SILK FIBROIN SOLUTION 5 % W/V IN TRYPTIC SOYA BROTH BEFORE AND AFTER STORAGE AT 4 °C, ROOM TEMPERATURE (RT) AND 37 °C FOR 14 DAYS. THE BROTH WAS INCUBATED AT BOTH ROOM TEMPERATURE AND AT 37 °C FOR 14 DAYS BEFORE BEING IMAGED. CONTROL IS TRYPTIC SOYA BROTH SPIKED WITH STERILE WATER 5% V/V. ASTERISKS DENOTE TURBIDITY OBSERVED. SCALE BAR 4CM (N = 3).	141
FIGURE 3-11. BACTERIAL GROWTH IN THE PRESENCE OF WATER WITH LB MEDIA. WATER IS SPIKED WITH LB MEDIA IN THE RATIO 75:25, 85:15, 95:5 OR 100:0 (WATER TO LB MEDIA). COLONIES COUNTED AFTER INCUBATION FOR 24 HOURS IN EACH CONCENTRATION OF WATER. (N = 3, ± SD) DATA ANALYSIS EVALUATED BY TWO-WAY ANOVA FOLLOWED BY TUKEY'S MULTIPLE COMPARISONS TEST. ASTERISKS DENOTE STATISTICAL SIGNIFICANCE DETERMINED USING POST-HOC TESTS AS FOLLOWS: *p < 0.05, **p < 0.01, ***p < 0.001, ****p < 0.0001.....	144
FIGURE 3-12. MINIMUM BACTERICIDAL CONCENTRATION OF SILK FIBROIN AQUEOUS SOLUTION. COLONIES PRESENT AFTER 24-HOUR INCUBATION IN EACH PURE SILK SPIKED SOLUTION CONCENTRATION (N = 3, ± SD). DATA ANALYSIS EVALUATED BY TWO-WAY ANOVA FOLLOWED BY ŠIDÁK'S MULTIPLE COMPARISONS TEST. ASTERISKS DENOTE STATISTICAL SIGNIFICANCE DETERMINED USING POST-HOC TESTS AS FOLLOWS: *p < 0.05, **p < 0.01, ***p < 0.001, ****p < 0.0001.	146
FIGURE 3-13. SIMULATED WOUND ENVIRONMENT AND THE PERFORMANCE OF SILK-FUNCTIONALISED WOUND PAD. (A) WOUND PAD DRY (CONTROL) OR SOAKED IN ETHANOL OR SILK REMOVED TO SHOW GROWTH ON LB AGAR AND SIMULATED WOUND FLUID AGAR. SCALE BAR 2 CM. (B) S. AUREUS AND P. AERUGINOSA WOUND PADS INCUBATED IN LB MEDIA AND COLONIES COUNTED. (N = 3, ± SD). DATA ANALYSIS EVALUATED BY ONE-WAY ANOVA FOLLOWED BY DUNNETT'S MULTIPLE COMPARISONS TEST. ASTERISKS DENOTE STATISTICAL SIGNIFICANCE DETERMINED USING POST-HOC TESTS AS FOLLOWS: *p < 0.05, **p < 0.01, ***p < 0.001, ****p < 0.0001.	149
FIGURE 3-14. IMPACT OF LIQUID SILK ON BACTERIAL CELL VIABILITY. (A) LIVE/DEAD FLUORESCENCE STAINING. GREEN AND RED INDICATE LIVE AND DEAD CELLS, RESPECTIVELY. (LEFT) S. AUREUS IN LB MEDIA, 1% W/V SILK, 5% W/V SILK AND WATER. (RIGHT) P. AERUGINOSA IN LB MEDIA, 1% W/V SILK, 5% W/V SILK AND WATER. SCALE BAR 200 μM. NUMERICAL RESULT N = 3. (B) PERCENTAGE OF DEAD CELLS IN EACH MEDIUM (N = 3, ± SD). DATA ANALYSIS EVALUATED BY TWO-WAY ANOVA FOLLOWED BY ŠIDÁK'S MULTIPLE COMPARISONS TEST. ASTERISKS DENOTE STATISTICAL SIGNIFICANCE DETERMINED USING POST-HOC TESTS AS FOLLOWS: *p < 0.05, **p < 0.01, ***p < 0.001, ****p < 0.0001.	152
FIGURE 4-1. PDMS MOULD DIAGRAM. PDMS WAS CAST WITH GROOVES 12 OR 16 μM APART IN LINEAR AND CONCENTRIC CIRCLE PATTERNS.....	167
FIGURE 4-2. CHAPTER AIMS. THE AIMS ARE SPLIT INTO 2 MAIN SECTIONS: WOUND HEALING, AND WATER FOULING. EACH AIM HAS OBJECTIVES LISTED UNDERNEATH.	174
FIGURE 4-3. SCHEMATIC OF SILK BOAT PRODUCTION. SILK FILMS ARE CAST AND AIR DRIED BEFORE BEING SUBMERGED IN 80% METHANOL. THE FILMS ARE THEN DRIED AND UNDERGO WATER ANNEALING IN A PRESSURISED CHAMBER. FILMS ARE THEN FOLDED INTO ORIGAMI BOATS.	178

FIGURE 4-4. PATTERNED SILK FILMS. DIFFRACTION PATTERN ON THE SILK FILM SURFACE CREATING LIGHT DIFFRACTION RAINBOW EFFECT. ARROWS INDICATE CONCENTRIC CIRCLES ON SILK FILM SURFACE WITH 2 DIFFERENT CIRCLE WIDTHS.	189
FIGURE 4-5. SILK FILM PATTERNED WITH DIFFRACTION PATTERN ON SURFACE AFTER METHANOL TREATMENT. THE PATTERN IS PRESERVED AS THE LIGHT DIFFRACTION RAINBOW EFFECT IS VISIBLE.	191
FIGURE 4-6. A. SILK FILM WITH LINEAR PATTERN AND 1% (W/W) IRON (III) OXIDE PARTICLES INCORPORATED. B. SILK FILM WITH IRON (III) OXIDE PARTICLES INCORPORATED AFTER METHANOL TREATMENT. THE IRON (III) OXIDE PARTICLES ARE STILL VISIBLE IN THE SILK FILM ALONGSIDE THE PATTERN.	193
FIGURE 4-7. SILK HYDROGELS IN THE SOL-GEL STATE ADDED TO PDMS CASTS FOR PATTERNING. CIRCULAR PATTERNED PDMS, LINEAR PATTERNED PDMS AND FLAT PDMS OF VARYING SEPARATION.	195
FIGURE 4-8. PATTERNED SILK HYDROGELS WITH CONCENTRIC CIRCLES WITH 12 μ M AND 16 μ M GAPS.	197
FIGURE 4-9. SLIDE PLACED ON SURFACE OF HYDROGEL ON PDMS CAST FOR REMOVAL.	198
FIGURE 4-10. NIH3T3 FIBROBLASTS GROWN ON PATTERNED GELS. (N=1)	200
FIGURE 4-11. SILK ORIGAMI. TOP: UNFOLDED SILK FILM ON THE LEFT AFTER BEING FOLDED TO FORM THE BOAT ON THE RIGHT. BOTTOM: SILK BOAT ON THE LEFT FOLLOWED BY PAPER BOATS OF VARIOUS SIZES TO THE RIGHT.	202
FIGURE 4-12. THE DIMENSIONS OF MECHANICALLY CUT SILK FIBRES. (A) HISTOGRAMS OF LENGTH AND WIDTH. REFERENCE LINES SHOW THE MINIMUM, AVERAGE AND MAXIMUM DIMENSIONS. N = 30. (B) EXEMPLAR IMAGES OF SILK FIBRES AT 10 \times MAGNIFICATION. SCALE BAR = 1 MM.	204
FIGURE 4-13. THE DIMENSIONS OF MECHANICALLY CUT SILK FIBRES. (A) HISTOGRAMS OF LENGTH AND WIDTH. REFERENCE LINES SHOW THE MINIMUM, AVERAGE AND MAXIMUM DIMENSIONS. N = 30. (B) EXEMPLAR IMAGES OF SILK FIBRES AT 10 \times MAGNIFICATION. SCALE BAR = 1 MM.	205
FIGURE 4-14. SILK FILM PROCESSING. SILK SOLUTION WAS DOPED WITH IRON OXIDE (1) OR SILK FIBRES (2) AND CAST AT 3 DIFFERENT THICKNESSES (3) TO ASSESS THE IMPACT OF EACH INDEPENDENTLY. SURFACE MODIFICATION WAS PERFORMED (4) TO PRODUCE AZOSILKS. THE THICKNESS OF FILMS SHOWED DIFFERENCES ONCE MODIFICATION HAD TAKEN PLACE AT EACH CASTING VOLUME DIFFERENCE. ERROR BARS ARE HIDDEN IN THE BARS AND PLOT SYMBOLS WHEN NOT VISIBLE, \pm SD, N = 3. MULTIPLE FACTORS WERE EVALUATED BY TWO-WAY ANALYSIS OF VARIANCE (ANOVA), FOLLOWED BY ŠIDÁK'S MULTIPLE COMPARISON, SIMPLE EFFECTS POST-HOC TEST. ASTERISKS DENOTE STATISTICAL SIGNIFICANCE DETERMINED USING POST-HOC TESTS AS FOLLOWS: *P < 0.05, **P < 0.01, ***P < 0.001, ****P < 0.0001.	206
FIGURE 4-15. SEM IMAGES OF NATIVE AND AZOSILK FILMS AFTER WATER ANNEALING WITH 0 AND 0.1 % (W/W) IRON OXIDE PARTICLE LOADS.	208
FIGURE 4-16. FTIR BAND ASSIGNMENTS AND SCHEMATIC KEY. SECONDARY STRUCTURE CONTENT OF SILK FILMS DROP-CASTED WITH VARYING IRON OXIDE PARTICLE CONCENTRATIONS. SECONDARY STRUCTURE CONTENT (%) WAS CALCULATED FROM THE RELATIVE AREAS OF PEAKS IN THE SECOND-DERIVATIVE SPECTRUM. UNTREATED SILK FILMS WERE USED AS NEGATIVE CONTROLS FOR B-SHEET CONTENT. THE EXTRAPOLATED ONSET TEMPERATURE OF DECOMPOSITION (T ₀) OF SILK FILMS FROM FIRST-CYCLE DSC. ERROR BARS ARE HIDDEN IN THE BARS AND PLOT SYMBOLS WHEN NOT VISIBLE, (N = 3, \pm SD)	210
FIGURE 4-17. THE EFFECT OF AQUEOUS ENVIRONMENTS ON SILK FILMS. (A) WATER CONTACT ANGLE OF AZOSILK AND NATIVE SILK MEDIUM THICKNESS FILMS WITHOUT IRON OXIDE AND OF NATIVE CONTROL THICKNESS SILK FILM CONTAINING 0.1 % (W/W) IRON OXIDE. (N = 3, \pm SD). (B) EXEMPLAR IMAGES OF WATER CONTACT ANGLES FOR AZOSILK AND NATIVE SILK FILMS. SCALE BARS = 0.5 CM. (C) WEIGHT CHANGE OF NATIVE SILK AND AZOSILK FILMS FOLLOWING IMMERSION IN ULTRAPURE WATER. (N = 3, \pm SD)	212
FIGURE 4-18. A) THE TIME WINDOW FOR FOLDING SILK FILMS WHILE PLASTICISED FOLLOWING WATER ANNEALING. B) THE TIME TAKEN FOR INITIATION OF CONTRACTION AND INITIATION OF RELAXATION BY FILMS LYING ON THE AIR-WATER INTERFACE WAS USED A MEASURE OF STRUCTURAL STABILITY IN WET ENVIRONMENTS (N = 3, \pm SD).	214
FIGURE 4-19. THE CHANGE IN PIXEL CHANNEL INTENSITIES UPON (A) LOADING MEDIUM THICKNESS FILMS CONTAINING 0.1% (W/W) IRON OXIDE PARTICLES WITH ANTHOCYANIN FOR SENSING PH, HEAVY METAL SALTS AND SURFACTANTS AND WITH CURCUMIN FOR SENSING HEAVY METAL SALTS AND SURFACTANTS. (B) MEDIUM THICKNESS FILMS CONTAINING 0.1% (W/W) IRON OXIDE PARTICLES WERE LOADED WITH CURCUMIN FOR SENSING PH AND UNLOADED IN 0.1 M AQUEOUS NaOH. SCALE BARS = 0.5 CM (N = 3, \pm SD)	215

FIGURE 4-20. THE CHANGE IN COLOUR AND MEAN PIXEL CHANNEL INTENSITIES OF CURCUMIN-LOADED AND ANTHOCYANIN-LOADED AZOSILK AND NATIVE SILK MEDIUM THICKNESS FILMS CONTAINING 0.1% (w/w) IRON OXIDE PARTICLES IN RESPONSE TO pH, SURFACTANTS, AND HEAVY METAL SALTS. SCALE BARS = 0.5 CM (N = 3, ± SD).	217
FIGURE 4-21. THE RELATIVE COLOUR CHANGES OF CURCUMIN AND ANTHOCYANIN-LOADED NATIVE SILK AND AZOSILK FILMS VARYING pH, SURFACTANT AND HEAVY METAL SALT. MULTIPLE FACTORS WERE EVALUATED BY TWO-WAY ANALYSIS OF VARIANCE (ANOVA), FOLLOWED BY ŠIDÁK'S MULTIPLE COMPARISON, SIMPLE EFFECTS POST-HOC TEST. ASTERISKS DENOTE STATISTICAL SIGNIFICANCE DETERMINED USING THE T-TEST AND POST-HOC TESTS AS FOLLOWS: *p < 0.05, **p < 0.01, ***p < 0.001, ****p < 0.0001.	219
FIGURE 4-22. SEMI-AUTONOMOUS MOVEMENT OF ORIGAMI SILK BOATS ACROSS WATER USING A MAGNET AND DISTANCE TRAVELLED FOR BOTH NATIVE AND AZOSILK ORIGAMI BOATS.	221
FIGURE 4-23. THE CHANGE IN COLOUR OF CURCUMIN-LOADED AND ANTHOCYANIN-LOADED SILK FILMS WITH pH AND ENVIRONMENTALLY RELEVANT CONCENTRATIONS OF CATIONIC, NEUTRAL, AND ANIONIC SURFACTANTS AND HEAVY METAL COMPLEXES, MEASURED WITH THE MODE INTENSITIES IN THE RGB COLOUR SPACE. THE MODE INTENSITIES OF THE RED, GREEN, AND BLUE CHANNELS WERE EXTRACTED FROM THE RGB HISTOGRAMS FOR CURCUMIN-SILK AND ANTHOCYANIN-SILK FILMS. THE NATIVE SILK AND AZOSILK FILMS, FOLLOWING LOADING AND WASHING WITH ULTRAPURE H ₂ O, SERVED AS THE CONTROLS. (N = 3, ± SD). ERROR BARS ARE HIDDEN IN THE BARS AND PLOT SYMBOLS WHEN NOT VISIBLE. SCALE BARS = 0.5 CM. MULTIPLE FACTORS WERE EVALUATED BY TWO-WAY ANALYSIS OF VARIANCE (ANOVA), FOLLOWED BY ŠIDÁK'S MULTIPLE COMPARISON, SIMPLE EFFECTS POST-HOC TEST. SAMPLE PAIRS WERE ANALYSED USING THE INDEPENDENT T-TEST. ASTERISKS DENOTE STATISTICAL SIGNIFICANCE DETERMINED USING THE T-TEST AND POST-HOC TESTS AS FOLLOWS: *p < 0.05, **p < 0.01, ***p < 0.001, ****p < 0.0001.	223

Abbreviations

ANOVA	ANALYSIS OF VARIANCE
BCA	BICINCHONINIC ASSAY
CFU	COLONY FORMING UNITS
DMEM	DULBECCO'S MODIFIED EAGLE MEDIUM
DSC	DIFFERENTIAL SCANNING CALORIMETRY
ECM	EXTRACELLULAR MATRIX
FBS	FOETAL BOVINE SERUM
FDA	FOOD AND DRUG ADMINISTRATION
FTIR	FOURIER TRANSFORM INFRARED
LB	LENNOX BROTH
MBC	MINIMUM BACTERICIDAL CONCENTRATION
MIC	MINIMUM INHIBITORY CONCENTRATION
MRSA	METHICILLIN RESISTANT <i>STAPHYLOCOCCUS AUREUS</i>
PBS	PHOSPHATE BUFFERED SALINE
PDMS	POLYDIMETHYLSILOXANE
SD	STANDARD DEVIATION
SDS PAGE	SODIUM DODECYL-SULFATE POLYACRYLAMIDE GEL ELECTROPHORESIS
SEM	SCANNING ELECTRON MICROSCOPY
SWF	SIMULATED WOUND FLUID

TGA

THERMOGRAVIMETRIC ANALYSIS

TSB

TRYPTIC SOYA BROTH

Table of Contents

DECLARATION	II
ABSTRACT	III
RESEARCH OUTPUTS	IV
ACKNOWLEDGEMENTS	VI
LIST OF FIGURES	VII
ABBREVIATIONS	XII
TABLE OF CONTENTS.....	XIV
1. INTRODUCTION	1
1.1 INTRODUCTION	2
1.2 WOUNDS	2
1.2.1 Skin wounding.....	2
1.2.2 Cell biology of wound repair	5
1.2.3 Chronic wounds	10
1.2.4 Skin microbiome	13
1.2.5 Infection of a wound.....	14
1.2.6 Treatment and Management	14
1.3 SILK.....	25
1.3.1 Background of Silk	25
1.3.2 Bombyx mori Silk.....	25
1.3.3 The structure of silk.....	28
1.3.4 Formats of silk.....	30
1.3.5 Silk uses in healthcare.....	34
1.3.5.1 Current use of silk in wound care	36
1.3.5.2 Biological Response to Silk.....	42
1.3.6 Biological response to silk fibroin	44
1.4 HYPOTHESIS, AIMS AND OBJECTIVES.....	46
2. CHAPTER 2 “IMPACT OF SILK HYDROGEL SECONDARY STRUCTURE ON HYDROGEL FORMATION, SILK LEACHING AND IN VITRO RESPONSE”	48
2.1 Introduction.....	50
2.2 Experimental	54
2.2.1 Silk solution production	54
2.2.2 Preparation of sonicated hydrogels.....	54
2.2.3 Preparation of Electro-gels	55
2.2.4 pH investigation	57
2.2.5 Silk quantity and efficiency determination	58
2.2.6 Secondary structure determination.....	58
2.2.7 Silk leaching determination	59
2.2.8 SDSPAGE	60
2.2.9 Cell proliferation	61
2.2.10 Cell migration.....	63
2.2.11 Wound healing.....	66
2.2.12 Phosphorylation assay	66
2.2.13 SEM	67
2.2.14 Statistical Analyses.....	67
2.3 Results	69
2.3.1 Silk Quantity and Efficiency Testing	69
2.3.2 pH testing.....	71

2.3.3 BCA leaching	75
2.3.4 FTIR	77
2.3.5 Thermal Analysis	79
2.3.6 SEM	88
2.3.7 SDSPAGE	91
2.3.8 Cell proliferation	93
2.3.9 Cell migration	95
2.3.10 Wound healing	97
2.3.11 Phosphorylation assay	100
2.4 Discussion	102
2.5 Conclusion	110
3. CHAPTER 3 “INVESTIGATING THE ANTIBACTERIAL EFFECTS OF SOLUBILIZED <i>BOMBYX MORI</i> SILK FIBROIN WITH COMMON WOUND PATHOGENS”	111
3.1 Introduction	113
3.2 Experimental	117
3.2.1 Silk solution preparation and conductivity assessment	117
3.2.2 Silk secondary structure analysis by Fourier transform infrared spectroscopy	117
3.2.3 Sterility testing	118
3.2.4 Culture Preparation	121
3.2.5 Bacterial growth in presence of water	121
3.2.6 Minimum Bactericidal Concentration of Silk	122
3.2.7 Simulated Wound Dressing	124
3.2.8 Bacterial Viability	126
3.2.9 Sodium Carbonate detection and bactericidal effects	126
3.2.10 Statistical Analyses & Data Sets	127
3.3 Results	128
3.3.1 Pure Aqueous Silk Solution	128
3.3.2 Secondary Structure Analysis of Silk	134
3.3.3 Sterility of Aqueous Silk Fibroin	136
3.3.4 Bacterial growth in the presence of silk	143
3.3.5 Performance of Silk Fibroin-functionalised Wound Pad	147
3.3.6 Bacterial Viability	151
3.4 Discussion	154
3.5 Conclusion	161
4. CHAPTER 4 “MANIPULATING SILK TO CONFORMABLE SHAPE AND PATTERNED FUNCTIONAL BIOMATERIAL”	163
4.1 Introduction	165
4.2 Experimental	175
4.2.1 Silk patterning	175
4.2.2 Fabrication and water annealing of silk films	176
4.2.3 Heterogeneous diazonium coupling	179
4.2.4 Extraction of anthocyanin	179
4.2.5 Anthocyanin loading	180
4.2.6 Curcumin loading	181
4.2.7 Characterisation of silk films	181
4.2.8 Electromagnetic field strength	184
4.2.9 Contraction and relaxation on water	185
4.2.10 Thickness and folding assessment	185
4.2.11 Characterization of silk origami boats	185
4.2.12 Statistical analyses	187
4.3 Results	188
4.3.1 Micropatterning	188
4.3.2 Micropatterning hydrogels	194

4.3.3 Silk film production	201
4.3.4 Origami Film parameters	205
4.3.5 Locomotion and floating testing	213
4.4 Discussion	224
4.5 Conclusion	228
5. CHAPTER 5 GENERAL DISCUSSION AND CONCLUSIONS	229
5.1 General Discussion	230
5.2 Recommendations for future research.....	236
5.3 Conclusion	239
BIBLIOGRAPHY.....	240

1. Introduction

This chapter introduces the topic of wound healing by introducing the current paradigm within the field and identifying opportunities for engineered solutions. The issues that interfere with and prolong wound healing are discussed such as inflammation and infection. Silk is introduced as a biomaterial with a wide-reaching potential for the application of improving wound care by overcoming prolonged inflammatory stages through its unique properties. The current uses of silk in healthcare are discussed and the future potential of this biomaterial is explored. Finally, the overall hypothesis of this thesis is introduced with the aims and objectives set out.

1.1 Introduction

The process of wound healing is a highly complex process with a defined sequence of events, that is sensitive to disruption. Sometimes, this means that the healing process requires managing and intervention to prevent regression of healing and infection of the wound. Some wounds are difficult to heal, and in vulnerable patients such as diabetics, immune-compromised or babies, can progress into chronic wounds which have a high risk of infection and lead to more serious complications if left untreated. Therefore, it is important to develop mechanisms to help progress wound healing and prevent and treat infections early if they are present. Silk fibroin is a versatile biomaterial that has been used for health care applications, such as sutures and dressings. In this chapter the pathways of wound healing, the background of silk and the uses in healthcare are explored in the context of the use of silk in wound healing applications.

1.2 Wounds

1.2.1 Skin wounding

The skin is the largest organ in the body, covering humans from head to toe. There are three layers of the skin; the epidermis, the dermis, and the hypodermis. The structure of the skin protects the body internal organs from UV light, chemicals, injury, and pathogens, serving as the first line of defence. As such, it is most vulnerable to wounding, and quick healing is vital to maintaining the health of the body. Within wound healing, there are cellular and molecular responses which elucidate the repair of the skin (Takeo, et al., 2015, Yousef, et al., 2022). The three

layers of skin can be further subdivided, with each layer having a role in the protection and regulation of the body.

SKIN ANATOMY

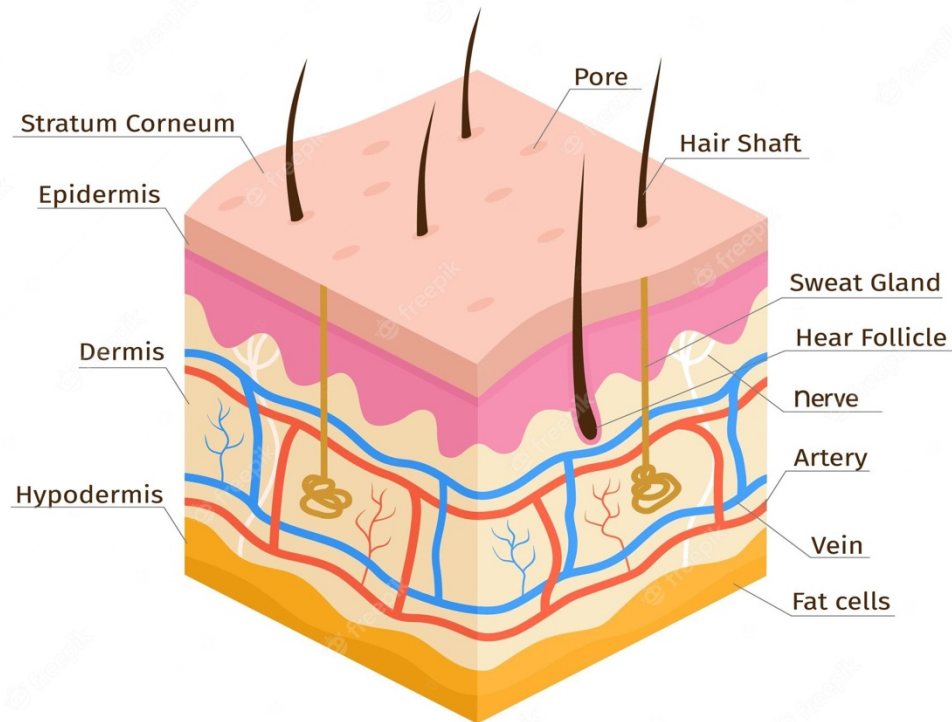


Figure 1-1. Layers of the skin. Image from Freepik.com available at https://www.freepik.com/premium-vector/human-skin-layers-anatomy-dermis-epidermis-hypodermis-tissue-skin-structure-veins-sweat-pores-hair-follicles-vector-infographic_23859333.htm

Wounding occurs when the skin is damaged, and an assortment of wound types can be formed depending on the mechanism of damage. Wounds can be broadly categorised into two groups; acute and chronic, which are classified according to the time frame in which they heal. Surgical wounds, bites, burns, abrasions, lacerations,

crush, and gunshot wounds can all be classified as acute wounds (Bowler, et al., 2001). Acute wounds will follow a series of pathways of healing, resulting in a shorter time frame until the skin regains integrity, whilst chronic wounds tend to get stuck in the cycle of healing and can take far longer to heal, reoccur or may never heal (Raziyeva, et al., 2021). In general, four phases of wound healing can be identified in the acute wound healing pathway. These phases overlap and can be described as haemostasis, inflammation, proliferation, and remodelling. It does not matter how an injury occurs or the type of wound caused, acute wounds are expected to heal within a predictable timeframe, with the treatment varied according to the type of wound, site of the wound and depth of the wound (Bowler, et al., 2001).

The skin is regenerative, with the epidermis being replaced approximately every 4 weeks via differentiation, proliferation, and migration of cells within the epidermis. This process ensures a continuous barrier is maintained, protecting the dermis where important blood vessels and nerves lie. As the outermost layer, the epidermis is subjected to various forms of injury. In the event of failure to repair the epithelial layer of skin, the body is open to dehydration and infection (Takeo, et al., 2015). Alongside re-epithelialisation, restoration of the dermis relies on the proliferation and migration of fibroblasts. Fibroblasts release growth factors that lead to further fibroblast migration and proliferation when wounding occurs, and they help instrument the immune response by releasing inflammatory cytokines (Takeo, et al., 2015). Another key role of fibroblasts in wound healing is the creation of new extracellular matrix (ECM). Fibroblasts can differentiate into myofibroblasts which

can contract and produce ECM proteins to induce wound closure (Li & Wang, 2011, Bainbridge, 2013, Cialdai, et al., 2022).

There are many different factors that contribute to the mechanisms behind wound healing which can greatly affect the outcome for the patient. When damage occurs to the epidermal layer in healthy individuals, the repair mechanisms are efficient, and the wound will heal quickly without leaving any lasting mark or scar. If the dermal layer is damaged more deeply, it may result in scar formation which will cause the original function and structure to be lost. When this repair mechanism does not work as intended, there are two main outcomes. This can result in an ulcerative skin defect, also known as a chronic wound, or excessive scar tissue being formed, such as a hypertrophic scar or keloid. (Frykberg & Banks, 2015)

1.2.2 Cell biology of wound repair

Wound healing occurs through four phases: haemostasis, inflammation, proliferation, and remodelling (Eming, et al., 2014, Sun, et al., 2014).

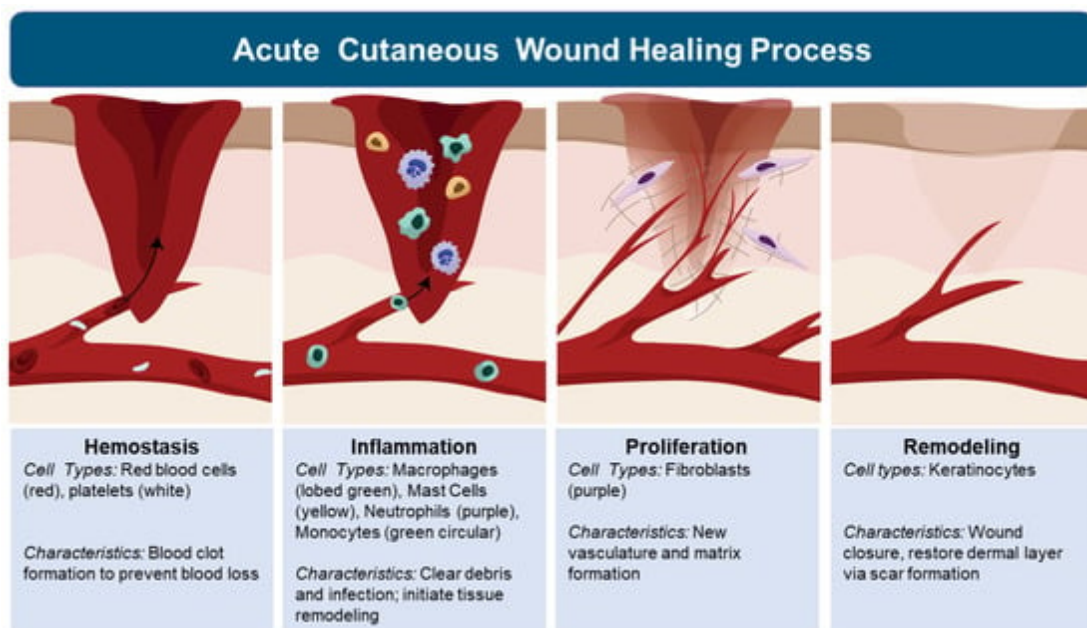


Figure 1-2. Cutaneous wound repair process. The 4 stages of wound healing are described by haemostasis, inflammation, proliferation, and remodelling. Image from (Andrade, et al., 2022)

Once an injury occurs, haemostasis commences quickly to stop blood loss and is characterised by vasoconstriction and blood clotting. This provides the matrix for cell migration to occur. The platelets within the blood will recruit endothelial cells, fibroblasts, and cells of the immune system by secreting cytokines and growth factors. The inflammatory phase can last for a week, with phagocytic cells producing reactive oxygen species that with help to remove cellular debris and ward off bacterial contamination. The tissue macrophages are formed from blood monocytes, and the purpose of these are to remove any bacterial contamination and non-viable tissues by phagocytosis. The other function of these cells is to secrete growth factors and cytokines that will attract fibroblasts, keratinocytes, and endothelial cells to help to repair the damaged blood vessels. The immune cells will undergo apoptosis,

signalling the end of the inflammatory phase, and allowing the proliferation phase to commence.

The proliferation phase includes granulosin, angiogenesis and epithelialisation. When the epithelium becomes broken, the body will begin to repair from both edges of the wound and from sweat glands. In a mouse model it has been seen that there are several gene upregulations that will occur from the wound edge epithelium as far back as 70 rows of cells (Canadian Agency for Drugs and Technologies in Health, 2013, Rice, et al., 2014, Shankaran, et al., 2013). The intermediary genes Ap1, Fos, Jun and krox zinc finger transcription factors are the first gene upregulations seen. This is thought to perform as the transcriptional activation machinery for more genes to be upregulated as the body begins to heal which will cause an increase in cell proliferation and the associated epidermal migration of keratinocytes at the interface between a scab and the healthy wound granulation tissue. The late activated genes are silenced by histone methylation marks deposited by the polycomb family of epigenetic regulators. These polycombs are downregulated and the marks are removed soon after wounding so the silenced genes can be activated by transcription. As the keratinocytes migrate forward, they change the cell-to-cell matrix adhesion. This changes from bonded basal epidermal cells to the basement membrane to being able to migrate over a new fibrin rich matrix, which is formed depending on the wound type. In order to do this, several integrins are turned off so that the cells can detach from the basement membrane and other integrins will facilitate the movement of the cell. It has been shown that in keratinocyte-specific knockout beta-1 integrins in mice will result in poor re-epithelialisation of the wound.

The desmosomal junctions that link the keratinocytes will become weaker and calcium dependent. This change is thought to be triggered by protein kinase C alpha dependent, as PKCalpha1-1 mice will not show this change and therefore will have slower wound healing. (Demidova-Rice, et al., 2007) The key factors are proteases such as matrix metalloproteases (MMPs) as they will remove the bond between integrins and collagen as the epidermis grows over the wound substratum (Edmonds, 2012).

Fibroblasts migrate into the wound, and in the wound site they are active. When they migrate into the wound site, they change their morphology and produce and secrete proteases to aid their movement from the ECM to the wound site (Shultz, et al., 2011). Fibroblasts move by attaching to fibronectin, vitronectin or fibrin via integrin receptors, binding to specific arginine-glycine-aspartic acid (RGD) or binding sites. The cell uses a cytoskeleton network of actin fibres to pull itself along (Shultz, et al., 2011). The directional element of fibroblast movement can be influenced by chemotactic growth factors, cytokines, chemokines, and the alignment of fibrils, along which the fibroblasts will travel. Fibroblasts will also secrete enzymes such as MMPs (Shultz, et al., 2011).

Granulation tissue, composed of collagen and proteoglycans, is deposited by fibroblasts. The activity of fibroblasts is controlled by growth factors, namely platelet-derived growth factor (PDGF) and transforming growth factor-beta (TGF- β). Proliferation, chemotaxis, and collagenase expression is stimulated by PDGF, whilst ECM deposition is regulated by TGF- β . Both growth factors are expressed from platelets and macrophages (Shultz, et al., 2011).

The re-epithelialisation of the wound is triggered by growth factors. These include hepatocyte growth factor (HGF) and at least one fibroblast growth factor (FGF) and epidermal growth factor (EGF) families. During wounding the epidermal cells are lost and as such they must be replaced. This is done by proliferation which occurs back from the migrating epidermis. (Shultz, et al., 2003)

Angiogenesis involves the replacement of damaged vasculature to maintain and re-establish a blood supply within the tissue. There are many angiogenic signals which trigger endothelial cells to extend and link vessels, which are released by the other cells involved in the proliferative stages of wound healing such as fibroblasts, vascular endothelial cells, epidermal cells, and macrophages. Oxygen levels in the tissue also regulates the level of angiogenesis required; with an increase in oxygen saturation of the tissue the decrease of the angiogenic factors through activation of hypoxia-inducing factor (HIF) which binds to oxygen is seen (Shultz, et al., 2011, Semenza, 2002).

Granulation tissue is granular in appearance, in part due to the formation of capillary tufts, and is a transitional tissue for the normal dermis. The tissue has a strong network of capillaries and blood vessels. This tissue matures into a scar during the remodelling phase of wound healing.

The proliferation phase can last for a year to 2 years, or even longer. Throughout this phase, the provisional matrix is remodelled into more organised and structured collagen bundles (Shultz, et al., 2003, Falanga, 2005).

1.2.3 Chronic wounds

The classifications of chronic wounds include vascular ulcers which will be venous or arterial ulcers, diabetic ulcers, and pressure ulcers. If a wound fails to heal within 3 months, it can be considered chronic. These wounds can possess excessive inflammation over a prolonged period, a persistent infection, drug resistant antimicrobial films and the inability of the dermal or epidermal cells to respond to reparative stimuli. These features together create a wound that fails to heal properly. Chronic wounds do not follow the usual progression of healing. Histological studies of chronic venous leg ulcers display a hyperproliferative epidermal edge, and the ulcer base is covered with exudate that contains necrotic debris. There are vessels with a fibrin cuff surrounding them in response to the venous hypertension, and little wound granulation tissue. There is also limited vessel sprouting and a lack of myofibroblasts. An increased inflammatory response is usually triggered which is indicated by the presence of neutrophils, and the phenotype of these cells can be different to those found in a normal healing acute wound. (Herrick, et al., 1992) Hyperpigmentation can be seen at the wound site, even past the wound healing, which is caused by melanocytes being used at the wound site. At the edge of the wound site keratinocytes will express a gene signature which reflects partial proliferative activation with several cell cycle genes. Cyclins are upregulated and checkpoint regulators such as p53 are suppressed, and this leads to the epidermal hyperproliferation at the ulcer edge. The fibroblasts present are senescent and have a reduced migratory capacity, as well as being unresponsive to growth factor signals. This is reflected in the drastically reduced tgf beta receptors and signalling cascade

components (Pastar, et al., 2010). The reduced growth factor signals could also be a symptom of the increased level of MMPs which are present in chronic wounds in greater numbers than in acute wounds. As the number of MMPs is larger than the inhibitors, this leads to the destruction of the extracellular matrix and the degradation of growth factors and the receptors. This will restrict the proliferative phase and attract more inflammatory cells (McCarty & Percival, 2013).

The most recognisable symptom of chronic wounds is persistent inflammation due to the increased recruitment of the inflammatory cells. This could be caused by the open wound being continually exposed to microbes. The immune response can be beneficial in some cases, such as with a diabetic foot ulcer, increased numbers of Langerhans cells in the epidermis can be associated with a more favourable healing result (Stojadinovic, et al., 2013). In most cases, however, the large numbers of immune cells from the innate system can restrict and inhibit some repair processes. It has been shown that the bactericidal and phagocytic functions of the immune cells may be compromised (Naghibi, et al., 1987). As the immune cells produce reactive oxygen species, in low concentrations this will inhibit bacterial growth, but in the large concentrations present in chronic wounds, it will damage the extracellular matrix proteins and cause cell damage.

Due to the reduced phagocytic function of the cells one key drawback found is the accumulation of necrotic debris at the edge of the wound site, and the usual treatment of this is debridement of the wound which creates a new wound surface, so the body can restart the epithelialisation once again.

Diabetic wounds often contain similar microbial flora to venous leg ulcers and pressure ulcers have the most variability in the microbial activity present. Some of the pathogens that can be present will affect the healing process by interfering with keratinocytes or wound fibroblasts, or indirectly by modulating the immune response.

The senescence of cells present in chronic wounds is another factor which will impair the healing process. This leads to a cell population with impaired proliferation and secretions which will make them unresponsive to healing signals (Shultz, et al., 2003). Pressure and venous ulcers studies have shown that the fibroblasts are senescent and will not proliferate as productively, which will lead to a failure of the wound to heal correctly. Other senescent cell types are keratinocytes, endothelial cells, fibroblasts, and macrophages (Bourguignon, 2014, Wall, et al., 2008). Cellular senescence is thought to arise from oxidative stress leading to DNA becoming damaged which will ultimately interrupt the cell cycle, or in diabetic patients will lead to metabolic changes, affecting the intracellular biochemical pathways such as GSK-3beta/Fyn/Nrf2 (Telgenhoff & Shroot, 2005, Biltar, 2012).

Mesenchymal stem cells have also been attributed to the wound healing process (Ennis, et al., 2013), as they are recruited into the circulation and will graft themselves into the remodelling microvasculature. In animals or patients with chronic wounds or diabetes, they have also been shown to be deficient and defective (Ennis, et al., 2013, Rodriguez-Menocal, et al., 2012). As such, these should be considered when treating chronic wounds as some patients may require a donor of healthy MSCs.

The balance of cytokines, growth factors and proteases which can facilitate the healing of a chronic wound should be restored to help the patient recover. The wound will not undergo complete reepithelialisation and therefore not heal correctly.

Chronic wounds affected around 3.8 million patients in the UK in 2017-18, with 49 % of chronic wounds healing in this timeframe. In the presence of infection, 45 % of wounds healed. The annual cost of wound management to the NHS is around £8.3 billion, with £5.6 billion being attributed to managing unhealed wounds (Guest, et al., 2020). The risk factors of developing a chronic wound are poor circulation, diabetes (Velickovic, et al., 2023), aging, and poor nutrition (Raeder, et al., 2020), and the rates of infection are around 45 % (Simel & Rennie, 2009).

1.2.4 Skin microbiome

The skin is host to millions of bacteria, which can be referred to as the skin microbiome (Byrd, et al., 2018). The bacteria present vary depending on the conditions for which they live in, such as moisture, pH, and nutrient availability. Many of these bacteria are of benefit to the body (symbiotic) or are of no benefit to the body but cause no harm (commensal). The skin microbiome can play a protective role for the host body, reducing the colonisation of pathogenic organisms, but occasionally these organisms can become pathogenic in a state of dysbiosis. The skin microbiome has natural antimicrobial properties and microorganisms may act competitively or synergistically with mutual benefits on the surface of the skin. Many common skin diseases are thought to be due to a dysbiosis in the commensal bacteria

on the surface of the skin, and chronic wounds are thought to be affected by the skin microbiome (Byrd, et al., 2018, Eming, et al., 2014).

1.2.5 Infection of a wound

All wounds are colonised to some degree, and the role of the inflammatory phase of wound healing is to control the level of colonisation, bringing it to a level that the body can tolerate (Eming, et al., 2014). Infection of a wound occurs when the virulence factors by microorganisms in a wound outcompete with the hosts natural immune system. The invasion of these microorganisms results in local and systemic host responses which can be characterised by purulent discharge, swelling, pain and fever or spreading redness at the wound site, with cellulitis developing if the infection progresses to the deeper layers of the skin (Peel, 1992). The infection of a wound can be influenced by the site and size of the wound, the depth of the wound, the exposure to contaminants, the levels of blood perfusion to the wound site, the microbial load and the general health and immune system strength of the host (Bowler, et al., 2001). In polymicrobial wound infections, some species of bacteria can increase their virulence factor and their number through formation of biofilms. The healing of wounds can be greatly delayed by the colonisation of harmful bacteria. The most common genera in chronic wounds are *Staphylococcus*, *Pseudomonas* and *Corynebacterium*, whilst the diversity of the microbiome is reduced compared to healthy skin around the wound (Gontcharova, et al., 2010)

1.2.6 Treatment and Management

Wounds should be assessed to determine the best route of treatment. There are lifestyle and health factors that can affect the wound healing process and help dictate

appropriate wound management. These factors vary from age, to smoking habits and comorbidities and medications. The wound assessment must look at the type of wound, location, and the stage of healing (Dealey, 2012).

Epidermal cells travel across the wound surface through well-defined ECM, but in devitalised tissue, these conduits are lost due to degradation or disruption. To improve the movement of cells, this devitalised tissue must be removed. Debridement of a wound is the removal of such tissue and can be performed through several methods, each with advantages and disadvantages (Manna, et al., 2022). Surgical debridement is the quickest method and can allow a non-healing chronic wound to adopt an acute wound environment and help the healing process (Shultz, et al., 2003). This method of debridement is commonly used on large areas and where there is a risk of infection, but this method requires skill as knowledge of the area around the wound is required and not too much tissue should be removed. Autolytic debridement employs the use of macrophage and endogenous proteolytic enzymes that can digest necrotic tissue and eschar, separating it from healthy tissues (Shultz, et al., 2003). Enzymatic degradation is the use of exogenous enzymes which combine with endogenous enzymes in the wound and break down devitalised tissues. This technique is useful for removing hard necrotic eschar if surgical debridement is not able to be used (Shultz, et al., 2005). Larval debridement is performed using sterile larvae which secrete digestive enzymes to break down devitalised tissues and leave healthy tissue behind (Gray, 2008). This method can also reduce bacterial infection as the larvae are bactericidal and can breakdown biofilms. They also increase the pH of the wound which can make the environment more inhospitable for bacteria

(Manna, et al., 2022). Mechanical debridement covers the use of wound irrigation and wet to dry dressings. This method is usually more painful than others, and can remove healthy tissues alongside necrotic tissue, impeding healing further (Manna, et al., 2022).

Wound bed preparation is often said to be the key to wound management, particularly those which have difficulty healing. The concept of wound bed preparation focuses on removing barriers to healing to encourage the normal wound healing pattern. The aim of the preparation of the wound bed is to remove devitalised tissues, reduce bacterial loads and inflammation, lower the volume of exudate, and encourage healthy granulation tissue to form (Halim, et al., 2012). The concept of wound bed preparation was first brought about by Dr Vincent Falanga and Dr Gary Sibbald in 2000 and has been developed in the following years (Falanga, 2000, Falanga, 2002, Sibbald, et al., 2000, Sibbald, et al., 2003).

One method of wound assessment is the TIME framework, which stands for Tissue, Infection/Inflammation, Moisture and Edge. The TIME framework can be used to help wound assessment at the point of each dressing change, with chronic wounds assessed every 4 weeks. This is to improve the wound bed preparation to aid the healing of chronic wounds (Halim, et al., 2012, Dowsett & Newton).

Tissue management looks at the type of tissue in the wound bed. There are different types of tissue formed through the healing process such as granular or epithelialisation tissues, sloughy and necrotic tissue, or eschar. Clinicians' assess the wound bed for cell debris that could be impairing wound healing. The treatment is

usually debridement of the affected tissue either mechanically or through enzymatic or biological methods. This is hoped to restore the wound base and encourage the deposit of ECM proteins to encourage wound closure (Dowsett & Newton, Halim, et al., 2012).

Infection can be identified through odour and confirmed through identifying the organisms present by microbiological culturing. Prolonged inflammation and high bacterial counts are indicators of infection. Pain is also monitored, with the frequency, location and severity all being important measures. When infection is present, there will be an increase in inflammatory cytokines and protease activity, and growth factor activity will be reduced. The treatment of infection is commonly through the use of antimicrobial agents and anti-inflammatories. As proteases can break down ECM proteins and foreign material to encourage new tissue to grow, if there is an increase in protease activity, it can alter the balance between new tissue growth and tissue breakdown prolonging the healing process. As such, it is also important to control the proteases in the wound bed (Wounds International, 2011, Dowsett & Newton, 2005). The treatment should reduce the number of bacteria in the wound bed and control the inflammation by lowering the inflammatory chemokines and proteases.

Moisture in the wound can be judged through the colour of the skin surrounding the wound, as excess fluid can turn the skin a lighter shade. The volume of exudate can be assessed by the number of dressings exudate can seep through. Excessive fluid can cause maceration of the wound margins which can prolong healing. To control the moisture in the wound bed, dressings which have moisture balancing properties

can be applied, such as occlusive dressings which can protect the wound from bacterial infection and external moisture by creating an airtight and watertight covering. If the wound is too moist Hydrofiber dressings can be used which will absorb the excess moisture in the wound bed (Barnea, et al., 2010). These dressings could also incorporate Cadexomer iodine which can provide antimicrobial effects and absorb exudate (Sibbald & Elliott, 2017). Compression or negative pressure therapies could also be applied to remove excess moisture from the wound bed (Dowsett & Newton, 2005).

Finally, the edge of the wound must be monitored. The dimensions of the wound and the margins of the wound are important factors to assess. Maceration, oedema, and erythema on the wound border are indications that the healing could be delayed (Black Country Partnership NHS Foundation Trust, 2016). If the edge of the wound is non advancing or undermining, then this could be due to imbalanced protease activity or abnormalities in the ECM. The treatment for these issues on the edge of the wound are debridement or skin grafting, or the use of biological agents to restore the protease activity balance. Once the wound edge is seen to be advancing then the therapies can be considered successful (Dowsett & Newton, 2005).

The application of a dressing onto a chronic wound can help protect the wound from contamination, infection, and further damage, and new advances in wound dressings can help target specific problems in the chronic wound healing pathways as identified through the TIME method (Britto, et al., 2022).

Traditional dressings such as gauze, cotton pads and bandages are commonly used to cover wounds. These are a low-cost option and can provide a quick solution to

protecting wounds, but they have many drawbacks. One drawback is that these dressings make it difficult to control the wound bed and can absorb all of the exudate from a wound, making the wound too dry. This can also cause adherence of the dressing to the wound surface, disturbing the wound bed when the dressing is removed, prolonging wound healing. Modern dressings have attempted to redress this balance with improved biocompatibility, degradability, and moisture retention. Common types of modern dressings include hydrogels, hydrocolloids, alginates, foams, and films. Hydrogels are useful for retaining moisture in a wound bed and removing necrotic tissues, so are commonly used in pressure ulcers, surgical wounds, and burns. They can be made of many materials but are commonly a network of hydrophilic polymer chains. Hydrogels can also be loaded with agents to improve their properties, such as silver nanoparticles or zinc nanoparticles which can maintain antibacterial effects over longer periods of time (Li, et al., 2018). More recently, zwitterionic hydrogels have been developed to act as an optical sensor to monitor the pH and glucose level of the wound. Zwitterionic groups can bind water molecules and can have effective antifouling properties (Zhu, et al., 2019).

Hydrocolloid dressings are a hybrid of a hydrogel mixed with rubber and sticky materials which are suited to absorbing exudate in a wound bed. They are formed of two layers, with the inner layer providing the absorbent properties whilst the outer layer protects the wound from contamination (Barnes, 1993). Alginate is a material formed from seaweed which can also absorb exudate and maintain haemostasis. These dressings are suited to infected wounds with lots of exudate (Lee & Mooney, 2012). Foams can be made of polyurethane or silicone and have the advantage of

being semi-permeable. They can offer antimicrobial activity and thermal insulation and so are suited to infected wounds. Finally, films are usually made of polyurethane and are thin, transparent, porous, and adhesive. The purpose of these films is to protect the wound from contamination as they are impermeable to bacteria and liquid but can offer autolytic debridement. Due to the thin nature of the films, they are best suited to aid the reepithelialisation of wounds with little exudate. (Shi, et al., 2020)

Dressings loaded with silver are often cited as providing improved wound healing and reduced infection, and zinc oxide can also improve the rate of wound healing with greater tissue regeneration (Ongarora, 2022).

Due to the nature of chronic wound healing, ideal dressings and treatment would include biocompatible materials that can reduce inflammation, prevent infection, and increase tissue regeneration to close the wound faster and improve the patient outcomes. A summary of moisture retentive dressings can be found in the table below.

Table 1. Moisture retentive dressings. Table adapted from (Powers, et al., 2013)

<i>Dressing Type</i>	<i>Advantages</i>	<i>Disadvantages</i>	<i>Examples</i>
<i>Films (polyurethane)</i>	Adherent, transparent, bacterial barrier	Fluid collection, removal can disturb healing	<ul style="list-style-type: none"> • Tegaderm (3M Healthcare) • Polyskin II (Kendall Healthcare)

		<ul style="list-style-type: none"> • Bioinclusive (Johnson & Johnson medical) • Blisterfilm (The Kendall Co.)
<p><i>Foams (bilaminate sheets containing polyurethane and silicone)</i></p>	<p>Absorbent, Adherence to Moist wounds if environment, exudate dries conforms to contours</p>	<ul style="list-style-type: none"> • Polymem (Ferris Corp.) • Allevyn (Smith and Nephew United) • Biopatch (Johnson & Johnson Medical) • Curafoam (the Kendall co.) • Flexzan (Dow B. Hickam, Inc.)

Hydrogels (96 % water, cross linked hydrophilic polymer)

Comfortable,
Absorbent,
Promotes
autolytic
debridement

Non-adherent
Macerations of
skin around
wound

- Hydrasorb
(Tyco/Kendall Co.)
- Lyofoam
(ConvaTec)
- Vigilon (CR Bard)
- Nu-gel
(Johnson & Johnson Medical)
- Tegagel (3M)
- FlexiGel
(Smith & nephew)
- Curagel (The Kendall Co.)
- Clearsite
(Conmed corp.)
- Curafil (the Kendall co.)

Hydrocolloids
(carboxymethylcellulose
on adhesive base)

			<ul style="list-style-type: none"> • Elasto-gel (SW Technologies) • 2nd Skin (Spenco Medical Ltd.) • Transigel (Smith & Nephew)
	Improved healing, Waterproof, promote granulation	Unpleasant odor, overstimulation of granulation, fluid drainage can be gel-like	<ul style="list-style-type: none"> • Duoderm (ConvaTec) • NuDerm (Johnson & Johnson Medical) • Comfeel (Coloplast Sween, Inc.) • Hydrocol (Dow Hickman) • Cutinova (Smith & Nephew)

				<ul style="list-style-type: none"> • Replicare (Smith & Nephew United) • Tegasorb (3M)
<i>Alginates (Natural polysaccharides from kelp and algae)</i>	Absorbent, hemostatic properties	Not useful for dry wounds, frequent changes may be required		<ul style="list-style-type: none"> • Algiderm (Bard) • Algisite (Smith & Nephew) • Algisorb (Calgon-Vestal) • Curasorb (The Kendall co.) • SeaSorb (coloplast) • Kalginate (DeRoyal)

Antimicrobial agents can be used in the management of wounds. Systemic agents such as ciprofloxacin can be used topically to increase the rate of wound healing.

Other topical agents such as benzoyl peroxide, silver zinc allantoinate cream and povidone iodine ointment can be applied to wounds and show improved healing and wound closure (O'Meara, et al., 2000).

1.3 Silk

1.3.1 Background of Silk

Silk has been used for two millennia as a suture material and it possesses unique mechanical properties that can be utilised in modern medicine. One advantage of silk is that it can be processed into many different material formats. These include fibres, fabrics, films, scaffolds, particles, and hydrogels. The silk used in these formats is typically everyday silk from the common *Bombyx mori* silkworm. These silkworms have been selectively bred and the characteristics have been chosen which help to obtain silk fibres with key properties such as improved toughness, easy reeling from the cocoon and a higher yield of silk (Seib, 2018).

1.3.2 *Bombyx mori* Silk

The domesticated silkworm, *Bombyx mori*, is typically used for commercial sericulture, or silk farming. It is the most common silk used in biomedical applications due to its excellent mechanical properties and the availability of the fibres (Seib, 2018).

The lifecycle of the silkworm consists of four main stages; the egg laid by the female moth which hatches and develops into a larva, moulting four times before it spins the cocoon around itself and becomes a pupa which would then develop into a moth which would emerge from the cocoon. The silkworm will consume vast quantities of mulberry leaves from the moment it hatches until it spins the cocoon. Once the

silkworm reaches the 5th and final instar of its life, it will consume mulberry leaves continuously for around one week to produce the volume of liquid silk it will need to produce the protective cocoon. The liquid silk is stored in the exocrine gland during this process and can reach a concentration of around 25% w/v. This silk solution does not aggregate unlike other solutions of high protein concentrations. This is interesting as silkworms are poikilothermic and as such the internal temperature can vary between 25° and 30°, and the silk does not aggregate with the movement of the silkworm either. This demonstrates how the silk has evolved to overcome these challenges as these factors can cause aggregation out-with the silk gland (Kronqvist, et al., 2017, Li, et al., 2016).

Once enough silk has been produced within the silk gland, the silkworm will begin to build the cocoon over a period of three days. The silk cocoon is constructed from a single thread of silk which can be up to 1500m in length. The thread is 10-25 µm thick, although this can vary over the length of the strand (Seib, 2018).

The silk thread is composed of two filaments (i.e., bifilar) and each filament is produced independently arising from the paired silk glands. The silk solution is triggered to assemble into a silk fibre in response to cues for example by a reduction in the pH within the silk gland (Domigan, et al., 2015). The fibre is coated in sericin, another protein produced by the silkworm, as it leaves the gland to bind the silk fibres together to produce a single thread. This thread is then spun from the spinneret at the head of the silkworm. This thread builds the cocoon as the silkworm winds it in a figure of 8 motion.

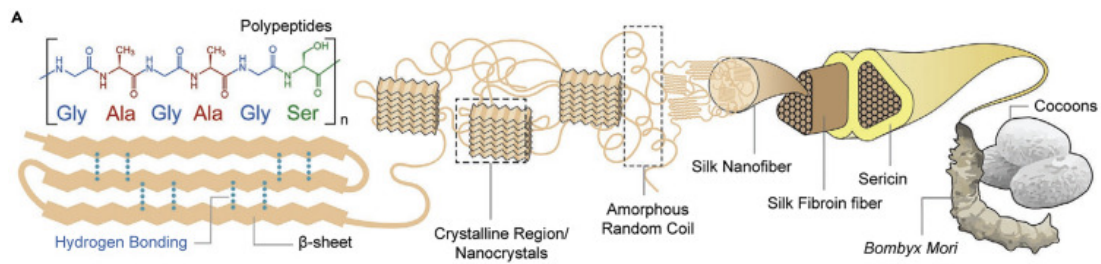


Figure 1-3. Silk thread composition. Image from (Wu, et al., 2022)

Sericin is involved in the process of spinning a cocoon and coats the fibroin which protects the silkworm from enemies and infections. Sericin can prevent the premature conversion of soluble silk into beta sheets (Kwak, et al., 2017). The role of sericin has been debated, for example sericin may provide an anti-bacterial effect that would help the silkworm remain protected once inside the cocoon. However, conflicting evidence has been reported. Akiyama (1993) and Seves (1998) both conducted studies and concluded that sericin does not contribute to any antibacterial properties of the fibre and that micrococcus bacteria would grow or were even aided by the presence of sericin. In contrast to this Sarovart (2003) and Khalifa et al. (2012) both concluded that sericin was an antibacterial substance.

There are environmental factors that can also affect the silk fibres produced by the silkworm, such as humidity and temperature, which can affect the morphology, mechanical properties, colour, and stiffness of the silk being spun by the silkworm (Offord, et al., 2016).

Silk has a high tensile strength and is very ductile. The fibre can withstand high forces before deformation will occur, which is comparable to Kevlar on a weight-weight basis. Therefore, silk has been used in load bearing applications such as bulletproof vests, parachute cords and in aerospace technology (Seib, 2018). Silk has also found

use in many biomedical applications. This includes wound closures (such as sutures) and Sofregen have the patents for a surgical mesh to use in reconstructive surgery and for vocal fold reconstruction with injectable regenerated silk protein (Sofregen Medical Inc).

The unique properties possessed by silk can be attributed to the structure of the silk fibre. The molecular size of the silk will vary between the different strains of *Bombyx mori* silkworm.

1.3.3 The structure of silk

The silk is composed of a heavy chain (~390 kDa, 5263 amino acids), a light chain (26kDa, 262 amino acids) and glycoproteins (30kDa, 220 amino acids). A thread of silk is mainly constituted by glycine (43%), alanine (30%) and serine (12%), which are joined to make a large protein chain (200-400kDA) (Kaplan, 1998). The ratio of these components is around 6:6:1 with heavy chains, light chains, and glycoprotein respectively. The heavy chain and light chain are connected by a single disulphide bond at the twentieth residue from the carboxyl terminus of the heavy chain (cys-c20) and cys-172 of the light chain. An intramolecular disulphide bond is formed at the cys-c4 and cys-c1 of the heavy chain. (Tanaka, et al., 1999)

The 5263-residue polypeptide chain of the heavy chain consists of 12 low complexity crystalline domains, which are constituted by Gly-X repeats which covers 94% of the sequence. These blocks are hydrophobic. The X can either be Alanine (65%), Serine

(23%) or Tyrosine (9%) for the repeats. The rest of the chain consists of a non-repetitive header sequence (151 residues), 11 copies of an identical spacer sequence (43 residues) and a C-terminal sequence (58 residues). The header sequence is homologous to other fibroins N-terminal sequence with the differences between them found in the crystalline regions. Within the crystalline regions of *Bombyx mori* silk fibroin, sub domains of around 70 residues are found which each begin with repeats of the GAGAGS hexapeptide and the GAAS tetrapeptide can be found at the end. Within the semi-crystalline region's sequences such as GAGAGY, GAGAGV and GAGAGVGY containing aromatic residues are found. These are not so repetitive. The hydrophobic sections of the chain have a different composition depending on their position within the chain. In support of the Pauling-Corey model, the Gly-X alternance is uniform in these sub domains, as beta sheets align in layers of Gly-Gly and X-X contact. Zhou et al. (2000) suggests that the subdomains form beta strands with each crystalline domain composed of a 2 layered beta 'sandwich', where these sheets lie parallel as opposed to lying anti-parallel as suggested in other papers.

In the silk gland, the silk is believed to exist as spherical micelles in solution around 100-200 nm in diameter. The micelles consist of a hydrophobic core made of the crystalline and amorphous regions, covered in the hydrophilic exterior formed by C- and N- terminal domains. The self-assembly of the silk is triggered by the pH in the silk gland and orchestrated by the n-terminal. When the pH drops to create an acidic environment, the acidic side chains of the silk heavy chain protonate and form hydrogen bonds. This mechanism helps to stabilise the silk gel-like state by causing the spherical micelles to aggregate. The resulting shear forces in the silk gland cause

the aggregated micelles to elongate and this forms the silk fibre. There is conflicting evidence that suggests the silk matures after being spun by the silkworm. These types of study are difficult to conduct because silk will mature with time (Hu, et al., 2020, Jin & Kaplan, 2003).

Much of the secondary silk fibre structure can be characterised as beta sheets, but other structures are present. These can be described as helices, turns and unordered secondary conformation. The distribution of these structures varies depending upon the conformation of the silk. The silk within the posterior silk gland adopts a silk I conformation, which consists of random coils, helices, and hydrated Beta sheets. The silk within the anterior silk gland, however, adopts a silk II conformation, which consists of beta- sheets, due to the low pH. Within the silk fibre the beta sheets are aligned parallel to the fibre axis, and within the amorphous matrix these nanocrystalline units are dispersed. To produce interlocking nanofibrils, the crystallinity, size and distribution of these crystallites dictate how this will occur. Nanofibrils are the components that twist together to produce the interconnected segments which make up a silk fibre. This structure contributes to the mechanical properties that silk possesses (Asakura, 2021). There is a third silk structure, silk III, which has three-fold polyglycine II-like helices (Vidya & Rajagopal, 2021, Lefevre, et al., 2007, Wilson, et al., 2000).

1.3.4 Formats of silk

Silk can be processed into many different formats with tuned properties that can be used in many diverse applications. Silk can be processed into silk nanoparticles, silk

films, silk fibres, silk coatings and silk hydrogels (Li & Sun, 2022). Silk hydrogels are a promising format of biomaterial due to the ability of the hydrogel to trap and deliver therapeutic payloads. Silk can be used for drug delivery, in which the drug and chemical modification to the silk can affect the final performance of the silk hydrogel (Haghighattalab, et al., 2022, Yavuz, et al., 2020, Numata, 2014). Silk hydrogels have also been investigated as a cell delivery system (Osama, et al., 2018, Seib, 2018). The silk is processed to best mimic the environment in which it will be implanted, with the goal being to mimic the extracellular matrix. This has the potential to support stem cell proliferation and self-renewal and differentiation into the required cell type. The presence of chemically reactive groups at known sites within the silk chain allows for functionalisation at these locations. For example, this strategy can be deployed to functionalise silk with integrin binding domains that are absent in *Bombyx mori* silk. These self-assembling silk hydrogels can be injected due to shear thinning and show minimal swelling as they undergo the solution-gel transition (Phuagkhaopong, et al., 2021, Osama, et al., 2018). Another branch of silk hydrogel are self-healing hydrogels. These hydrogels have ligand-mediated self-assembly and as such are chemically modified self-healing hydrogels that have potential uses in biomedicine (Meng, et al., 2020, Liu, et al., 2019). Silk hydrogels can be classified into chemically and physically crosslinked systems.

Chemically crosslinked silk hydrogels have been synthesised through the use of chemical crosslinking agents such as ethylene glycol diglycidyl ether or enzymatic crosslinkers like horseradish peroxidase to crosslink the phenol groups of tyrosine amino acids (Farokhi, et al., 2021). These hydrogels can withstand shear strain of

100% and a compressive strain of more than 70%. The crosslinked hydrogels are optically clear and more elastic than physically crosslinked hydrogels, which contain nanocrystalline regions which are capable of scattering light. The drawbacks to chemically crosslinked hydrogels are the need to add chemicals to the silk which can compromise the immunogenicity of the silk hydrogel and reduce the biocompatibility. Horseradish peroxidase is immunogenic and cannot be proven to be completely removed (Volkov, et al., 2015, Chirila, et al., 2017, Su, et al., 2017).

Physically crosslinked silk hydrogels can be manufactured through several different methods exploiting the innate self-assembly process of silk. Methods to trigger self-assembly include vortexing, ultrasound, temperature, osmotic stress, pH, CO₂ acidification, electrical fields and polymers (Farokhi, et al., 2021, Floren, et al., 2016, Samal, et al., 2014, Kim, et al., 2004). These trigger the self-assembling behaviour of silk by causing the entanglement and hydrogen bonds forming between the hydrophobic domains of the silk block copolymer. In most silk hydrogels, these can trigger a change in the secondary structure which means the formation of beta sheets, which can have strong intermolecular forces that can stabilize the silk network and produce a solid hydrogel structure which can be irreversible in most cases. Within the silk gland, the micelle concentration will reach a critical point at which the high concentration silk is in a gel-like state. Work done with reverse engineering the silk has found that the solution concentration will affect the silk hydrogel self-assembly and structure. When hydrogels are derived from low concentration silk solutions (1% w/v) the structure is micellar, as opposed to

hydrogels derived from higher concentration solutions (20% w/v) which show silk II structures in fibrillar networks (Seib, 2018).

Shearing of the silk solution can be achieved by vortexing or sonication. The agitation of the solution speeds up the process to minutes as opposed to hours if the reverse engineered silk is left to form a hydrogel by itself. The shear forces induce the transition from a silk I structure to a silk II structure containing high amounts of beta sheets, but excessive forces can damage the silk (Toprakcioglu & Knowles, 2021, Floren, et al., 2016, Onder, et al., 2022).

The formation of silk hydrogels by the alteration of the pH of the solution is due to the amphiphilic nature of the molecule, as the N-terminus of the silk heavy chain is acidic and the C terminus is basic, and the C terminus of the light chain is acidic. These acidic groups attract the protons at low pH, which allows the structure to become more ordered due to the reduced repulsion of the charges. This causes the formation of beta sheets (Onder, et al., 2022, Hirabayashi, et al., 1990, Nagarkar, et al., 2009).

The silk hydrogel formed when an electric current is applied has a different morphology to the silk hydrogels formed by other methods (detailed above). These hydrogels are referred to as e-gels and will deposit on the positive electrode when an electric current is applied to the silk solution. It is thought that this is due to the local pH change at the electrode caused by the hydrolysis of the water in the silk solution. When the pH drops to below the isoelectric point of silk, the silk is deposited on the electrode. The pH change is the trigger in this solution-gel transformation, but the properties of these gels are different to those produced by pH alone. The secondary structure of the silk hydrogel shows a change from random coil to the helical

conformation and the beta sheet content is unchanged compared to other silk hydrogels. The silk hydrogel is also reversible, as if the current is reversed the gel formed at the electrode will dissociate and a new silk hydrogel will form on the new positive electrode. This is repeatable for many cycles. The e-gels formed by this method are sticky with adhesive properties (1 - 1.5 mJ) and are highly elastic compared to other silk hydrogels which usually cannot withstand strains of greater than 10% and tend to be brittle. The unique properties of e-gels make them a promising tool for use in biomedical applications (Kojic, et al., 2012, Leisk, et al., 2010).

1.3.5 Silk uses in healthcare

There are many potential uses of silk in healthcare applications due to the diverse formats and properties. These include the clinically approved use of silk for load-bearing applications which is supported by the biocompatibility of silk, the ability of the silk to degrade and the useful mechanical properties as well as the ease of production of *Bombyx mori* silk.

The IUPAC definition of biocompatibility is the ability of a material to perform with an appropriate host response in a specific application within biomedical therapy (Vert, et al., 2012). Silk is regarded as biocompatible in the fibre format for use as sutures. Silk hydrogels will need to undergo further testing to be classified as biocompatible. Any foreign body introduced into an existing ecosystem will elicit an immune response from the host, but this reaction can vary widely. Silk does produce an immune response, although this is comparable to other synthetic materials currently used in the human body such as polycaprolactone and polylactic acid, used

as medical implants that will degrade over time. Silk films and scaffolds have been widely used and are typically regarded as biocompatible across a wide spectrum of applications. Silk hydrogels are biocompatible, although this definition varies with factors such as the site of implantation and the volume of product implanted. This will also vary between hosts (Holland, et al., 2019, Vepari & Kaplan, 2007, Roy, et al., 2022). Silk has demonstrated a favourable immune response, with a low systemic inflammatory response and a low local inflammatory response in neutrophils and macrophages (Gorenkova, et al., 2021, Thurber, et al., 2015).

The degradability of a silk biomaterial can be manipulated in order to suit different biomedical applications. This can vary from targeted drug delivery to meshes for tissue regeneration. Although the US Pharmacopeia classified silk sutures are non-resorbable due to the maintained stability for the duration of the suture, there is evidence that the sutures degrade within a year and can be completely resorbed within 2 years. Cao and Wang (2009) proposed that the degradation of silk is controlled by a proteolytic enzyme such as chymotrypsin, actinase and carboxylase, and hydrolysis reactions that are catalysed by an enzyme. This is not thought to produce any toxic by-products which is ideal in a biomedical capacity. Numata and Kaplan (2010) proposed that the proteolytic degradation is driven by the breakdown of beta-sheet crystals, and therefore that the rate of degradation could be influenced and controlled by the regulation of the crystalline state. Although there have been studies into the degradation of silk films and scaffolds, there is not much research into silk hydrogels. However, a study was performed where sonicated silk hydrogels were implanted subcutaneously in a rat model. An increase in the pore size of the

hydrogel and vascularisation was seen over the time that the implant was monitored. This change was credited to the degradation of the silk hydrogel (Li, et al., 2018, Zhang, et al., 2022).

1.3.5.1 Current use of silk in wound care

Silk is a diverse biomaterial that is currently used and under investigation for use in different formats for healthcare, including its use in wound dressings. The table below summarises some of the key commercially available products that incorporate the use of silk fibroin in various stages of production.

Table 2. Commercially available or in development products containing silk fibroin for healthcare uses

Product	Use	Silk format and additives	Stage of development	Reference
Sofregen Silk Voice	Vocal fold insufficiency	Silk-HA protein injectable	US FDA cleared for use	(Brown, et al., 2019)
Sofregen Seri Surgical Scaffold (discontinued 2021)	Surgical scaffold to strengthen soft tissue	Silk fibroin	US FDA cleared for use in soft tissue scaffolding	(Jewell, et al., 2015)
Fibroheal Woundcare PVT Ltd.	Various wound care solutions	Silk and silver based formulas as	ISO accredited and available for	(Forbes India, 2023)

			ointment	or	purchase online,			
			dressings		not CE marked			
SilkTears	Dry	eye	Silk	derived	Available	for	(Silk	Tech,
	relief		protein	with	purchase		2022)	
			polysorbate-		2023/2024	with		
			80		FDA approval			

Many other formats of silk have been investigated for use in other healthcare applications and these are discussed in the next sections.

1.3.5.1.1 Silk Fibroin Solution

One format of silk that can be used in wound healing applications is silk fibroin solution. This silk fibroin solution has been tested both in vivo and in vitro on a scratch wound model with NIH 3T3 cells. Park et al. (2017) concluded that the introduction of silk fibroin into a wound will increase the expression of growth factors by activating the NF- κ B signalling pathway in both in vitro and in vivo wound healing processes. The results they observed suggested that the silk fibroin promotes wound healing by acting on the proliferative and remodelling stages of the wound healing process previously described. Silk fibroin has also been used as eye drops to improve corneal scratch wound healing (Vidya & Rajagopal, 2021, Abdel-Naby, et al., 2017).

1.3.5.1.2 Electrospun nanofibers

One format currently used in wound dressings are electrospun nanofibers. They have the ability to form porous, non-woven and membrane-based materials. Their structure is like that of collagen fibres in tissues which makes them ideal for skin

tissue engineering (Repanas, 2016). One format used included silver nanoparticles (AgNPs) coated with the electrospun silk fibroin nanofibers. These dressings were shown to inhibit the growth and spread of staphylococcus aureus and pseudomonas aeruginosa (Uttayarat, 2012). The AgNPs were shown to diffuse to the bacterial cell membrane and bind to the proteins and organelles present, disrupting cell function and leading to cell death. (Sondi & Salopek-Sondi, 2004, Suresh, 2010). Jeong et al. (2009) conducted a study into the hydrophobicity of silk fibroin wound dressings using gas plasma treatments. O₂ plasma treatments were shown to increase the hydrophilicity by affecting the surface properties of the silk fibroin nanofiber, whereas CH₄ plasma treatments decreased the hydrophilicity. O₂ treated silk fibroin nanofibers displayed better skin cell activity compared to untreated silk fibroin nanofibers. The functional groups on silk fibroin nanofibers that induce attachment and spreading of keratinocytes and fibroblasts showed increased characteristics after O₂ plasma treatment.

1.3.5.1.3 Silk Fibroin Films

Silk fibroin films could be useful in wound care due to their ease of characterisation and design. When used to treat full thickness skin wound in mice, the silk film reduced the area of the wound by 10 % after 14 days and 21 days later the wound was covered by regenerated epidermis. When a traditional hydrocolloid dressing (DuoActive) was used the wound showed a reduced recovery over 14 days compared to the silk film and only a partial epidermal regeneration could be seen after 21 days. The healing time was reduced by a week when using the SF film compared to the DuoActive

dressing. When the silk fibroin film was compared to Alloask D, a porcine dermis dressing used for burns, ulcers, inflammation and bed sores, the histological results showed a reduced inflammatory response and greater collagen regeneration (Sugihara, et al., 2000). Another study reported that silk fibroin films had no adverse effect on the growth and secretion of VEGF from endothelial cells. The films did not influence the production of platelet-derived growth factor (PDGF), VEGF, fibroblast growth factor-2 (FGF-2), or angiopoietin 1 (Ang-1) by normal human foetal lung fibroblasts (Liu, et al., 2010). Silk fibroin films have shown that they can be advantageous due to the ease of getting the material and making it sterile. It is also transparent and has improved healing outcomes in acute wounds (Padol, et al., 2011) (Zhang, et al., 2017). A human study involving the use of silk films for wound dressings has been used in a clinical trial, with biocompatibility criteria being met and improved wound size reduction (Zhang, et al., 2017).

1.3.5.1.4 Silk Fibroin Sponges

Tissue engineering often uses sponges as scaffolds for cell growth as they are porous with a high surface area within the defined space which will allow cells to attach and form tissues around these pores. Silk fibroin solutions can be processed to form sponges by freeze-drying, gas forming or through the use of porogens and electrospun fibres (Zhang, et al., 2012, Sultan, et al., 2018). Silk sponges can be fragile when dry, so hybrid sponges incorporating other materials have been produced. A silk fibroin- alginate blended sponge has been tested on a full thickness wound model in rats. When the composite sponge was compared to both silk fibroin and alginate

alone, the half healing time was reduced, and the re-epithelialization was increased, but the rate of collagen deposition was unchanged. (Roh, et al., 2006)

1.3.5.1.5 Silk Fibroin Hydrogels

Pure silk fibroin hydrogels can be classified as either physically or chemically crosslinked hydrogels. Physical crosslinking occurs through the use of shear forces, temperature changes, ultrasound, pH, electric field or surfactants, whilst chemical crosslinking involves the use of chemical agents, enzymes or irradiation (Zhang, et al., 2022, Floren, et al., 2016).

Physical crosslinking occurs through the physical interactions between the silk molecules, transforming the solution into a hydrogel with a defined 3D network structure. Temperature is an important factor to control when controlling self-assembly of hydrogels, as an increase in temperature can increase the molecular collisions and therefore aggregation of silk fibroin. This then forms beta sheets which are irreversible and stable (Zhang, et al., 2022). Ultrasound can accelerate the intermolecular interactions of silk fibroin through the creation of bubbles. When the bubbles collapse, the fluid is accelerated rapidly, creating collisions between the silk fibroin molecules, inducing self-assembly without the use of chemical agents, producing a pure silk fibroin hydrogel (Floren, et al., 2016, Gorenkova, et al., 2019). Electric fields can also be used to generate silk fibroin hydrogels through the increase of protons at the cathode, reducing the pH in the vicinity and triggering aggregation of the silk molecules. These hydrogels have unique properties, in that they are adhesive, and the formation of these hydrogels is reversible upon reversing the

polarity of the voltage applied through the solution (Floren, et al., 2016, Kojic, et al., 2012).

Chemical crosslinking can be useful to overcome limitations of physically crosslinked hydrogels, improving features such as the porosity, mechanical strength, biodegradability and swelling of hydrogels for diverse applications. Enzymatic agents commonly used are horseradish peroxidase (HRP), glutaminase and tyrosinase. HRP can produce elastic hydrogels with tuneable degradability (Zhang, et al., 2022).

Silk hydrogels are used in a wide range of biomedical applications. The silk can also be combined with naturally derived polymers such as collagen, hyaluronic acid, chitosan, alginate, and gelatin. Ju et al. (2014) produced a silk hydrogel with a combination of carboxymethyl cellulose and calcium alginate which was compared with medical gauze and Purilon Gel (PG) for cytotoxicity, adhesive strength, and water content. The cell toxicity was tested with NIH 3T3 fibroblasts and showed that after 1 day the hydrogels promoted cellular growth. The adhesive strength of the hydrogel was less than the gauze and PG, but the hydrogel had good cell viability. When the hydrogel was tested in vivo on rats with second degree burns over 3 weeks, the hydrogel allowed collagen deposition and dermal formation which suggests it would be a suitable burn wound dressing.

One material used currently is chitosan (CS) as a skin substitute, due to its biocompatibility, biodegradability, and antimicrobial behaviour. It is thought that the wound healing is accelerated by the synthesis of collagen by fibroblast cells to improve tensile strength at the wound site (Luangbudnark, et al., 2012, Kweon, et al., 2001). Thangavel et al. (2016) developed a chitosan-based hydrogel loaded with silk

fibroin and L-proline (LP) by crosslinking for use with tissue engineering and wound healing applications. L-proline is an amino acid used for collagen synthesis. The characterization of the gels showed them to be thermally stable and possess a good surface morphology. The loaded hydrogels increased antioxidant activity and increased cell viability with NIH 3T3 L1 cells. The cells also showed improved migration and proliferation. Skin tissue engineering applications have recognised the potential for silk fibroin blends to be suitable as scaffolds. A hydrogel consisting of β -cyclodextrin, polyethyleneimine to increase the swelling ratio, and silk fibroin was produced to aid in the healing of pressure sores. The gel also included centella asiatica extract which was added by submerging the gel in an aqueous solution containing it. The pressure sores healed within 6 days whilst the unloaded gels healed within 10 days (Lee, et al., 2012).

Overall silk hydrogels show potential to be crosslinked or loaded with other beneficial materials to improve wound healing outcomes, whilst showing excellent biocompatibility and degradability with pure physically crosslinked hydrogels.

1.3.5.2 Biological Response to Silk

The use of silk fibroin in wound healing has been shown to help the process by increasing cell growth and proliferation (Fini, 2005, Kim, 2016, Martinez-Mora, et al., 2012). The use of silk fibroin solution has been shown to increase the adhesion and proliferation of human fibroblasts (Chiarini, et al., 2003, Petrini, et al., 2001) and the proliferation and migration of primary human dermal fibroblasts and NIH 3T3 cells in a wound scratch model (Park, et al., 2017). The use of nanofibers has been shown to increase fibroblast cell proliferation in culture for a week (Yamada, et al., 2004). The

studies done thus far demonstrate the properties that silk fibroin possesses which could aid wound healing when applied as a dressing. Silk has been shown to have an effect of different cell types and by aiding both the proliferative and migratory stages of the wound healing process.

The cellular pathway through which the silk fibroin functions has been started to be investigated with the aim to understand how it impacts wound healing. The cellular pathways AKT/mTOR and MAPK signalling have a pertinent role in wound healing. The activation of c-Jun N-terminal kinases 1/2 (JNK1/2) and extracellular signal related kinases1/2 (ERK1/2) are responsible for cell migration. Martinez-Mora et al. investigated the role of SF on these kinases in the presence of specific inhibitors for certain cell signalling pathways. The investigation showed that MEK, JNK and PI3K pathways are involved in the migration of cells in the presence of fibroin and that inhibition of these kinases prevented the upregulation of c-Jun and phosphorylation. When the fibroin was tested in human keratinocyte cells HaCaT, the results were similar, showing that fibroin initiates cell migration through activation of the MEK, JNK and PI3K signalling pathways ending in c-Jun activation. (Martinez-Mora, et al., 2012) The inflammatory pathway is modulated by NF- κ B which produces signals used in scratch injuries, corneal epithelial wound healing, and cutaneous wound healing. Silk fibroin has been shown to induce healing by activating this pathway (Park, et al., 2017). NF- κ B has been shown to regulate the silk healing pathway by modulating the proteins involved such as vimentin, fibronectin, VEGF, and cyclin D1. There are cytokines and growth factors that also play a key role in wound healing. These are tumour necrosis factor- α (TNF- α), interleukin-1 β (IL-1 β), interleukin-6 (IL-6),

interleukin-8 (IL-8), interleukin-10 (IL-10) and growth factors such as transforming growth factor (TGF- α or TGF- β), vascular endothelial growth factor (VEGF) and epidermal growth factor (EGF). Silk fibroin has been shown to reduce these pro-inflammatory cytokines during the inflammatory phase when they are increased which helps to protect the cells and tissues whilst they heal. (Aykac, et al., 2018, Ju, et al., 2016)

These studies have shown the potential of silk fibroin to promote wound healing through several pathways. The presence of silk can induce and increase the speed of wound regeneration by improving cell migration, proliferation, and differentiation. (Sultan, et al., 2018) However, many questions about the efficacy of silk fibroin remain, some of which have been worked on in this thesis.

1.3.6 Biological response to silk fibroin

Silk fibroin has been shown to exhibit low haemostasis response and does not accumulate in the body, being degraded into benign products. The timescale of this will depend on many factors such as the site in the body, quantity of silk used and the silk secondary structures present (Gorenkova, et al., 2021). Silk fibres retain more than 50 % of their mechanical properties 2 months after implantation. Silks degrade by the action of proteases, such as α -chymotrypsin and collagenases (Vepari & Kaplan, 2007). Enzymatic degradation of the silk fibroin leads to smaller polypeptides before becoming amino acids, which are absorbed or metabolized in vivo (Guo, et al., 2020). The inflammatory response of degummed silk fibres have shown a lower

inflammatory response than polystyrene, collagen films and PLA films (Vepari & Kaplan, 2007). Amyloid proteins are insoluble protein aggregates with a “cross- β ” structure and occur naturally and most often do not result in disease. It has been reported, however, that amyloid may increase in response to a physiological challenge and can be involved in other human pathologies such as Alzheimer’s Disease and Parkinson’s disease, where an accumulation of these folded proteins can result in neurodegeneration. Fibroin β sheets have similar characteristics to amyloid and have been shown in mice to accelerate amyloid accumulation (Madden, et al., 2020). Silk fibroin β sheets have been shown to not exhibit cytotoxic effects on human neural cells where amyloid β sheets have, thought to be due to the lack of surface charge on the silk peptides. Silk can occasionally cause amyloidogenesis but has a low potential for amyloidosis (Tsukawaki, et al., 2016).

1.4 Hypothesis, Aims and Objectives

The overall hypothesis of my thesis is that silk fibroin is an adaptable biomaterial that has properties desirable for reducing the duration of wound healing by preventing bacterial infection and improving closure of wounds. The main hypothesis has been broken down into specific aims and objectives:

The aim of Chapter 2 was to determine the cellular impact of silk fibroin in wound healing context. The objectives of Chapter 2 were to produce silk hydrogels by sonication and electro-gelation, to characterise the differences between these hydrogels and the subsequent release of silk. The final objective was to monitor the response of fibroblasts to the silk released from the hydrogels to determine the biocompatibility and potential benefits of the presence of silk.

The aim of chapter 3 was to determine the antibacterial effects of silk fibroin. The objectives of chapter 3 was first to determine the inherent sterility of silk fibroin solution by monitoring bacterial growth in media and on agar. The next objective was to assess the bactericidal effects of silk fibroin solution when spiked with common wound pathogens. The final objective was to monitor the bactericidal effects when silk is applied in a surrogate wound dressing on simulated infected wounds to investigate the limitations of silk fibroin in an antibacterial context.

The aim of chapter 4 was to determine the versatility of silk fibroin and explore the contexts for use out-with biomaterials. The initial objective was to produce micropatterned silk fibroin hydrogels and films and monitor the cellular response to these patterned surfaces. The next objective developed into monitoring the ability of silk films to be folded into origami boats. This objective also involved the spiking of

silk films with curcumin and anthocyanin, natural dyes that react to their environmental pH. The final objective was to monitor the response of spiked films in the presence of different environmental agents to determine the feasibility of using spiked silk origami films for eco sensing applications.

2. Chapter 2 “Impact of silk hydrogel secondary structure on hydrogel formation, silk leaching and in vitro response”

Silk can be processed into a broad spectrum of material formats and is explored for a wide range of medical applications, including hydrogels for wound care. The current paradigm is that solution-stable silk fibroin in the hydrogels is responsible for their therapeutic response in wound healing. Here, I generated physically cross-linked silk fibroin hydrogels with tuned secondary structure and examined their ability to influence their biological response by leaching silk fibroin. Significantly more silk fibroin leached from hydrogels with an amorphous silk fibroin structure than with a beta sheet-rich silk fibroin structure, although all hydrogels leached silk fibroin. The leached silk was biologically active, as it induced vitro chemokinesis and faster scratch assay wound healing by activating receptor tyrosine kinases. Overall, these effects are desirable for wound management and show the promise of silk fibroin and hydrogel leaching in the wider healthcare setting.

This chapter was published as an original article (Egan, et al., 2022) and has been adapted accordingly for this thesis. Data acquisition and analysis for figures was conducted by myself. Data acquisition and analysis for thermal analysis (Figure 2-9)

was conducted in collaboration with Saphia Matthew. As the first author of this study,
I wrote the manuscript with input from the other authors.

2.1 Introduction

The current treatment strategies for chronic wounds typically include application of standard and advanced wound dressings (Carter, et al., 2010) and compression bandaging (Amsler, et al., 2009). Ultrasound (Cullum & Liu, 2017), debridement (Mohd Zubir, et al., 2020) and skin substitutes (Greaves, et al., 2013, Onida, et al., 2021) are more advanced therapeutic interventions, but the treatment of chronic wounds remains challenging and still requires orthogonal treatment strategies. Examples include physical methods, such as negative pressure wound therapy (Norman, et al., 2020) and real-time sensing applications that can support clinical decision making (e.g. when to change dressings (Milne, et al., 2015)) and enable the early detection of infection (Ward, et al., 2018) (e.g. WoundSense, Ohmedics Ltd). Electrical stimulation to accelerate healing by reducing infection and increasing tissue perfusion is also promising (Han & Ceilley, 2017, Thakral, et al., 2013, Ud-Din & Bayat, 2014). A number of new products are now being approved for use in humans (e.g., WoundEL, PosiFect RD, Procellera).

Despite these advances, wound dressings continue to be the key staple of wound management; therefore, a broad spectrum of both synthetic and natural materials are now utilized (reviewed in (Han & Ceilley, 2017, Farokhi, et al., 2018)). One of the natural materials emerging as a promising biomaterial for wound care is silk. The silk fibroin protein is a clinically approved biomaterial that is widely used for load-bearing applications (e.g., sutures, surgical meshes) (Holland, et al., 2019). In 2019, the first reconstituted silk fibroin injectable (Silk Voice®, Sofregen Inc, Medford, MA, USA)

gained clinical approval for vocal fold augmentation. The Silk Voice® product has demonstrated that reconstituted silk fibroin can be acceptable for registration in the medical regulatory frameworks (e.g., The United States Food and Drug Administration). A small ongoing clinical trial (NCT04085822) sponsored by Silk Medical Aesthetics Inc (Medford, MA, USA) is examining the use of this technology to improve aesthetic, with the study completing in 2020 and the results are eagerly awaited. Small-scale clinical trials using fibroin formulated as silk films (Zhang, et al., 2017), sponges (Noda, et al., 2021) and knitted scaffolds (Schiefer, et al., 2021) (Scheifer, et al., 2020) have also shown favourable outcomes for both wound repair and aesthetics. This work is now being complemented by preclinical studies. For example, topical application of self-assembling silk hydrogel in a rabbit ear hyperplastic scar model showed significant therapeutic efficacy (Li, et al., 2020). Liquid silk is currently used in cosmetics for topical application to the skin (e.g., Silk Therapeutics Inc).

Silk fibroin hydrogels that can self-assemble in vitro are capable of supporting comparable human fibroblast proliferation and keratinocyte migration to that obtained with collagen hydrogels (Chouhan, et al., 2018). In vivo, these silk hydrogels can serve as a support matrix for healing third-degree burn wounds in mice by guiding the local tissue response from a wound-mediated inflammatory response to the proliferative stage by orchestrating cell recruitment, cytokine signalling and extracellular matrix deposition (Chouhan, et al., 2018). Second-generation silk hydrogels have also shown improvements in wound healing in rodent models (Wang,

et al., 2020, Ju, et al., 2016), while silk hydrogels loaded with fibroblast growth factor 1 (He, et al., 2019, Xu, et al., 2017) and mesenchymal stem cells (Zheng, et al., 2020) improved the healing rate, function and aesthetic appearance in vivo over their respective controls.

The current paradigm is that the successful therapeutic response of these products is due to their content of solution-stable silk. However, this paradigm is now questioned by the finding that local application of soluble silk as a treatment for dry eye increased tear production, improved the smoothness of the cornea and reduced corneal epithelial detachment and inflammation (Kim, et al., 2017). Treatment of injured rabbit corneas with soluble silk accelerated the acute corneal epithelial healing process, resulting in the recovery of a robust multi-layered epithelium with increased tight function and focal adhesions (Abdel-Naby, et al., 2017)(reviewed in (Tran, et al., 2018)). The soluble silk is expected to adopt a random coil/alpha-helical secondary structure (Leisk, et al., 2010).

Therefore, emerging evidence suggests that soluble silk also has a significant impact on wound healing and raises the possibility that soluble silk leaching from hydrogels may also play an important role.

No studies have yet assessed whether soluble silk can leach from silk fibroin hydrogels. One aim of this study was therefore to produce physically crosslinked silk hydrogels with tuned crystallinity to investigate the impact of the silk secondary structure on silk fibroin leaching. A second aim was to determine the biological

response to this leached silk. The silk hydrogel secondary structure was tuned using electro-gelation and sonication. The silk fibroin content of the hydrogels was measured and the efficiency of the solution–gel transition was quantified. The biological response to leached silk was measured through fibroblast response by determining cell proliferation, migration, and downstream molecular signalling.

2.2 Experimental

2.2.1 Silk solution production

The silk solution was prepared as described previously by Leisk (Leisk, 2010). Briefly, *Bombyx mori* silk cocoons sourced from Scientific Centre on Sericulture, Vratsa, Bulgaria. Cocoons were cut into 5x5 mm pieces. 5 g of these were then degummed in 0.02 M Na₂CO₃ (Sigma Aldrich, UK) solution for 30 minutes. The purified silk fibroin was rinsed in Milli-Q ultrapure water a total of 3 times for 20 minutes each, before being stretched and left to dry overnight. Next, the dried silk fibroin fibres were packed into a beaker and dissolved in a 9.3 M LiBr (Sigma Aldrich, UK) solution at 60°C for up to 4 hours. The resulting solution was dialyzed (MW cut off 3500 g/mol, Thermo Scientific, Waltham, MA) for 48 hours in ultrapure water to remove the LiBr salt. When loading the dialyzer, the excess air was removed with a syringe to ensure the contact area with the membrane was maximised. The water was changed regularly to maintain the concentration gradient, totalling 6 changes through the 48-hour period. The resulting silk fibroin solution was cleared by centrifuging at 9418 x g, 5 °C, for 20 minutes, twice. A 1 ml sample of the resulting silk fibroin solution was dried overnight at 60 °C; the residual mass was weighed, and the weight percentage of the solution was calculated. The silk fibroin solution was stored at 4 °C until use.

2.2.2 Preparation of sonicated hydrogels

Physically cross-linked silk fibroin hydrogels were produced using sonication or electro- gelation.

Sonication of a 5 % w/v silk fibroin solution was performed by adding the solution to a centrifugation tube and submerging in an ice bath to minimise heating. Next, the sonicating probe (Sonoplus HD 2070, Bandelin, Berlin, Germany) was submerged in the solution so that the end was near the base, but not touching. A 45- amplitude wave with a cycle of on/off/on in 30 second intervals was used. The solution was then transferred to a covered dish and left to solidify at room temperature for 1 hour before being stored at 4 °C.

2.2.3 Preparation of Electro-gels

Electro-gelation of the silk solution was performed using 5 % w/v silk solution. 10 ml of solution was added to a beaker and stainless-steel electrodes were submerged to a depth of 1 cm. The electrodes were connected to a Solartron SI 1286 (Ametek, Hampshire, UK) and a galvanostatic input with parameters set at 0.5 mA for 1.5 hours. The gel began to form on the anode. The gel was removed from the positive electrode using a spatula and transferred to a petri dish and used immediately.

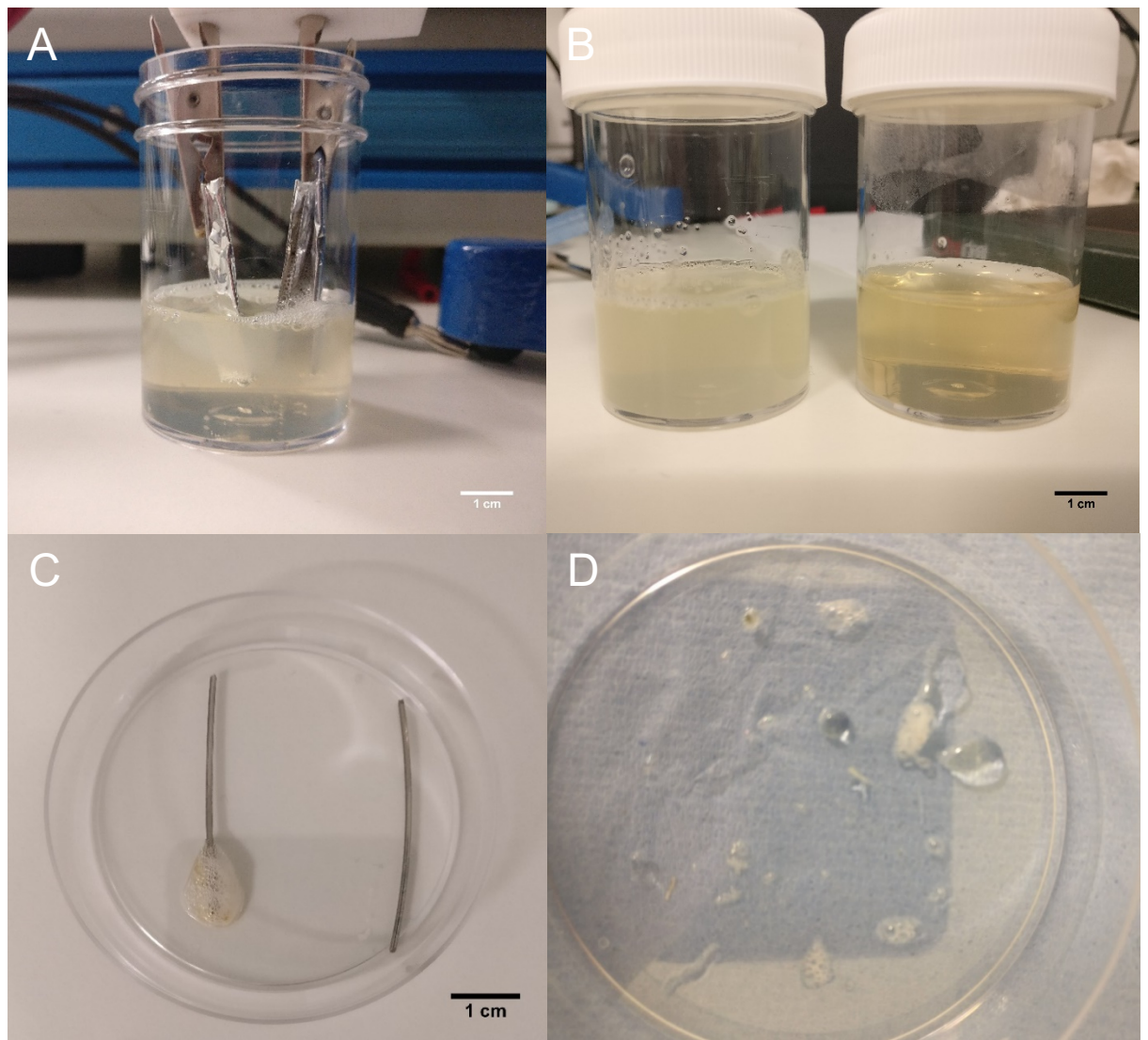


Figure 2-1. Electrodeposition of silk fibroin solution. A) shows tin foil electrodes in silk solution with cloudiness observed around the anode indicating the formation of hydrogel. B) left shows the silk solution after it has undergone electrogelation. Cloudiness was observed in the silk solution when compared the right, control silk solution before electrogelation. C) shows an electrogel formed on a wire electrode. D) shows electrogel on a petri dish once removed from the electrode.

2.2.4 pH investigation

The pH of silk fibroin hydrogels was investigated by two methods: pH indicator strips (litmus paper) and a phenol red indicator. The hydrogels were prepared either through sonication or by electrical current.

Briefly, a 5 % silk fibroin solution was prepared as previously described and further processed into a hydrogel through either the application of an electric current or by sonication. The electro- gel was removed from the electrode and placed on the pH indicator strip (Haobase, China) whilst wet. The solution around the other electrode was tested by dipping the indicator strip into the immediate area and noting the colour change. The sonicated gel was tested by submerging the pH strip into the solution in the sol-gel phase and once again before the gel was fully formed.

The second method involved the use of phenol red. Firstly, a 300 mg/l phenol red solution was produced by dissolving phenol red powder (Sigma Aldrich, Dorset, UK) in deionized water and added to the 5 % silk fibroin solution in a ratio of 1:20, yielding a final concentration of 15 mg/l. An electric current was then applied to trigger the self-assembly of the hydrogel and the colour change noted. This was repeated with sonication and pictures were taken throughout the process.

2.2.5 Silk quantity and efficiency determination

The quantity of silk in both silk fibroin hydrogels was determined by gravimetric analysis with dried samples. The efficiency of the silk hydrogel production was calculated by comparing the content of the hydrogels with the quantity of silk in the starting solution.

2.2.6 Secondary structure determination

The secondary structures of silk samples were determined by Fourier transform infrared (FTIR) spectroscopy (Tensor II Bench ATR IR, Bruker, MA, USA). Each FTIR measurement was run for 128 scans at a 4 cm^{-1} resolution in absorption mode over the wavenumber range of $400\text{--}4000\text{ cm}^{-1}$. Silk hydrogel samples were dried before undergoing FTIR analysis. The silk solution after the electro-gelation was assessed by collecting the solution and drying the samples prior to FTIR analysis. For silk leaching experiments (detailed below), the samples were freeze-dried (Epsilon 2-4, Martin Christ, Germany). Reference samples with a low and high beta sheet content were prepared by drying the silk fibroin solution to form a film. A high beta sheet (silk II) content was induced by treating the film with 70% v/v ethanol for 2 h (silk II), whilst low beta sheet films were left untreated (silk I). All FTIR data were deconvoluted following two methods. The first method followed Hu et al. (2006). The correlation coefficient was calculated using air-dried silk film or freeze-dried silk solution as the comparator for all samples while the second derivative of the absorbance spectra was processed and smoothed with a seven-point Savitzky-Golay function with a

polynomial order of 2 as detailed previously. Outlier analysis was performed where high variance was observed with Z-scores. Significance ($Z > 2$).

2.2.7 Silk leaching determination

A micro bicinchoninic acid protein assay (BCA) (Pierce Biotechnology, Thermo Scientific, IL, USA) was performed to determine the protein content of the solution removed from each sample (i.e., leached). Briefly, a 5 % silk fibroin solution was prepared as previously described and further processed into hydrogels using either agitation from a sonic probe or an electric current altering local pH and triggering the self-assembly of the gels. A sample of each gel was placed in a 1.5 ml Eppendorf tube and water, or phosphate buffered saline (PBS, Sigma Aldrich, MO, USA) was added in a ratio of 1 ml per 0.02 g of gel. The samples were stored at 37°C. The supernatant was removed at set intervals and replaced with fresh solution to assess the quantity of silk leached from the gel at these times. The removed solution was stored at 4°C for up to 48 hours.

The BCA assay was performed according to manufacturers' instructions: briefly, a silk fibroin standard curve was produced with concentrations ranging from 0 µg/ml to 14 µg/ml and 150 µl pipetted onto a microplate in triplicate. 150 µl of each sample was also placed on the microplate. The working reagent was mixed using the stated ratio (25 A: 4 B: 1 C) and 150 µl was added to each well before the plate was covered and incubated at 37°C for 2 hours. This was then cooled to room temperature and read using a plate reader at 570 nm (Thermo Multiskan Ascent, Thermo Labsystems, Finland).

A standard curve was produced using known concentrations of silk fibroin protein and interpolated using GraphPad Prism software (GraphPad Software Inc, CA, USA).

2.2.8 SDS-PAGE

The collected samples were also subjected to sodium dodecyl sulphate polyacrylamide gel electrophoresis (SDS-PAGE) to assess the fibroin molecular weights. Samples were lyophilized and reconstituted in Milli-Q water at a concentration of 5 mg/ml⁵⁷. The protein concentration was determined with the BCA assay, and the silk samples were diluted in Milli-Q water to 5 mg/ml. All samples were separated using a mini-PROTEAN TGX Precast Gel (4 – 20 %) (Bio-Rad, Hertfordshire, UK) and a running buffer consisting of 25 mM Tris, 192 mM glycine and 0.1 % SDS, pH 8.3. Samples were reduced using 2× Laemmli buffer and β -mercaptoethanol, followed by heating at 90 °C for 5 minutes. A 10 μ L sample was then loaded and separated at 200 V, with a 30 to 35 mA current for 30 to 40 minutes. The gel was stained with the SilverXpress Staining Kit according to the manufacturer's instructions (ThermoFisher, Renfrew, UK). Images were acquired with a 12.2 MP megapixel Google Pixel 3 phone, and the pixel density was analysed by ImageJ v1.52n (National Institutes of Health, Bethesda, MD, U.S.A).

2.2.9 Cell proliferation

Cell proliferation was measured in response to the presence of silk fibroin leached from hydrogels over 72 hours. A fibroblast cell model was chosen to mimic cells found in a wound environment. An MTT assay was chosen to determine cellular metabolism by which the number of cells in each well can be derived.

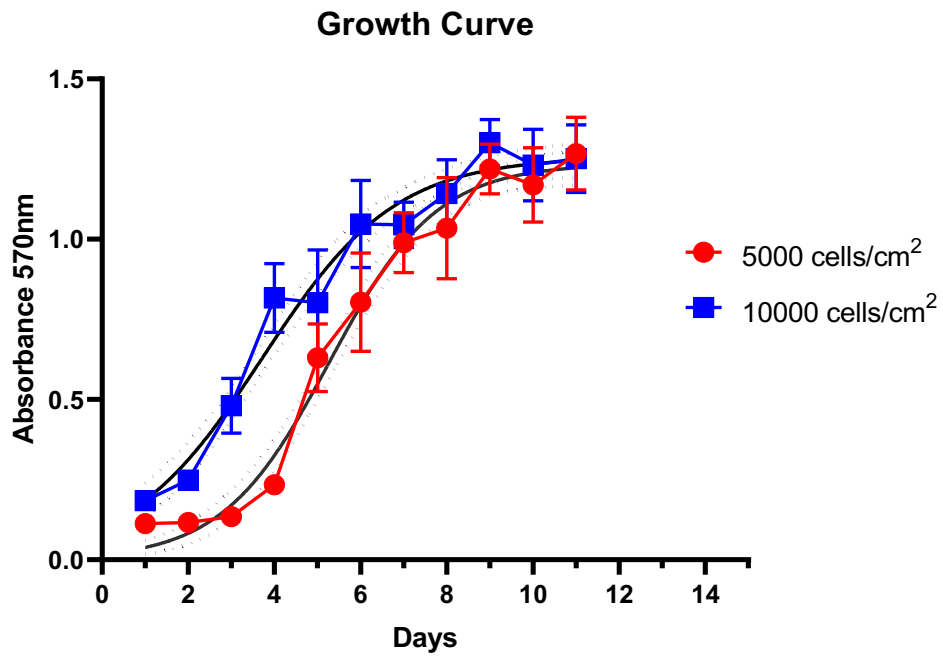


Figure 2-2. Standard growth curve observed when cells are seeded at two different densities. The absorbance of 570nm light indicates the metabolic activity of the cells over 12 days.

NIH-3T3 cells (ATCC CRL-1658, ATCC, England, UK) were cultured as monolayers in Dubellcos Modified Eagle Medium, (DMEM, ThermoFisher Scientific, Paisley, UK) supplemented with 10 % (v/v) foetal bovine serum, 50 U/ml penicillin and 50 µg/ml streptomycin. Culture conditions were maintained within a humid incubator set at 37 °C.

NIH-3T3 cells were seeded into 96-well tissue culture treated polystyrene plates (Corning Inc. Costar, Kennebunk ME, USA) at 5×10^4 cells/cm² in 100 µl of culture medium. The plates were then incubated for 24 hours before the medium was removed. A gradient of silk solution was added with culture medium, ranging from 0 µg/ml to 2100 µg/ml. After 72 hours an MTT assay was performed. 20 µl of (3-(4,5-dimethylthiazol-2-yl)-2,5-diphenyltetrazolium bromide (MTT; 5 mg/ml in PBS) was added and incubated for 5 hours. Next, the MTT was aspirated and 100 µl of dimethyl sulphoxide was added to dissolve the formazan crystals and incubated for a further 15 minutes. The absorbance was read on a spectrophotometer (Thermo Multiskan Ascent, Thermo Labsystems, Finland) at 570 nm.

2.2.10 Cell migration

Cellular migration was determined through use of a chemotaxis assay. The principle of this method determines the mode of cellular migration through a filter which can be stained and counted for cells. The placement of the cells on the filter can help to surmise that cells will move by chemotaxis (i.e., towards or away from a chemical

trigger along a concentration gradient) or cells move chemokinetically (i.e., in a random manner regardless of the presence of chemical agent).

NIH-3T3 cells (ATCC CRL-1658, ATCC, England, UK) were cultured in Dubellcos Modified Eagle Medium, DMEM (ThermoFisher Scientific, Paisley, UK) supplemented with 10% (v/v) foetal bovine serum (FBS), 50 U/ml penicillin and 50 µg/ml streptomycin. After 24 hours the complete culture medium was removed, cells were washed with PBS and un-supplemented DMEM was added overnight.

Cells were harvested with Accutase Cell Detachment Solution (BioLegend, San Diego CA, USA) and resuspended in non-supplemented DMEM. ChemoTx Disposable Chemotaxis Plates (Neuroprobe, Gaithersburg MD, USA) coated with 1 µg/ml fibronectin (Sigma Aldrich, Scotland, UK) were prepared with 30 µl of medium and 30 % silk solution in a gradient of concentration in the bottom wells. The filter was then replaced and contact between the surface of the liquid and cell site area was ensured. A silk concentration gradient was also then added to the top filter before 21 µl of medium containing cells to produce a cell density of 1×10^5 cells/cm². Cells were incubated for 3.5 hours before the cells on the underside of the filter were fixed and stained with 0.5 % crystal violet (Sigma Aldrich, Scotland, UK) and counted under a microscope.

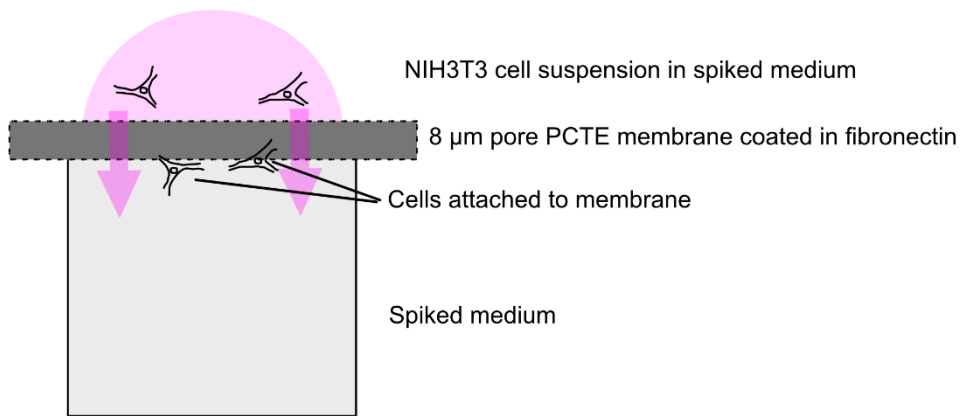


Figure 2-3. Cell migration assay diagram. ChemoTx disposable chemotaxis plates consisting of a PCTE membrane over a 96 well plate. Image displays the placement of spiked medium and cells. Cells can travel through the pores and will adhere to the fibronectin coated membrane for counting.

2.2.11 Wound healing

The ability of the presence of silk to aid in wound healing was determined through a scratch wound healing assay. The closure of a wound of a prescribed width was measured over time to determine the effect silk had on the rate of healing.

NIH-3T3 cells (ATCC CRL-1658, ATCC, England, UK) were cultured in Dubellco's Modified Eagle Medium (DMEM, ThermoFisher Scientific, Paisley, UK) supplemented with 10 % (v/v) foetal bovine serum (FBS), 50 U/ml penicillin and 50 µg/ml streptomycin and maintained at 37°C in a humidified, 5 % CO₂ incubator. After 24 hours the complete culture medium was removed, cells were washed with PBS and non-supplemented DMEM was added overnight.

Cells were harvested with Accutase Cell Detachment Solution (BioLegend, San Diego CA, USA) and resuspended in DMEM. Cells were seeded in a 12 well plate at a density of 5×10^4 cells/cm² and left to attach for 24 hours. Medium was removed and un-supplemented DMEM was added overnight. A scratch was made with pipette tip and the medium removed. Un-supplemented DMEM was added back before being supplemented with 30 % total volume of either water, FBS or 1600 µg/ml silk solution. At the wound edge 1 µg/ml nocodazole (Sigma Aldrich, Paisley, Scotland) was added and the cells were imaged over 7 hours.

2.2.12 Phosphorylation assay

The mouse phosphorylation array (Mouse Phospho-RTK Array ARY014, R&D Systems LTD, Minneapolis, MN, USA) was used as detailed previously (Lescarbaeu, et al., 2012) to examine the molecular response of fibroblasts. Briefly, cells were grown to

confluence and exposed for 30 minutes to (i) 1600 µg/ml silk solution, (ii) water or (iii) DMEM with 10 % foetal bovine serum and (iv) without any treatment. Cell lysates were then harvested on ice with lysis buffer containing 10 µg/ml aprotinin (Sigma Aldrich, Paisley, UK), 10 µg/ml leupeptin (Tocris Bioscience, Bristol, UK) and 10 µg/ml pepstatin (Tocris Bioscience). The protein content of each lysate was measured with the BCA assay. The cell lysates were then added at 200 µg protein per array and developed using autoradiography film (UltraCruz, Dallas, TX, USA). The film was digitized using a scanner (HP Envy 4250, HP Inc UK Limited, UK) and processed using Image J software v1.53c (National Institutes of Health, USA).

2.2.13 SEM

To image the hydrogels and leached samples, known quantities of each were freeze-dried before samples were attached to aluminium stubs with carbon adhesive pads. Samples were sputter coated (ACE200, Leica Microsystems, Wetzlar, Germany) with gold to reduce charging in the SEM. Samples were viewed with a Hitachi SU6600 Field Emission SEM at voltage 5 kV under standard vacuum settings at magnifications of 300 x, 1000 x and 10000 x.

2.2.14 Statistical Analyses

Statistical analyses were carried out using Origin Pro 2018 (Northampton, Massachusetts, USA) and GraphPad Prism v.9.1.1 (San Diego, CA, USA). One-way analysis of variance, followed by Bonferroni's post hoc test, was conducted between multiple groups, or two-way analysis of variance followed by Tukey's multiple comparisons or Šidák's multiple comparisons test. Normality and homogeneity of

variances were assumed. Asterisks denote statistical significance as follows: *P < 0.05, **P < 0.01, and ***P < 0.001. All data are presented as mean values \pm standard deviation, and the number of independent experiments (n) is noted in each figure legend.

2.3 Results

2.3.1 Silk Quantity and Efficiency Testing

Physically cross-linked silk hydrogels were generated using sonication energy and electro-gelation (Figure 2-4A). Gravimetric analysis of the silk content of both hydrogel types indicated significant differences (Figure 2-4B). The sonicated hydrogel had a 100% solution–gel conversion efficiency, whereas the electro-hydrogel had a significantly lower efficiency ($4.77 \pm 3.24\%$) (Figure 2-4C). The sonicated hydrogel showed a lower solid silk content (5% w/v) and less release, whilst the electro-hydrogels contained more silk ($14.46 \pm 3.91\%$ w/v) but also released significantly more silk.

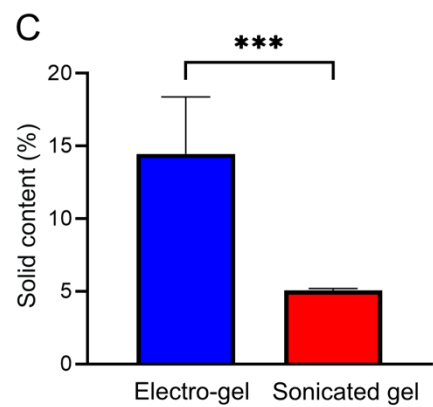
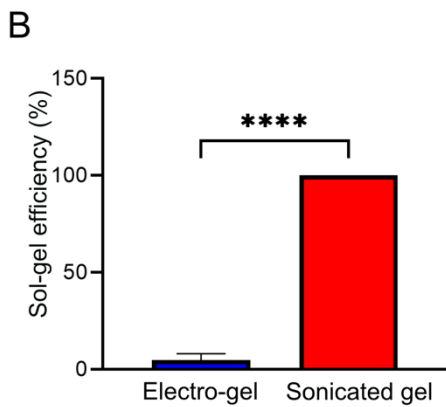
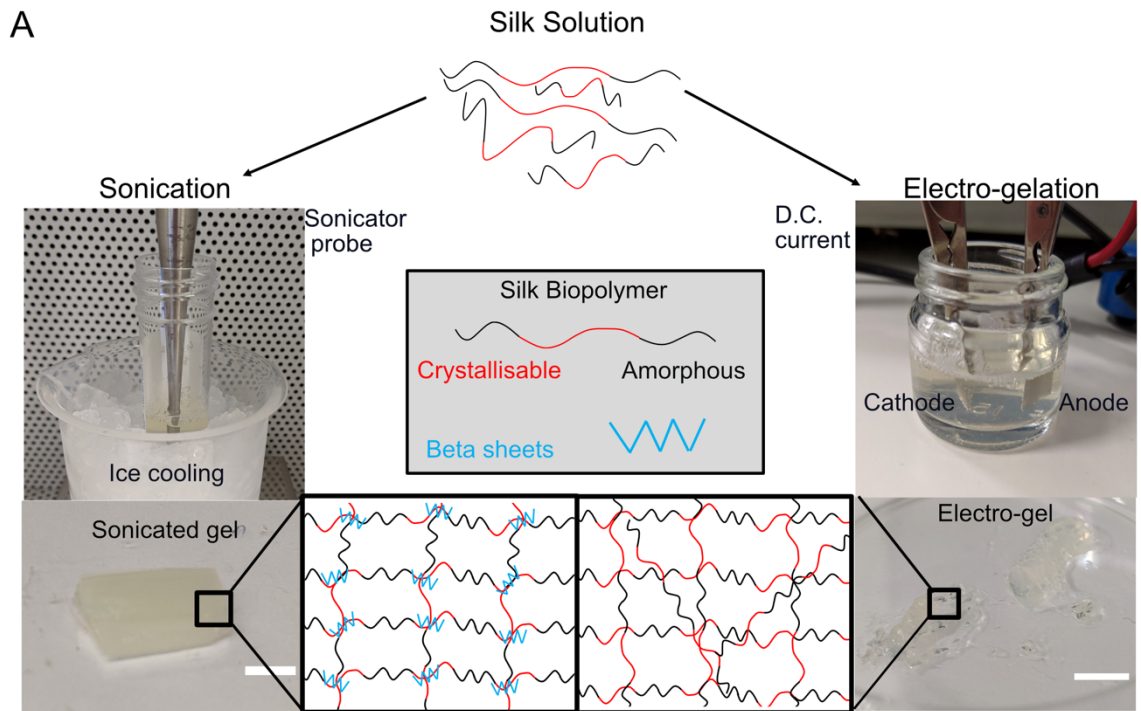


Figure 2-4. A) processing of silk solution into hydrogels by sonication or electro gelation. Graphic depicts the expected alignment of the secondary structures of the hydrogels. B) the efficiency of the gelation process, C) the silk content of each hydrogel. Data analysis evaluated by unpaired t-test ($n = 4$, \pm SD). Asterisks denote statistical significance as follows: * $p < 0.05$, ** $p < 0.01$, *** $p < 0.001$, **** $p < 0.0001$.

2.3.2 pH testing

The pH of both hydrogels was indicated by both phenol red and pH indicator strips (Figure 2-6, Figure 2-7). The phenol red was a pink colour when added to the silk solution. The pH indicator strips were submerged in the silk solution before the silk was treated, indicating When the solution underwent sonication, the pink colour remained throughout each application, and when left to set. When the silk solution was sonicated and the pH indicator strip was submerged in it, the colour changed to green/blue showing a consistent pH of around 6-7.

In contrast to this, when the solution underwent electro-gelation, a strong colour change with the phenol red was seen on the positive electrode. This was from pink to yellow. The pH indicator strips were dipped in silk solution and the colour changed to green/blue. When the silk solution had the current applied, the solution tested around the positive electrode with pH indicator strips turned yellow, and when a section of gel was placed on the strip, the colour changed to yellow. The remaining solution tested with the strips changed colour to green/blue. This indicated the pH was lower in the electro-gel compared to the sonicated gel and silk solution.

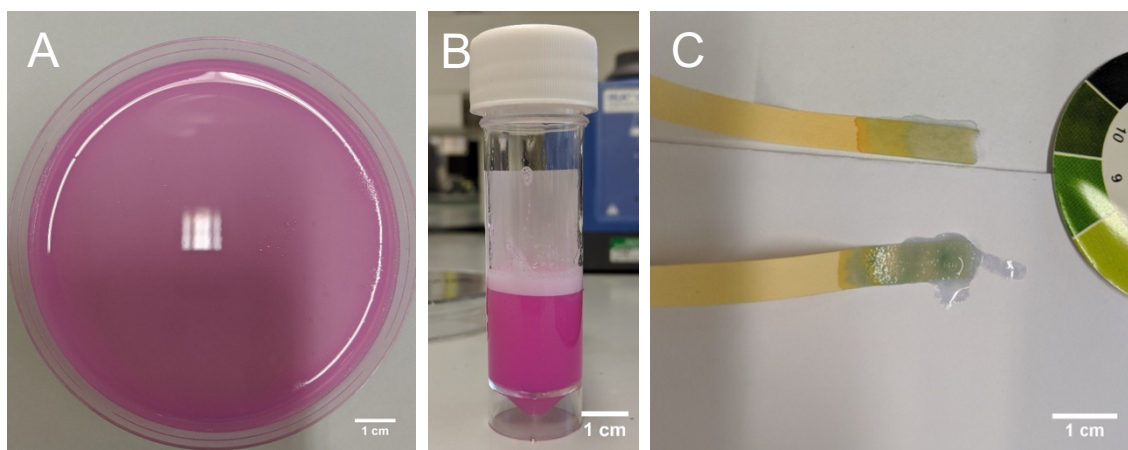


Figure 2-5. pH testing of sonicated hydrogel with phenol red and pH paper. A) B) No colour change from the pink phenol red is seen when undergoing sonication. C) pH paper indicates that the pH remains neutral when undergoing sonication.

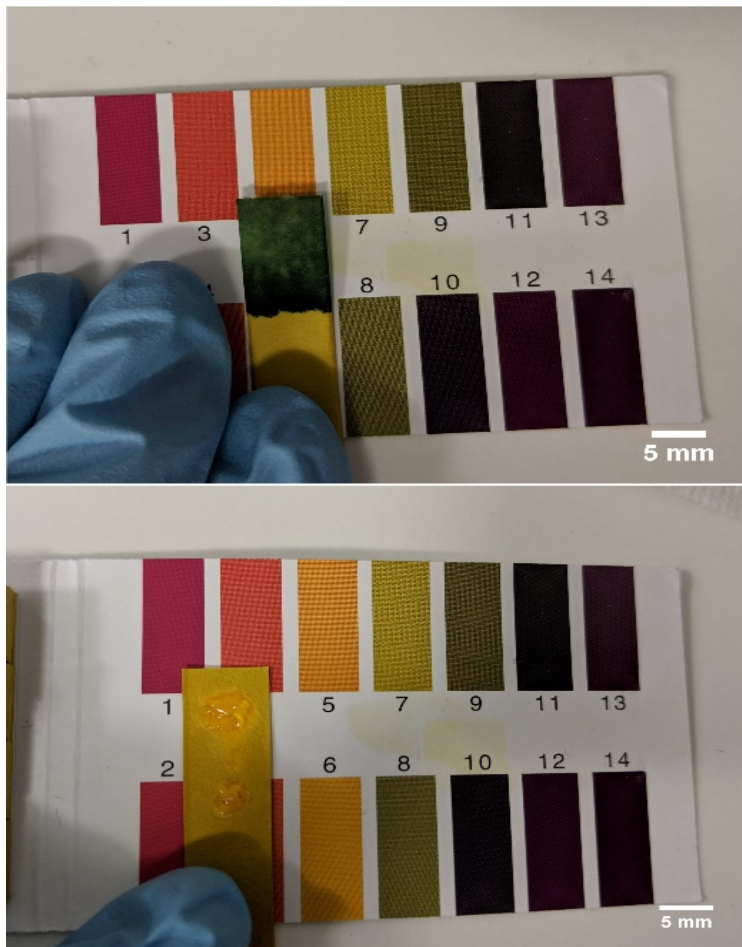


Figure 2-6. pH testing electro gel with pH paper. TOP pH of silk solution before electro gelation. BELOW electro-gel placed on the pH paper. A colour change to yellow can be seen on the pH paper indicating a drop in pH.

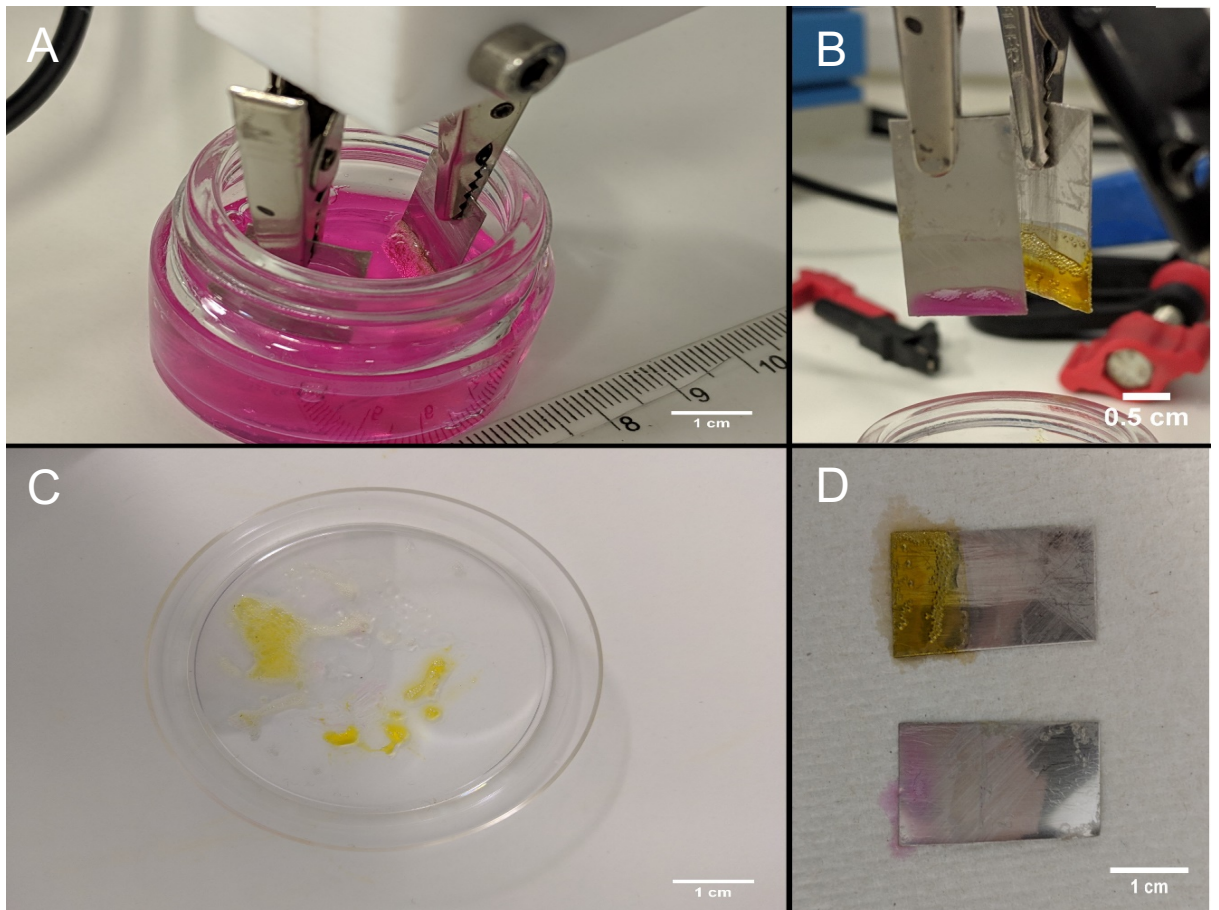


Figure 2-7. pH testing electro-gel with phenol red. A) Silk solution is pink when phenol red is added indicating a neutral-basic pH. B) D) Once electro-gelation occurs, only a local colour change to yellow is seen as the electro gel forms on the electrode. C) The colour remains once removed from the electrode.

2.3.3 BCA leaching

The ability of the gel to retain the incorporated silk was also examined and quantified over 72 h (Figure 2-8). For sonicated hydrogels, the percentage release from the starting concentration was 0.57 ± 0.05 % in water and 0.41 ± 0.18 % in PBS, with no significant difference between the release media. The pattern of release followed a zero order. By contrast, the electro-hydrogel showed a first order release profile, with most of the release occurring within the initial 12 h. The average cumulative release values at 72 h at 37°C were 34.19 ± 23.27 % and 47.40 ± 20.83 % in water and PBS, respectively.

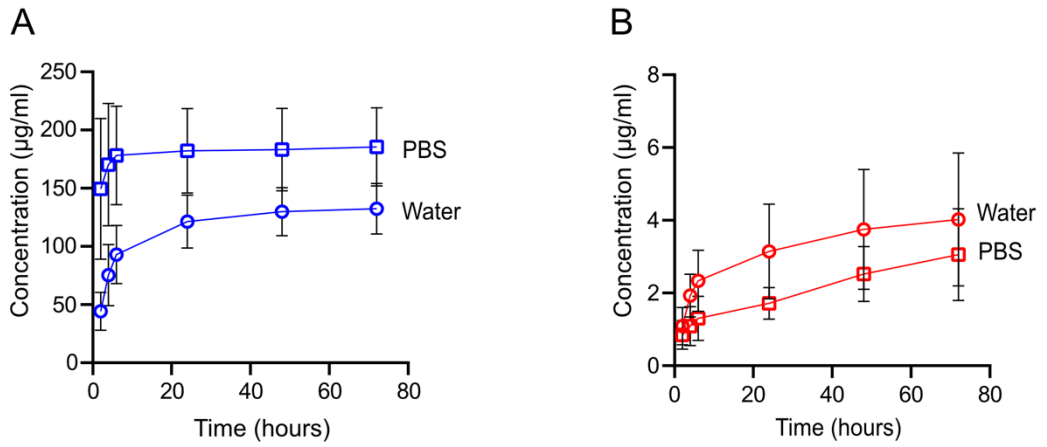


Figure 2-8. Protein release and characterisation from silk hydrogels measured by protein quantification and gel electrophoresis. (A) Electro-gel protein release in water and PBS over 72 hours. (B) Sonicated hydrogel protein release in water and PBS over 72 hours.

2.3.4 FTIR

2.3.4.1 Method 1

The secondary structure of the silk fibroin as silk films and as hydrogels was measured using FTIR (Figure 2-10). The untreated silk film has a greater number of turns, alpha helices, and random coils than the 70 % ethanol treated silk film, which has increased beta sheets and side chains. The sonicated gel indicates a similar structure to the ethanol treated control, with a peak at 1621, displaying the presence of beta sheets. The untreated silk film has a peak around 1640, the amorphous region, with the silk film from the remaining silk solution of the electro-gel showing a similar peak. The electro-gel has a slight peak at both 1621 and 1640, showing the secondary structure to be more balanced, with beta sheets and alpha helices, turns and random coil structures present.

The lyophilized leached samples of both sonicated and electro-gels both show a peak at 1621, which indicates the structure is rich in beta sheets.

2.3.3.2 2nd derivative method

The deconvolution method of the FTIR data was performed with the second derivative as detailed in the methods (2.2.6). The deconvoluted data indicated that the sonicated hydrogel was dominated by intermolecular beta sheets ($33.14 \pm 1.07\%$), with beta turns and antiparallel amyloid beta sheets being the next most common secondary configuration ($21.98 \pm 0.61\%$ and $20.28 \pm 0.05\%$, respectively). This contrasts with the electro-hydrogels, which displayed a different, statistically significant, distribution of secondary structures within the amide I region. Alpha and

random coil structures were the most abundant ($30.22 \pm 3.55\%$), followed by beta turns and intermolecular beta sheets ($27.11 \pm 2.90\%$ and $25.57 \pm 2.92\%$), while the number of native beta sheets had increased significantly in electro-hydrogels to $15.98 \pm 3.39\%$ compared to $4.86 \pm 1.90\%$ in sonicated hydrogels. The switch in secondary structure for both hydrogels was readily apparent when they were compared to the untreated silk film control, which contained less intermolecular beta sheet and beta turn content and more amorphous structures. Substantial differences in secondary structures of sonicated hydrogels and air-dried silk films (Silk I) were supported by the low correlation coefficient (Table 1) (0.25). In contrast, electro-gels had a higher correlation coefficient (0.60) indicating that these hydrogels were more similar to a Silk I secondary structure.

Table 3. Correlation coefficient for FTIR against silk solution

	Correlation Coefficient (\pm SD)
Sonicated Gel	0.251550 \pm 0.026454
Electro-gel	0.602864 \pm 0.136176
Leached Sonicated Gel	0.368774 \pm 0.045787
Leached Electro-gel	0.412926 \pm 0.039905

The crystallinity of the leached silk was also assessed from the FTIR data (Figure 2-10). These results indicated that the silk released from the electro-gel had significantly more native beta sheets, and less intermolecular beta sheets and antiparallel amyloid beta sheets than the silk released from sonicated hydrogels. Both leached samples

also contained significantly less alpha and random coil structures than silk solution controls (28.881 ± 7.08 % for leached electro-gel, 22.125 ± 1.12 % for leached sonicated gel and 48.00 ± 0.55 % for silk solution). Large standard deviations were noted for the leached electro-gel samples. However, outlier analysis produced z-scores that were not significant. Leached sonicated and leached electro-gel silk samples had a lower correlation coefficient to air dried silk than electro-gels (0.37 and 0.41, respectively (Table 1). This indicated that these leached samples were less like air-dried Silk I (or the electro-gels). The correlation coefficient when compared to freeze dried silk solution indicated that electro-gels were most similar (0.98) whilst the sonicated hydrogel was least similar (0.33) to this beta sheet-rich film. Whilst the silk released from electro-gels had a high correlation to freeze dried silk (0.96), the silk released from sonicated hydrogels did not (0.42). These results indicate leached samples were not identical to the silk hydrogels nor the freeze-dried silk. This observation of an 'intermediary silk secondary structure' was supported by thermal analysis.

2.3.5 Thermal Analysis

Thermogravimetric analysis (TGA) was used to determine the effect of gelation method on the thermal stability of silk hydrogels (Table 2, Figure 2-9). Silk hydrogels and leached silk contained 8–11 % w/w adsorbed water. The onset of decomposition of sonicated gels (248.6 °C) was significantly delayed compared to the freeze-dried powder, silk I control (237.6 °C). Compared to the sonicated hydrogels, the electro-gels showed a reduced thermostability, but the onset of decomposition (244.1 and 245.7 °C, respectively) remained significantly higher than that of the silk I control. The

onset of decomposition of leached silk obtained from electro-gels (240.7 °C) were comparable to the silk I control. This lower stability to thermal degradation suggests that the leached silk secondary structure is composed of a lower crystalline fraction compared to the hydrogel architecture and the electro-gel leached portion is similar to the silk I control.

Table 4. First-cycle thermal analysis data of the gel and leached portions from sonicated gels and e-gels

Thermal Property	+Silk I		Gel portion		Leached portion				
	Freeze-dried silk		Sonicated	E-gel	Sonicated	E-gel			
$T_{o,des} / ^\circ\text{C}$	48.46 ± 0.72	±	41.82 ± 3.40	±	51.04 ± 0.28	±	50.82 ± 1.89	±	50.87 ± 1.89
$T_{des} / ^\circ\text{C}$	77.55 ± 2.18	±	75.43 ± 0.79	±	79.8 ± 5.56	±	79.52 ± 1.73	±	83.83 ± 2.11
$T_{des}' / ^\circ\text{C}$	60.08 ± 3.27	±	58.12 ± 2.62	±	66.08 ± 1.00	±	64.04 ± 1.52	±	66.89 ± 1.97
$\Delta H_{des} / \text{J g}^{-1}$	-235.8 ± 22.7	±	-163.6 ± 27.1	±	-204.7 ± 15.8	±	-138.4 ± 21.6	±	-208.4 ± 38.9
$T_g / ^\circ\text{C}$	184.2 ± 2.1		195.1 ± 3.5		180.4 ± 1.8		187.1 ± 1.6		182.1 ± 0.4
$\Delta C_p / \text{J g}^{-1} \text{ } ^\circ\text{C}^{-1}$	-0.62 ± 0.03	±	-0.40 ± 0.03	±	-0.48 ± 0.04	±	-0.57 ± 0.03	±	-0.62 ± 0.04
$T_{o,c} / ^\circ\text{C}$	207.5 ± 1.2		235.3 ± 2.7		213.4 ± 0.8		217.3 ± 0.4		204.4 ± 5.1
$T_c / ^\circ\text{C}$	250.0 ± 0.9		246.3 ± 4.9		233.8 ± 0.5		253.2 ± 0.6		243.6 ± 0.4
$\Delta H_c / \text{J g}^{-1}$	59.44 ± 2.60	±	2.163 ± 2.914	±	11.60 ± 1.18	±	32.02 ± 4.57	±	25.10 ± 2.53
$T_{o,dec} / ^\circ\text{C}$	261.8 ± 0.0		263.8 ± 0.7		266.9 ± 0.8		263.0 ± 0.4		253.4 ± 1.7
$T_{dec}' / ^\circ\text{C}$	262.6 ± 0.5		267.8 ± 0.8		268.7 ± 0.8		267.2 ± 0.0		254.8 ± 1.1

DSC

TGA	[H₂O] / %	11.10	±	10.14	±	10.05	±	8.22 ± 0.79	11.07 ±
		1.26		0.30		0.27			1.97
	T_{o,dec} / °C	234.3 ± 3.8		248.6 ± 0.5		246.2 ±		235.0 ± 1.6	235.7 ±
						1.3			1.6
	T_{des'} / °C	72.43	±	66.72	±	75.10 ±		69.78	± 70.83 ±
	5.99		4.63		4.83		4.79	1.21	

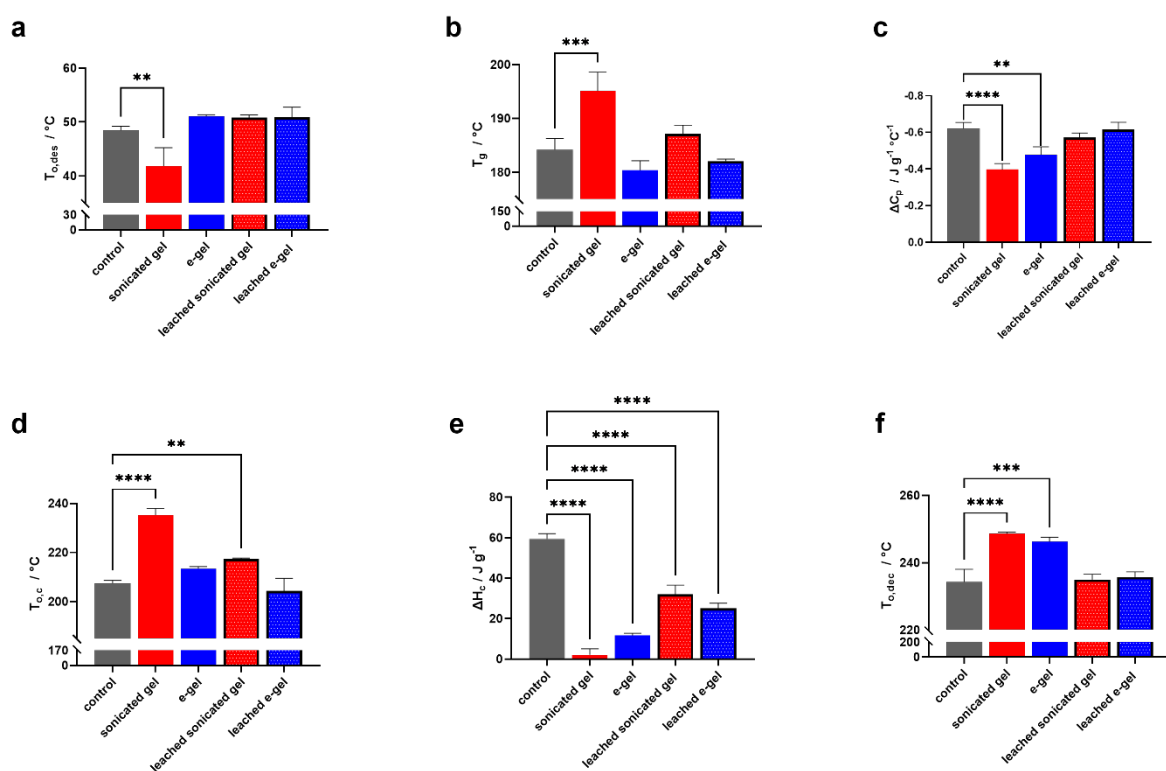


Figure 2-9. Sonicated silk hydrogels were more crystalline than e-gels while the leached silk from both hydrogel types displayed a silk I-like thermal signature. The variation in (a) onset of desorption ($T_{0,des}$), (b) ISO glass transition temperature (T_g), (c) ISO change in heat capacity (ΔC_p), (d) onset of crystallization ($T_{0,c}$), and (e) enthalpy of cold crystallization (ΔH_c) from first-cycle DSC and (f) the extrapolated onset of decomposition from first-cycle TGA. Error bars are hidden in the bars and plot symbols when not visible ($n = 3, \pm SD$).

Differential scanning calorimetry (DSC) measurements confirmed that hydrogels manufactured using sonication were composed of a greater crystalline fraction than electro-gels, and both gel types were more crystalline than the silk I control. The silk leached from both hydrogels was significantly less crystalline than the silk retained in the hydrogels, with a similar crystallinity to the silk I control. The desorption enthalpy required to remove adsorbed water ranged between -138.4 and -204.7 J g^{-1} . Compared to the silk I control (-235.8 J g^{-1}), the desorption enthalpy was significantly lower for the hydrogel (-163.6 J g^{-1}) and leached silk (-138.4 J g^{-1}) obtained by sonication. The onset of desorption ranged from 41.8 to $51.2 \text{ }^\circ\text{C}$ and was significantly lowered from $48.5 \text{ }^\circ\text{C}$ for the silk I control to $41.8 \text{ }^\circ\text{C}$ for the sonicated hydrogels. The glass transition of the sonicated hydrogels at $194.4 \text{ }^\circ\text{C}$ was also shifted to a higher temperature compared to the silk I control ($182.0 \text{ }^\circ\text{C}$). This suggests that the amorphous secondary structure content of silk molecules was reduced upon their integration into the hydrogel architecture, while the leached silk from both hydrogels shows a similar molecular mobility to the silk I control. The onset of the random coil to β -sheet crystallization, present for the silk I control at $207.4 \text{ }^\circ\text{C}$, was delayed for the sonicated hydrogels ($235.3 \text{ }^\circ\text{C}$) and their leached silk ($217.3 \text{ }^\circ\text{C}$). Similarly, the enthalpy of crystallization for the sonicated hydrogels (2.163 J g^{-1}) and electro-gels (11.60 J g^{-1}) were significantly lower than the silk I control (59.44 J g^{-1}). The enthalpy of crystallization of the silk leached from the sonicated hydrogels (32.02 J g^{-1}) and the electro-gels (25.10 J g^{-1}) were higher than those of the bulk hydrogels but remained lower than that of the silk I control. The temperature of the maximum rate of decomposition of electro-gels ($267.2 \text{ }^\circ\text{C}$), sonicated hydrogels ($267.8 \text{ }^\circ\text{C}$) and the

leached portion of sonicated hydrogels (267.2 °C) were significantly higher than that of the silk I control (262.6 °C). In contrast, the temperature of maximum rate of decomposition of the silk leached from the silk leached from the electro-gels (254.8 °C) was lower than for the silk I control.

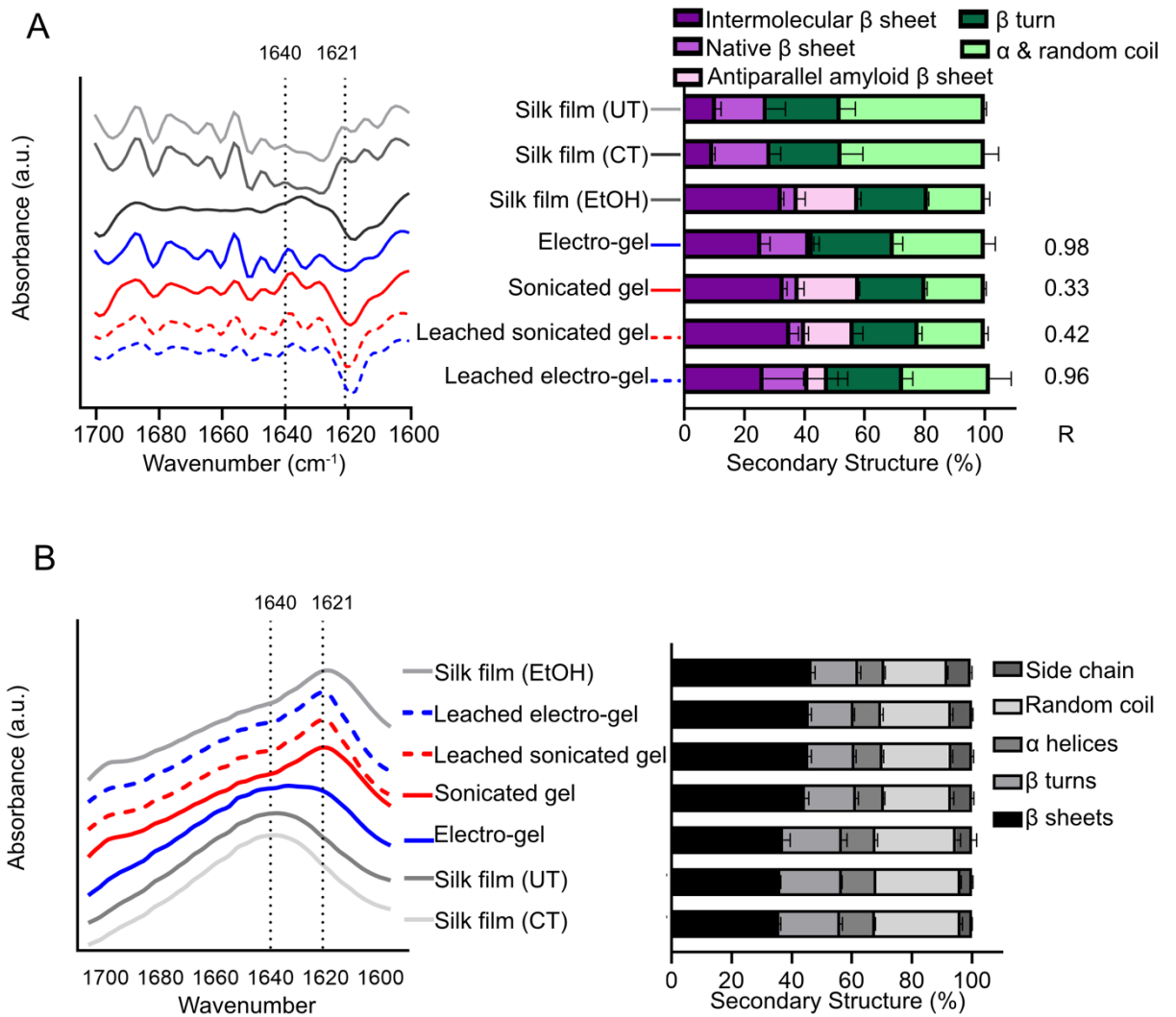


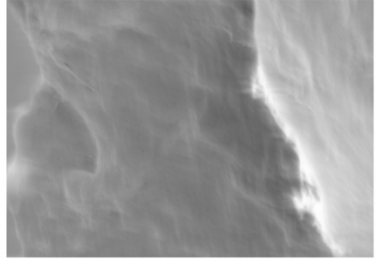
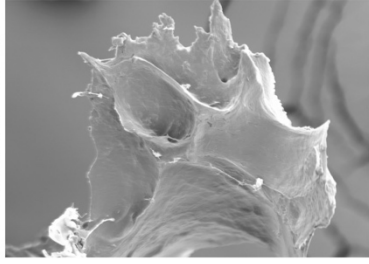
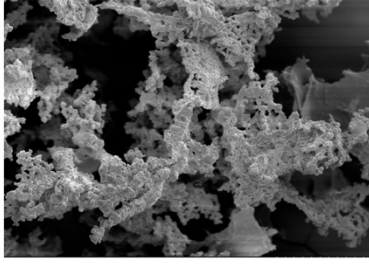
Figure 2-10. FTIR absorbance spectra of the amide I region of electro-gels and sonicated gels. Controls included were untreated air-dried silk film (UT), ethanol treated silk films (EtOH) and the current treated solution remaining after removal of the electro-gel (CT). Leached samples in water of both electro-gel and sonicated gel after 72 hours are included here. Lines at 1640 and 1621 indicate the amorphous and crystalline region, respectively ($n = 3$). (A) 2nd derivative method result (B) Hu et al.

*method. Data analysis evaluated by two-way ANOVA followed by Tukey's multiple comparisons test. (n = 4, ± SD). Asterisks denote statistical significance determined using post-hoc tests as follows: *p < 0.05, **p < 0.01, ***p < 0.001, ****p < 0.0001.*

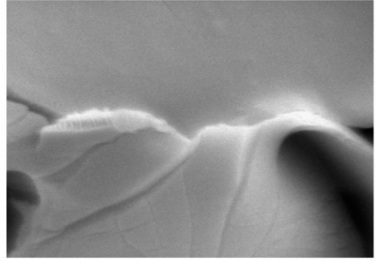
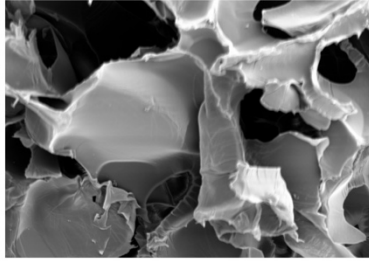
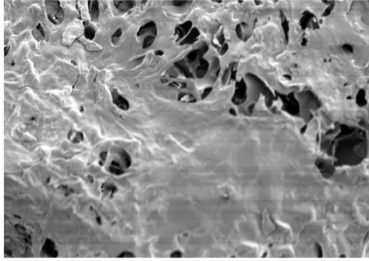
2.3.6 SEM

Scanning electron microscopy (SEM) of sonicated hydrogels showed a porous network of silk with sharp edges while electro-gels appeared smoother with an interconnected structure (Figure 2-11). The leached electro-gel and sonicated hydrogel samples appeared very different in their structure with a fibrous and lamellar structure, respectively. Leached silk from the electro-gel also showed an abundance of micro-sized droplet-like structures that were rare in leached silk from sonicated hydrogels.

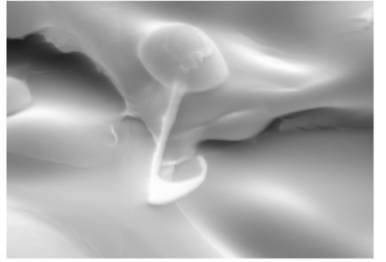
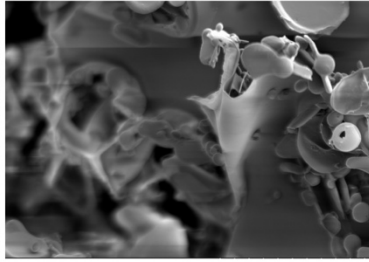
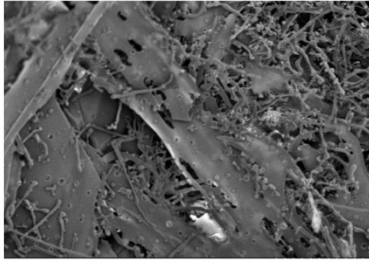
Sonicated hydrogel



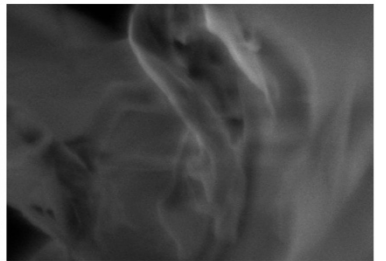
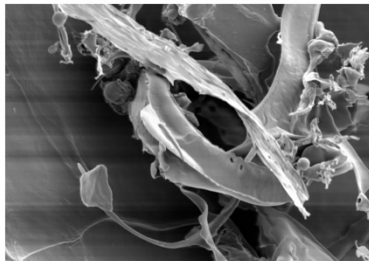
Electro-gel



Leached electro-gel



Leached sonicated hydrogel



Silk solution

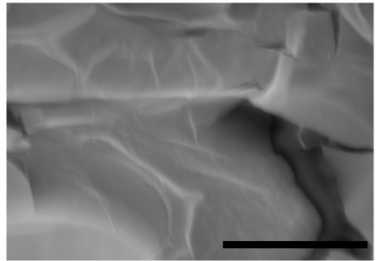
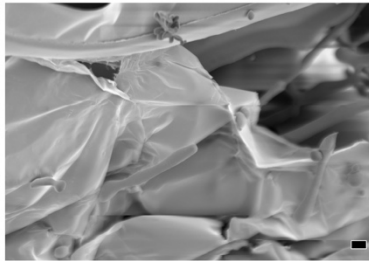
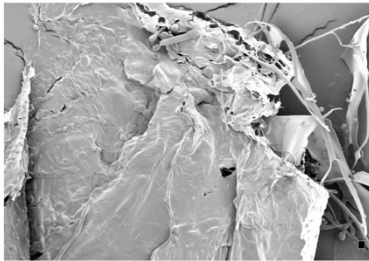


Figure 2-11. SEM images of sonicated hydrogels, electro-gels, and the leached silk from both. Silk solution is included as a reference. Scale bar 5 μm .

2.3.7 SDS PAGE

The protein size distribution in silk solution and from leached samples was examined using SDS PAGE as described (Figure 2-12). The silk solution and freeze-dried silk solution showed a longer peak from 200 – 31 kDa whereas both the sonicated and electro-gel samples showed a peak from 200 - ~36.5 kDa which suggested proteins > 36.5 – 6 kDa were no longer present. Freeze dried silk solution showed a band at ~ 31 kDa which can also be seen in the sonicated hydrogel but not in the electro-gel or silk solution samples. The sonicated hydrogel also had less intensity with the bands below 6 kDa than sonicated and both silk solution samples, indicating these silk fibroin fragments were present in a lower quantity.

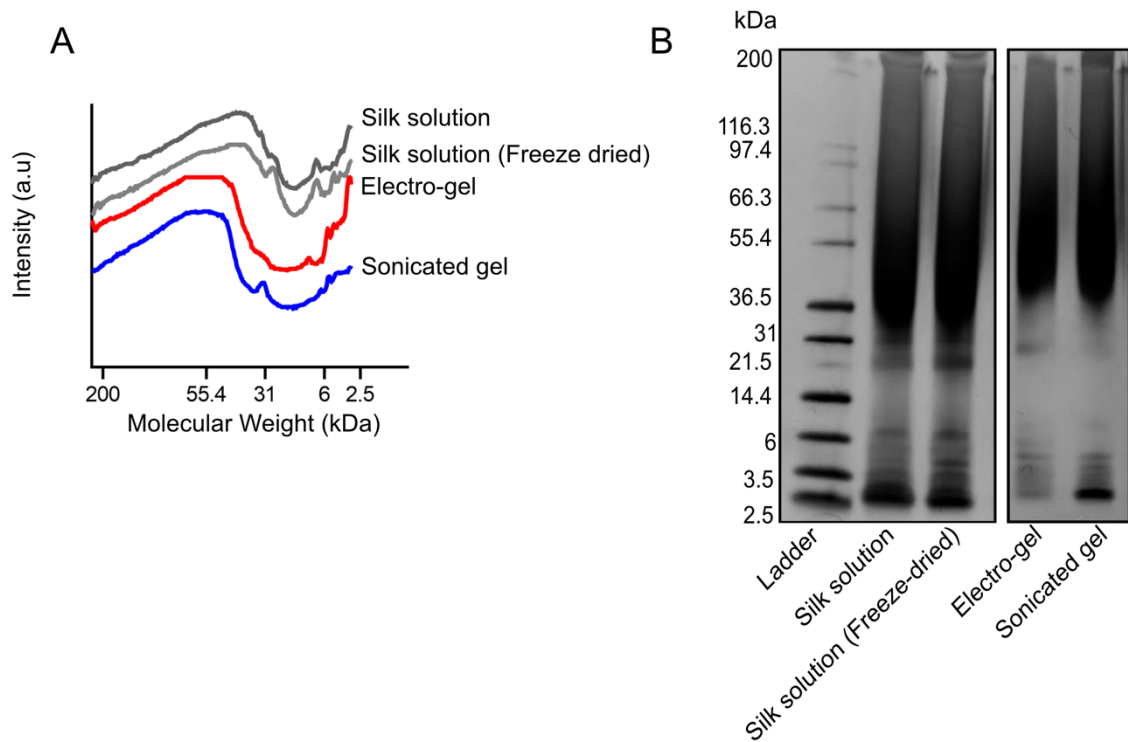


Figure 2-12. SDS PAGE of protein released from electro-gels and sonicated gels. Standards included are silk solution and freeze-dried silk solution reconstituted in water. (B) Densitometry analysis of SDS PAGE.

2.3.8 Cell proliferation

The impact of leached silk on the fibroblast response was also assessed in vitro (Figure 2-13). First, the influence of soluble silk on cell proliferation was determined. A broad concentration range, from 0 to 2,100 $\mu\text{g}/\text{ml}$ silk, was used (Figure 2-13B). For these studies, the culture medium was spiked with silk. No significant effect was observed on cell proliferation over this broad concentration range. Possible differences in cellular response were taken into account by comparing the silk solution to leached silk samples collected from both sonicated and electro-hydrogels. These samples were tested at three concentrations (2, 20 and 200 $\mu\text{g}/\text{ml}$) and compared to fresh silk solution samples. No significant differences were detected among any of these samples.

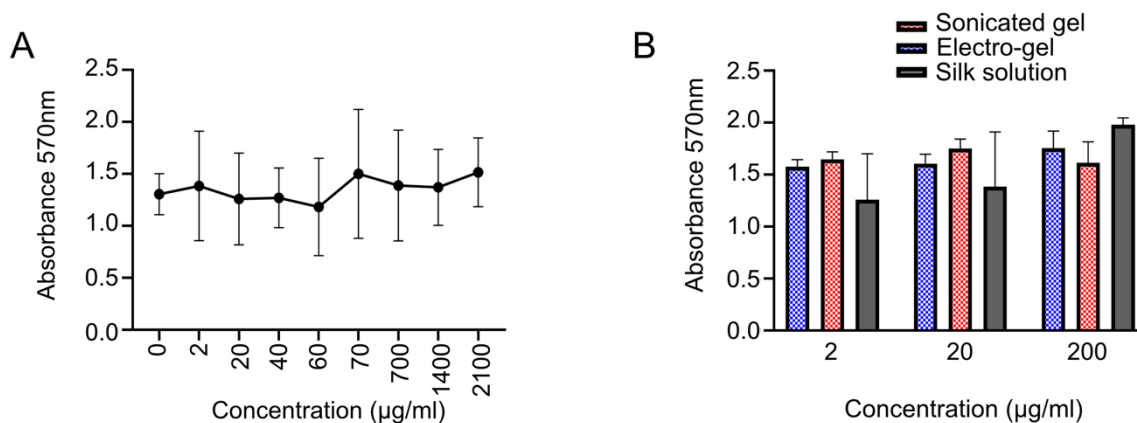


Figure 2-13. *In vitro* studies with silk fibroin. NIH 3T3 mouse fibroblasts were used throughout. (A) Cell proliferation of NIH3T3 fibroblasts incubated with silk solution for 72 hours and cell viability measured with an MTT assay ($n = 3$). (B) Cell proliferation of NIH3T3 fibroblasts incubated with leached samples of silk from electro-gels, sonicated gels, or silk solution after 72 hours ($n = 3$). Data analysis evaluated by two-way ANOVA followed by Tukey's multiple comparisons test. ($n = 3$, \pm SD). Asterisks denote statistical significance determined using post-hoc tests as follows: * $p < 0.05$, ** $p < 0.01$, *** $p < 0.001$, **** $p < 0.0001$.

2.3.9 Cell migration

Cell migration is critical for wound healing; therefore, the response of fibroblasts to soluble silk was tested using a checkerboard design to differentiate between chemokinesis and chemotaxis. The presence of soluble silk fibroin substantially influenced the movement of NIH3T3 fibroblasts. Little chemotactic movement was observed from a low to a high concentration, but NIH3T3 cells responded to the 1,600 $\mu\text{g/ml}$ silk fibroin concentration by displaying a marked increase in cellular mobility indicative of chemokinesis. The 1,600 $\mu\text{g/ml}$ silk fibroin concentration was compared to a positive control (FBS) and negative control (water only) (Figure 2-14). The negative control showed a low number of migrating cells (25 ± 11.89), while FBS positive control showed a similar number of migrated cells (no statistical difference between FBS and silk fibroin).

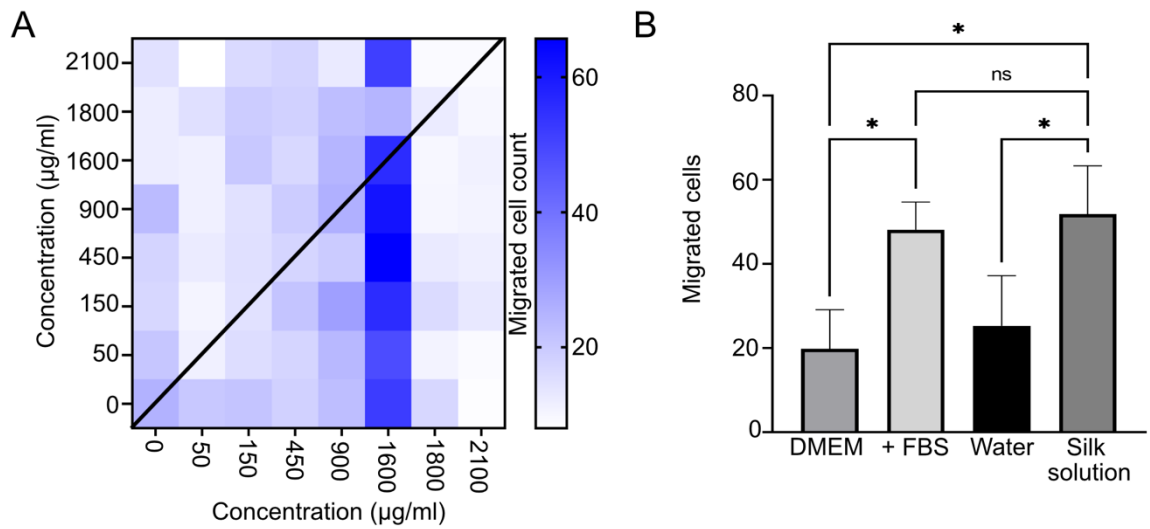


Figure 2-14. (A) Cell migration across a permeable membrane after exposure to silk solution for 3.5 hours ($n = 4$). (B) Cell migration at 1600 $\mu\text{g/ml}$ silk solution and controls with the presence of FBS as a positive control and water as the negative control. Data analysis evaluated by two-way ANOVA followed by Tukey's multiple comparisons test. ($n = 4$, \pm SD). Asterisks denote statistical significance determined using post-hoc tests as follows: * $p < 0.05$, ** $p < 0.01$, *** $p < 0.001$, **** $p < 0.0001$.

2.3.10 Wound healing

The in vitro scratch assay was used to measure functional outcomes in response to soluble silk fibroin (Figure 2-15). Wound site reduction assessed at both 4 and 7 hours showed similar trends for the different treatment groups at both time points (Figure 2-16). The presence of 1,600 $\mu\text{g/ml}$ silk fibroin significantly increased the rate of healing by reducing the wound site distance by $11 \pm 7 \%$ at 7 h, whereas, in the absence of silk, the wound distance was reduced by only $4 \pm 2\%$. FBS, which served as the positive control, gave a $14 \pm 7\%$ reduction in the wound site, thereby matching the silk fibroin response.

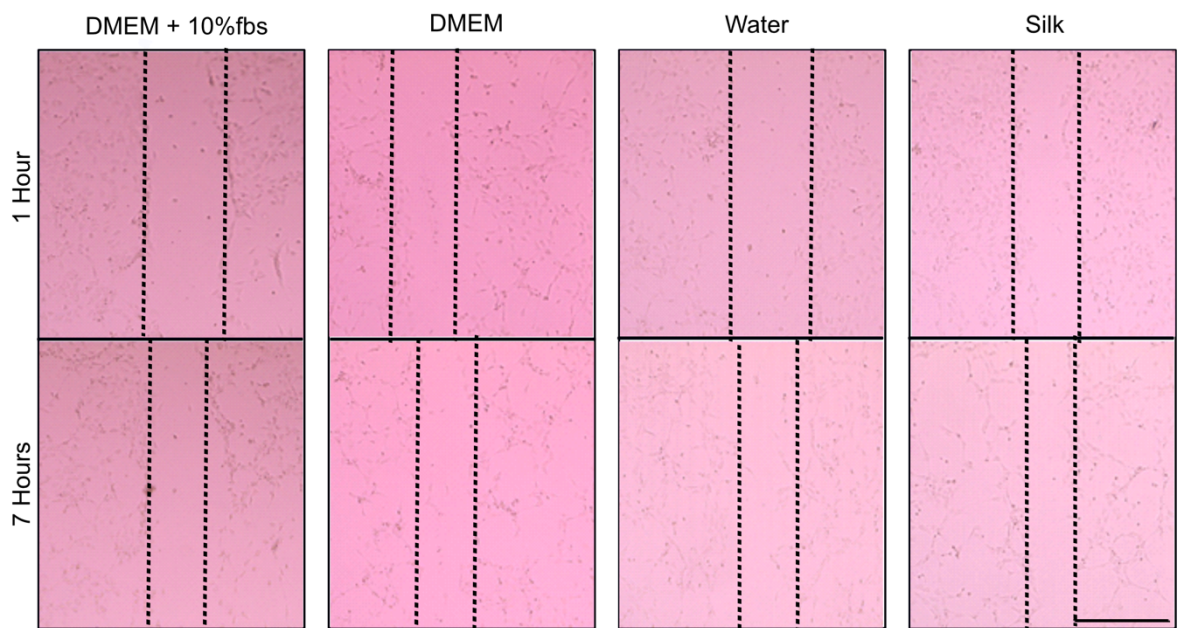


Figure 2-15. Wound closure assay with NIH3T3 fibroblasts at 1 and 7 hours. Broken lines indicate the border of cell growth. Scale bar 400 μm.

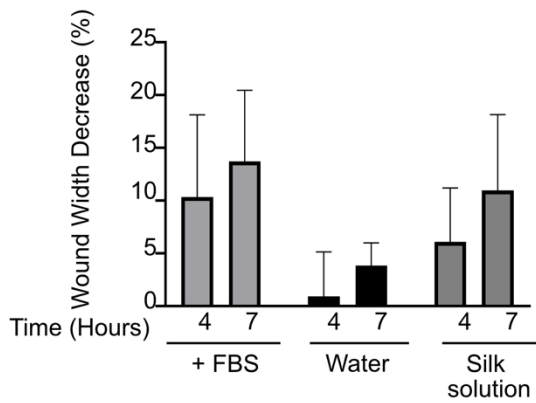


Figure 2-16. Wound closure assay width over 4 and 7 hours in the presence of silk solution, water or FBS. Data analysis evaluated by two-way ANOVA followed by Šidák's multiple comparisons test ($n = 4, \pm SD$). Asterisks denote statistical significance determined using post-hoc tests as follows: * $p < 0.05$, ** $p < 0.01$, *** $p < 0.001$, **** $p < 0.0001$.

2.3.11 Phosphorylation assay

The molecular response of fibroblasts exposed to soluble silk was assessed by monitoring the tyrosine phosphorylation of receptor tyrosine kinases (Figure 2-17). The epidermal growth factor family of receptor tyrosine kinases were impacted by soluble silk fibroin. For example, ErbB2 and to a lesser extent ErbB3, were phosphorylated in response to both soluble silk fibroin and the positive FBS control. ErbB4 was also activated, albeit to a lower extent. Strong activations in response to both soluble silk and FBS were observed for PDGF α . Soluble silk induced a stronger activation of Dtk than was observed for the FBS control. FBS also simulated the receptor tyrosine kinase TrkC receptor, but this response was not observed in cells treated with soluble silk fibroin.

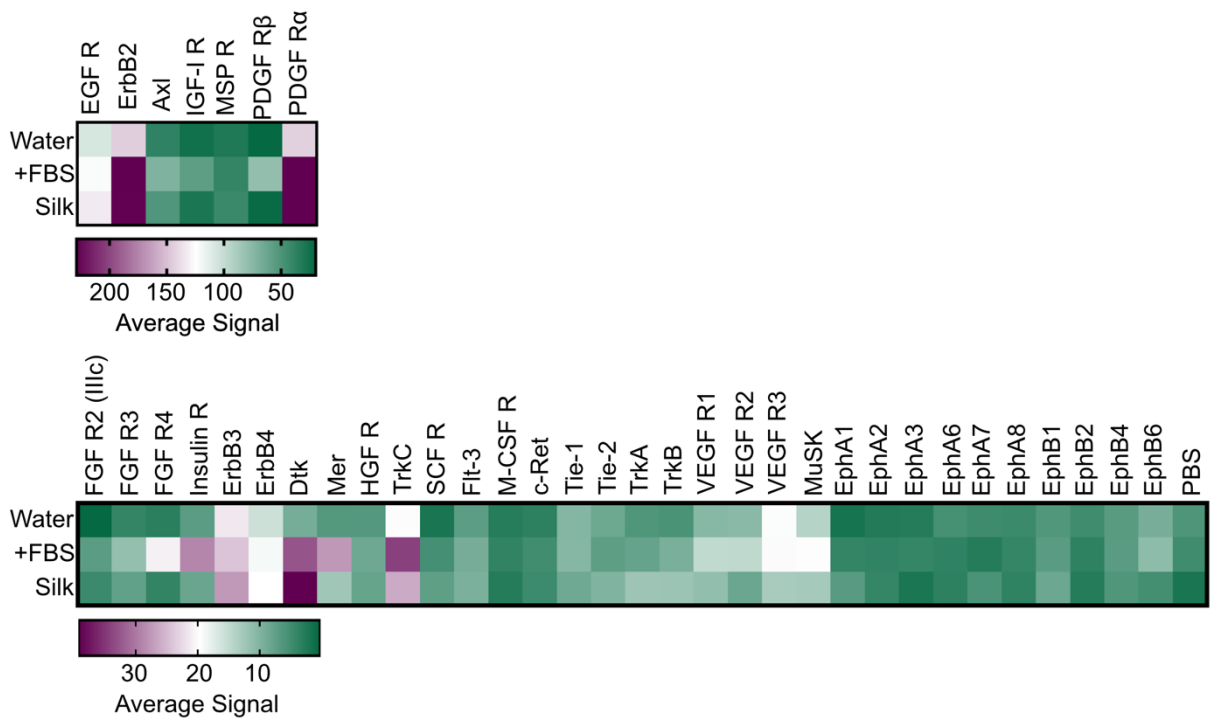


Figure 2-17. Phosphorylation array in the presence of silk solution, water or FBS.

2.4 Discussion

Silk fibroin has desirable material attributes (Holland, et al., 2019, Janani, et al., 2019), including biocompatibility across a broad spectrum of applications (e.g. blood (Maitz, et al., 2017, Seib, et al., 2014, Seib, et al., 2012), brain (Fernandez-Garcia, et al., 2016, Fernandez-Garcia, et al., 2018, Gorenkova, et al., 2019, Osama, et al., 2018), musculoskeletal (Neubauer, et al., 2021) etc.). The ability to unspin the silk fibre and apply diverse processing strategies to liquid silk has opened up a wide material landscape (Rockwood, et al., 2011). For example, silk fibroin hydrogels are being explored for numerous applications, including wound care (Farokhi, et al., 2018). Silk hydrogels can be generated using covalent crosslinking, physical crosslinking, or a combination of both (Phuagkhaopong, et al., 2021, Seib, 2018). For this work, I used physical crosslinking by sonication energy and DC current to tune the secondary conformation. These manufacturing regimens are robust for triggering the solution–gel transition without the need for chemical crosslinkers, which can be toxic (Seib, 2018). However, our current understanding of silk leaching from physically crosslinked hydrogels is limited. Obtaining a better understanding is important because preclinical assessments of silk hydrogels have overlooked silk leaching as a potential mechanism of action. The clinically approved regenerated silk Silk Voice also uses physical crosslinking, but information regarding the impact of silk leaching on overall performance is currently not in the public domain.

The efficiency of the solution-gel transition for electro-hydrogels is significantly lower than for sonicated hydrogels (which approaches 100% efficiency), the relative

amount of silk incorporated into sonicated hydrogels was significantly lower than the amount incorporated into electro-hydrogels. Hydrogel assembly at the positive electrode is triggered by the hydrolysis of water, which creates a local drop in pH that drives hydrogel self-assembly (Kojic, et al., 2012). The drop in pH was verified using pH indicator paper which changes colour in response to the presence of hydrogen ions (Lab Pro, 2021), and by using phenol red, a commonly used indication of alkalinity in cell culture (Pub Chem, 2023). In the future, more accurate testing could be done with a pH meter that is able to be used with hydrogels (PharmaState, 2023). The silk content for electro-hydrogels varied significantly, possibly due to a change in the electric field triggered by the build-up of the hydrogel at the positive electrode. I used a relatively low current, creating an electric field of 3.5 V/cm, whereas other studies have reported using a constant voltage of 25 V or an electric field of 50 V/cm (Lin, et al., 2013). I specifically selected this low voltage to determine if these conditions enable hydrogel formation because this lower voltage is more suited to the healthcare contexts (e.g., in situ hydrogel formation in the wound bed etc). This lower voltage also created electro-gels that leached silk to ultimately trigger cell migration.

I verified the silk secondary structure of both electro-hydrogels and sonicated hydrogels. Sonicated hydrogels were rich in beta sheets, confirming the transition from silk I to silk II. By contrast, electro-hydrogels contained significantly lower amounts of beta sheets and retained the more amorphous silk I state that more closely resembled native silk or a regenerated silk fibroin solution. These data are in good agreement with the literature (Leisk, et al., 2010, Wang, et al., 2008), despite

the use of substantially higher voltages in these earlier studies (Kojic, et al., 2012, Lin, et al., 2013, Leisk, et al., 2010). This suggests that a critical threshold exists for triggering silk self-assembly, but little difference occurs in the secondary structure once that threshold is passed. However, one difference may be the solid content of the hydrogel and the how tightly the silk fibroin protein is packed within the hydrogel. Overall, the use of sonication and DC current enables the assembly of physically cross-linked hydrogels with tuned crystallinity that impacts both the physical and biological properties.

Based on previous work with films and scaffolds (Guo, et al., 2020), the silk crystallinity is also expected to affect the solution stability and the degradation of the silk hydrogels, but experimental proof is limited. It is shown here that electro-hydrogels leached significantly more silk protein over 72 h into both water and PBS when compared with sonicated hydrogels that have a high beta sheet content. When comparing the sonicated hydrogels to the electro-gels, the lower desorption temperature and enthalpy, combined with the lower enthalpy of crystallization, shallower glass transition profile and delayed onset of decomposition suggest that the sonicated hydrogels contain a greater crystalline fraction than the electro-gels. Both hydrogel types show a higher crystallinity than the silk I control, due to the higher enthalpies of crystallization, shallower glass transitions and higher onsets of decomposition of the hydrogels compared to the silk I control. The silk secondary conformation therefore appears to be a key factor determining silk leaching because the silk is more amorphous in electro-hydrogels than in sonicated silk hydrogels. This suggests that electro-hydrogels have a less tightly bound silk structure that is prone

to leaching, as nearly half the original silk content was lost over 72 h. By contrast, sonicated hydrogels released only very small amounts of silk (as a percentage in relation to the total amount present), indicating that crystallinity locks silk into the hydrogel structure and leaves little free silk that can escape. Morphological differences were apparent too. Sonicated hydrogels showed porous sharp features that were mostly absent in electro-gels. One might speculate that these sharp features were due to tighter silk binding mediated by beta sheet-rich silk fibroin structures. Morphological differences of the leached silk were evident too; the high abundance of globular structures was typical for leached electro-gel samples and are a hallmark for silk I (Leisk, et al., 2010).

Unexpectedly, the silk protein released from both hydrogel types can be beta-sheet rich. This is especially surprising for the silk leached from the electro-gel. The differences in correlation coefficients for leached silk indicated that the beta sheet content was higher than pristine Silk I. However, the silk secondary structure of the leached silks was also different to the respective hydrogel (based on FTIR and thermal analyses). The lower onsets of crystallization, larger crystallization exotherms, steeper glass transition profiles and lower onset of decomposition of leached silk compared to the hydrogel architecture reinforced the greater amorphous content of leached silk determined by FTIR. This indicates that the leached silk had undergone a conformational transition forming an 'intermediary silk secondary structure'. I speculate that this conformational switching occurred during the incubation period in the bulk aqueous phase, rather than during the integration into the hydrogel

network, because (i) beta sheets provide physical anchoring points within the silk hydrogel network, thereby impeding leaching and (ii) silk in solution has a greater degree of conformation flexibility than when integrated into a hydrogel network. Overall, this work proves that silk hydrogels leach silk.

I also assessed the impact of leached silk on cell behaviour via a fibroblast model. NIH3T3 fibroblasts were chosen as previous studies have successfully used this cell line to demonstrate migration in scratch wound assays (Ranzato, et al., 2010, Freiesleben, et al., 2017, Park, et al., 2017). This is an important initial assessment because the cellular response is critical for wound healing. However, the underlying mechanism by which silk fibroin hydrogels improve wound healing is currently poorly understood and is expected to be multifaceted. Other studies have shown that both in vitro and in vivo self-assembled silk hydrogels upregulated talin 1 expression, resulting in increased cell proliferation and expression of adhesion/migration related proteins (Guan, et al., 2020). Similarly, soluble silk increased the in vitro phosphorylation of ERK1/2, c-Jun, and JNK1/2 (Martinez-Mora, et al., 2012). Soluble silk also activated NF- κ B signalling both in vitro, and in a rat wound model (Park, et al., 2017). NF- κ B activation upregulated the expression of cyclin D1, vimentin, fibronectin, and vascular endothelial growth factor (Park, et al., 2017). Silk proteins have also been shown to regulate Notch signalling by suppressing *Hes-1* (Kim, et al., 2010). Other studies with silk-gelatin bio inks have shown that there is a negative regulatory role on the IHH signalling pathway and Wnt/ β -catenin signalling pathway to control hypertrophy in bone marrow stromal cells (Chawla, et al., 2017, Chawla, et al., 2017, Chakraborty & Ghosh, 2020).

In the present study, fibroblasts exposed to soluble silk were assessed for the activation status of 39 key proteins. For example, the ErbB family is capable of homo-, heterodimer and higher order oligomer formation, which is orchestrated by growth factor ligands. ErbB3 showed an increased expression in silk-treated cells when compared to cells exposed only to water or supplemented medium. ErbB3 can form heterodimers with other members of the ErbB family, including ErbB2, which was also activated by exposure to soluble silk. ErbB signalling ultimately stimulates intracellular protein-tyrosine kinase activity. Autophosphorylation can also occur, and this can initiate signal transduction cascades (e.g., MAPK, Akt, JNK etc.) that regulate a plethora of cellular responses, including cell proliferation. AXL is also involved in cell proliferation and survival (Axelrod & Pienta, 2014). The activation level of AXL in response to silk was similar to that in the controls. Signalling pathways downstream of AXL include NF- κ B, which was not assessed here but has been reported to be activated by soluble silk (Park, et al., 2017). Dtk activation was higher in the silk samples than in the controls, and Dtk signalling is associated with Axl and Mer (Rothin, et al., 2015). PDGF α was highly activated and affected cell signalling pathways that regulate cell growth and differentiation. The receptor tyrosine kinases TrKA and TrKB were not changed, but the expression of TrkC was lower in silk-treated cells than in the medium-treated controls. This TrkC activation could impact several other pathways, including the phosphorylation of PI3 Kinase (Huang & Reichardt, 2003). Overall, this snapshot of receptor tyrosine kinase signalling showed that soluble silk, similar to FBS, supported fibroblast functions relevant for cell survival, proliferation and motility.

The impact of leached silk on cell function was also investigated. Silk fibroin release from physically crosslinked hydrogels had little impact on fibroblast proliferation or cytotoxicity. No significant difference was detected in the biological response towards leached silk and a silk fibroin solution over the tested concentration range. These findings are at odds with the work by Park et al. (Park, et al., 2017), who found that the presence of silk fibroin induced a dose-dependent cell growth. A possible explanation for this discrepancy could be differences in the silk processing protocols that could result in different silk molecular weight distributions.

Cell migration is a key aspect of wound healing. I therefore assessed the effects of soluble silk on cell migration and whether migration might be mediated by a gradient (i.e., chemotaxis) or by a stimulation of cell mobility (i.e., chemokinesis). The measured response clearly indicated that silk was not chemotactic but instead induced significant chemokinesis, especially at a concentration of 1600 µg/ml. The observed migration at the key silk concentration was unexpected. It was predicted that cell migration would increase with concentration and then remain at a high level. I speculate that I observed off-target receptor-mediated migration. This relatively high silk concentrations triggered chemokinesis (i.e., the signalling threshold) suggesting an off-target effect rather than high fidelity receptor activation. Silk concentrations beyond this threshold abrogated migration possibly by receptor down regulation. These experimental results suggest a complex biological response towards silk that requires more work to elucidate the mechanism of action. However, I expect that the principle of leached silk to mediated chemokinesis is relevant both in vitro and in vivo. Gradient formation and high local silk concentration are feasible

and can be further tuned by adjusting the volume of administered hydrogel. To achieve such a specific silk concentration in vivo would require further research into tuning the silk released from hydrogels over time to ensure a steady concentration was present to allow cell migration to occur. The sonicated silk hydrogel appears to be more suited to a slow steady release of silk fibroin so the volume and concentration of the silk in the hydrogel could be altered to achieve the desired leaching of silk into the surrounding environment. The in vitro scratch wound assay showed that the presence of soluble silk fibroin caused the cells to migrate more rapidly into the scratch than they did in the absence of silk. This study was performed over 7 hours due to equipment constraints but many studies have shown the trend in migration within this timeframe (Liang, et al., 2007, Suvarna, et al., 2018) and it is possible a significant difference would have been seen over a longer timeframe. Many scratch wound assay studies are performed over 24 hours (Jonkman, et al., 2014, Liang, et al., 2007) to allow a better understanding of the cell migration into a wound area but cell proliferation should be noted as affecting results beyond this (Axion Biosystems, 2023). Cell migration is dependent upon microtubule polymerization of the cytoskeleton. The cellular mechanism of action of silk is currently not fully known, but one possibility is that the VITTDSDGNE and NINDFDED sequences found in the N-terminal region of silk fibroin (Yamada, et al., 2004) promoted chemokinesis in fibroblasts. Overall, silk is emerging as a powerful fibroblast chemokinesis stimulator, suggesting that the presence of leached silk could accelerate this aspect of wound healing. This hypothesis is supported by in vivo data in a corneal wound model where animals treated with liquid silk showed significantly

faster wound healing than saline controls (Abdel-Naby, et al., 2017). Similar observations were also made for a skin wound model in rats (Park, et al., 2017).

2.5 Conclusion

Silk hydrogels with tuned secondary structures can be formed by sonication or electro-gelation. The elution of silk from the hydrogels is significantly greater for electro-hydrogels, due to their more amorphous structure and lower beta sheet secondary structure. The leached silk from such gels is biologically active. No significant effect was noted on cell proliferation; however, soluble silk promoted the phosphorylation of receptor tyrosine kinases and stimulated chemokinesis. These effects are desirable for wound management; therefore, silk fibroin hydrogels show promise for wide use in the healthcare setting.

3. Chapter 3 “Investigating the antibacterial effects of solubilized *Bombyx mori* silk fibroin with common wound pathogens”

Antibacterial properties are desirable in wound dressings. Silks, among many material formats, have been investigated for use in wound care. However, the antibacterial properties of liquid silk are poorly understood. The aim of this study was to investigate the inherent antibacterial properties of a *Bombyx mori* silk fibroin solution. Silk fibroin solutions containing $\geq 4\%$ w/v silk fibroin did not support the growth of two common wound pathogens, *Staphylococcus aureus* (*S. aureus*) and *Pseudomonas aeruginosa* (*P. aeruginosa*). When liquid silk was added to a wound pad and placed on inoculated culture plates mimicking wound fluid, silk was bacteriostatic. Viability tests of the bacterial cells in the presence of liquid silk showed that cells remained intact within the silk but could not be cultured. Liquid silk appears to provide a hostile environment for *S. aureus* and *P. aeruginosa* and inhibits growth without disrupting the cell membrane. This effect could be beneficial for wound healing and supports future healthcare applications for silk. This observation also indicates that liquid silk stored prior to processing is unlikely to experience microbial spoilage.

This chapter was submitted for peer review as an original article and has been adapted accordingly for this thesis. Data acquisition and analysis for figures was

conducted by myself. As the first author of this study, I wrote the manuscript with input from the other authors.

3.1 Introduction

Wound care is a key area of healthcare and can have long-lasting adverse effects on quality of life if wound infection is not treated correctly by medical professionals. Wound healing typically follows a pathway consisting of 4 clear stages: haemostasis, inflammation, proliferation, and remodelling (Wilkinson & Hardman, 2020); however, this order is disrupted in chronic wounds, making treatment of these wounds an especially difficult challenge. The inflammation stage can also be prolonged by contamination by microbial pathogens present in the environment, the surrounding skin, or various mucous membranes (Guo & DiPietro, 2010).

Two of the most common pathogens that cause wound infection are the bacteria *Staphylococcus aureus* and *Pseudomonas aeruginosa* (Bowler, et al., 2001, Bessa, et al., 2015). *S. aureus* is a gram-positive bacterial species that can grow aerobically or facultatively anaerobically (Taylor & Unakal, 2021) and is found in the environment and on human skin and mucous membranes as part of a healthy skin flora. However, this microbe can cause serious infections if it enters the bloodstream or internal tissues. *P. aeruginosa* is a gram-negative motile bacterium found on the skin, in the throat, and in stool samples of healthy individuals. However, *P. aeruginosa* can become pathogenic by the release of virulence factors, such as pyocyanin. *P. aeruginosa* can form intractable biofilms, which make subsequent wound treatment difficult (Iglewski, 1996, Prasad, et al., 2020). Biofilms are groups of bacteria that can attach to a surface and each other embedded in a self-produced matrix. This matrix is composed of proteins, polysaccharides, and extracellular DNA which provide the

bacteria with a method of improved survival. In the matrix, composed of 90 % extracellular matrix, nutrients are trapped for metabolic utilization and water is retained through hydrogen bond interactions with the hydrophilic polysaccharides. Enzymes secreted by the bacteria also allow modification of the composition in response to nutrient availability (Kostakioti, et al., 2013). Biofilms can hide bacteria from the host immune system which allows them to cause more damage and can lead to an infection. Whilst the bacteria are within the biofilm, they adapt to the altered conditions by changing metabolism, gene expression, and protein production, which can improve the resistance of the bacteria to antimicrobial therapies (Vestby, et al., 2020).

Wound dressings are a commonly used method for preventing infection and providing an environment that favours wound healing. Our ability to unspin the silk fibre and generate novel material formats (Seib, 2017, Seib, 2018) has sparked a renewed interest in silk, including its use in wound care applications (e.g. (Egan, et al., 2022, Schiefer, et al., 2021, Kim, et al., 2017), reviewed (Chouhan & Mandal, 2020)).

Bombyx mori silk has long been used in humans for wound care, especially as a suture material, and the *B. mori* silk fibroin protein is a clinically approved biomaterial for use in load-bearing applications in humans (e.g., sutures, meshes etc.) (Holland, et al., 2019). Silk fibroin films, sponges (Zhang, et al., 2017), hydrogels (Noda, et al., 2021) and knitted scaffolds (Schiefer, et al., 2021) have also shown potential uses in wound repair and aesthetic restorations in small-scale clinical trials. Soluble silk has

also improved epithelial healing in a rabbit eye cornea model (Kim, et al., 2017, Abdel-Naby, et al., 2017). Overall, silk fibroin is emerging as a useful tool in wound healing, but wound dressings should help to prevent or overcome pathogen infection in wounds. Although some research has investigated the antimicrobial properties of silk fibroin, most studies focused on a potential role for sericin, one of the components of raw silk (Kaur, et al., 2013), and the results have been conflicting (Seves, et al., 1998, Akiyama, et al., 1993, Nuchadomrong, et al., 2009, Pandiarajan, et al., 2011), reviewed in (Schafer, et al., 2022). Many studies focus on the silk as spun in the cocoon, and the effects of silk when developed into sutures or scaffolds (Ghalei & Handa, 2022). Silk fibres in the cocoon of the silkworm have been shown to provide a substrate for bacterial biofilm growth, thought to provide protection to the cocoon from environmental stresses (Seves, et al., 1998, Ghalei & Handa, 2022). Silk fibroin films have been found to have strong microbial attachment, immobilizing microbes, thought to be due to the glycine, alanine and serine amino acids present in the silk fibroin (Tabei, et al., 2011). Processing of the silk fibroin has been linked to the antibacterial effects of silk films, with silk processed with lithium bromide showing a higher degree of antibacterial activity than films processed with Ajisawa's reagent (Abdel-Fattah, et al., 2015). Other studies have combined silk fibroin with other components, including polyethyleneimine (Calamak, et al., 2014), graphene oxide (Wang, et al., 2018) or plant extracts (Basal, et al., 2010), to improve its antibacterial effects. More research is still needed to characterise the antimicrobial properties of silk fibroin for its use in wound dressings in other formats, such as aqueous solution.

Healthcare products, like wound dressings, that are destined for use in clinical applications typically must also be sterile. However, with silk fibroin, this requirement introduces new challenges because the sterilisation methods that are deemed acceptable by regulatory agencies can adversely affect this biomaterial (Rnjak-Kovacina, et al., 2015, Gil, et al., 2014, George, et al., 2013, Hofmann, et al., 2014). Current methods of sterilisation include autoclaving, irradiation (e.g., ultraviolet, gamma), immersion in 70% v/v ethanol, filtering, or exposure to ethylene oxide. Some studies have indicated that autoclaving a silk solution decreases the molecular weight, increases the protein aggregation, and ultimately affects the final product by altering these physical properties of the silk (Wu, et al., 2011). Filtering a silk solution through a 0.22 µm filter is only feasible with low molecular weight silk (i.e., low viscosity solutions) and at low concentrations to minimise losses in sample concentration and final volume (Rnjak-Kovacina, et al., 2015).

A knowledge gap presently exists regarding the sterility of silk fibroin solutions and the effects of silk fibroin on bacterial growth. One aim of the present work was to produce sterilised and non-sterilised silk solutions and to assess their sterility over time under various storage conditions. A second aim was to use live/dead bacterial staining and colony counting to assess the viability of *S. aureus* and *P. aeruginosa* after inoculation into a silk fibroin solution. The final aim was to mimic wound conditions using nutrient agar to determine whether adding silk fibroin-soaked wound pads would eliminate bacterial growth on the agar plates.

3.2 Experimental

3.2.1 Silk solution preparation and conductivity assessment

The silk solution was prepared as detailed previously (Matthew, et al., 2020) (Totten, et al., 2017). Briefly, *Bombyx mori* silk cocoons were cut into 5 × 5 mm pieces, and 5 g samples were degummed in 0.02 M Na₂CO₃ solution for 30 minutes. The purified silk fibroin was rinsed three times for 20 minutes in Milli-Q ultrapure water and then stretched and left to air dry at room temperature overnight. The dried silk fibroin fibres were then packed into a beaker and dissolved in a 9.3 M LiBr solution at 60 °C for up to 4 h. The resulting solution was dialysed (MW cut off 3500 g/mol, Thermo Scientific, Waltham, MA) for 48 h in Milli-Q water to remove the LiBr salt. Salt removal was monitored by taking conductivity measurements of the dialysate at 20 to 21.5 °C (Haiqingxin Shenzhen Purification Technology Co. Ltd, China). At the end of the dialysis procedure, the resulting silk fibroin solution was cleared by centrifuging twice at 9418 × g and 5 °C for 20 minutes. The silk fibroin content was determined gravimetrically. The silk fibroin solution was stored at 4°C until use, unless otherwise stated.

3.2.2 Silk secondary structure analysis by Fourier transform infrared spectroscopy.

The secondary structures of silk samples were determined by Fourier transform infrared (FTIR) spectroscopy (Tensor II Bench ATR IR, Bruker, MA, USA). Each FTIR measurement was run for 128 scans at a 4 cm⁻¹ resolution in absorption mode over the wavenumber range of 400–4000 cm⁻¹. Reference samples with low beta sheet content were prepared by air-drying 5% w/v silk fibroin solution to form a water-

soluble film. Aqueous 1 and 5 % w/v silk fibroin samples were incubated in a rocker-shaker at 150 rpm overnight at 37 °C, and then collected and air-dried into films. All FTIR data were deconvoluted as described previously (Hu, et al., 2006).

3.2.3 Sterility testing

A silk solution (5% w/v) was divided into different treatment and storage conditions. The samples were either filter sterilised (0.22 µm Millex PES membrane, Merck Millipore Ltd, Cork, Ireland) or left unsterilised. The concentration of sterilised silk solutions was measured gravimetrically and adjusted prior to testing. The silk samples were then divided for storage at either 4 °C, room temperature (25 °C) or 37 °C for 14 days in sealed aseptic containers.

The sterility of the silk solutions was tested by two methods. For the first method, tryptic soy broth (TSB) was produced according to manufacturer's instructions by dissolving 40 g tryptone soya broth powder (Oxoid, Hampshire, England) in 1 L Milli-Q H₂O and autoclaving for 20 minutes at 121 °C. Next, 1 ml of silk solution (freshly prepared or stored for 14 days) was added to 9 ml TSB and incubated at either room temperature or 37 °C for 14 days, and then imaged. The turbidity of the solutions was visually assessed to determine the presence of contamination. Positive control samples were also prepared by spiking TSB with known concentrations of *Staphylococcus aureus* and *Pseudomonas aeruginosa* and imaging before and after incubation for 24 hours to indicate bacterial growth of these strains for a visual aid.

Bacterial colonies were then counted after 24 hours to assess growth rate and turbidity detection.

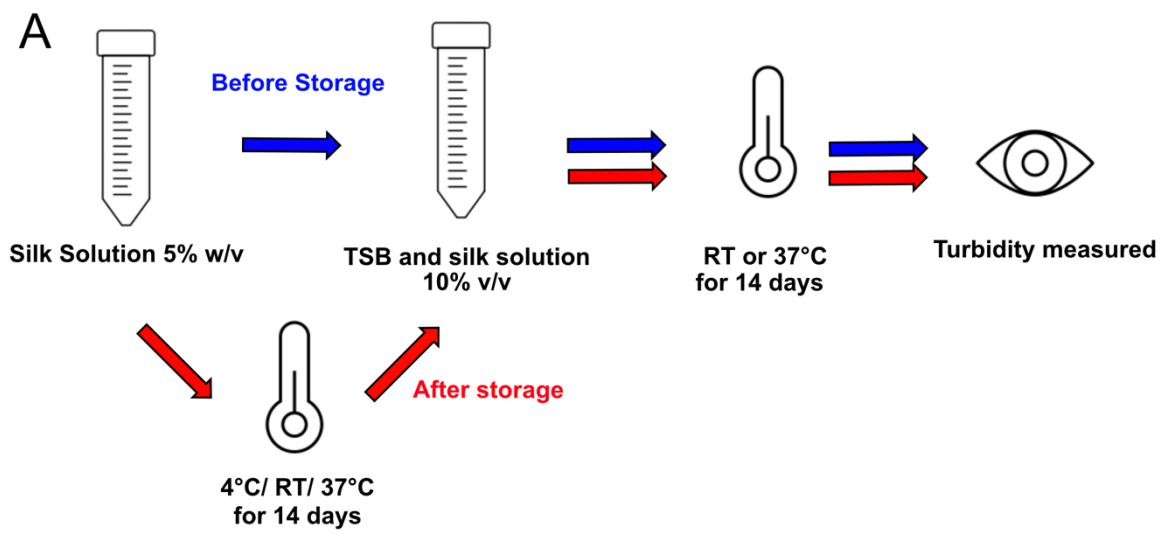


Figure 3-1. Sterility testing of silk fibroin solution (5% w/v) in tryptic soya broth (TSB) before and after storage at 4 °C, room temperature (RT) and 37 °C for 14 days. (A) TSB was incubated at both room temperature and at 37 °C for 14 days and then examined for growth (i.e., turbidity).

The second method used blood and chocolate agar plates. Briefly, blood and chocolate agar were prepared by dissolving 40 g blood agar base (Fluka analytical, Buchs, Switzerland) in 1 L Milli-Q H₂O and autoclaved for 20 minutes at 121 °C. The blood and chocolate agar were prepared following the manufacturer's instructions with defibrinated horse blood and stored at 4 °C until use. The silk solution was tested by streaking 10 µL samples of each condition onto both blood and chocolate agar plates and storing them either in aerobic or anaerobic conditions at 37 °C for 72 h and imaging them after visually assessing growth.

3.2.4 Culture Preparation

The bacteria used for this study were *Staphylococcus aureus* (NCTC 8325) and *Pseudomonas aeruginosa* (PA 14) grown in Lennox LB medium, prepared with 10 g tryptone, 5 g NaCl and 5 g yeast extract in 1 L Milli-Q H₂O autoclaved for 20 minutes at 121 °C. LB agar plates were prepared by the addition of 20 g agar to LB medium before autoclaving, and 20 ml was poured into 9 cm diameter Petri dishes, then cooled. Stock cultures were produced by inoculating 10 ml of LB medium with a single colony and incubating overnight at 37 °C in a shaker-incubator at 150 rpm (ES-20, Grant instruments, Cambridge, UK).

3.2.5 Bacterial growth in presence of water

The growth and survival of bacteria in the presence of water was determined. Briefly, overnight cultures of *S. aureus* and *P. aeruginosa* were prepared as described in 2.4. Samples were centrifuged at 12,100 × g for 5 minutes and the supernatant was removed. The bacterial pellet was resuspended in sterile water and centrifuged again. This washing step was repeated twice. A sample of bacteria suspended in

water was taken for colony counting. Colony counting was performed by performing a serial dilution and plating 10 x 10 µl drops on an agar plate and incubating overnight. The colonies were counted and totalled across the 10 drops and from this the total concentration can be calculated. All samples were spiked with bacteria in the order of 10⁸ CFU/ml. The bacteria were then centrifuged once more and then suspended in either 0 %, 75 %, 85 %, 95 % or 100 % sterile water with LB medium. The samples were incubated for 24 h at 37 °C in a shaker-incubator (ES-20, Grant Instruments, Cambridge, UK). A 10 µL sample of each inoculated silk mixture was streaked onto an LB agar plate and incubated overnight. The colonies were counted at time 0 and after 24 h of growth.

3.2.6 Minimum Bactericidal Concentration of Silk

The minimum bactericidal concentration (MBC) of silk was determined in a similar method to that use for determination of bacterial survival in water . Briefly, overnight cultures of *S. aureus* and *P. aeruginosa* were prepared as described in section 2.4. Bacterial samples were prepared as described in section 2.5. All samples were spiked with bacteria in the order of 10⁸ CFU/ml. The bacteria were suspended in either 1 %, 3 %, 4 % or 5 % w/v filter-sterilised aqueous silk solution and incubated for 24 h at 37 °C in a shaker-incubator (ES-20, Grant Instruments, Cambridge, UK). A 10 µL sample was taken from each inoculated silk mixture, streaked onto an LB agar plate, and incubated overnight. The colonies were counted at time 0 and after 24 h of growth.

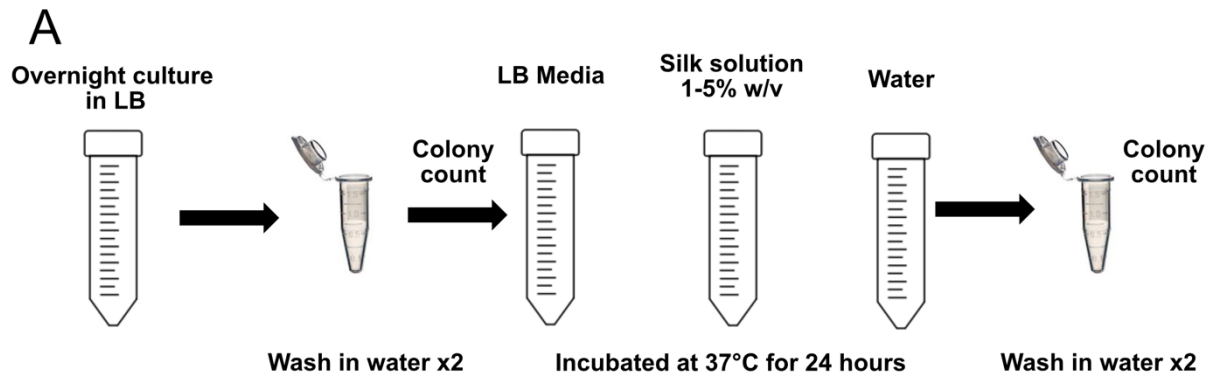


Figure 3-2. Minimum bactericidal and inhibitory concentrations of silk fibroin testing strategy. Overnight cultures of *S. aureus* and *P. aeruginosa* were incubated in LB media before being centrifuged at 12,100 x g for 5 minutes and the supernatant removed. This was repeated with water to wash the cells. The cells were then resuspended in LB media, water or aqueous silk solution and incubated at 37°C, 150 rpm in an orbital incubator overnight. The cells were again washed through centrifugation and with water, as before. Colony counting was performed before the cells were suspended in the solution and after the final wash to determine viability.

3.2.7 Simulated Wound Dressing

The antibacterial effect of the silk solutions was tested in the presence of bacterial nutrients. Briefly, simulated wound fluid agar was prepared by adding heat-inactivated foetal bovine serum (Biosera, East Sussex, UK) to a physiological salt solution at a ratio of 1:1 at 56 °C. The physiological salt solution was prepared with 142 mM NaCl, 2.5 mM CaCl₂ and dH₂O and autoclaved. The LB agar plates were prepared as before.

To mimic the application of a dressing, the wound pad of a fabric plaster (Elastoplast, Beiersdorf, Hamburg, Germany) was cut and soaked in either 5% w/v silk solution or 70% v/v ethanol. Overnight cultures of *S. aureus* or *P. aeruginosa* were prepared as before. These were then diluted to a final concentration of 10⁶ CFU/ml when 100 µl solution was placed in the centre of 4 quadrants of the agar plates. Freshly soaked wound pads were placed over the bacterial suspension and incubated at 37 °C overnight. The wound pad was then removed, and the plates were imaged. Infection levels were determined by placing the wound pad in LB broth for 15 minutes and then performing colony counting (detailed above).

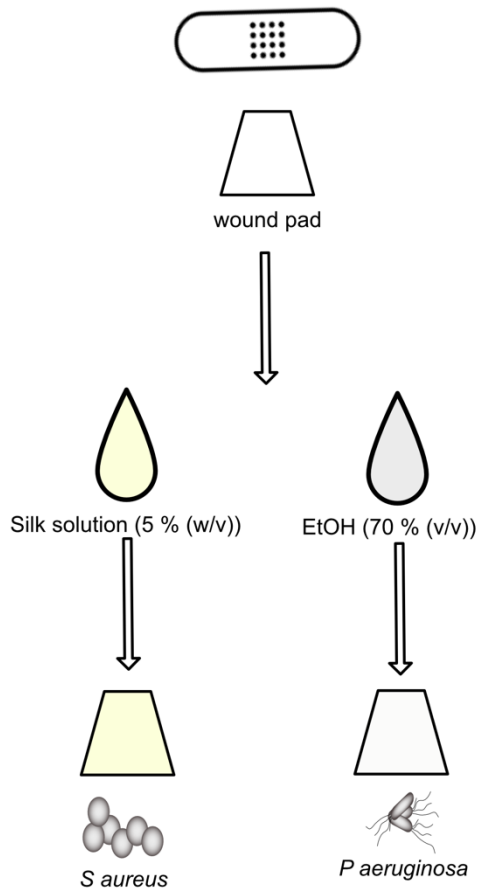


Figure 3-3. Woundpad dressing procedure. Woundpad was removed from a standard plaster dressing before being soaked in silk solution or ethanol and placed on either *S aureus* or *P aeruginosa* on agar plates. Growth was then observed after incubation overnight.

3.2.8 Bacterial Viability

Bacterial viability was measured with a live/dead BacLight staining kit (ThermoFisher Scientific, UK). Briefly, overnight cultures were prepared and exposed to silk (detailed above). Bacterial samples were prepared as described in section 2.5. The samples were then resuspended in either 4 ml of LB medium, water, 1 % w/v silk solution or 5 % w/v silk solution and incubated overnight at 37 °C at 151 rpm. Samples (1 ml) were collected the following day, centrifuged at 12,100 × g for 5 minutes, washed once with water, and resuspended in sterile 0.85 % w/v NaCl. The viability kit was then used according to the manufacturer's protocol. Samples were added to microscope slides and imaged using an epifluorescence microscope (Nikon Eclipse E600) with excitation/emission 470/515 nm (green filter, viable cells) and 530/635 (red filter, dead cells). Images were processed and analysed with ImageJ software v1.53f51 (National Institutes of Health, USA).

3.2.9 Sodium Carbonate detection and bactericidal effects

Sodium carbonate was detected with a sodium ion selective electrode (perfectION, Mettler Toledo AG, Switzerland). Briefly, solutions used to degum silk fibroin were produced at 0.02 M Na₂CO₃ and the concentration of sodium was measured before and after silk degumming. Silk was then rinsed in 1 L water 3 times and samples were taken for sodium detection. Finally, the silk solution (5 % w/v) was tested and the sodium within the solutions was recorded. Aqueous sodium carbonate solutions were then produced at the concentrations measured in the silk solution and water rinses to determine the minimum bactericidal concentration. The samples were tested as detailed in section 2.5.

3.2.10 Statistical Analyses & Data Sets

Statistical analyses were carried out using Origin Pro 2018 (Northampton, Massachusetts, USA) and GraphPad Prism v.9.1.1 (San Diego, CA, USA). Normality and homogeneity of variances were assumed. One-way analysis of variance (ANOVA), followed by Bonferroni's post hoc test, was conducted between multiple groups, or two-way analysis of variance (ANOVA) was conducted, followed by Tukey's multiple comparisons. Asterisks denote statistical significance determined using post-hoc tests as follows: * $p < 0.05$, ** $p < 0.01$, *** $p < 0.001$, **** $p < 0.0001$. Statistical analyses are noted in figure legends. All data are presented as mean values \pm standard deviation, and the number of independent experiments (n) is noted in each figure legend.

3.3 Results

3.3.1 Pure Aqueous Silk Solution

The dialysis progress was monitored using conductivity measurements of the dialysate, which served as a proxy (Figure 3-4). At the first water change, the conductivity was $4863.50 \pm 335.40 \mu\text{S}/\text{cm}$, and the conductivity value dropped at each water change. For example, at the start of day 2, the conductivity was $588.5 \pm 93.54 \mu\text{S}/\text{cm}$ and dropped to $14.75 \pm 10.21 \mu\text{S}/\text{cm}$ by the end of the day. The final conductivity was $9 \pm 2.45 \mu\text{S}/\text{cm}$, which is less than the conductivity of tap water ($50 \mu\text{S}/\text{cm}$).

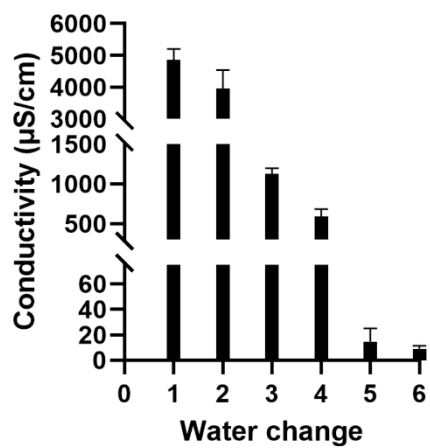


Figure 3-4. Conductivity measurements of the dialysate over 72 h resulting in an aqueous silk fibroin solution.

Next, the sodium carbonate remaining in silk fibroin solution was measured. The sodium content was verified at 0.02 M before silk degumming, increasing to 0.021 M after boiling. The water used to rinse the silk after degumming decreased with each rinse from 0.9 ± 0.2 mM on rinse 1, to 6 ± 4 μ M on rinse 2 and 0.2 ± 0.06 μ M on the final rinse. The concentration of sodium in the final silk solution (5 % w/v) was 50 ± 3 μ M (Figure 3-4).

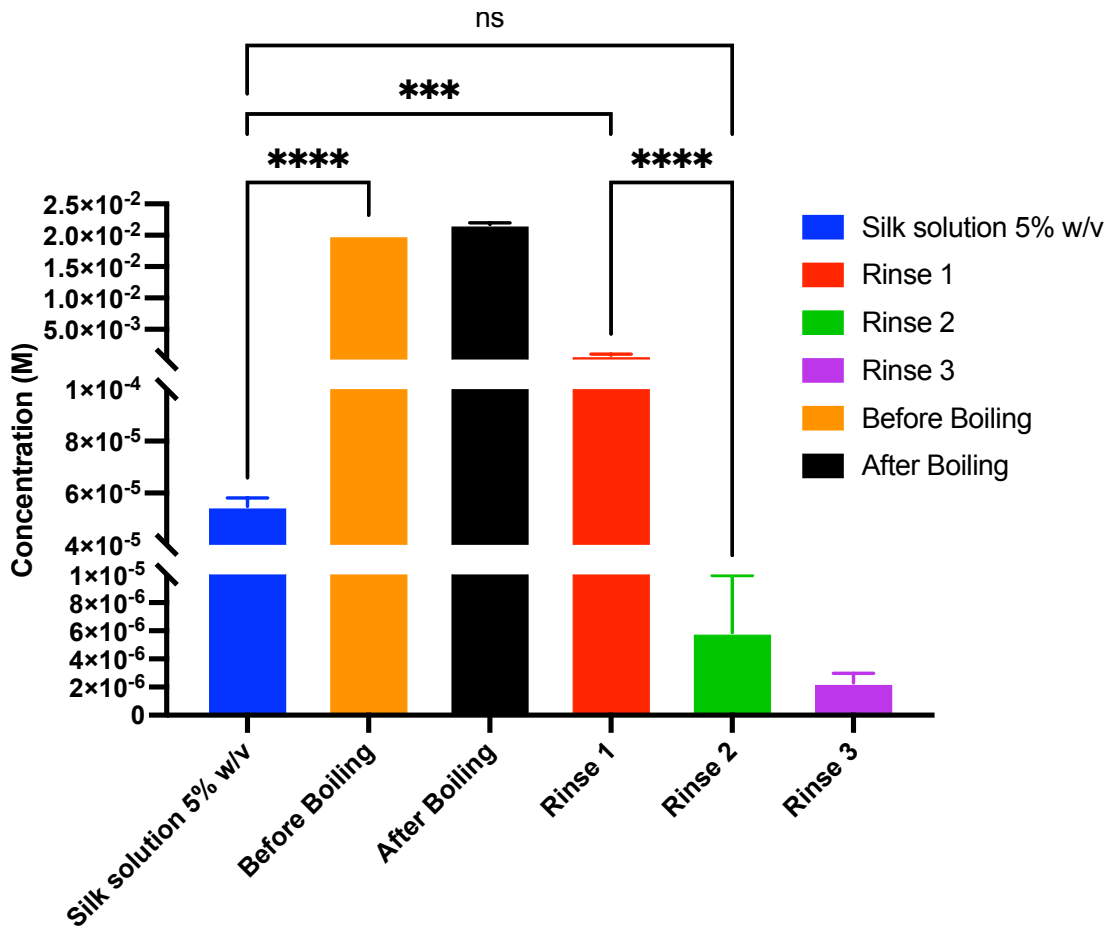


Figure 3-5. Concentration of sodium carbonate in water before and after silk degumming, silk rinsing and in the final silk solution. Data analysis evaluated by one-way ANOVA followed by Tukey's multiple comparisons test ($n = 3, \pm SD$) Asterisks denote statistical significance determined using post-hoc tests as follows: * $p < 0.05$, ** $p < 0.01$, *** $p < 0.001$, **** $p < 0.0001$.

As some sodium carbonate is still present in the silk solution, the bactericidal effects of this were determined (Figure 3-5). As the concentration of sodium carbonate increased, the number of viable bacteria significantly decreased. However, there were still viable bacteria present in the solution at concentrations above what is found in silk solution.

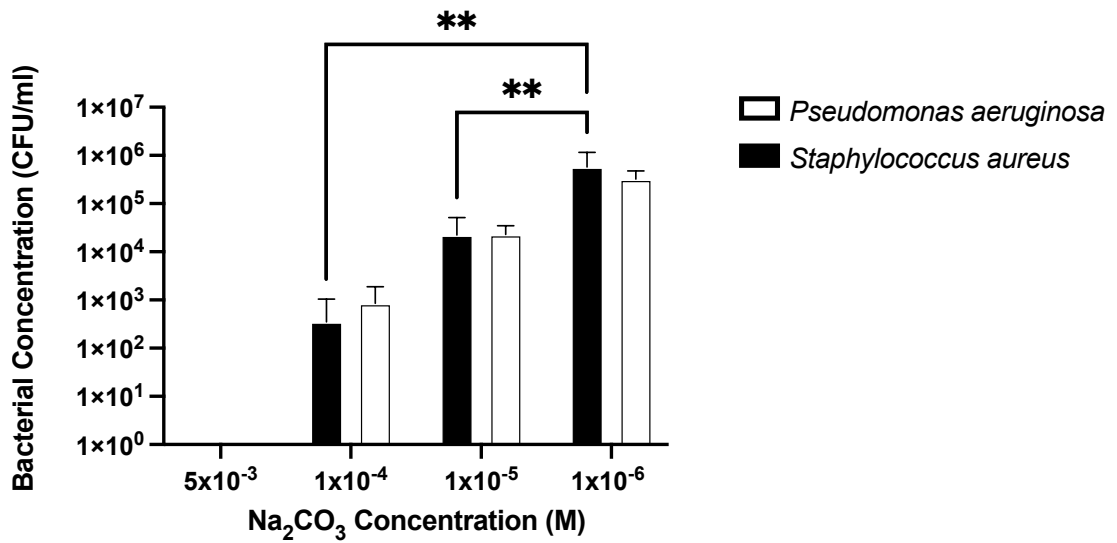


Figure 3-6. Minimum bactericidal concentration of sodium carbonate in water over 24-hour incubation with *Staphylococcus aureus* and *Pseudomonas aeruginosa* Data analysis evaluated by two-way ANOVA followed by Tukey's multiple comparisons test. ($n = 4, \pm SD$). Asterisks denote statistical significance determined using post-hoc tests as follows: * $p < 0.05$, ** $p < 0.01$, *** $p < 0.001$, **** $p < 0.0001$.

3.3.2 Secondary Structure Analysis of Silk

For some of the microbial assays, I exposed silk fibroin to shear forces and elevated temperatures. I therefore felt that assessing possible structural changes was important. I used FTIR to determine the secondary structures of silk fibroin in 1 and 5 % w/v solutions before and after incubation in the orbital incubator at 37 °C, 150 rpm (Figure 3-6). Samples of silk solution were cast and air dried to form silk films. Amorphous control silk films were produced from silk fibroin solution stored at 4 °C. The most common secondary structures were detected in the following order: beta sheets > random coils > turns and > alpha helices. Deconvolution showed that the beta sheets in the amorphous control, 1 and 5 % w/v silk films were 33.91 ± 1.14 , 33.43 ± 1.19 and 35.21 ± 1.43 %, respectively. No statistically significant differences were noted in beta sheet content in the amorphous control films ($p = 0.6572$ for 5 % silk and $p = 0.0601$ for 1 % silk). The other secondary structures also showed no significant differences. By contrast, the ethanol-treated silk film showed an increase in crystalline beta sheets (46.61 % versus 33.91 %).

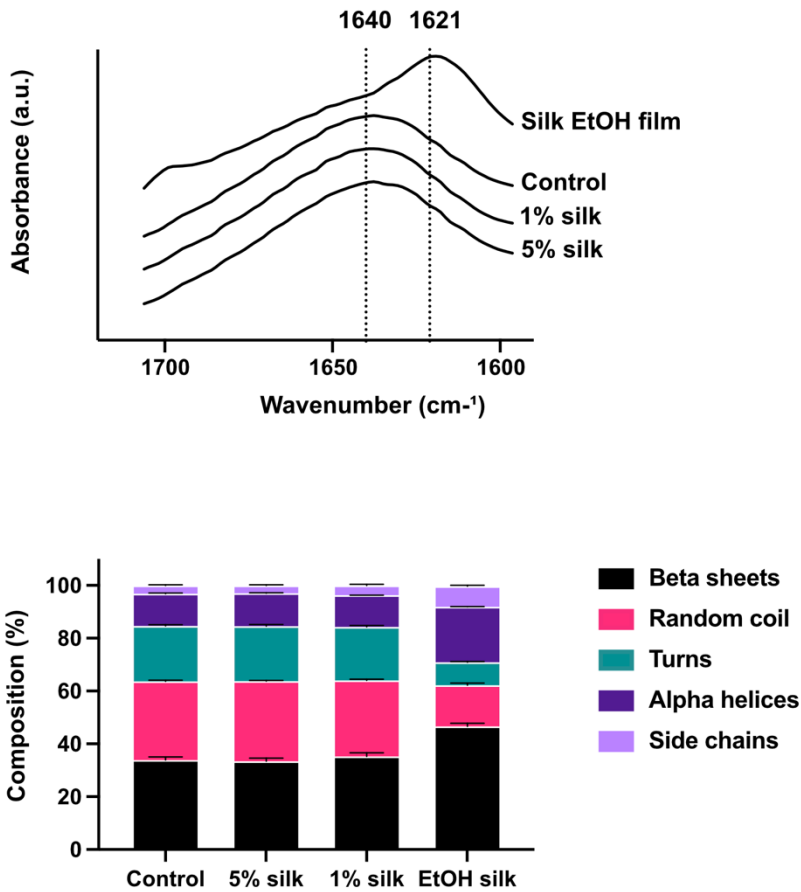



Figure 3-7. FTIR spectra and (C) FTIR analysis of silk fibroin solution incubated in the orbital incubator at 37 °C 150 rpm for 24 h. Silk was air dried into films for analysis. Air-dried amorphous control and ethanol (EtOH) treated crystalline silk film controls (data from chapter 2). Data analysis evaluated by one-way ANOVA followed by Tukey's multiple comparisons test. Asterisks denote statistical significance determined using post-hoc tests as follows: * $p < 0.05$, ** $p < 0.01$, *** $p < 0.001$, **** $p < 0.0001$. ($n = 3, \pm SD$)

3.3.3 Sterility of Aqueous Silk Fibroin

Aqueous protein solutions typically provide a preferred environment for bacterial growth over protein in its dry state. I therefore examined the susceptibility of liquid silk to bacterial spoilage. For my studies, 9 ml tryptic soya broth (TSB) was spiked with a 1 ml silk fibroin 5 % w/v solution. This silk fibroin solution was exposed to various processing conditions. First, freshly prepared silk fibroin solution samples were assessed either "as-obtained" or after filter sterilisation. When fresh as-obtained silk fibroin solution was added to TSB and incubated at either room temperature or 37 °C, turbidity was observed in the solutions at the end of this incubation period. This suggested that the freshly prepared silk solution was contaminated with bacteria. However, turbidity was observed only after 14 days of incubation, suggesting that the bacteria were present at initially low numbers and/or were slow growing. The absence of cloudiness for the filter-sterilised silk solution demonstrated the effectiveness of the filter sterilisation process at removing bacteria (Figure 3-7, "Before storage" column). The turbidity of TSB was assessed according to control experiments (Figure 3-8) but it should be noted that TSB will support growth of any organisms which may display differently to the bacterial controls used. When TSB was spiked with a low number of bacterial cells, initially no turbidity is seen, but after 24 hours of incubation turbidity can be seen at all concentrations of spiked bacteria. This indicates that if contaminants were present even in small numbers, after 24 hours growth should be visible in the TSB.

		Before storage		After storage	
		TSB Incubation for 14 days		TSB Incubation for 14 days	
Silk Storage temp		25°C	37°C	25°C	37°C
Filtered	4°C				
	25°C				
	37°C				
Unfiltered	4°C				
	25°C				
	37°C				



Green box: No growth
Yellow box: Growth

Figure 3-8. Sterility testing of silk solution with TSB. Green and yellow colour coding indicates no growth and growth, respectively. (n = 3)

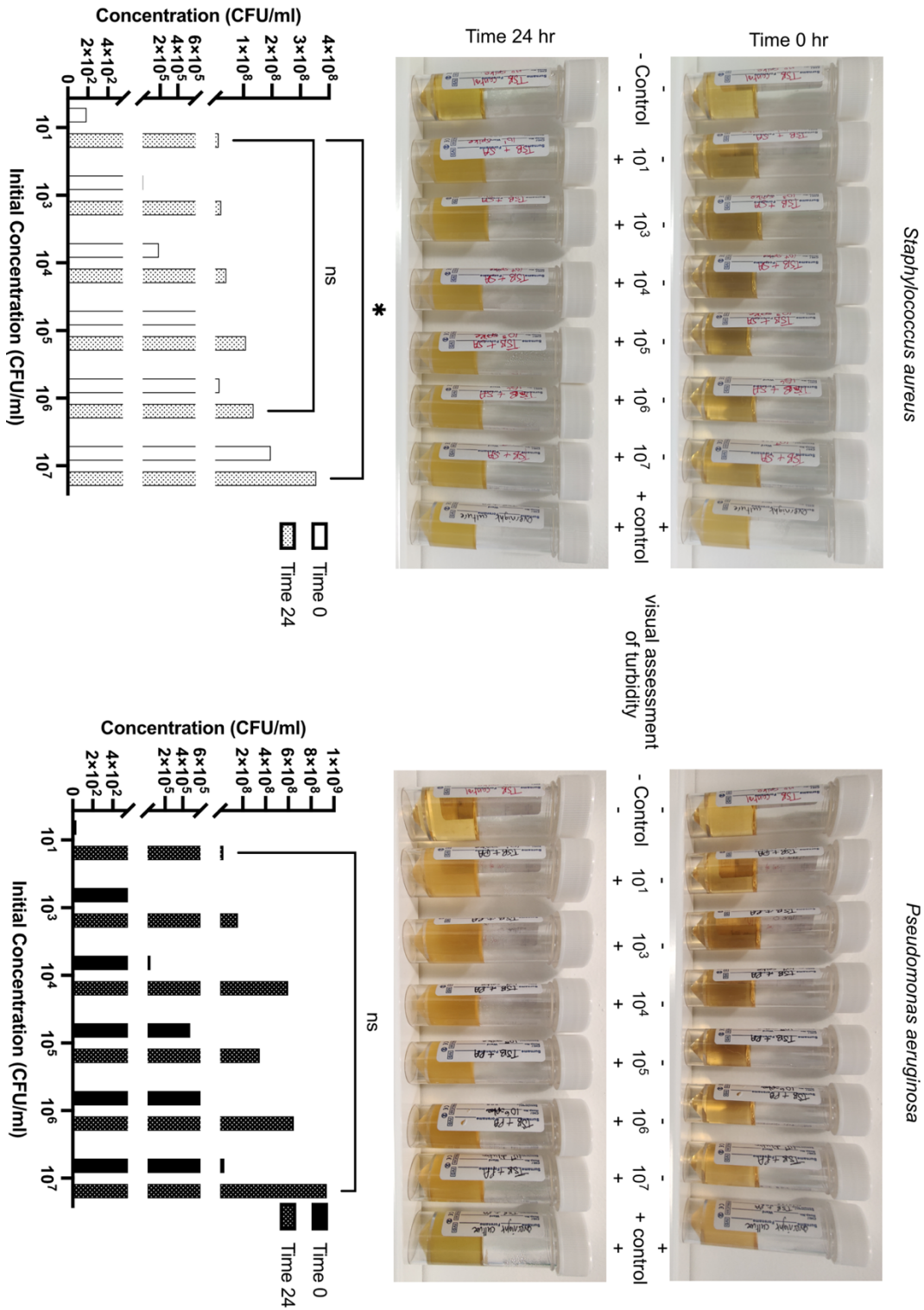


Figure 3-9. Tryptic soya broth (TSB) control testing. Spiked TSB with *Staphylococcus aureus* and *Pseudomonas aeruginosa* at concentrations 10^1 - 10^7 CFU/ml after 24 incubations. Colonies were counted at time 0 and time 24, and solutions were imaged

*and visually assessed for turbidity, indicating contamination. Experiment run in triplicate, n = 1 shown with corresponding images for counted colonies in graphs below. Data analysis evaluated by two-way ANOVA followed by Tukey's multiple comparisons test. Asterisks denote statistical significance determined using post-hoc tests as follows: * $p < 0.05$, ** $p < 0.01$, *** $p < 0.001$, **** $p < 0.0001$.*

I also exposed sterile-filtered and as-prepared silk fibroin solutions to different temperature storage conditions (4 °C, room temperature [~25 °C] or 37 °C) for 14 days. I then used the stored silk samples to spike TSB and incubated the spiked solutions for 14 days at either room temperature or 37 °C. Interestingly, no turbidity was observed in any of these samples (Figure 3-10), suggesting that, although the silk solution was contaminated during preparation, the culture environment was not conducive to bacterial growth and/or survival. Therefore, bacterial growth was only seen before storage of the silk solution, suggesting that bacteria are likely introduced during silk solution processing, but their viability is not supported during storage.

Besides the TSB, I also used agar to identify any colonies that would grow. The sterility of the silk solutions was confirmed by streaking samples of the sterilised and non-sterilised silk fibroin solution, before and after storage for 14 days, onto blood and chocolate agar plates. These plates were incubated either aerobically or anaerobically before final assessment. These enriched agar growth media are formulated for the isolation of pathogenic bacteria (Frobose, et al., 2021). The agar plates showed no growth when plated with silk fibroin before or after storage, broadly supporting the TSB results.

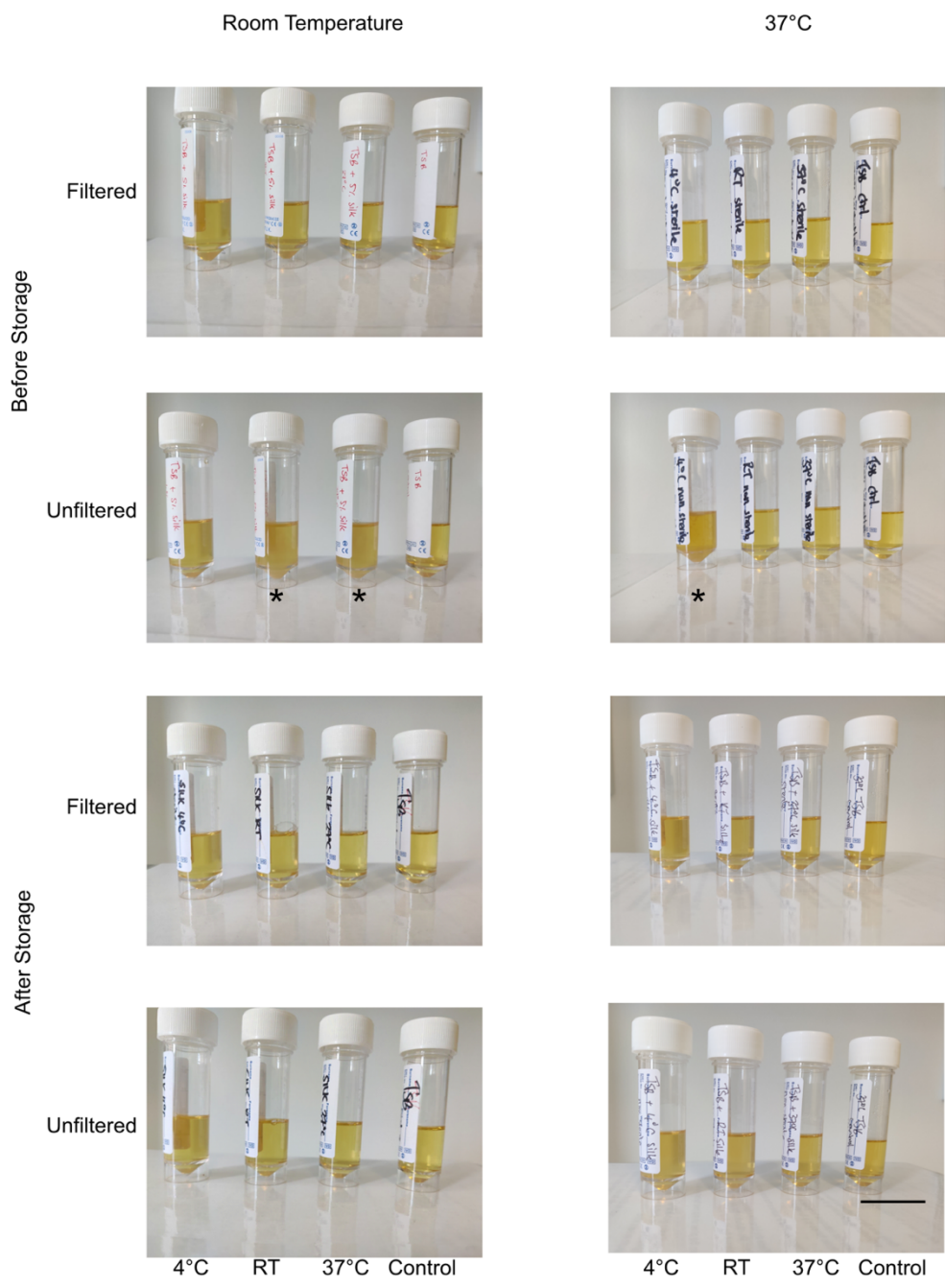


Figure 3-10. Sterility testing of silk fibroin solution 5 % w/v in tryptic soya broth before and after storage at 4 °C, room temperature (RT) and 37 °C for 14 days. The broth was incubated at both room temperature and at 37 °C for 14 days before being imaged.

Control is tryptic soya broth spiked with sterile water 5% v/v. Asterisks denote turbidity observed. Scale bar 4cm (n = 3).

3.3.4 Bacterial growth in the presence of silk

Next, the growth of bacteria in the presence of minimum quantities of liquid silk was determined because aqueous liquid silk fibroin exhibits antibacterial properties. I also conducted control experiments to exclude possible confounders, especially the impact of water on bacterial colony count. Colony counts in water and Luria Bertani Lennox (LB) served as benchmarks for low and high growth conditions, respectively. Water controls were important because an aqueous silk fibroin solution was spiked with pathogens to determine its minimum inhibitory concentration. Specifically, I examined the impact of water on the bacterial strains *S. aureus* and *P. aeruginosa* because these are common wound pathogens (Bowler, et al., 2001) (Bessa, et al., 2015) (Figure 3-11). The contents of sterile water added were 75 %, 85 %, 95 % and 100 % of the total volume, with the remaining volume comprising LB media to control for the presence of nutrients. Silk is an aqueous solution; thus, water control provides the impression of bacterial growth in stronger aqueous solutions. Water was spiked with the pathogens, and colony counting was performed before and after 24-hour incubation.

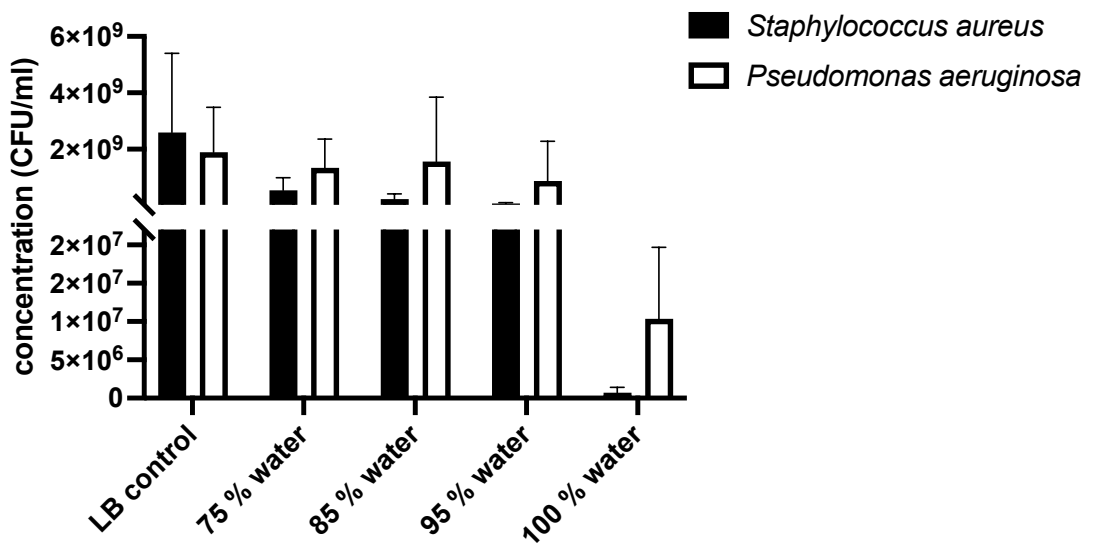


Figure 3-11. Bacterial growth in the presence of water with LB media. Water is spiked with LB media in the ratio 75:25, 85:15, 95:5 or 100:0 (water to LB media). Colonies counted after incubation for 24 hours in each concentration of water. ($n = 3, \pm SD$) Data analysis evaluated by two-way ANOVA followed by Tukey's multiple comparisons test. Asterisks denote statistical significance determined using post-hoc tests as follows: * $p < 0.05$, ** $p < 0.01$, *** $p < 0.001$, **** $p < 0.0001$.

No significant difference was observed in bacterial growth in 75 %–100 % water compared to the 100 % LB control with *S. aureus*, which showed a significant increase ($p = 0.0054$). As compared to spiked 100% water, I observed a significant increase in growth in 75% water with *P. aeruginosa* ($p = 0.0377$) and a more significant increase in LB media ($p = 0.0041$); however, I did not observe any significant change in bacterial colony count in 85–100% water after 24 hours. There was no significant decrease in bacterial growth in up to 95% water, suggesting that the presence of water did not impact the bacteria or their ability to use the nutrients supplied to them by the LB media present in the solution. For the 100% water condition, bacterial growth was reduced. However, these bacteria became viable after water exposure, as demonstrated by LB agar colony enumeration. *P. aeruginosa* was less affected by the presence of water than *S. aureus*.

Next, the impact of silk solution concentrations on *S. aureus* and *P. aeruginosa* colony count was assessed (Figure 3-11). A silk content of 1–5 % w/v affected bacterial growth significantly; both *S. aureus* and *P. aeruginosa* had a significant reduction in the number of bacterial colonies at all concentrations after a 24-hour exposure when compared to the LB control ($p = <0.0001$ at all silk concentrations). Compared to the spiked 100% water control, all silk solution samples showed a significant reduction in bacterial colony numbers with both *S. aureus* and *P. aeruginosa* ($p = 0.0060$ and 0.0821 , respectively). No *S. aureus* colonies were formed at 3 % w/v silk solution and above, whereas *P. aeruginosa* did form a few colonies at 3 % w/v but no growth occurred at 4 % w/v and above.

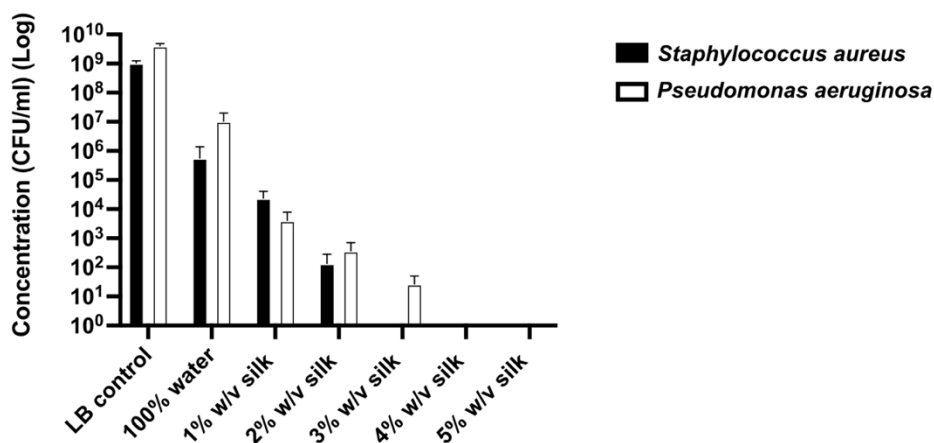


Figure 3-12. Minimum bactericidal concentration of silk fibroin aqueous solution. Colonies present after 24-hour incubation in each pure silk spiked solution concentration ($n = 3, \pm SD$). Data analysis evaluated by two-way ANOVA followed by Šidák's multiple comparisons test. Asterisks denote statistical significance determined using post-hoc tests as follows: * $p < 0.05$, ** $p < 0.01$, *** $p < 0.001$, **** $p < 0.0001$.

3.3.5 Performance of Silk Fibroin-functionalised Wound Pad

As silk does not support growth in the absence of nutrients, I next determined its ability to act as an antimicrobial agent when applied topically to a bacterial suspension. The bacterial inhibition of the silk solution was determined by monitoring the bacterial growth of a silk-functionalised wound pad by exposing it to both LB agar and simulated wound fluid (SWF) agar (Figure 3-12). After wound pad removal, bacterial growth was observed on both types of the agar. *S. aureus* formed light-coloured spherical colonies when cultured on agar plates. On the LB agar plates, the dry sterile wound pad left a growth pattern. The wound pad pores were visible with no growth, implying that the wound pad aided growth on the agar when in direct contact with the surface. When the pad was soaked in 70% v/v ethanol, some growth was still observed at the pad borders, and some cloudiness was left beneath the pad. This suggests that the bacteria in contact with the wound pad surface could not grow, but the moisture may have enabled them to migrate and grow elsewhere. The silk-soaked pad left clearly defined growth borders around the wound pad. On simulated wound fluid agar plates, I observed a similar pattern, with clearly borders around the silk-soaked wound pad, with less defined borders in the ethanol-soaked pad and the dry sterile pad.

The bacterial count of the wound pads after incubation in LB media for 15 minutes showed that when inoculated with *S. aureus*, the wound pad containing 70% v/v ethanol had significantly less bacterial growth than both the sterile dry pad and the silk solution-soaked pad. In contrast, *P. aeruginosa* showed no significant difference

in any of the wound pads. These results, combined with the images of the dressing borders, suggest that, although the silk solution does not increase the bacterial growth of *S. aureus* or *P. aeruginosa*, it also does not reduce it significantly. Thus, the silk solution does not directly kill bacteria, as they grow when nutrients are introduced into their environment.

Ethanol solution is a common antibacterial agent used to destroy pathogens on surfaces (Kampf & Hollingsworth, 2008). The ethanol-soaked wound pad disrupted bacterial growth better than the silk solution-soaked pad, which performed better than the dry pad at restricting growth under the pad on the agar for *S. aureus* (Figure 3-13). The silk solution did not interrupt growth when in direct contact with the bacterial surface, because some growth was still observed under the wound pad around the edge, but the colonies found in and around the pad were not fewer than those observed under dry pad.

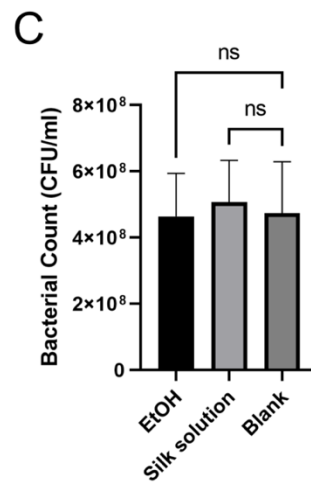
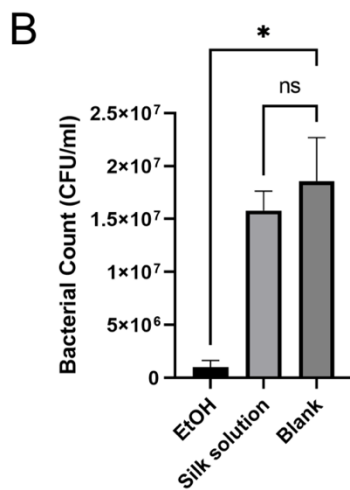
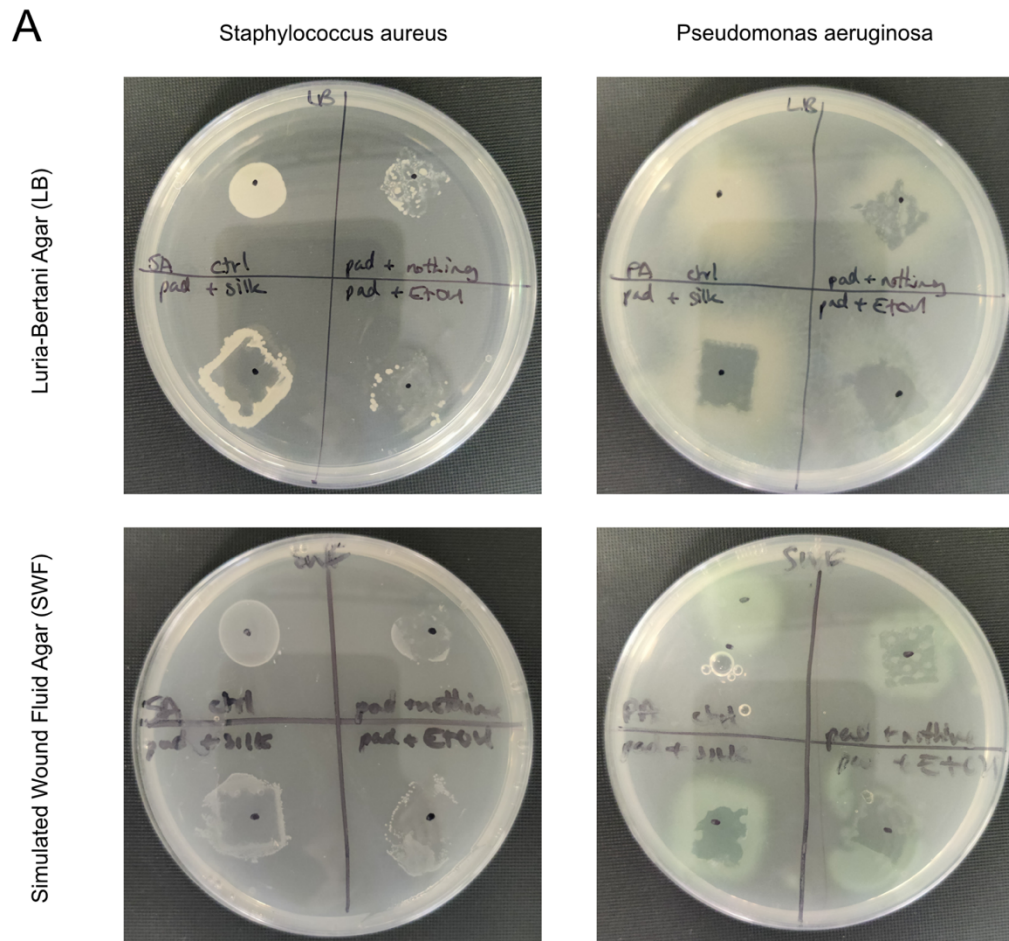


Figure 3-13. Simulated wound environment and the performance of silk-functionalised wound pad. (A) Wound pad dry (control) or soaked in ethanol or silk removed to show growth on LB agar and simulated wound fluid agar. Scale bar 2 cm.

*(B) S. aureus and P. aeruginosa wound pads incubated in LB media and colonies counted. (n = 3, ± SD). Data analysis evaluated by one-way ANOVA followed by Dunnett's multiple comparisons test. Asterisks denote statistical significance determined using post-hoc tests as follows: *p < 0.05, **p < 0.01, ***p < 0.001, ****p < 0.0001.*

3.3.6 Bacterial Viability

Bacterial viability after exposure to the silk fibroin solution was measured through live/dead imaging (Figure 3-13). A reduction in the number of live cells was observed for 100% water, 1% w/v aqueous silk solution and 5% w/v aqueous silk solution for both *S. aureus* and *P. aeruginosa*. The percentage of dead cells increased with the percentage of silk fibroin. The percentages of live *S. aureus* cells were 69% in the LB media and 70% in water. However, 61% and 13% of the cells were alive in 1% and 5% w/v silk solutions, respectively. Similar trends were observed for *P. aeruginosa* in LB media with 72% live cells, decreasing to 48% in 100% water and 48% and 28% in 1% and 5% w/v silk solutions, respectively. To confirm the viability of the stained cells, in parallel studies, samples were streaked onto LB agar. No growth occurred for either bacterial strain when exposed to a 5% w/v silk solution, while some growth occurred for the 1% w/v silk solution.

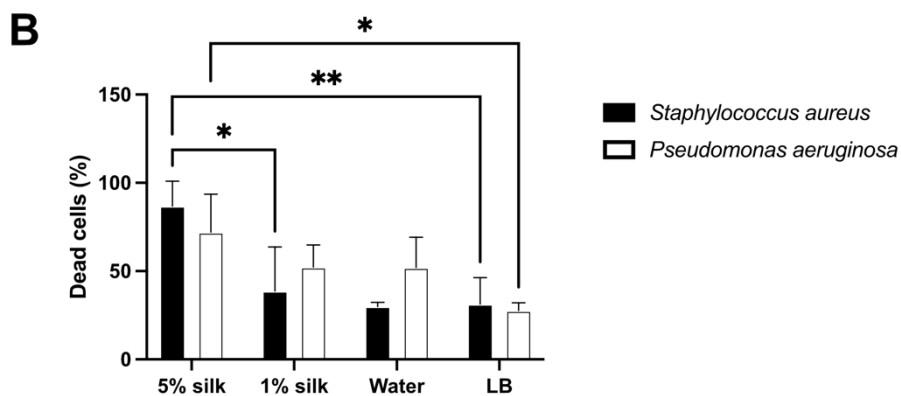
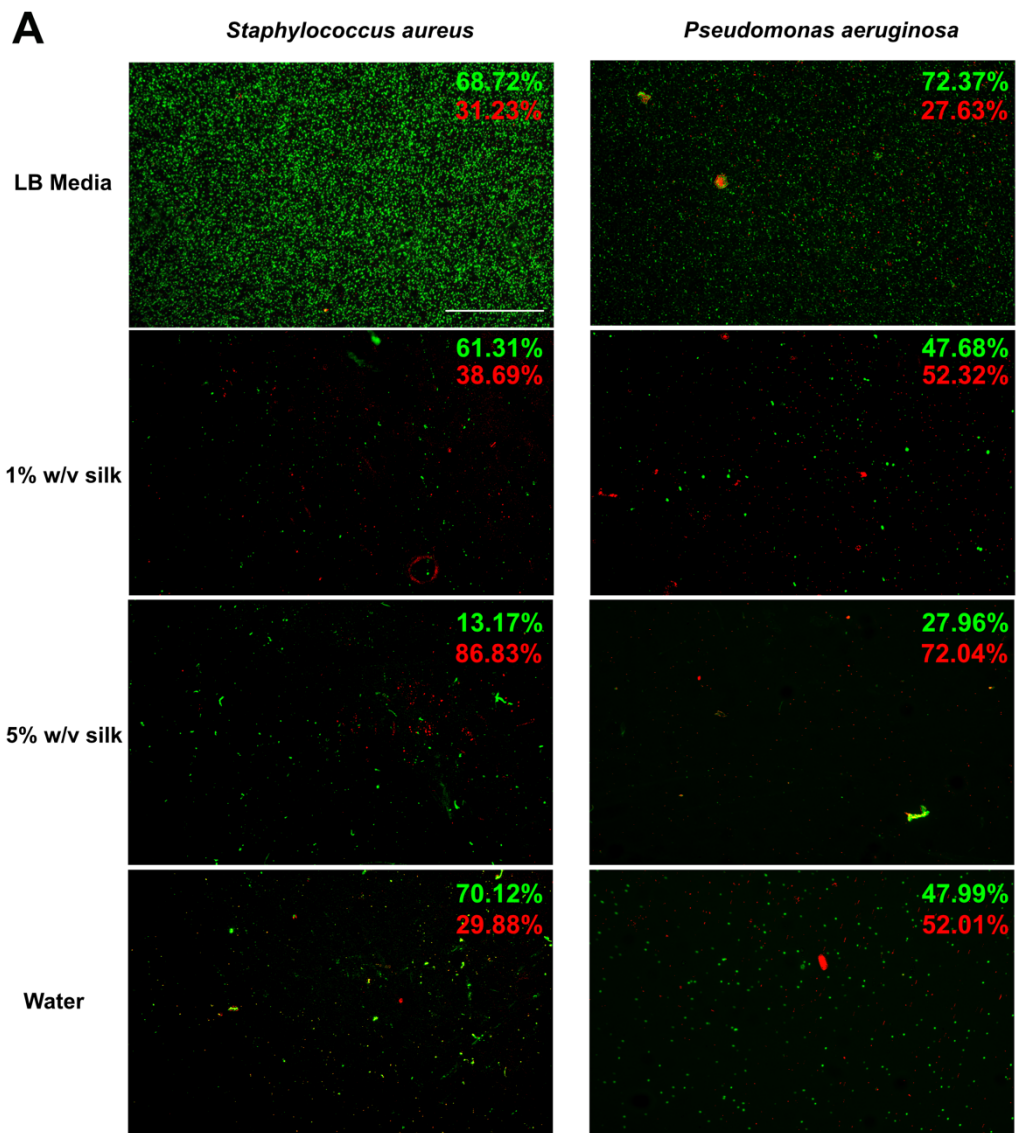


Figure 3-14. Impact of liquid silk on bacterial cell viability. (A) Live/dead fluorescence staining. Green and red indicate live and dead cells, respectively. (Left) *S. aureus* in LB media, 1% w/v silk, 5% w/v silk and water. (Right) *P. aeruginosa* in LB media, 1% w/v silk, 5% w/v silk and water. Scale bar 200 μ m. Numerical result $n = 3$. (B) Percentage of dead cells in each medium ($n = 3$, \pm SD). Data analysis evaluated by two-way ANOVA

*followed by Šídák's multiple comparisons test. Asterisks denote statistical significance determined using post-hoc tests as follows: * $p < 0.05$, ** $p < 0.01$, *** $p < 0.001$, **** $p < 0.0001$.*

3.4 Discussion

Silk fibroin has many desirable attributes that lend themselves to diverse applications, such as biocompatibility and biodegradability. One area in which silk is making inroads is wound healing, and soluble silk fibroin has been found to be an effective treatment for dry eye and can improve tear production and epithelial healing. Despite this, the inherent biocompatibility has not been investigated with antibacterial properties. This work investigates the inherent sterility of regenerated silk.

This evaluation is important because the reverse engineering of silk fibres into a silk fibroin solution requires that the silk molecule be dissolved to dismantle higher order structures. For example, I used a 9.3 M lithium bromide (LiBr) solution to disrupt robust beta sheet secondary structures. Therefore, contaminating LiBr could impact bacteria viability. Previous studies have shown that the choice of silk fibroin extraction protocol can influence the antibiotic activity of silk films (Abdel-Fattah, et al., 2015), and how much of this reported effect can be attributed to contamination remains to be determined. In the present work, the reduction in conductivity to baseline levels suggests that lithium bromide was quantitatively removed. Similarly, sodium carbonate can have bactericidal effects at elevated concentrations (Jarvis, et al., 2001). The results suggested that there was sodium carbonate remaining in the silk solution which could be an influence on the bactericidal effects seen. As silk solution was found to obtain around 50 μ M sodium carbonate, I proposed that the bactericidal effects of silk could not be fully attributed to the presence of sodium

carbonate. The numbers of both bacteria were reduced as sodium carbonate concentration increased, indicating a correlation between survival of bacteria and the presence of sodium carbonate.

Elevated temperatures and shearing forces can trigger structural changes in an amorphous silk solution (Toprakcioglu & Knowles, 2021). Therefore, monitoring the impact of incubation and shear on secondary structure was also deemed important. In the case of secondary structure changes, I expected a higher percentage of beta sheets and a reduced percentage of amorphous structures. No conformational changes were observed, indicating that the crystallinity of the silk fibroin solution was unaffected by incubation at 37 °C and rocking at 150 rpm for 24 h.

The contamination of TSB samples was only seen before storage of silk solution in any condition, which may suggest that bacteria could be present in the silk solution prior to filtration. This could be introduced at any stage in the silk production as the methods used are not sterile and are performed on an open bench. After storage, even at 37 °C, none of the silk solution in TSB showed any signs of contamination or bacterial growth. This result seems to suggest that although silk solution can become contaminated, the environment is not conducive to bacterial growth and, in fact, survival. TSB was examined visually for turbidity (Galvez, et al., 2014) but further quantification of turbidity should be performed using a spectrophotometer and can be compared against a McFarland standard (Carlotti, 2023) measuring the optical density of each solution (Metris, et al., 2003).

This sterility was verified with culturing on blood and chocolate agar in aerobic and anaerobic conditions to confirm that no fastidious species of bacteria were present.

The enriched growth medium would allow the isolation of pathogenic bacteria. The agar plates indicated no growth would occur before or after storage, which supports the TSB result, and indicates that if contamination was present, it was slow growing and would not grow without the presence of nutrients supplied by the TSB. The finding of samples that showed bacterial contamination with the TSB method suggested that growth was slow and required the nutrients supplied by TSB (and not available in the agar plates). Overall, these results suggest that the regenerated silk fibroin solution has an inherent ability to attain and maintain sterility for 2 weeks. This is an interesting discovery because many sterilisation techniques adversely affect the silk molecule (through molecular weight reduction, polydispersity etc.) and the silk solution properties (e.g. premature self-assembly) (Rnjak-Kovacina, et al., 2015, Zhao, et al., 2011, Hashimoto, et al., 2020, George, et al., 2013).

The ability of two strains of bacteria to survive and grow in water in the presence of LB media at different concentrations was assessed. There was no significant decrease in growth in up to 95 % water, suggesting that the presence of water has not impacted on the bacteria and their ability to utilize the nutrients available to them. At 100 % water, the growth of both pathogens was reduced over 24 hours, but there were still bacteria present and able to grow after incubation on LB agar. This indicates that both strains of bacteria do not die in water, but their growth would be impeded. *P aeruginosa* is less affected by the presence of water than *S aureus*. Water activity is defined as the ratio of the vapor pressure of water to that of pure water, which can be used to measure water that is available to be reacted with or attached to other materials. Higher water activity can support more microorganisms, with bacteria

requiring water activity levels of at least 0.91 to grow (Allen Jr, 2018). Distilled water has a water activity of 1. This is based on the fact that Milli-Q water has a water activity of >0.91, as bacteria do not proliferate well but do survive in this form of water (Hallsworth, 2022). I speculate that water forced the cells into a low or zero growth rate due to a lack of nutrients. The ability of water to preserve pathogens for long-term storage (>30 weeks) suggests that water cannot affect the survival and viability of some bacteria (Liao & Shollenberger, 2003).

In contrast to this, when silk solution was inoculated with either pathogen, bacteria seemed to be compromised and no longer viable. At the higher percentages of silk tested, no colonies were detected after incubation over 24 hours. In 100 % water cells were able to survive after incubation overnight, which suggests that the silk fibroin itself has an impact on the bacterial viability when the solution is directly contaminated. When the silk content was increased above 3% w/v in the aqueous solution, no colonies were detected. This suggests that the silk fibroin solution itself impacted bacterial viability, which is attributable to the alteration of water activity due to the addition of silk fibroin. Silk may decrease the amount of 'free' water, reducing the water activity below the threshold and allowing the solution to become self-preserving, as supported by previously obtained sterility results (Cundell, 2015) (Peleg, et al., 2015). Silkworms produce antimicrobial peptides (AMPs), such as cecropins, which effectively protect gram-positive and gram-negative bacteria from infection (Mastore, et al., 2021). Silk fibroin has a 5-amino-acid block 'glycine-alanine-glycine-alanine-glycine-serine' (GAGAGS) sequence, which can assemble into β sheets in crystalline form but remains open in amorphous form, such as in aqueous

solution. Glycine inhibits the growth of some bacteria and has been used as a non-specific antiseptic agent (Minami, et al., 2004); thus, the structure of silk can exhibit similar antiseptic effects on the bacteria in solution. One consideration is the degradation of silk by enzymes produced by the bacteria. Silk has been shown to be subject to biological degradation by proteolytic enzymes such as chymotrypsin, actinase, and carboxylase (Cao & Wang, 2009). Silk fibres have also been shown to degrade in soil due to bacterial presence (Seves, et al., 1998). Future studies could investigate the longevity of the effects of silk on bacteria and look into the effects of enzymes on the antibacterial properties of the silk solution.

The viability of the bacterial cells was determined by live/dead staining to confirm the results of colony counting. Interestingly, these results did not conclusively determine that all the bacterial cells in the presence of 5 % silk were “dead”, but rather that a smaller number of cells stained were “live” with more staining dead in the 5 % silk samples, and less with the water and LB media controls. The bacterial stain for dead cells can only enter cells when the membrane has been disrupted, which indicates that the method of silk inhibiting the bacteria is not solely by affecting the bacterial membranes. When the cells were cultured on LB agar to confirm the viability of the cells, there were no colonies present in 5 % silk. This result, combined with the staining result, suggests that bacteria may be intact in the soluble silk, but are unable to grow and survive, even if introduced to nutrients after being exposed to silk fibroin. Pelegrini et al (2008) have previously identified glycine-rich plant defence peptides for antibacterial purposes, determining that the interaction with

the lipid layer of the bacterial cell wall causes cell death. Silk fibroin is composed of a heavy and a light chain, with the amino acid composition of the heavy chain containing 46 % glycine. Silk solution contains amorphous regions which are not tightly packed, which may allow the glycine regions to have this effect on the bacteria when exposed to them.

The next stage was to determine if silk maintained the antibacterial effects in the presence of nutrients by monitoring growth on nutrient agars in the presence and absence of silk solution. Ethanol solution is a common antibacterial agent used to destroy pathogens on the surface. The ethanol-soaked wound pad appeared to disrupt growth more than the silk solution-soaked pad, which performed better than the dry pad at restricting growth under the pad on the agar. Silk solution does seem to interrupt growth when in direct contact with the bacterial surface, but the colonies found in and around the pad were not fewer than the dry pad. This indicates that in the presence of nutrients, the antibacterial effects of silk are limited, and the presence of a solution may allow bacteria to move around the antibacterial agent to grow and thrive elsewhere. In future, further studies can be done with a water-soaked pad to determine if the movement of bacteria is altered in the presence of a wet pad. A dry pad was used to determine the ability of an unaltered wound dressing to disrupt the growth of bacteria on the agar plates.

Therefore, I speculate that the silk solution displaced the bacteria around the wound pad. Bacteria may not grow directly in the presence of silk but are not killed; instead, they grow on the enriched agar medium around the pad. *P. aeruginosa* formed less-defined colonies, with green pyocyanin readily visible around the colonies. On the LB

agar plates, the sterile dry pad left a clear pattern of contact with the wound pad. The ethanol-soaked pad left a visible rough border of growth, while the silk-soaked pad left clear borders where growth did not occur on the agar plates. On simulated wound fluid agar plates, a similar growth pattern was observed, with borders around the ethanol-and silk-soaked wound pads and a visible pattern where the dry pad was previously placed. This is similar to the results obtained for the interaction with *S. aureus*, indicating that these strains act similarly in response to a silk solution and an ethanol solution.

These results are interesting, as pure aqueous silk shows sterility when stored over time, and when a pure silk solution is inoculated with pathogens directly, but used in addition to nutrient agar, bacterial growth occurs. This indicates that silk is bacteriostatic and not directly bactericidal.

This indicates that, in the presence of nutrients, the antibacterial effects of silk are limited. The presence of a solution can also enable bacteria migration, ultimately allowing them to navigate away from the antibacterial agent to grow and thrive elsewhere. Antibacterial effects of *Bombyx mori* silk have been postulated because the silk cocoon, and the raw silk fibre, demonstrate antibacterial effects (Dong, et al., 2023). This property has been attributed to seroins and sericin that are present in raw silk (Zhu, et al., 2020). Sericin has shown high antibacterial activity (Kaur, et al., 2013, Singh, et al., 2014, Rajendran, et al., 2011). However, Jaseet Kaur and colleagues showed that pure silk fibroin and fibres lacked antibacterial properties against *Escherichia coli* contrasting earlier studies. This discrepancy was attributed to

residual processing chemicals present in earlier studies (Kaur, et al., 2013, Seves, et al., 1998).

This study also demonstrates that, in the presence of silk (e.g., 5% w/v), some viable bacterial cells still exist (albeit at much lower levels than the controls). However, when these silk-exposed cells were subsequently cultured on LB agar, no colonies were detected. Overall, these results suggest that some bacteria still had an intact plasma membrane after exposure to soluble silk but were unable to grow and ultimately survive, even in favourable growth conditions. Pelegrini et al. (2008) identified glycine-rich plant defence peptides for antibacterial purposes, determining that the interaction with the lipid layer of the bacterial cell wall causes cell death. A silk fibroin heavy chain contains 46% glycine (Zhou, et al., 2000); however, the silk fibroin molecule also contains amorphous regions in the heavy chain, which provides flexibility and mobility to the molecule. I speculated that this allows the glycine-rich silk fibroin regions to have their antibacterial effect.

3.5 Conclusion

A silk fibroin aqueous solution has inherent antimicrobial effects. A silk solution with $\geq 4\%$ w/v silk fibroin could inactivate *S. aureus* and *P. aeruginosa* contaminations. The silk solution did not support bacterial growth or survival. This opens up the possibility of using aqueous silk in biomedical applications. Importantly, liquid silk stored prior to processing is unlikely to experience microbial spoilage. This simplifies the handling and processing of liquid silk. However, this study also shows when liquid silk was applied to a simulated infected wound in the presence of nutrients, the antibacterial

effects of the silk solution are not as effective. Overall, these results indicate that liquid silk is unlikely to spoil during storage, but terminal sterilization of the final product is recommended.

4. Chapter 4 “Manipulating silk to conformable shape and patterned functional biomaterial”

Here, an initial study into the production of hydrogels and silk films to be cast with micropatterns was performed. This work began before the Covid-19 pandemic forced the University closures which affected the progress of these results. Upon reopening of the University, a tangential study was undertaken where the ability of silk films to be loaded with magnetic iron oxide nanoparticles and curcumin was tested. This study was initiated to maximise outputs during restricted lab access. The folding of silk films was also monitored alongside the swelling and locomotion of films. Finally, the response of the curcumin loaded films to pH changes was measured.

Much of this work presented in this chapter has been published as an original article (Matthew, et al., 2022) and has been adapted accordingly for this thesis. Data acquisition and analysis for figures 4-1 – 4-11, and 4-17 – 4-20, was conducted by me. This included fabrication of silk films and water annealing, curcumin loading, iron oxide and silk fibre loading, colour change of curcumin in response to pH and pollutants, swelling analysis, electromagnetic field strength and semi-autonomy testing and thickness assessment of films. Data acquisition and data analysis for figures 4-12 – 4-20, which included anthocyanin extraction and loading, and diazonium coupling, SEM, water contact angle, thermal analysis and FTIR was performed by Saphia Matthew. Matthew was supported by Dr Kimia Witte, Dr Suttinee Phuagkhaopong, Jirada Kaechuchuen and Dr John Totten. As joint lead

author of this paper, Saphia Matthew and I contributed equally to the data acquisition and analysis.

4.1 Introduction

Micropatterns

Micropatterns are patterned microstructures on a substrate with sizes ranging from nanometres to micrometres and can often be exhibited in nature. These micropatterns often perform functions such as modified hydrophobicity and antifouling properties, adhesive properties, and for colour through interaction with light (Wang, et al., 2023). Recent studies have involved the investigation of micropatterned bacterial cellulose for scar free wound healing by encouraging cell-oriented growth (Liu, et al., 2023). Silk fibroin/gelatine composites have also been investigated with micropatterns for wound healing which were able to guide cell growth along patterns to promote wound closure and angiogenesis (Li, et al., 2023). Pure silk fibroin has been manufactured with micropatterns previously (Youn, et al., 2021, Sun, et al., 2021, Wang, et al., 2019) using methods such as photolithography which requires photoreactive acrylate groups. Silk has been mixed with eumelanin nanoparticles to produce bioelectric films with diverse potential for tissue engineering and bioelectronics (Youn, et al., 2021). Silk films can have conformational changes induced by exposure to water vapour, UV radiation or methanol. Wrinkled structures were formed through polar interactions altering the hydrogel bonding within the silk film and inducing beta-sheet formation which results in an insoluble film (Wang, et al., 2019). Another method of micropatterning used with silk is inkjet printing on electro spun silk scaffolds with I3K peptide nanofibers (Sun, et al., 2021). Silk films have previously been cast on polydimethylsiloxane (PDMS) to incorporate microfluidic designs (Bettinger, et al., 2007), for patterning films for corneal epithelial

wound healing (Luo, et al., 2021), and for drug delivery mechanisms (Lecomte, et al., 2015). Silk hydrogels have also been micropatterned through different methods such as using HFIP as a crosslinking agent on a PDMS stamp to create a pattern (Gu, et al., 2021).

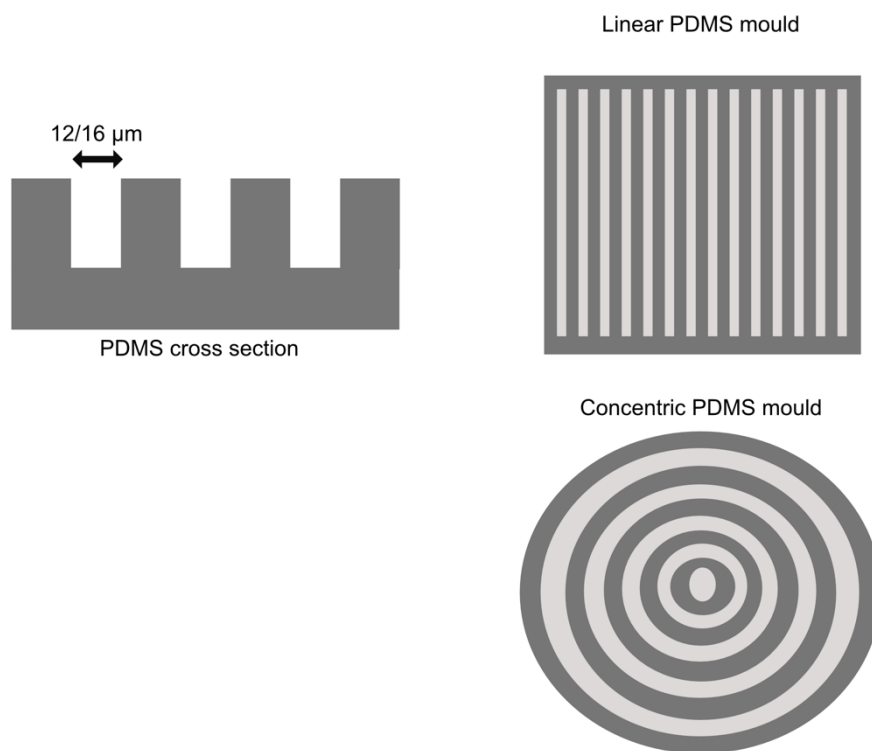


Figure 4-1. PDMS mould diagram. PDMS was cast with grooves 12 or 16 μm apart in linear and concentric circle patterns.

Cells respond to topographical changes, although specific responses to differing features have not yet been defined (Ventre, et al., 2014). Cells can potentially be influenced by the topography of a surface through the signalling pathways relating to stem cell differentiation (Kang, et al., 2019), cell migration (Lawrence, et al., 2012), cellular alignment and focal adhesion localisation (Lawrence, et al., 2012). Topographical changes can alter the surface tension which can direct tissue shape and growth (Ehrig, et al., 2019, Heller & Fuchs, 2015). Wang et al. (2017) found cell morphology differences, with HUVEC cells able to attach and spread on flat silk films, remaining flat and circular. In comparison, when the cells were grown on linear patterns with varied well length, cells stretched and displayed an elongated morphology.

Bacterial cell walls and morphology have been investigated as the mechanism of survival in diverse environments (Yang, et al., 2016). Bacteria will colonise on a surface before forming a biofilm through a cascade of signalling and development. A biofilm is formed when bacteria secrete an extracellular matrix that protects the bacteria from external interruption with antibiotics or cells from the immune system. Disrupting the formation of the biofilm is a key method of reducing infection and colonisation of bacteria (Sharma, et al., 2019, Donlan & Costerton, 2002). Many current methods of reducing biofilm formation involve the use of chemical or antimicrobial drugs which can damage surfaces or risk increasing the rate of antimicrobial resistance (Francolini & Donelli, 2010, Lewis, 2008). Micro patterns on surfaces have been demonstrated to reduce bacterial colonisation and biofilm formation. The reason for this has been hypothesised to be that bacteria cannot

adhere to the surface in a way to support colonisation (May, et al., 2014, Ghavamian, et al., 2021, Mendez, et al., 2018). This method of utilising patterned surfaces to reduce bacterial fouling of surfaces can be implemented on a variety of surfaces with a broad variety of uses (Cuello, et al., 2020). Commonly infected surfaces such as implantable biomaterials could make use of micropatterns to influence cell behaviour on the surface and reduce bacterial colonisation without resorting to the use of chemical or antibiotic drugs, improving patient outcomes and biomaterial longevity (Xu, et al., 2017).

Silk in drug delivery

Silk has been used as a drug carrier due to the proven biocompatibility, tunable degradation and capacity to maintain the function of the drugs bound. Many formats have been investigated, such as nanoparticles for anticancer drugs (Xiao, et al., 2016). Silk nanoparticles have been used to deliver paclitaxel, doxorubicin, and curcumin, which has shown biological activity when attached to silk (Wani & Veerabhadrapa, 2018).

Natural Agents and their applications in wound healing

The turmeric plant has three curcuminoids, one of which is curcumin. It is thought that curcumin can have an effect on the physiological and molecular processes involved in the inflammatory and proliferative phase of wound healing (Kumari, et al., 2022, Akbik, et al., 2014, Hewlings & Kalman, 2017). Within the inflammatory phase, curcumin has a protective effect, reducing the expression of pro-inflammatory cytokines (Dai, et al., 2017, Emiroglu, et al., 2017). Anthocyanins are phenolic water soluble pigments that can be found in berries, currants, grapes, grains, roots, tubers,

and purple coloured leafy vegetables (Khoo, et al., 2017). Anthocyanins have been shown to have antioxidant and anti-inflammatory effects with many nutraceutical properties that can help health, and when applied to wounds have been shown to improve wound healing by having a cytoprotective effect, reducing inflammation, and improving angiogenesis (Xu, et al., 2013)

Silk Origami and Water Fouling

Silk adaptability

The craftsman art of origami has been used for over four centuries to change a flat material into a complex 3D shape (Li, et al., 2019). Folding is an easy, cost-effective and scalable fabrication method; (Li, et al., 2019) therefore, origami has inspired a variety of structures over a wide size range, from DNA-origami (Dey, et al., 2021) and soft robotics (Fang, et al., 2017, Ryu, et al., 2020) to metre-scale shelters (Melancon, et al., 2021). In soft robotics, tailoring the stiffness and softness of the flat material is important for obtaining a compliant, foldable architecture which preserves its final shape (Mintchev, et al., 2018). The origami folds can endow the structure with attractive mechanical properties, such as load bearing capacity (Li, et al., 2019, Zhai, et al., 2018) and impact absorption; (Qi, et al., 2021, Xiang, et al., 2020) consequently, folds are being increasingly incorporated into soft robotics (Ryu, et al., 2020, Mintchev, et al., 2018, Faber, et al., 2018).

Iron Oxide

Iron oxides possess potential in biomedicine due to the magnetism they exhibit. This has been investigated with coatings for iron oxide nanoparticles with organic or inorganic molecules, such as drugs, proteins, or enzymes, that can be directed to sites

within the body using an external magnetic field (Ali, et al., 2016). Iron and iron oxides are naturally found in the environment and are generally considered to be non-toxic (Wang, et al., 2016). The iron oxide can also be extracted by using a magnet from the environment, making it a sustainable option for eco-friendly applications. Iron oxides have also been used in medical imaging such as magnetic resonance imaging and was found not to be toxic to human monocyte-macrophages in vitro (Muller, et al., 2007).

Current techniques

Soft robots, which can convert external physical forces to mechanical force, have attracted growing interest for a diverse range of applications, including drug delivery, (Setti & Wiersma, 2020, Medina-Sanchez, et al., 2018) biomedical devices (Setti & Wiersma, 2020, Medina-Sanchez, et al., 2018, Wei, et al., 2017) and sensors (Wei, et al., 2017, Zhou, et al., 2018, Wang, et al., 2020). Examples of external stimuli used as energy sources for locomotion include thermal energy, (Kim, et al., 2020) humidity, (Zhou, et al., 2018, Xu, et al., 2020, Zhao, et al., 2020, Wani, et al., 2019, Ge, et al., 2018) chemical, (Wang, et al., 2020) and optical (Kim, et al., 2020, Jia, et al., 2020), and magnetic fields (Ji, et al., 2017). Among these sources, magnetic fields typically result in rapid and directional actuation over long ranges. Materials for smart actuators range from graphene (Jia, et al., 2021) and metal–organic frameworks (Park, et al., 2017) to synthetic polymers (Du, et al., 2020). However, these materials can raise environmental sustainability issues and require harsh, multi-step reaction conditions for production; therefore, emphasis is shifting to bioresorbable metals (Hartmann, et al., 2020) and eco-friendly polymers (Wang, et al., 2020, Zhao, et al., 2020, Wei, et al., 2021, Boonkanon, et al., 2020) that are naturally sourced,

renewable and biodegradable. The ecological footprint of waterborne robots is particularly important, as freshwater, and marine environments are already negatively impacted by plastic and chemical pollution (Aracri, et al., 2021).

Water fouling

A global need exists for in situ water quality monitoring of large or complex water distribution systems and wastewater effluents to mitigate the impact of environmental contaminants on health (Dhanwani, et al., 2021, Vikesland, 2018, Munoz & Pumera, 2020). Miniaturised optical (Vikesland, 2018), electrical (Vikesland, 2018) (Horne, et al., 2020), magnetic (Vikesland, 2018) and chemical sensors (Vikesland, 2018, Horne, et al., 2020, Nawaz, et al., 2021, Kim, et al., 2021) capable of on-site detection provide a promising alternative to slow traditional analytical methods. These technologies should be inherently green themselves, so interest is growing in developing non-toxic, natural colourimetric indicators loaded within a biopolymer matrix as eco-green chemical sensors. For example, curcuminoids from turmeric and anthocyanins from red-pigmented plants are metal and pH-responsive dyes (Chen, et al., 2020, Wiczowski, et al., 2013) and have been used with biodegradable polymers including chitosan (Halasz & Csoka, 2018, Fernandez-Marin, et al., 2022), corn and tapioca starch (Boonkanon, et al., 2020, Chen, et al., 2020, Luchese, et al., 2017) as visual pH-sensing films. However, at present, no silk fibroin matrices or complete examples of portable eco-green sensors have been reported. The folding of biocompatible (DeBari, et al., 2021) silk fibroin films into reusable origami robots could serve as a simple approach for the fabrication of eco-friendly early warning systems for waterborne pollutants.

Chapter Aims

In this chapter the ability of sonicated silk hydrogels and films to adopt a micropattern is investigated. The effect the micropattern has on fibroblasts was then recorded. In the present study, 3D silk structures were folded via cast moulding of liquid silk and plasticisation of the 2D film through water annealing. Liquid silk was also spiked with iron oxide particles to realise semi-autonomous films with an electromagnetic field strength of 1.8 mm g^{-1} at an iron oxide doping concentration of 0.1 % (w/w) of silk protein. The surface of water-insoluble films was also modified by diazonium coupling with benzene diazonium to increase hydrophobic repulsive forces, and this, in turn, increased the buoyancy and electromagnetic field strength of the resulting azosilk. Both native and azosilk films could be loaded with curcumin and anthocyanin to fabricate colourimetric 3D silk boats for detection of heavy metal salts and surfactants at harmful aqueous concentrations, thereby demonstrating their potential in pollution sensing applications. A summary of the aims of the chapter can be seen in Figure 4-2.

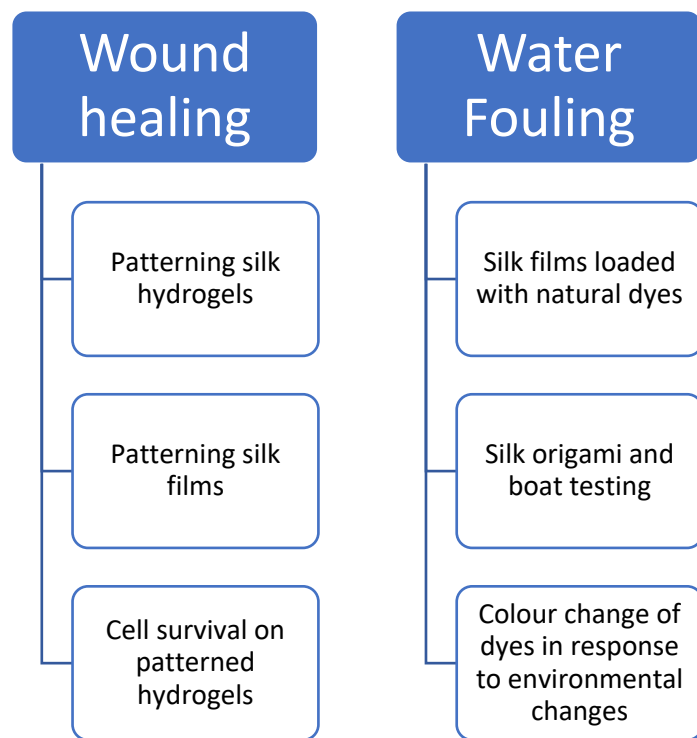


Figure 4-2. Chapter aims. The aims are split into 2 main sections: wound healing, and water fouling. Each aim has objectives listed underneath.

4.2 Experimental

Silk solution was prepared as before, described in Chapter 2.2.1.

4.2.1 Silk patterning

4.2.1.1 Silk film patterning

Silk solution was diluted to 3 % w/v before being added to a diffraction grate (Newport Corporation, New York, USA). Volumes up to 0.5 ml were added to the surface before being left to air dry overnight. Once the film was cast, the film was removed using tweezers to peel it apart from the diffraction grate surface. Films were also cast on PDMS surfaces with varying patterns of 10, 12 and 16 μm lines and concentric circle patterns. Similarly, up to 0.5 ml silk was added to the surface of these before air drying overnight. Once the films were dry, they were removed using tweezers once again.

4.2.1.2 Silk hydrogel patterning

Silk solution was diluted to 3 % w/v before undergoing sonication to induce sol-gel transitioning. The solution was kept on ice during the process to reduce heat and sonicated at 45 amplitude for 4-6 30 second cycles of on-off-on. Before the gel had set, the sol-gel solution was cast on patterned PDMS with linear channels at 10, 12 and 16 μm and concentric circles at the same distance, and blank control PDMS surfaces. This was left to gelate at room temperature for 1 hour before being transferred to the fridge and stored at 4 °C. To produce sterile hydrogels for cell studies, silk solution was filtered using 0.2 μm filters before dilution to 3 % (w/v) silk solution with sterile water.

NIH3T3 mouse fibroblasts were cultured as described previously (Chapter 2.2.9). Prior to cell seeding, hydrogels were incubated in DMEM overnight. Briefly, patterned hydrogels were placed in 12- well tissue culture plates (Corning Costar, Arizona, USA) and 1 ml of supplemented Dubelco's Modified Eagle Medium (DMEM) was added before the plates were placed in an incubator overnight at 37 °C. The DMEM was removed from the hydrogels before a cell suspension (1×10^4 cells/ml) in DMEM was added and the hydrogels were once again incubated overnight. Hydrogels were then viewed under a light microscope and images recorded on a 12MP OnePlus 7 phone camera.

4.2.2 Fabrication and water annealing of silk films

Liquid silk was mixed with a 10% w/v aqueous suspension of silk fibre ($1241.9 \pm 790.4 \mu\text{m} \times 21.0 \pm 2.9 \mu\text{m}$) or 1% w/v iron(III) oxide (synthetic spherical particles with 99.995% < 325 mesh [$\sim 45 \mu\text{m}$] size, > 96.8% purity, 4.6 g/cm³ solid density and 0.8–1.2 g/cm³ bulk density from Inoxia Ltd, Sweden) to give a final suspension of 3% w/v silk containing 0.1, 1.0 or 10.0% dopant weight per silk weight. The liquid silk and silk suspensions were mixed slowly before casting in silicone moulds (Sika Everbuild Building Products Ltd, Leeds, UK) on a Perspex base (RuudraScott Plastic, Glasgow, UK) in air for 16 h.

Four moulds and silk volumes were used in the study. The control mould (8 × 6 cm; 7.45 ml) was used to screen iron oxide and silk fibre loads and to cast 3 % w/v silk with 0.1 % (w/w) iron oxide for loading with natural indicators. The film thickness was screened by increasing the casting volume in a 10 × 14.5 cm mould from 15 ml for thin films to 22.5 ml for medium films and 30 ml for thick films. The medium thickness

mould was used to cast 3 % w/v silk with 0.1 % (w/w) iron oxide for origami. Films were removed by scoring with a knife at a distance of at least 0.5 mm from the silicone mould boundary. All films were stored under vacuum in a dry environment before measurement to avoid structural changes.

Films for curcumin loading were directly treated with methanolic curcumin. Films for diazonium coupling and anthocyanin loading were weighed and annealed with 80% v/v methanol/ultrapure water (10 ml per 0.1 g film) for 0.5 – 1 h. The films were then dried overnight at room temperature and weighed before diazonium coupling or loading.

Dried films loaded with anthocyanin and curcumin were water annealed in a water-filled vacuum desiccator using an 85.7 kPa vacuum (70 % humidity) for at least 6 h at room temperature to produce a water-insoluble, plasticised film. The films were removed from the vacuum desiccator, folded into an origami architecture within 10 minutes, and allowed to dry for at least 2 h. Films were refolded into alternative shapes by repeating the water annealing process.

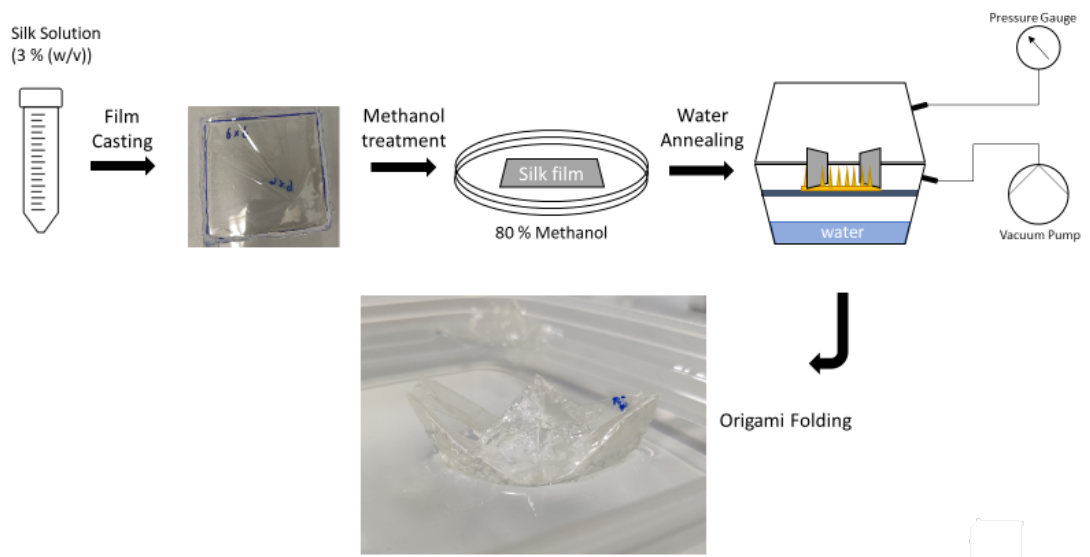


Figure 4-3. Schematic of silk boat production. Silk films are cast and air dried before being submerged in 80% methanol. The films are then dried and undergo water annealing in a pressurised chamber. Films are then folded into origami boats.

4.2.3 Heterogeneous diazonium coupling

A cooled solution of 0.2 M aniline (1.25 ml) in acetonitrile and a 1.6 M aqueous solution of p-toluenesulfonic acid (0.625 ml) were combined with a cooled aqueous solution of 0.8 M NaNO₂ (0.625 ml). The mixture was placed in an ice bath for 15 minutes with continuous stirring. A silk film in 1:1 acetonitrile/0.1 M borate buffer pH 9 (total solution volume 10 ml/0.1 mg) was combined with the stock diazonium salt solution (~0.98 equivalents with respect to tyrosine, assuming 288 tyrosines and according to an H-chain molecular weight of 391 kDa), and the mixture was placed in an ice bath. After combining the silk and diazonium salt, the reaction was allowed to proceed for 1 h. The film was then treated with ultrapure water (30 ml) for 1 h. This step was repeated two further times before drying the film at room temperature in the dark.

4.2.4 Extraction of anthocyanin

Red cabbage (East Lothian, Scotland, Billy Logan, Class 1, 00096, DWW, selected on 12 July 2021) (400 g) was cut into approximately 5 × 5 mm pieces and boiled, with manual stirring, in ultrapure water (850 ml) at 98–105 °C for 0.5 h. Insoluble matter was separated from the anthocyanin solution with a sieve. The solution was concentrated at 80 °C to a final volume of 200 ml. The solution was left to cool to room temperature and then filtered through 12–15 µm qualitative filter paper (VWR, Radnor, PA, USA) and stored at 4 °C for 17 h before use.

4.2.5 Anthocyanin loading

Native silk and azosilk films (6 × 4.5 cm and 6 × 8.5 cm) containing 0.1% iron oxide (w/w) were submerged in the anthocyanin solution (100 ml g⁻¹) for 17 h under constant movement on a tilt table (SSL4 see-saw rocker, Stuart®, Staffordshire, U.K.) at 10 osc minutes⁻¹ at 25 °C. The films were then removed and washed in ultrapure water (100 ml) three times for 20 minutes each on an orbital shaker (Yellowline OS 5 basic, IKA, Staufen, Germany) at 240 rpm. The films were protected from light throughout the loading and washing process. Finally, the films were left to dry in the dark before being imaged on an iPhone SE (Apple, Cupertino, CA, USA) reverse camera at a focal length of 9.7 cm. Loading was repeated in triplicate for the 6 × 4.5 cm film size.

The photographs were standardised using a Datacolor SpyderCheckr® 24 (v1.3, Datacolor, NJ, USA) colour chart under the same lighting conditions. The calibration photo was imported to Adobe Lightroom Classic (Adobe, San Jose, CA, USA), the angle corrected, chromatic aberration removed, perspective profile corrected using the auto or full setting, a full transformation completed, and the image cropped. The white balance was altered using cell E2, adjusting the exposure, highlights, shadows, whites, and blacks to achieve RGB values of 90% at cell E2 and 4% at cell E4. The image was then edited in SpyderCheckr® using the colourimetric mode. The resulting colour profile was applied to all images under the same lighting conditions. The edited images were exported as 300 ppi JPG files, and a grid overlay was placed in ImageJ® v1.52n (National Institutes of Health, Bethesda, MD, U.S.A). The RGB values

were measured for 4 boxes on the grid (595952 pixels) and the averages were calculated.

4.2.6 Curcumin loading

Native silk and azosilk fibroin films (6 × 4.5 cm and 6 × 8.5 cm) containing 0.1% iron oxide (w/w) were submerged in a 2.5 mg ml⁻¹ solution of curcumin in methanol (100 ml g⁻¹) for 30 minutes under constant movement on a tilt table (SSL4 see-saw rocker, Stuart®, Staffordshire, U.K.) at 10 osc minutes⁻¹. The films were then removed and washed in ultrapure water (100 ml) three times for 20 minutes each on an orbital shaker at 240 rpm (Yellowline OS 5 basic, IKA, Staufen, Germany). The films were protected from light throughout the loading and washing process. Finally, the films were left to dry in the dark before being imaged on an iPhone SE (Apple, Cupertino, CA, USA) or a OnePlus 8 (48MP, f/1.8 ISO320) reverse camera at a focal length of 9.7 cm. Standardisation was undertaken as for anthocyanin loading. Loading was repeated in triplicate for the 6 × 4.5 cm film size.

4.2.7 Characterisation of silk films

4.2.7.1 Colour change of silk films across pH and pollutant concentration

Silk films loaded with curcumin or anthocyanin were imaged after being submerged for 2 minutes in the following solutions: 0.2 M potassium phosphate buffer (pH 4.37, pH 7 and pH 9.15); 897 mg L⁻¹ SDS; 660 mg L⁻¹ CTAB; 370 mg L⁻¹ Triton X-100; 242.3 mg L⁻¹ CoCl₂; 341.5 mg L⁻¹ Co(NO₃)₂; 3.265 mg L⁻¹ CuSO₄; 0.15748 mg L⁻¹ AgNO₃; 979.2 mg L⁻¹ MgCl₂; 999.2 mg L⁻¹ MgCO₃; or 600.0 mg L⁻¹ MgOH₂. The images were processed as for loading. Films were washed three times in ultrapure water for 0.25

h, dabbed dry with a tissue and dried at room temperature for 0.17 h before submersion in a new solution. The relative colour change (S) was calculated by subtracting the mode and mean intensities in the red (Ro), green (Go), and blue (Bo) channels of the loaded film from the red (R), green (G) and blue (B) intensities in the films following exposure to each medium, according to equation 1. (Dey, et al., 2021)

$$S (\%) = 100 \times \frac{(|R - R_o| + |G - G_o| + |B - B_o|)}{R + G + B} [1]$$

4.2.7.2 Scanning electron microscopy

For surface imaging, samples were added to aluminium stubs with sticky carbon tabs, with the surface uppermost. For section imaging, a titling SEM stub was used to rotate the samples to 90° with the cross-section uppermost. Samples were sputter coated (ACE200, Leica Microsystems, Wetzlar, Germany) with a 20 nm gold layer to minimise charging in the SEM. Samples were viewed with a Hitachi TM4000Plus SEM operated at beam voltage 10000eV, probe current setting 2, standard vacuum level (M) and with data collected in backscattered electron mode at magnifications of 100×, 1000× and 10000×.

4.2.7.3 Contact angle measurement

The films were placed on a glass slide. The contact angle was measured using a DSA30 drop shape analyser (KrussGmbH, Hamburg, Germany) equipped with a manual syringe and needle (diameter 0.8 mm). Droplet size was controlled manually. Results were analysed in Advance software (KrussGmbH, Hamburg, Germany) with manual droplet shape fitting.

4.2.7.4 *Fourier Transform Infrared Spectroscopy analysis*

Positive silk II controls were provided by autoclaved silk films and silk films treated with 70% v/v ethanol/ultrapure H₂O, while air-dried silk films and freeze-dried silk were used as positive controls for silk I structure. Secondary structures of silk films, freeze-dried powders and freeze-dried particles were analysed by Fourier transform infrared spectroscopy (FTIR) on an ATR-equipped TENSOR II FTIR spectrometer (Bruker Optik GmbH, Ettlingen, Germany). Each FTIR measurement was recorded in absorption mode over the wavenumber range of 400 to 4000 cm⁻¹ at 4 cm⁻¹ resolution for 128 scans and then corrected for atmospheric absorption using Opus (Bruker Optik GmbH, Ettlingen, Germany). The second derivative of the background-corrected FTIR absorption spectra was analysed in OriginLab 19b® (Northampton, Massachusetts, USA) by adapting a literature protocol (Fang, et al., 2017). The second derivative was smoothed twice using a seven-point Savitzky-Golay function with a polynomial order of 2. The amide I region was analysed by interpolation of a non-zero linear baseline between 2–3 of the highest values in the 1600–1700 cm⁻¹ range. Peak positions were identified by applying the second derivative, and the peaks were fitted in the amide I region using non-linear least squares with a series of Gaussian curves. The position, width and height of each peak were allowed to vary, while peak area could take any value less than or equal to 0. Deconvoluted spectra were then area-normalised, and the relative area of each band was used to calculate the secondary structure content according to literature band assignments (Ryu, et al., 2020) (Melancon, et al., 2021).

4.2.7.5 Thermal analysis

First-cycle differential scanning calorimetry and thermogravimetric analysis were carried out on the dried samples (3–5 mg) in aluminium pans from 20–350 °C at a scanning rate of 10 °C minutes⁻¹ and under a nitrogen flow of 50 ml/minutes (STA Jupiter 449, Netzsch, Gerätebau GmbH, Germany). Thermograms were analysed using Proteus® (Netzsch, Gerätebau GmbH, Germany).

4.2.7.6 Swelling analysis

The swelling of silk fibroin films was monitored over 30 minutes. Each film was split into 3 pieces and placed in ultrapure water (20 ml), and the weight was measured at defined intervals. The films were removed, and any excess water on the film was dabbed dry with paper towels. This was repeated three times for each film.

4.2.8 Electromagnetic field strength

The strength of a magnetic field was measured by the ability to pull a floating rectangular silk film (0.1 g, 25 µm thickness) along the water-air interphase using a N52 round cylinder magnet (25 × 20 mm Rare Earth Neodymium). The magnet used in the study was moved across water-glass interphase (2 mm thickness) parallel to the water-air interphase (where silk was floating) at fixed distances defined by the volume of water in a 5000 ml glass beaker. Every added 50 ml was equivalent to a 1 mm increase in the distance between the silk film and the magnet.

4.2.9 Contraction and relaxation on water

The time of contraction from the original shape of the water-annealed dried silk films (ca. 7 × 5 cm) was measured in seconds as the films were placed in water (floating at the water-air interface). The relaxation and return to the original shape were followed by measuring time in seconds.

4.2.10 Thickness and folding assessment

Film thickness was measured with digital Vernier callipers (CM145 Clarke® Precision, Clarke®, London, U.K.) by stacking 3–4 films of the same type. The folding time after annealing for 17 h was measured by removing the films (ca. 9 × 13.5 cm) from the water annealing chamber and recording the time when the films first cracked or tore when being repeatedly folded and unfolded by hand.

4.2.11 Characterization of silk origami boats

4.2.11.1 Semi-autonomy

Origami sailboats (6 × 8.5 cm) containing 0.1% (w/w) iron oxide were placed on ultrapure water in a clear acrylic box (10.3 × 10.3 × 5 cm). An LED panel (RALENO, Seattle, WA, USA) was fixed at the back of the box to provide constant illumination at 5600K colour temperature and at 1% brightness. An N52 round cylinder magnet (25 × 20 mm Rare Earth Neodymium) was suspended from the bow of the boat at ca. 2 mm horizontally and from the highest point of the boat sail at ca. 2 mm vertically. The distance travelled over 30 s was captured on an iPhone SE (Apple, Cupertino, CA, USA) reverse camera at a capture speed and resolution of 240 fps and 1080 p using

FILMiC Pro (FiLMiC Inc., Seattle, WA, USA). In parallel, the movement of a folded origami boat manufactured without iron oxide was used as a negative control. Each condition was repeated with three origami boats manufactured with different silk batches. Images were extracted at 240 fps using FFmpeg (Mintchev, et al., 2018).

4.2.11.2 Sensing of pH and pollution

Films (4.5 × 4.5 cm) were loaded with anthocyanin and curcumin, water annealed and folded into origami canoes. Boat hulls were imaged on an iPhone SE (Apple, Cupertino, CA, USA) reverse camera at a focal length of 7.8 cm. Curcumin-silk canoes were placed on 0.2 M potassium phosphate buffer (pH 4.73 and 9.15), and anthocyanin-silk canoes were placed on 660 mg L⁻¹ CTAB and 979.2 mg L⁻¹ MgCO₃ for 2.5 mins before removal, drying in air and imaging. Photographs were standardised as described for loading of 2D films, the RGB values were measured for 2 boxes on the grid (42840 pixels) and the averages were calculated.

Equivalent origami sailboats (6 × 8.5 cm) were placed on 0.2 M potassium phosphate buffer (pH 9.15), 897 mg L⁻¹ SDS and 3.27 mg L⁻¹ copper sulphate in a clear acrylic box (10.3 × 10.3 × 5 cm). An LED panel (RALENO, Seattle, WA, USA) was fixed at the back of the box to provide constant illumination at 5600K colour temperature and at 1% brightness. The colour change was imaged on an iPhone SE (Apple, Cupertino, CA, USA) reverse camera at a capture speed and resolution of 60 fps and 2160 p using FiLMiC Pro (FiLMiC Inc., Seattle, WA, USA). Images were extracted at 60 fps using FFmpeg (Mintchev, et al., 2018).

4.2.12 Statistical analyses

Data were analysed using Microsoft Excel® 2019 (Microsoft Office 365 ProPlus Software, Redmond, WA, U.S.A), Minitab® (Minitab® Statistical Software, State College, PA, USA) and GraphPad Prism 8.2.1 (GraphPad Software, La Jolla, CA, U.S.A.). Normality of the data distributions was assumed throughout. The equivalence of variance for sample pairs and multiple groups was identified with the F-test and Bartlett's test. Sample pairs were analysed using the independent t-test. A two-way ANOVA was used to compare multiple groups across two independent variables, followed by Šidák's multiple comparison, simple effects post-hoc test. Statistical significance, identified using post-hoc tests, was as follows: * $p < 0.05$, ** $p < 0.01$, *** $p < 0.001$, **** $p < 0.0001$. All data are displayed as the mean \pm standard deviation, with the number of experimental repeats (n) shown in each figure legend.

4.3 Results

4.3.1 Micropatterning

Silk films were cast on diffraction grating (Figure 4-2) and PDMS molds of various designs (Figure 4-3). The films were able to be removed from the substrate by carefully lifting off. The negative of each pattern could be seen on each film. The film cast on the diffraction grating was able to diffract light as the grating had done, indicating a clear transfer of the pattern onto the silk.

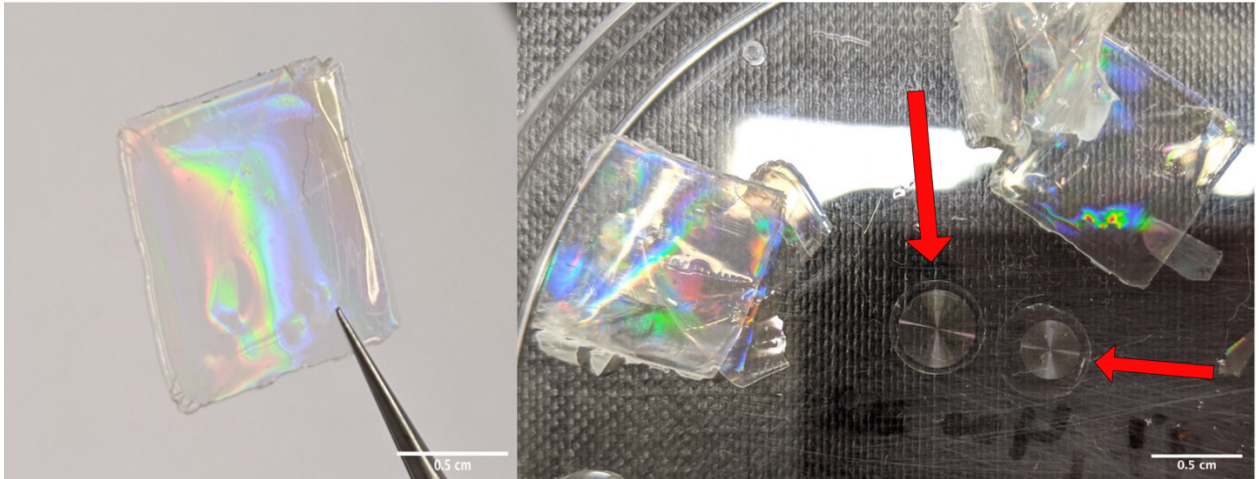


Figure 4-4. Patterned silk films. Diffraction pattern on the silk film surface creating light diffraction rainbow effect. Arrows indicate concentric circles on silk film surface with 2 different circle widths.

Patterned silk films were then methanol treated to determine if the crystallization of the silk film would alter the pattern on the surface. The diffraction of light can still be seen on the surface of methanol treated films (Figure 4-3) indicating that the pattern was unaffected by the treatment of the films.

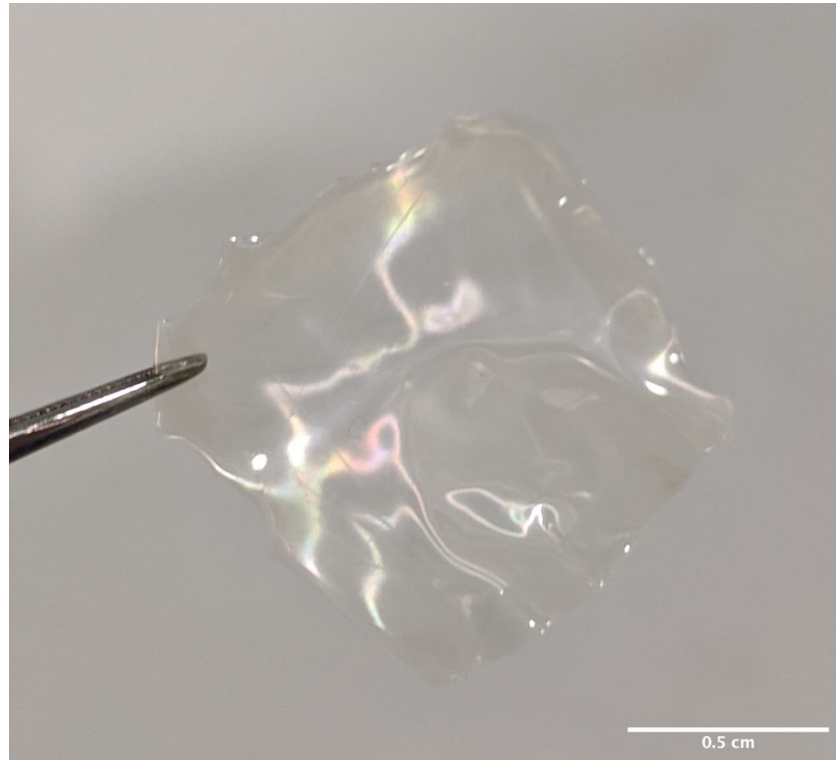


Figure 4-5. Silk film patterned with diffraction pattern on surface after methanol treatment. The pattern is preserved as the light diffraction rainbow effect is visible.

Silk films spiked with iron (III) oxide particles were then cast on the patterned PDMS mould. The films still displayed the micropattern clearly, with the iron (III) oxide microparticles visible. The pattern was also preserved when the films underwent water annealing and methanol treatment (Figure 4-4).

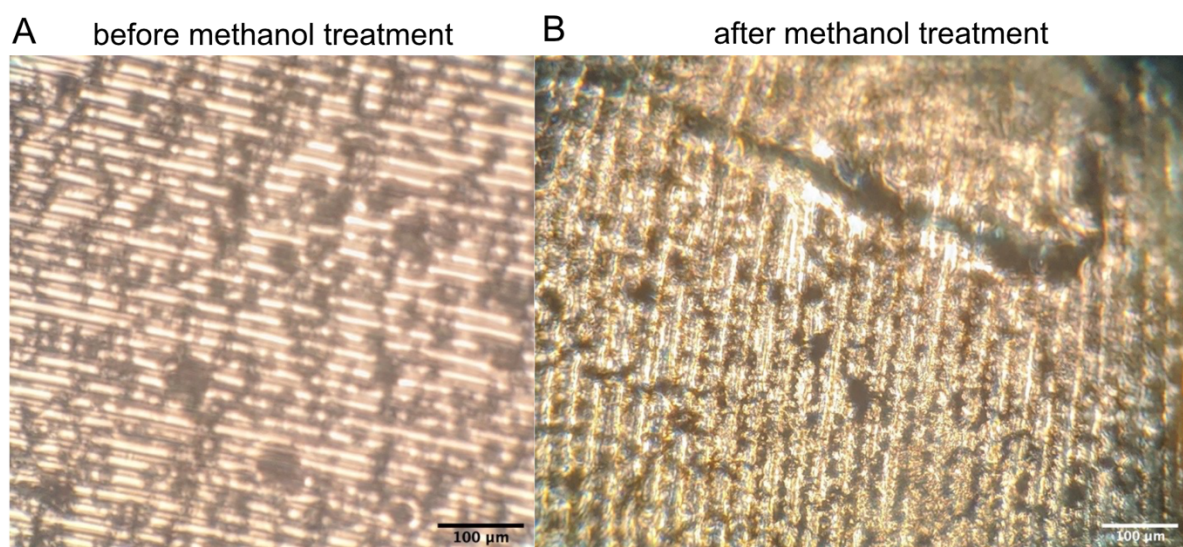


Figure 4-6. A. Silk film with linear pattern and 1% (w/w) iron (III) oxide particles incorporated. B. Silk film with iron (III) oxide particles incorporated after methanol treatment. The iron (III) oxide particles are still visible in the silk film alongside the pattern.

4.3.2 Micropatterning hydrogels

Silk hydrogels were then cast to determine if they could still retain the micropatterning. Silk solution underwent sonication until the sol-gel phase and was cast onto PDMS molds as shown in Figure 4-5.

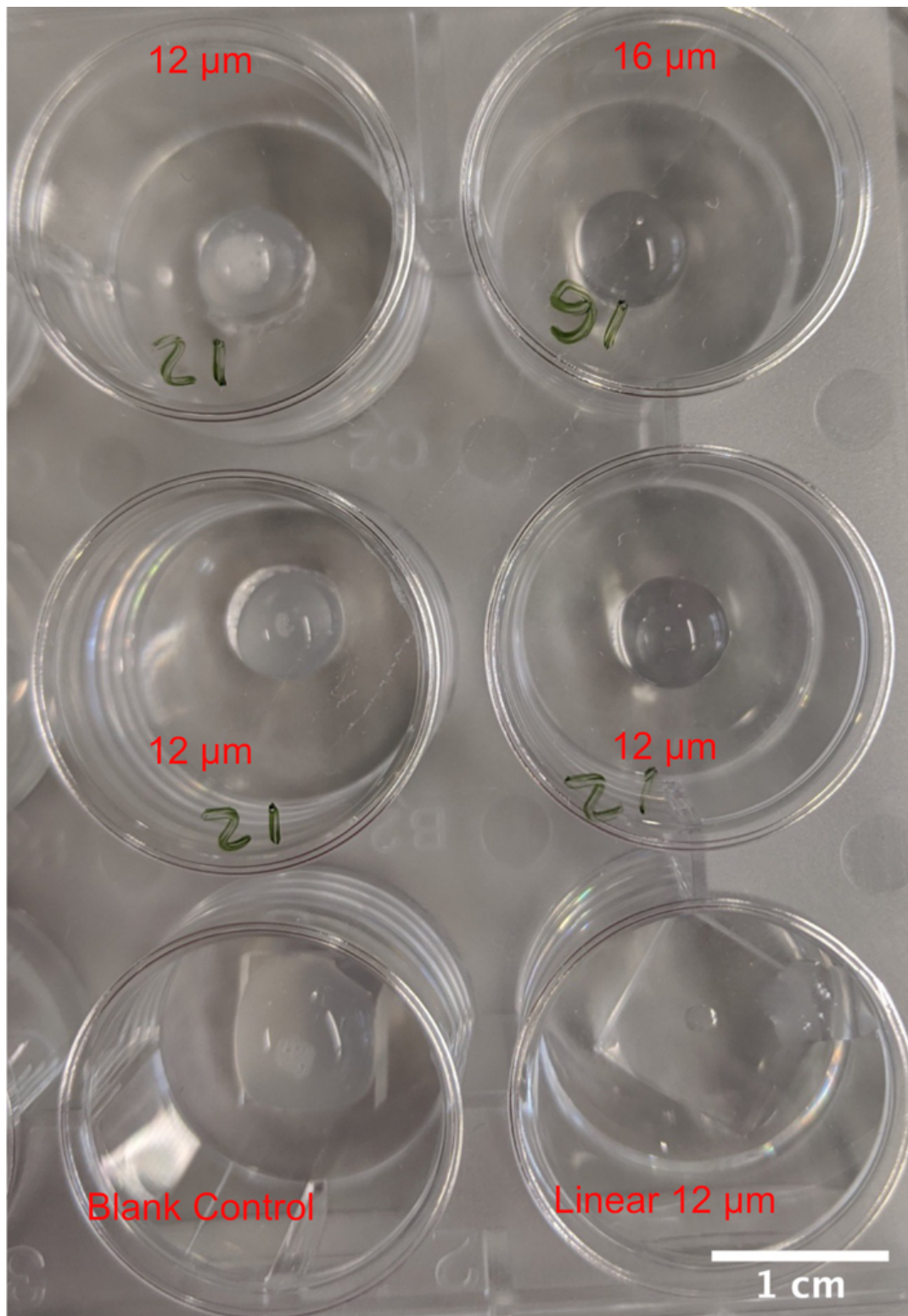


Figure 4-7. Silk hydrogels in the sol-gel state added to PDMS casts for patterning. Circular patterned PDMS, linear patterned PDMS and flat PDMS of varying separation.

When removing the silk hydrogels from the PDMS casts, the hydrogel was often fragile and would break. To improve stability a glass cover slide was placed on the top of the gel as it was setting. The other method used was freezing the gel for 1 hour before removal to harden the gel. This created small bubbles on the surface of the hydrogel (Figure 4-6).

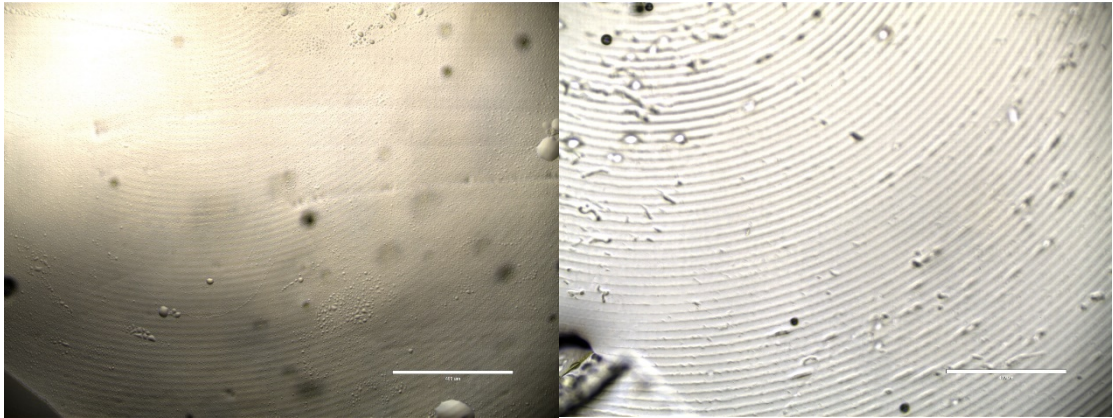


Figure 4-8. Patterned silk hydrogels with concentric circles with 12 μm and 16 μm gaps.

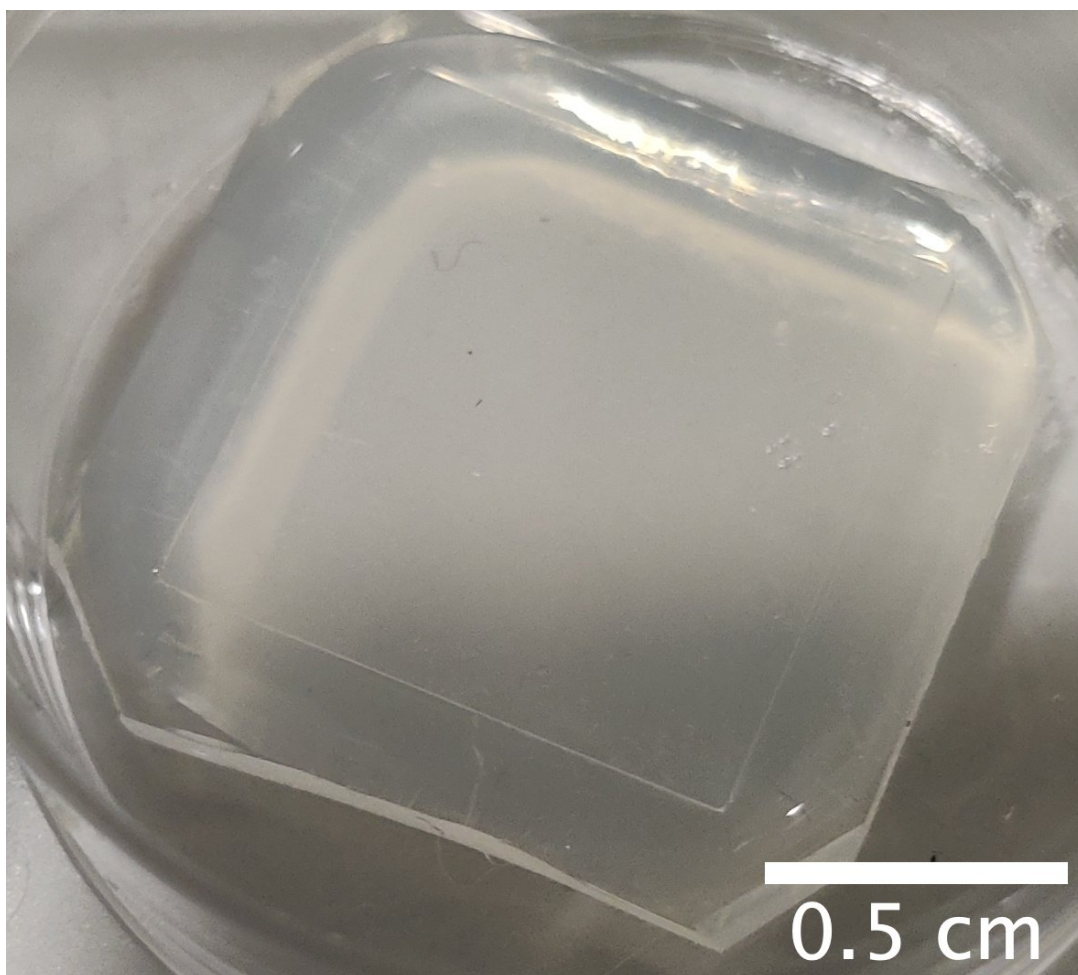


Figure 4-9. Slide placed on surface of hydrogel on PDMS cast for removal.

To determine if the micropattern on the silk hydrogel surface influenced cell morphology, hydrogels were seeded with NIH 3T3 mouse fibroblasts. Silk films were not tested with cells. Cells were grown overnight on the surface of the hydrogels and imaged. Cells did not appear to grow in the grooves of the micropattern but some changes to the patterning can be seen suggesting the cells can detect the changes in pattern.

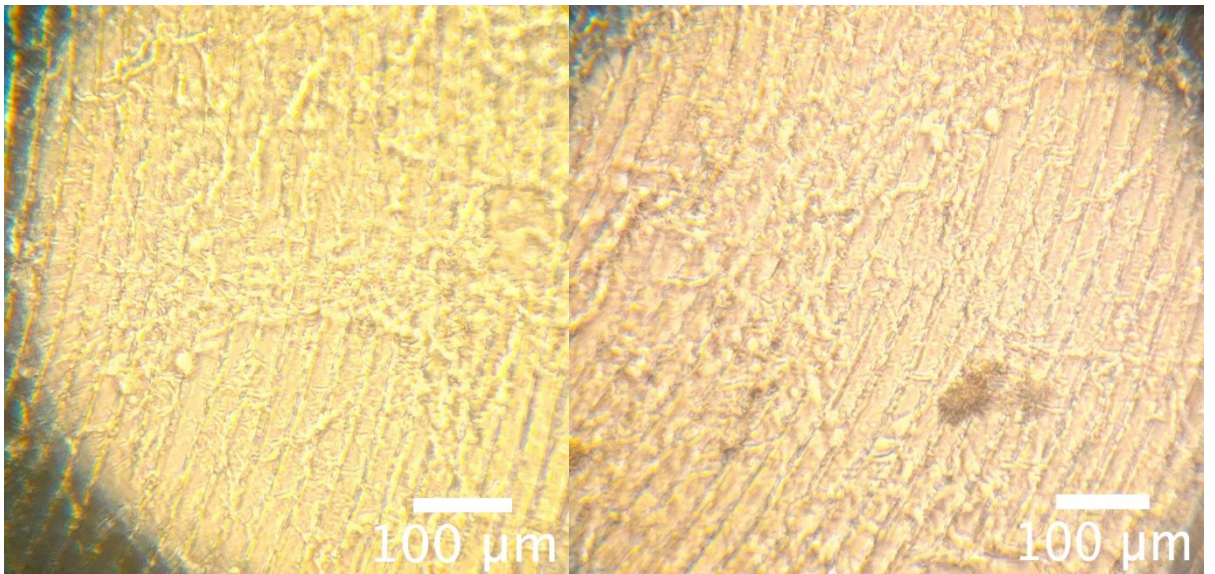


Figure 4-10. NIH3T3 Fibroblasts grown on patterned gels. (n=1)

4.3.3 Silk film production

Silk films can be cast, and methanol treated to induce crystallisation. This produces a film that will fracture upon folding but will not dissolve in water. To allow the folding of the silk film, the sheet must be placed in a water annealing chamber for a minimum of 1 hour to plasticise the silk film. This hydrates the beta sheets and allows the film to be folded before the water evaporates and the film becomes unable to be folded.

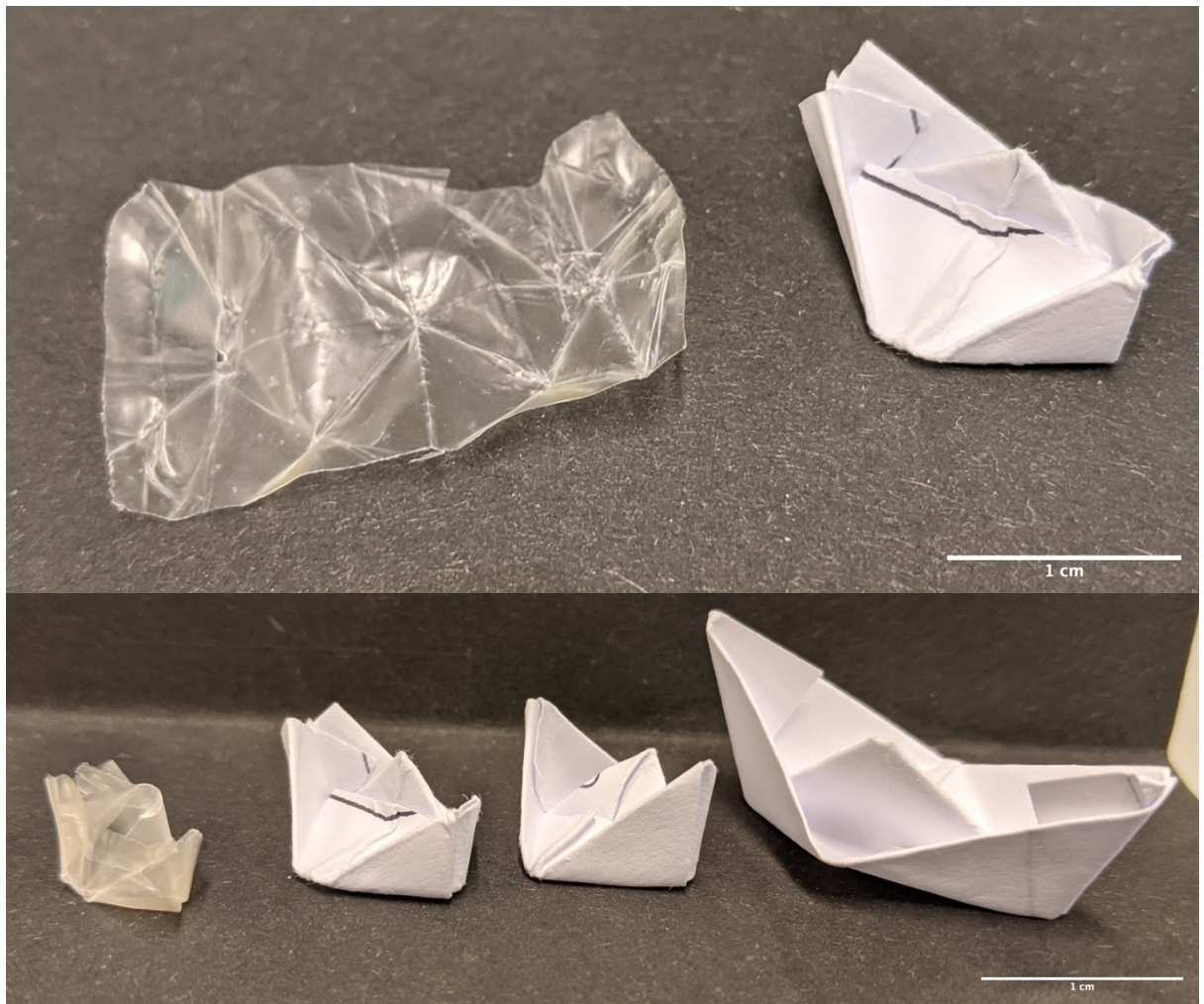


Figure 4-11. Silk origami. Top: Unfolded silk film on the left after being folded to form the boat on the right. Bottom: Silk boat on the left followed by paper boats of various sizes to the right.

Silk films may also be cast containing iron (III) oxide nanoparticles to produce a magnetic boat. The nanoparticles remain distributed evenly through the film and do not affect the folding properties. Casting conditions were first optimised for semi-autonomy by varying the iron oxide particle concentration, the time window for folding by tuning film thickness, and the longevity of folds upon water by increasing silk fibre ($1241.9 \pm 790.4 \mu\text{m} \times 21.0 \pm 2.9 \mu\text{m}$) concentration and hydrophobicity (Figure 4-13). The film thickness was tuned by increasing the volume of liquid silk for mould casting. Diazonium coupling generally increased the film thickness compared to native films (Figure 4-14) and resulted in an increase in the water contact angle, indicating a greater hydrophobicity (Figure 4-17).

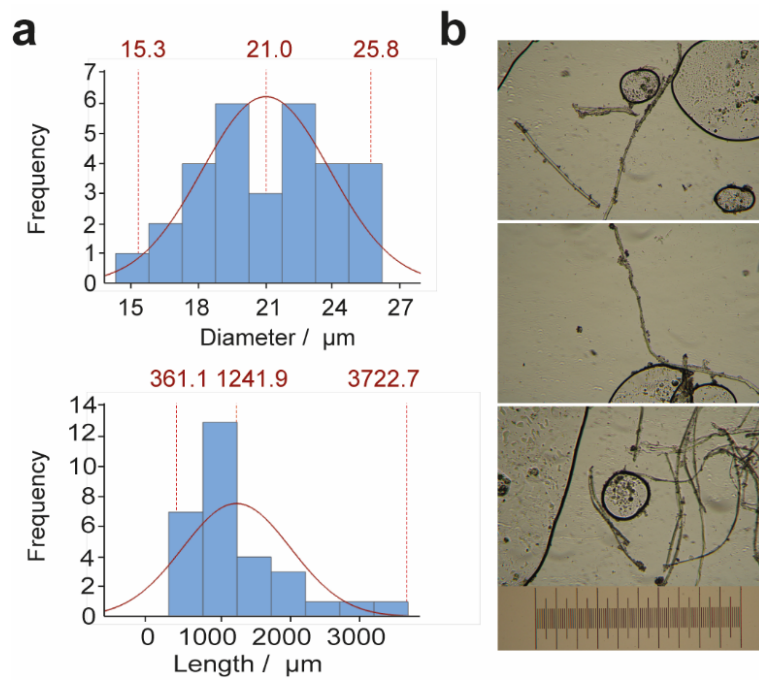


Figure 4-12. The dimensions of mechanically cut silk fibres. **(a)** Histograms of length and width. Reference lines show the minimum, average and maximum dimensions. $n = 30$. **(b)** Exemplar images of silk fibres at 10 \times magnification. Scale bar = 1 mm.

Silk films were folded following an origami boat pattern as shown in Figure 4-9. Paper boats were produced first to determine sheet size of silk film required and to demonstrate flexibility of the silk film when compared to paper. Silk films were able to be folded into a small boat before drying out following water annealing. The films can then be unfolded without breaking along seams.

4.3.4 Origami Film parameters

The casting of silk films was performed at three volumes to produce three thicknesses. The thinnest film measured at 0.031 ± 0.004 mm, the medium film was 0.048 ± 0.006 mm and the thickest film measured 0.068 ± 0.011 mm. The thicknesses were significantly different from one another ($p = 0.002$ thin and thick, $p = 0.037$ medium to thick). The folding time of the three thicknesses was also measured. The time for the film to be unable to fold increased with the increasing thickness measured. The thinnest film was unable to fold after 140 seconds. The medium thickness film was unable to fold after 210 seconds. The thickest film was unable to fold after 244 seconds. Following plasticisation by water annealing, the time of plastic endurance of the azosilk and native silk films in air increased with thickness due to the reduced surface area percentage for evaporation of the thicker films (Figure 4-11). Across all thicknesses, azo-modification reduced the plasticity time window (Figure 4-15).

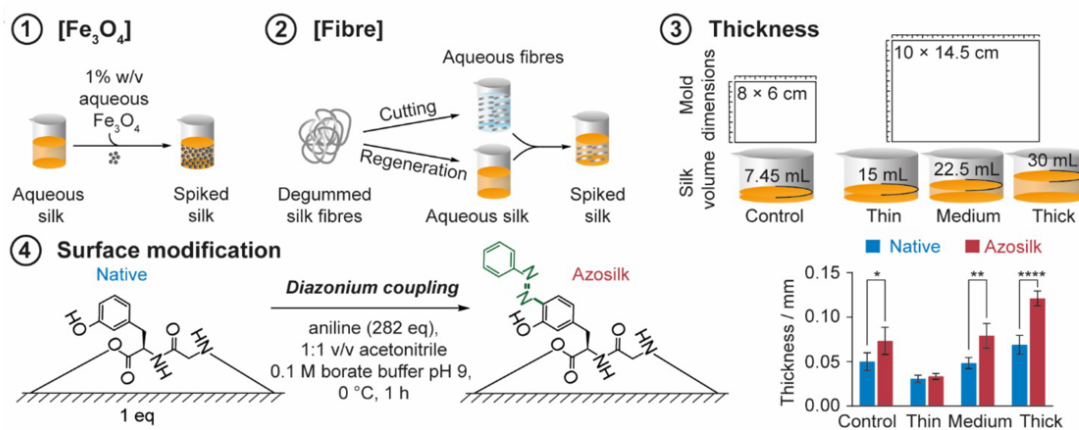


Figure 4-14. Silk film processing. Silk solution was doped with iron oxide (1) or silk fibres (2) and cast at 3 different thicknesses (3) to assess the impact of each independently. Surface modification was performed (4) to produce azosilks. The thickness of films showed differences once modification had taken place at each casting volume difference. Error bars are hidden in the bars and plot symbols when not visible, \pm SD, $n = 3$. Multiple factors were evaluated by two-way analysis of variance (ANOVA), followed by Šidák's multiple comparison, simple effects post-hoc test. Asterisks denote statistical significance determined using post-hoc tests as follows: * $p < 0.05$, ** $p < 0.01$, *** $p < 0.001$, **** $p < 0.0001$.

Scanning electron microscopy (SEM) confirmed that iron oxide particles were incorporated into, and retained within, the silk film matrix following post-processing methods (Figure 4-12). The cross section of the iron loaded azosilks revealed a more irregular surface when compared to the native silks.

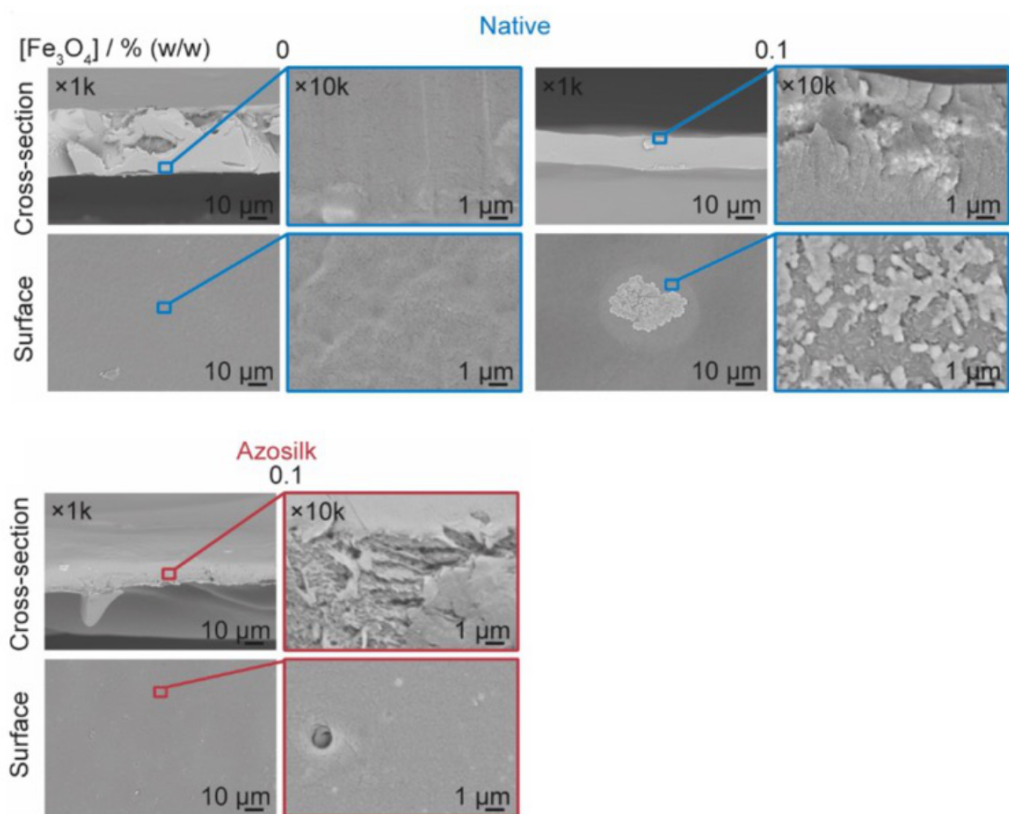


Figure 4-15. SEM images of native and azosilk films after water annealing with 0 and 0.1 % (w/w) iron oxide particle loads.

All films showed stability in water due to the dominant β -sheet secondary structure, which ranged from 55 to 61% (Figure 4-13). The thermal decomposition of silk films occurred at temperatures above 250 °C, which was consistent with a high β -sheet content (DeBari, et al., 2021), and azo-modification generally increased the thermal stability (Figure 4-13).

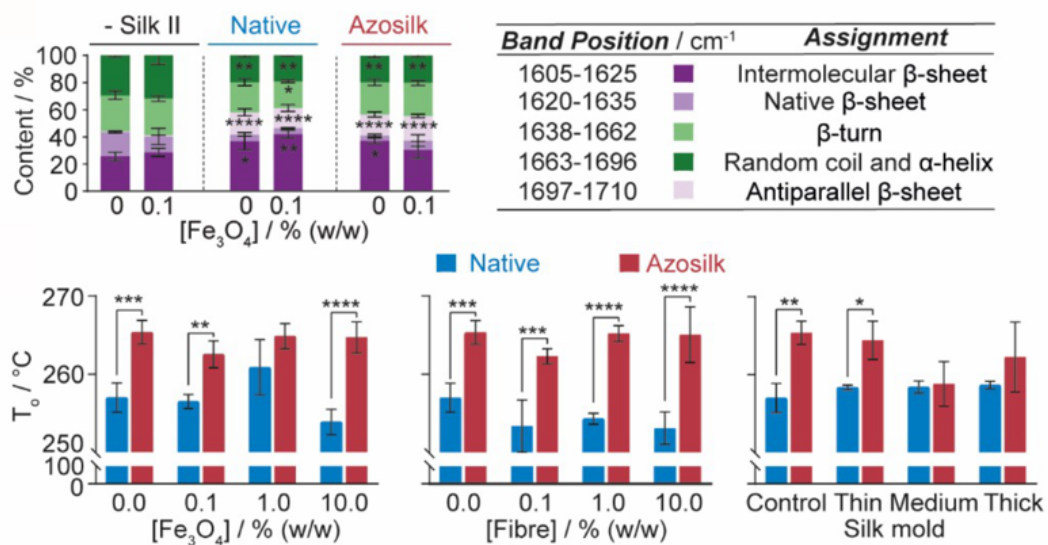


Figure 4-16. FTIR band assignments and schematic key. Secondary structure content of silk films drop-casted with varying iron oxide particle concentrations. Secondary structure content (%) was calculated from the relative areas of peaks in the second-derivative spectrum. Untreated silk films were used as negative controls for β -sheet content. The extrapolated onset temperature of decomposition (T_0) of silk films from first-cycle DSC. Error bars are hidden in the bars and plot symbols when not visible, ($n = 3, \pm SD$)

To determine the effects of water on the films the swelling was measured by weight of film over 30 minutes. The 0.1 % fibre film showed the largest initial increase, with 56.43 ± 15.89 % in the first minute, but this decreased to a 46.31 ± 11.63 % weight increase after 30 minutes. The 1% fibre film showed a much lower initial weight increase (17.97 ± 15.25 %) and grew steadily to 30.08 ± 6.44 % of the initial weight. The 10% fibre film also did not have as large an initial swelling, with a 30.51 ± 8.62 % increase after 1 minute, and 35.96 ± 6.42 % after 30 minutes.

The presence of 0.1 % Fe_3O_4 nanoparticles allowed the film to swell to 41.48 ± 3.58 % after 1 minute and 43.79 ± 12.56 % after 30 minutes. This consistent swelling was also seen in 1 % and 10 % Fe_3O_4 .

Finally, the thin film had an initial swelling of 30.36 ± 4.15 % and 29.83 ± 11.17 % after 30 minutes. The medium film had a lower initial swelling (20.28 ± 25.38 %) with large variability, and the final swelling was just as diverse (24.44 ± 24.25 %). The thickest film had a higher initial swelling of 31.55 ± 14.55 % and after 30 minutes had increased by 32.77 ± 4.93 %. Azosilk films showed varying swelling over 30 minutes with iron oxide particle doping. For example, a weight change of 35 % occurred at an iron oxide loading of 0.1 % (w/w), and this increased to 61 % at 1 % (w/w) iron oxide. Increasing the iron oxide content further to 10 % (w/w) resulted in a lower weight increase of 19 % over 30 minutes.

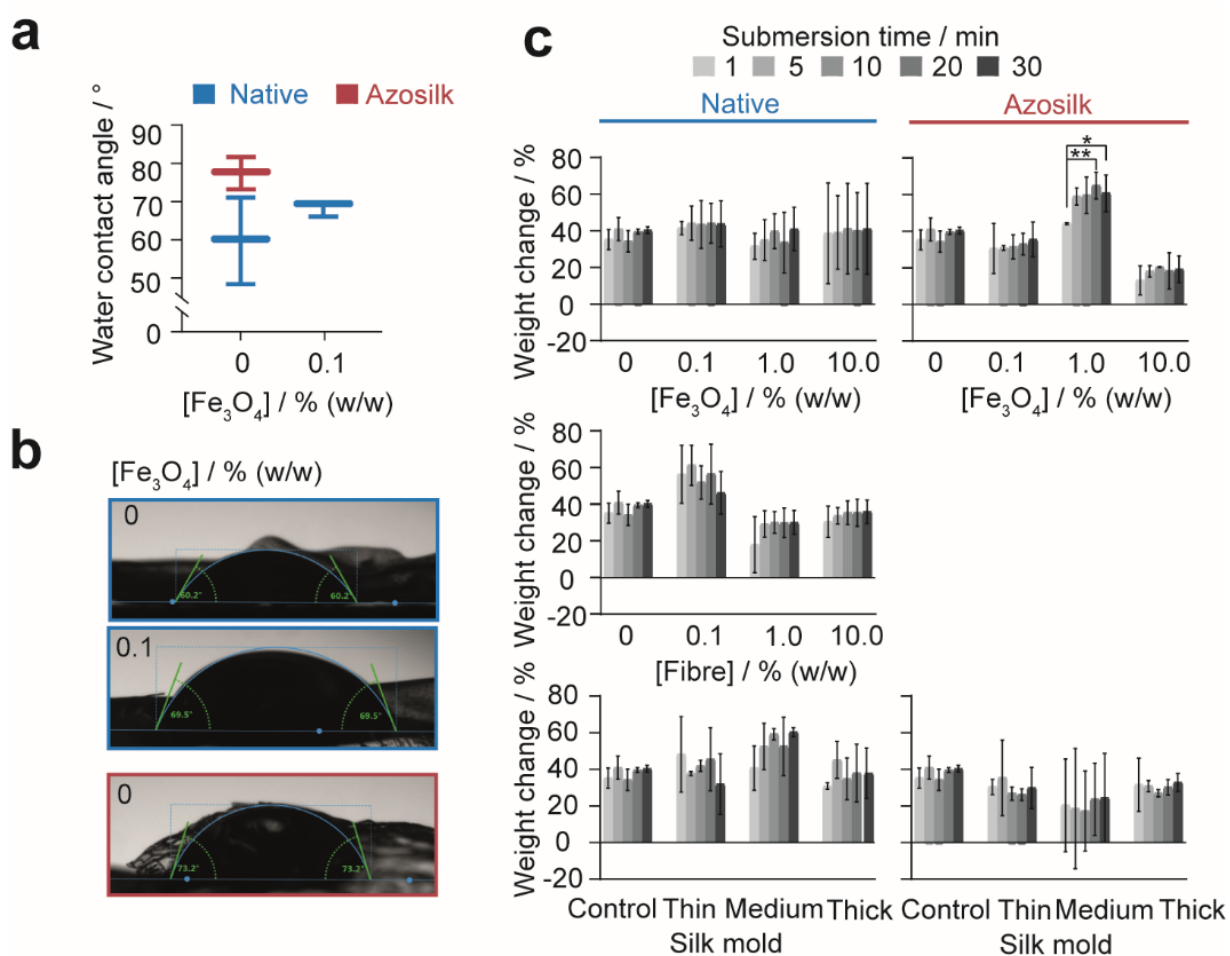


Figure 4-17. The effect of aqueous environments on silk films. **(a)** Water contact angle of azosilk and native silk medium thickness films without iron oxide and of native control thickness silk film containing 0.1 % (w/w) iron oxide. ($n = 3, \pm SD$). **(b)** Exemplar images of water contact angles for azosilk and native silk films. Scale bars = 0.5 cm. **(c)** Weight change of native silk and azosilk films following immersion in ultrapure water. ($n = 3, \pm SD$)

4.3.5 Locomotion and floating testing

The films were tested on the surface of water to determine if they would remain stable and if the weight of iron or fibres would alter the ability of the film to float. All films were able to float on the surface of water without sinking for up to 30 minutes. When folded into an origami boat, films began to unfold after 10 minutes. All films spiked with iron (III) oxide showed semi-autonomy on the water surface. They could be pulled along the air-water interface using a neodymium magnet. Increasing the iron oxide load from 0.1% to 10% (w/w) resulted in a decreased electromagnetic field strength required for magnetic response from 2.71×10^4 to $0.45 \times 10^4 \text{ m}^{-1}$.

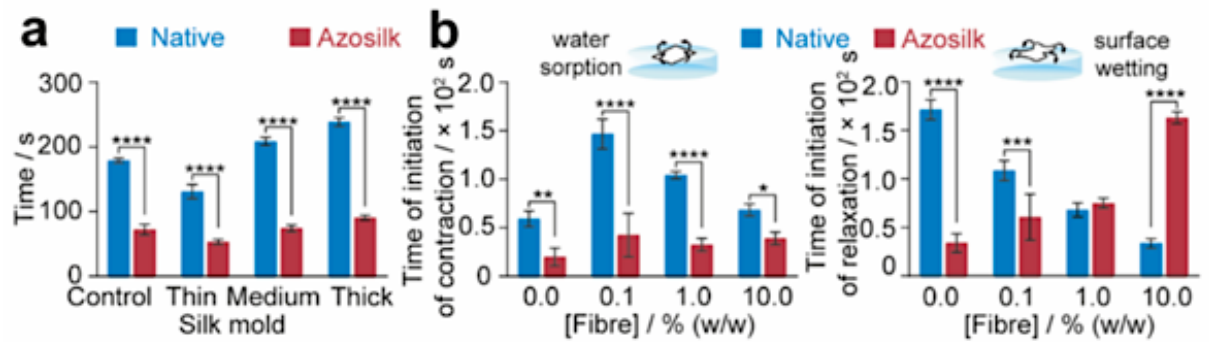


Figure 4-18. a) the time window for folding silk films while plasticised following water annealing. b) The time taken for initiation of contraction and initiation of relaxation by films lying on the air-water interface was used a measure of structural stability in wet environments ($n = 3, \pm SD$).

For sensing applications, silk films doped with 0.1 % (w/w) iron oxide particles and casted at medium thickness were loaded with curcumin extracted from turmeric rhizome and anthocyanin extracted from fresh red cabbage (Figure 4-16).

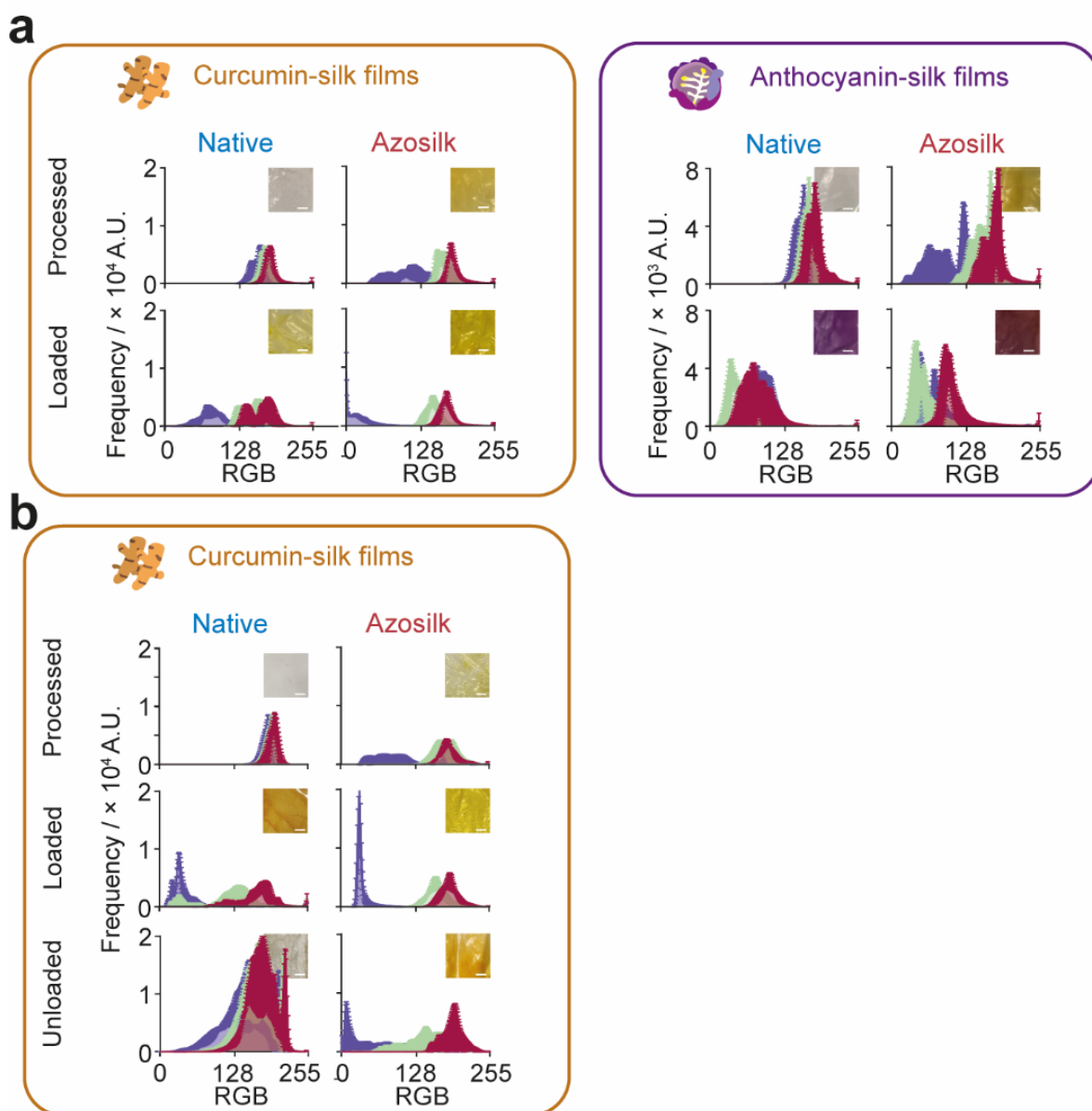


Figure 4-19. The change in pixel channel intensities upon **(a)** loading medium thickness films containing 0.1% (w/w) iron oxide particles with anthocyanin for sensing pH, heavy metal salts and surfactants and with curcumin for sensing heavy metal salts and surfactants. **(b)** Medium thickness films containing 0.1% (w/w) iron oxide particles were loaded with curcumin for sensing pH and unloaded in 0.1 M aqueous NaOH. Scale bars = 0.5 cm ($n = 3, \pm SD$)

Both native and azosilk films showed a visible colour change upon loading with the natural pigments (Figure 4-17) and could be used as colourimetric probes for pH changes (Figure 4-17, Figure 4-18). The colour of the azosilk and native curcumin-loaded films was yellow at pH 4.37, deep yellow at pH 7.00 and reddish-orange at pH 9.15.

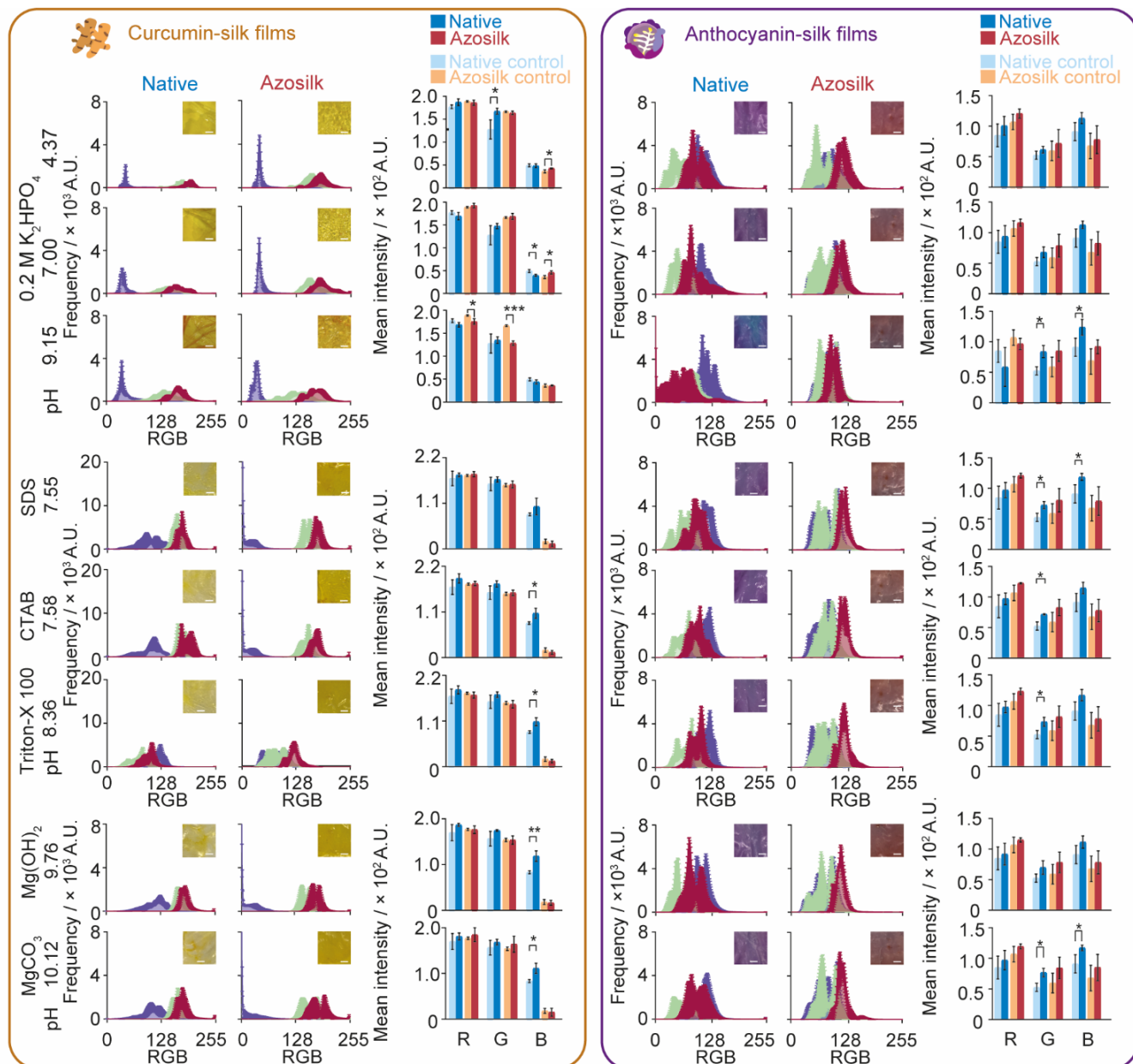


Figure 4-20. The change in colour and mean pixel channel intensities of curcumin-loaded and anthocyanin-loaded azosilk and native silk medium thickness films containing 0.1% (w/w) iron oxide particles in response to pH, surfactants, and heavy metal salts. Scale bars = 0.5 cm ($n = 3, \pm SD$).

The colour change was analysed in the RGB colour space and revealed a reduction in the blue channel intensity for native and azosilk films with increasing pH, in addition to a reduction in the red and green channel intensities of azosilk films at pH 9.15. Anthocyanin-silk films were more sensitive than the curcumin-silk films to pH, as the relative colour change was consistently greater than their curcumin counterparts at all pH values investigated (Figure 4-18).

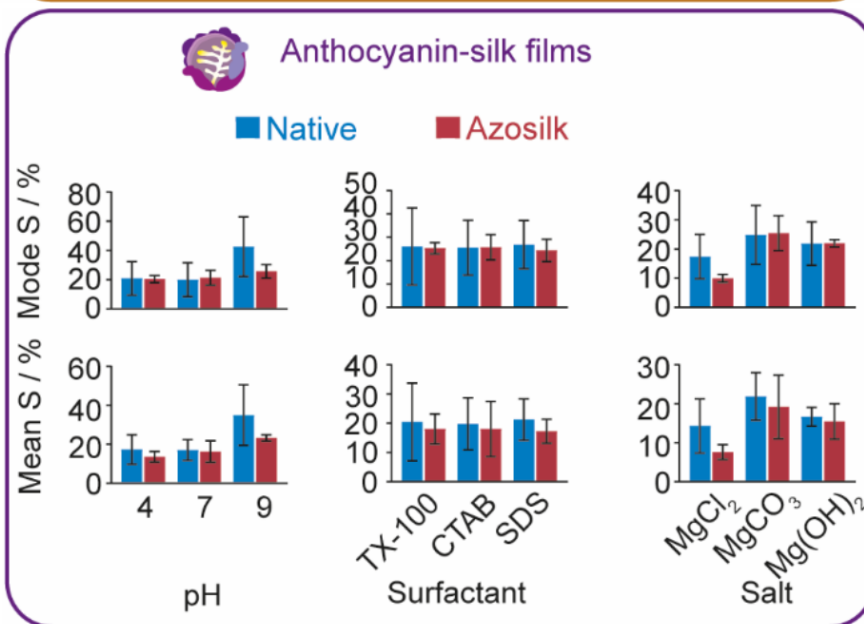
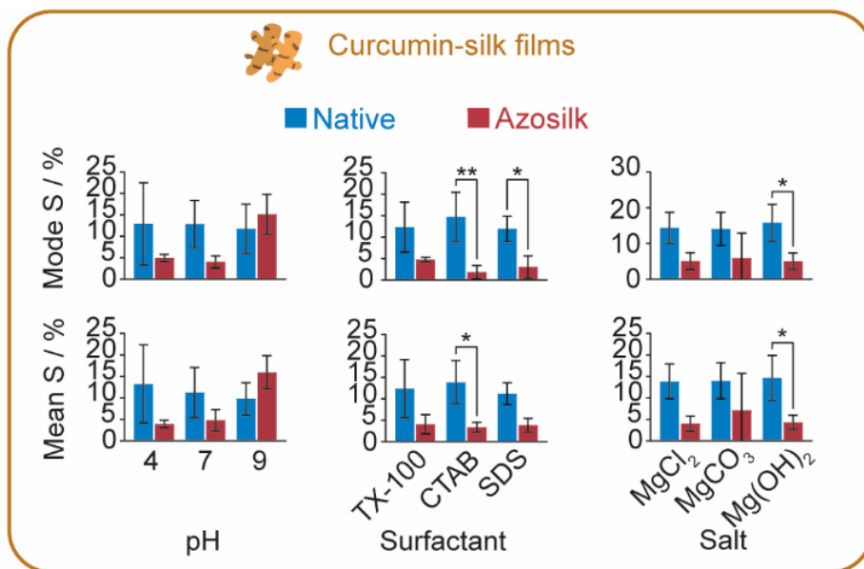


Figure 4-21. The relative colour changes of curcumin and anthocyanin-loaded native silk and azosilk films varying pH, surfactant and heavy metal salt. Multiple factors were evaluated by two-way analysis of variance (ANOVA), followed by Šidák's multiple comparison, simple effects post-hoc test. Asterisks denote statistical significance determined using the t-test and post-hoc tests as follows: * $p < 0.05$, ** $p < 0.01$, *** $p < 0.001$, **** $p < 0.0001$.

Curcumin-silk films could be unloaded by treatment with sodium hydroxide (Aboudiab, et al., 2020), allowing recycling of the film and loading with alternative indicators (Figure 4-16). However, unloading the azosilk increased the film brittleness and fracture.

As proof of principle, native and azosilk medium thickness silk films containing 0.1 % (w/w) iron oxide were then folded into a variety of 3D origami structures, including waterborne boats and airborne darts and spinners. Silk origami structures could be reused for at least five cycles prior to elastic failure upon folding, and the films could also be reloaded with chemical indicators. In addition, both native and azosilk examples of 3D silk origami sailboats remained structurally stable for at least 3 days on ultrapure water. An efficient method for the distribution and recovery of films using magnetic fields as the energy source for locomotion was achieved, as the silk origami retained semi-autonomy upon folding (Figure 4-19). Silk origami sailboats were then used as in situ pH probes and showed visible colour changes along their hulls within 2.5 minutes of exposure to a 0.2 M potassium phosphate buffer at pH 9.15. The silk canoe design enabled colourimetric analysis of the keel of the boat, as this region of interest consisted of a single layer. For example, the yellow to reddish-orange colour change as pH increased from 4.37 to 9.15 was detected by the decrease in green channel intensity of native curcumin-silk canoes. For the azosilk canoe, monitoring of this colour change was possible through the increase in red channel intensity. Detection of the model pollutants CTAB and magnesium carbonate was also possible using anthocyanin-silk canoes through increased intensities in the red, green, and blue channels.

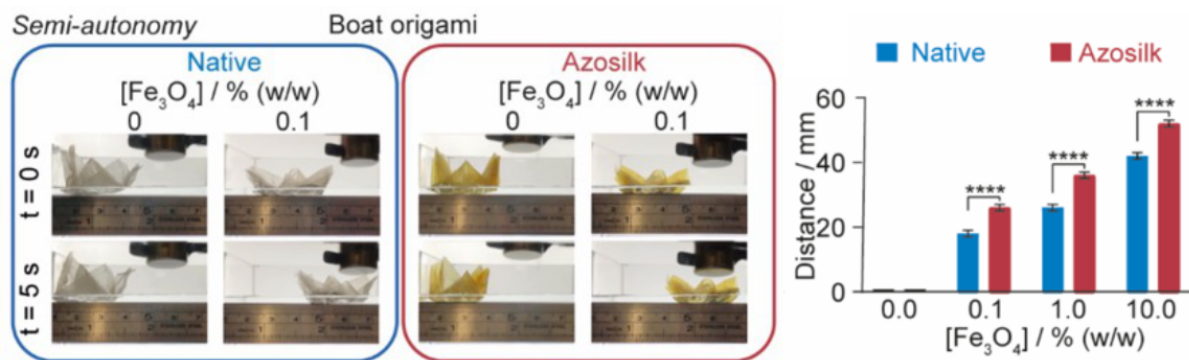
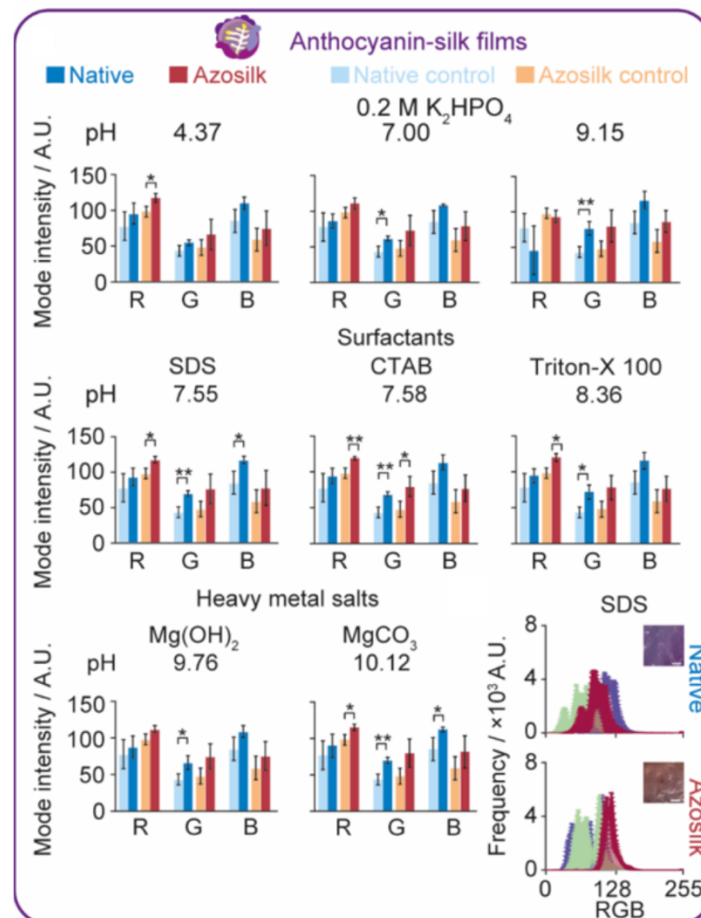
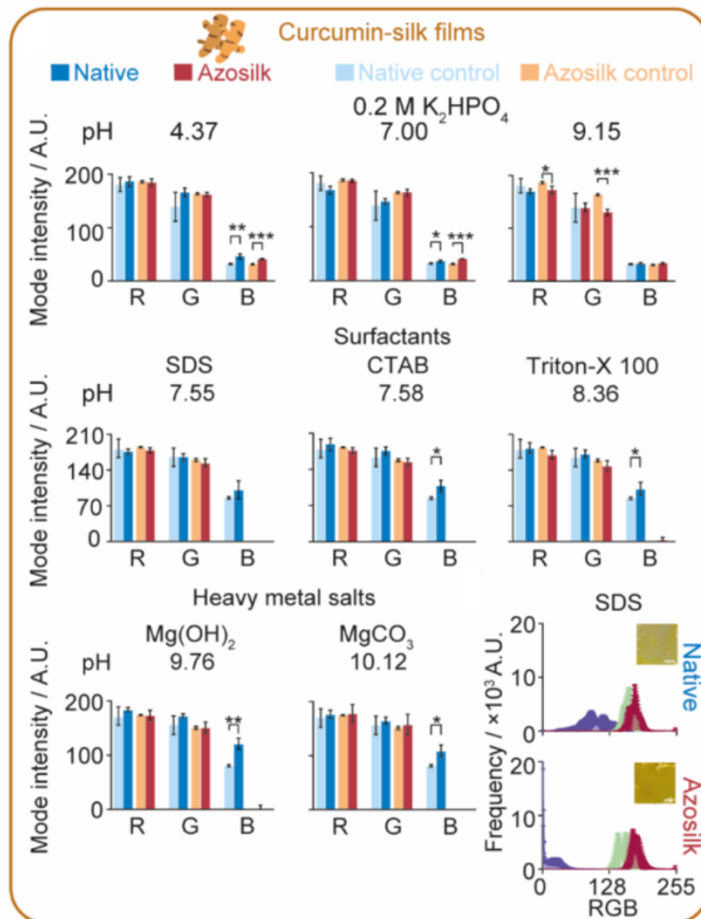


Figure 4-22. Semi-autonomous movement of origami silk boats across water using a magnet and distance travelled for both native and azosilk origami boats.



*Figure 4-23. The change in colour of curcumin-loaded and anthocyanin-loaded silk films with pH and environmentally relevant concentrations of cationic, neutral, and anionic surfactants and heavy metal complexes, measured with the mode intensities in the RGB colour space. The mode intensities of the red, green, and blue channels were extracted from the RGB histograms for curcumin-silk and anthocyanin-silk films. The native silk and azosilk films, following loading and washing with ultrapure H₂O, served as the controls. (n = 3, ± SD). Error bars are hidden in the bars and plot symbols when not visible. Scale bars = 0.5 cm. Multiple factors were evaluated by two-way analysis of variance (ANOVA), followed by Šidák's multiple comparison, simple effects post-hoc test. Sample pairs were analysed using the independent t-test. Asterisks denote statistical significance determined using the t-test and post-hoc tests as follows: *p < 0.05, **p < 0.01, ***p < 0.001, ****p < 0.0001.*

4.4 Discussion

The intentional spreading of cells and encouragement of directional growth can be used for improving wound healing and closure (Wang, et al., 2021, Schneider, et al., 2010, Molinie & Gautraeu, 2018) and silk has shown suitability for wound dressings throughout this thesis and work by others (Farokhi, et al., 2018). Micropatterning can direct cell growth (Li, et al., 2023, D'Ovidio, et al., 2019) and discourage bacterial biofilm formation. The initial aims of this chapter were to determine if silk hydrogels could be cast with micropatterns that would be maintained through handling. Silk films had the ability to retain micropatterns when cast on PDMS, and after crystallisation, maintained these micro-structures. This observation is in line with earlier work (Youn, et al., 2021, Wang, et al., 2019, Wang, et al., 2017). The patterns were also unaffected by the addition of iron particles. Silk hydrogels were also able to be micropatterned when cast on PDMS during the sol-gel transition. The characterisation of the micropatterns could be further investigated to fully understand the 3D nature of the patterning. Confocal microscopy was investigated as a potential method with DAPI stained hydrogels to view the depth of the micropatterns, but images were unsuccessful, and the patterns were not able to be discerned from the rest of the hydrogel. Other methods, such as atomic force microscopy (AFM) could be used to map the surface of hydrogels and films. Initial results with fibroblast cells on silk hydrogels suggest the growth is not influenced by the micropattern, but cells will survive when grown on silk hydrogels with patterns. This could be an important result with further research into how films and hydrogels degrade with the micropatterns, and how further culturing of cells could reveal

protein expression or cytoskeleton differences when cultured on flat and micropatterned surfaces. Another important characteristic of silk films investigated was the ability of films to be loaded and folded.

The crystallinity of silk fibroin films can increase with drying time (DeBari, et al., 2021); therefore, the films were methanol annealed to induce β -sheet self-assembly for scalable origami production and to enable the loading of lipophilic dyes during this step. Water annealing was used to increase the plasticity and fracture resistance of the semicrystalline films (Hu, et al., 2011, Jin, et al., 2005) during folding, while stiffness was regained upon drying. The post-casting modification of silk films by diazonium coupling (Murphy, et al., 2008, Zhao, et al., 2014) of benzene diazonium with tyrosine and histidine residues was used to increase the hydrophobicity of the film surface.

The effect of the thickness of the film on the ability to fold was measured over time. The time of plasticity of the films increased as the thickness increased, suggesting that due to the ratio of surface area to moisture in the film reducing, the evaporation rate was reduced and thus the film remained able to be folded for longer. The ability of silk films to swell with water have been documented previously (Lawrence, et al., 2010) with the hydration of the film altering the mechanical properties of the film.

When the films were submerged in water, the weight of the film changed which suggests the film was rehydrating. Films spiked with both iron oxide and silk fibres were also able to retain these folding properties for similar times. Films spiked with iron oxide were also able to be moved by a neodymium magnet across the surface of

water. Changing the concentration of iron oxide resulted in a change in the distance of magnetism which would allow the films to be altered for desired movement.

Curcumin was loaded onto films doped with 0.1 % iron oxide particles with medium thickness. Once curcumin was added to these films, a visible colour change was exhibited. Curcumin had a bright yellow/orange appearance when solubilised in methanol which was displayed on the films. The films with iron oxide were relatively transparent with a grey hue. Once loaded with curcumin, the films remained slightly transparent but had a strong yellow hue. To test the pH sensing ability of curcumin the films were then exposed to varying pH levels. Between pH 4.37 and pH 8.16 the films were yellow, yellow-orange between 9.15 and 10.50, and orange-red at pH 11.36. The colour change was reversible and would return to yellow when rinsed in pH 6.5 water. The colour change confirmed the reversible tautomerisation of curcumin from the predominant yellow keto form in the acidic and neutral environments to the red enol form as basicity increased above pH 8 (Chen, et al., 2020). Anthocyanin-loaded films were pink-purple at acidic pH due to the dominant cationic flavylum species (Chen, et al., 2020) (Fenger, et al., 2019), purple at pH 7.00 and blue at pH 9.15, as equilibrium favoured the quinoidal anhydrobase (Chen, et al., 2020, Fenger, et al., 2019). In the RGB colour space, the green channel intensity of native films increased with pH, while the red channel intensity decreased for azosilk films. Consequently, data from deployed silk origami eco-sensors could be monitored in near real-time using field conditions or remotely by aerially acquired images. Increasing alkalinity in wounds has been shown to influence the survival and proliferation of bacteria, with *Pseudomonas aeruginosa* producing virulence factors

such as alginate and proteinase at pH 8, and both *Pseudomonas aeruginosa* and *Klebsiella pneumoniae* had increased biofilm growth in alkaline conditions (Bennison, et al., 2017). Chronic wounds have also been found to be predominantly alkaline (Jones, et al., 2015). The curcumin and anthocyanin loaded silk films displayed visible colour changes when exposed to increasing alkalinity of their environment, indicating that the incorporation of these agents into wound dressings could offer a visual indication of the pH of the wound bed and therefore the risk of bacterial infection or progression of a wound healing.

The boats preserved their shape for at least 3 days on water and could exhibit colour changes within 1 minutes after exposure to solutions of basic metal salts and surfactants. These eco-green sensors demonstrate the practical importance of origami for engineering silk devices and enable a simple, deployable approach for direct monitoring of pH and pollution.

4.5 Conclusion

Silk can be manipulated into hydrogels that incorporate micropatterns which could be useful for directing cell proliferation into ordered patterns to improve healing outcomes and reduce infection by preventing biofilm formation. Silk films can be produced which can be folded into many shapes and dried, retaining the form. Curcumin can be loaded onto these films to improve wound healing outcomes by detecting pH changes locally and reducing the duration of inflammation.

5. Chapter 5 General Discussion and Conclusions

The following chapter summarises the research outputs included within this thesis including: (i) Chapter 2: the cellular impact of silk fibroin hydrogels in the context of wound healing (Egan, et al., 2022), (ii) Chapter 3: antibacterial effects and sterility of silk fibroin solution (Egan, et al., submitted), and (iii) Chapter 4: the versatility of silk fibroin as origami films for biological testing (Matthew, et al., 2022). The ability of silk films and hydrogels to maintain a micropattern is also reviewed. For future work, further investigation into the role of patterning in cellular alignment on silk fibroin films and hydrogels is proposed as the next steps. The thesis is then brought to an overall conclusion.

5.1 General Discussion

This thesis explored the use of silk fibroin in the context of wound care applications. The primary aim of this thesis was to investigate the biomaterials effects on wound closure and bacterial infiltration which was broken down into key aims and objectives to achieve this goal.

Since the start of this thesis, the area of wound care has continued to develop. New products are being tested with varied focus and results to improve the landscape of healthcare and reduce the burden of wounds on health services.

Wound dressing research has continued with new combinations of biomaterials being developed for the treatment of wounds with difficulty healing. In the realm of hydrogel wound dressings, polyethylene glycol with silver nitrate and the drug, deferoxamine, was monitored for diabetic and open wounds (Chen, et al., 2019). Another new dressing that has been developed is EHO-85 with antioxidant properties and stimulating granulation (Nguyen, et al., 2023). In the past five years, there have been 12 clinical trials published involving the use of hydrogel based wound dressings available on PubMed, indicating this area of research remains relevant and necessary. Likewise, silk fibroin research has continued, and new combinations and material formats have been investigated for various purposes as a biomaterial. In the area of silk fibroin as wound dressings, there have been 14 review papers published in the last five years, according to PubMed. Recent developments in the hydrogel wound dressing space include nanoparticle composite dressings, stem cell hydrogel composites, and curcumin- hydrogel composites (Zahra, et al., 2023). Silk fibroin solution based Nanosilk has been applied to diabetic skin samples, showing an

improvement in maximum load and modulus, strengthening the skin (Lehmann, et al., 2022). Work has also been done to investigate the use of silk fibroin as a biosensor due to the ability to immobilise enzymes such as uricase, phytase, and glucose oxidase (Lehmann, et al., 2022). Although there is much research in the area, no new clinical trials have been published involving silk fibroin as a wound dressing.

The advances in the field indicate the relevance of this thesis, as silk fibroin shows promise in a vast array of biomaterial formats in healthcare settings.

The first objective, covered in Chapter 2, was to determine the impact of silk fibroin hydrogels in a cellular capacity. Aqueous silk fibroin was processed into self-assembling hydrogels through electro-gelation or sonication to monitor the differences in these hydrogel types. Electro-gels contained significantly more silk than sonicated hydrogels of same weight (Figure 2-4), thought to be due to the electric field created when producing electro-gels. Electro-gels were also more amorphous than sonicated hydrogels, which were more crystalline. The silk release from both types of hydrogel were monitored in water and PBS at body temperature to mimic the application of the hydrogel topically. The secondary structure of the silk released from the hydrogels was then measured by FTIR and SDS PAGE, revealing that the silk released from both sonicated and electro-gels was rich in beta sheets (Figure 2-10). This indicated that there was a higher crystallinity of the silk released from the hydrogels when compared to aqueous silk solution. This was hypothesised to be due to an intermediate silk secondary structure in the incubation in the bulk aqueous phase when silk is more conformationally flexible and would be able to alter the secondary structure as once it is integrated into a hydrogel network, the silk is less

able to alter its conformation. The impact of the released silk was assessed on a fibroblast model in a scratch wound assay, proliferation assay, migration assay and phosphorylation assay. Receptor tyrosine kinase signalling showed that soluble silk supported fibroblast functions relevant for cell survival, proliferation, and motility. The proliferation of fibroblasts was unaffected in the presence of silk fibroin, which supported the hypothesis that silk was not cytotoxic to these cells. Cell migration was largely unaffected by the presence of silk, except at a key concentration of 1600 $\mu\text{g/ml}$. This response was thought to be an off-target effect, which suggests there is a complex biological response to silk fibroin which would require further investigation. In the scratch wound assay, cells exposed to silk fibroin showed a faster migration into the wound area. However, many questions remain that require further work, for example:

1. What is the effect of leached aqueous silk fibroin on other cell types such as epidermal cells?
2. Does the silk hydrogel itself affect the closure of a wound?
3. Does the silk hydrogel degrade over time and how does the silk break down?

From these questions, there are future experiments that could be done to further validate these results discussed. Other cell types could be analysed with the hydrogels and leached silk, and cell viability could be confirmed with other assays such as nucleic acid binding dyes to monitor the live cells present. Biodegradation is an important factor in this study due to the use of hydrogels topically. More work should be done to monitor and quantify the biodegradation over time in a simulated wound environment before progression to in vitro studies. The hydrogels can be

monitored for silk release over long periods and also imaged to view the breakdown of solid matter.

This work provided the first evidence of the potential use of aqueous silk fibroin leached from hydrogels in aiding wound healing.

The next objective, covered in Chapter 3, was to assess the antibacterial effects of aqueous silk fibroin and the inherent sterility of the solution. The processing of the silk solution was assessed to determine if remaining lithium bromide caused the solution to affect bacterial cells, but it was found to be removed. The secondary structure of the silk solution was also found to remain stable at increased temperatures and rocking (Figure 3-6). Silk solution was found to possess inherent sterility when incubated with TSB growth media and in aerobic and anaerobic conditions on blood and chocolate agar. This is interesting as silk is produced aseptically on the benchtop, and after storage for 14 days once produced, all samples did not contain microbial growth (Figure 3-1, 3-7). This result was reinforced by the spiking of sterile silk with known pathogens, *Staphylococcus aureus* and *Pseudomonas aeruginosa*. After spiking silk solutions $\geq 4\%$ (w/v), no viable bacterial cells were seen, suggesting that aqueous silk fibroin could impede bacterial growth and survival, thought to be due to the glycine present in the silk chains. However, many questions remain that require further work. For example:

1. How does aqueous silk fibroin interact with other bacterial cell types?
2. Does the processing of the silk affect the bactericidal effects? If silk is reverse engineered with other chemical agents such as sodium hydroxide (DeBari, et al., 2021)

3. Do the antimicrobial properties of aqueous silk fibroin translate across other formats such as hydrogels?

The work in this chapter provided a baseline measurement of the antibacterial effects of silk fibroin, but this work disagreed with some literature. Previous work in the area has found mixed results on the antibacterial effects of silk fibroin (Seves, et al., 1998), but the work reported in this thesis is unique in the processing of silk and bacterial strains studied. To address the contradictory results some future experiments can be undertaken to review the effects of silk. The sterility studies performed in this thesis were also monitored visually, where in future the use of a spectrophotometer to quantify the turbidity of the TSB solution. The sterility was verified with the use of blood and chocolate agar to back up these results.

The final objective was to investigate the versatility of silk fibroin and explore the uses out-with conventional biomaterials in an adjacent avenue (Chapter 4). Curcumin has been used previously for wound healing applications, so the ability of silk fibroin films to incorporate this could be beneficial for wound dressings. The curcumin and anthocyanin loaded films were able to detect contaminants in water through displaying colour changes in response to the environment. This could also be useful in a wound dressing context as bacterial infections in wounds could alter the alkalinity of a wound bed. There are many questions that still require answering, however.

Examples are:

1. What other contaminants could be detected with the loaded films?
2. How can the colour change of the silk boat be detected consistently in different solutions?

3. What is the lifespan of the silk boats in contaminated water and how quickly do the boats degrade?

The work in the final chapter was more focussed on the environmental sensing capabilities of the silk films produced. To verify the translation of these films to wound dressing sensing abilities, future work can be done to monitor the effects of the curcumin and anthocyanin topically, and the release from the silk films. Work should also be done to monitor the ability of silk hydrogels to incorporate these agents and exhibit beneficial colour changing or anti-inflammatory effects. The micropatterning work discussed in this chapter was very preliminary but the promising ability of silk to incorporate these micropatterns is encouraging for future research. The cell studies were only performed with the hydrogels and imaged once, so more work should be done in this area to verify the cells ability to adhere to the surface of patterned and non-patterned hydrogels, and these cells can be characterised to determine the effects of the patterned hydrogels on them.

5.2 Recommendations for future research

This project explored the application of silk fibroin in a wound environment to potentially improve healing processes and shorten the time it took to recovery. The project provides a strong starting point for future development into topical application of silk fibroin to improve prospects in wound management but requires further work and development before a final judgement can be made.

The project was impacted by the Covid-19 pandemic and university closure which means there were many limitations in the work undertaken. The main project affected was the micropatterning of hydrogels and films, and as discussed, the origami work was undertaken as a team to maximise outputs during restricted laboratory access.

To further investigate the micropatterning, I would recommend further imaging is performed to map the depth of the patterns. This work would also benefit from in vitro studies to monitor how live cells navigated the surface. This could involve morphological studies such as imaging and live-mapping of the cell distribution. Fibroblast cells could be stained to show the actin filaments which would indicate the movement and attachment of the cells. As part of this study, I would recommend surface wettability and water contact angle to be measured on the micropatterned surfaces. This would allow understanding of the effects that these features have on the cell attachment and motility. Studies have already indicated that cells can be aligned in micropatterns and if silk hydrogels can be adapted to have similar results this would be ideal for wound healing applications (Wang, et al., 2017, Youn, et al., 2021). Longevity studies would also need to be performed to identify the lifespan of

the hydrogels in situ, determining how the gel breaks down over time and how long the pattern lasts. I have shown that hydrogels release silk over time in water and PBS, so it is expected that the hydrogel will degrade. It would be interesting to know if the cells remain in the aligned state also. Finally, I would recommend bacterial studies are done on the micropatterned surfaces. Studies have indicated that in nature, micropatterns disrupt the formation of biofilms and can reduce bacterial adherence. Regarding silk release from hydrogels and the resultant effect on cells, these studies would benefit from a wider variety of cell types being tested with the silk fibroin. Although fibroblasts are a key cell type in skin and wound remodelling, other cell types such as keratinocytes, macrophages, and endothelial cells are key in the proliferative stages of wound healing (Wilkinson & Hardman, 2020). As such, it would be beneficial to understand how the presence of silk fibroin influences these cell types too to build a greater picture of the potential implementation in wound care. This work would also benefit from in vivo studies to monitor wound closure with the application of hydrogels or aqueous solution. The ability of the silk films to retain dyes was investigated, and this work would benefit from future studies investigating the ability of films and hydrogels to bind to drugs and monitor their release profiles as the biomaterial degrades. Relevant drugs could include antibiotics, such as penicillins or clindamycin, or antiseptics, such as iodine or chlorhexidine, that could be beneficial in a wound environment (Norman, et al., 2016).

Another recommendation for future work to further investigate the sterility and antibacterial effects of aqueous silk fibroin would be to test it with other bacterial cell lines that would be relevant in a wound environment such as *Klebsiella*

pneumoniae and *Proteus mirabilis* (Puca, et al., 2021). Bessa et al. (2015) found *Proteus mirabilis* in 10% of wounds cultured, third most commonly after *Staphylococcus aureus* (37%) and *Pseudomonas aeruginosa* (17%). *Proteus mirabilis* is a rod-shaped bacterium that commonly develops antimicrobial resistance which could be important to tackle if silk was to be used as a wound care agent (Shelenkov, et al., 2020). Antimicrobial resistance (AMR) is on the rise in other strains of bacteria, and new antibacterial agents are required to tackle the growing resistance amongst pathogenic bacteria (Murray, et al., 2022). As such, it would also be advisable to monitor the effectiveness of silk against bacterial strains with known antibiotic resistance, such as methicillin resistant *Staphylococcus aureus* (MRSA). Another future experiment could involve imaging the bacterial cells after exposure to silk through electron cryotomography to assess the morphology of the cells. This could help determine the mechanism through which silk appears to render the bacterial cells unviable. If the mechanisms employed by silk are unique, it could prove useful in the fight against AMR and reduce the mutations amongst bacteria to develop resistance to antibacterial agents.

The eco-sensing aspect of silk fibroin films could be further investigated with other natural dyes loaded onto films and in a greater array of contaminated waters. The ability of the colour change to be assessed by an arial imaging device on a body of water should also be recorded. This could indicate future uses of the eco-sensor canoe as the movement of water, what is beneath the surface of the water and a change in the colour of the boat may require more advanced imaging than a conventional camera.

5.3 Conclusion

In summary, this thesis demonstrates the diverse properties of silk fibroin and explores the potential future applications in wound care. Silk fibroin released from hydrogels has been shown to be biocompatible and can aid wound closure by stimulating fibroblast movement. Aqueous silk fibroin solution has been shown to possess antimicrobial properties and inherent sterility with the potential to reduce bacterial viability when inoculated or contaminated with bacteria. Again, this is desirable in wound care applications. Silk can be manipulated into origami structures and show great potential for loading chemicals. The curcumin, when loaded onto silk films, still exhibits colour change properties when exposed to environmental pH changes. Overall, this work explores the multipurpose uses of silk fibroin, although further work demonstrating these properties with more cell types and pathogens would improve our understanding of the potential applications of this ancient material. This thesis serves as a strong foundation for future research into aqueous silk fibroin hydrogels and films for more targeted wound care.

Bibliography

- Abdel-Fattah, W. I., Atwa, N. & Ali, G. W., 2015. Influence of the protocol of fibroin extraction on the antibiotic activities of the constructed composites. *Progress in Biomaterials*, Volume 4, pp. 77-88.
- Abdel-Naby, W. et al., 2017. Treatment with solubilized Silk-Derived Protein (SDP) enhances rabbit corneal epithelial wound healing. 12 (11).
- Aboudiab, B., Tehrani-Bagha, A. R. & Patra, D., 2020. Curcumin degradation kinetics in micellar solutions: Enhanced stability in the presence of cationic surfactants. Volume 592.
- Akbik, D., Ghadiri, M., Chrzanowski, W. & Rohanizadeh, R., 2014. Curcumin as a wound healing agent. *Life Sci*, 116(1), pp. 1-7.
- Akiyama, H., Torigoe, R. & Arata, J., 1993. Interaction of *Staphylococcus aureus* cells and silk threads in vitro and in mouse skin. *J Dermatol Sci*, 6(3), pp. 247-57.
- Ali, A. et al., 2016. Synthesis, characterization, applications, and challenges of iron oxide nanoparticles. *Nanotechnol Sci Appl*, Volume 9, pp. 49-67.
- Allen Jr, L., 2018. Quality Control: Water Activity Considerations for Beyond-use Dates. *Int J Pharm Compd.*, 22(4), pp. 288-293.
- Amsler, F., Willenberg, T. & Blattler, W., 2009. In search of optimal compression therapy for venous leg ulcers: a meta-analysis of studies comparing diverse [corrected] bandages with specifically designed stockings. *J. Vasc. Surg.*, Volume 50, pp. 668-674.
- Andrade, A. M. et al., 2022. Role of Senescent cells in cutaneous wound healing. *Biology*, 11(12), p. 1731.
- Aracri, S. et al., 2021. Soft Robotics for Ocean Exploration and Offshore Operations: A Perspective. 8(6).
- Asakura, T., 2021. Structure of Silk I (Bombyx mori silk fibroin before spinning) -type II B-turn, not a-helix. *Molecules*, 26(12), p. 3706.
- Axelrod, H. & Pienta, K. J., 2014. Axl as a mediator of cellular growth and survival. *Oncotarget*, Volume 33, pp. 8818-8852.
- Axion Biosystems, 2023. *Wound healing assay: what, why and how*. [Online] Available at: <https://cytosmart.com/resources/resources/wound-healing-assay-what-why-and-how> [Accessed August 2023].
- Aykac, A., Karanlik, B. & Sehirli, A., 2018. Protective effect of silk fibroin in burn injury in rat model. *Gene*, Volume 641, pp. 287-291.
- Bainbridge, P., 2013. Wound healing and the role of fibroblasts. *J Wound Care*, 22(8), pp. 407-8, 410-12.
- Barnes, H. R., 1993. Wound care: fact and fiction about hydrocolloid dressings. *J Gerontol Nurs.*, 19(6), pp. 23-6.

- Basal, G., Altioik, D. & Bayraktar, O., 2010. Antibacterial Properties of Silk Fibroin/Chitosan Blend Films Loaded with Plant Extract. *Fibers and Polymers*, 11(1), pp. 21-27.
- Bennison, L. et al., 2017. The pH of wounds during healing and infection: a descriptive literature review. *Wound Practice and Research*, 25(2), pp. 63-69.
- Bessa, L. J., Fazii, P., Giulio, M. D. & Cellini, L., 2015. Bacterial isolates from infected wounds and their antibiotic susceptibility pattern: some remarks about wound infection. *Int Wound J*, Volume 12, pp. 47-52.
- Bettinger, C. J. et al., 2007. Silk Fibroin Microfluidic Devices. 19(5), pp. 2847-2850.
- Biltar, M., 2012. The GSK-3beta/Fyn/Nrf2 pathway in fibroblasts and wounds of type 2 diabetes: on the road to an evidence based therapy of non-healing wounds. *Adipocyte*, Volume 1, pp. 161-163.
- Black Country Partnership NHS Foundation Trust, 2016. *NHS*. [Online]
Available at: <https://www.bcpft.nhs.uk/documents/policies/w/1444-wound-management-guidelines/file>
[Accessed April 2023].
- Boonkanon, C., Phatthanawiwat, K., Wongniramaikul, W. & Choodum, A., 2020. Curcumin nanoparticle doped starch thin film as a green colorimetric sensor for detection of boron. Volume 224.
- Bourguignon, L., 2014. Matrix hyaluronan-activated CD44 signalling promotes keratinocyte activities and improves abnormal epidermal functions. *Am J Pathol*, Volume 184, pp. 1912-1919.
- Bowler, P. G., Duerden, B. I. & Armstrong, D. G., 2001. Wound Microbiology and Associated Approaches to Wound Management. *Clin Microbiol Rev*, 14(2), pp. 244-269.
- Britto, E. J., Nezwek, T. A., Popowicz, P. & Robins, M., 2022. Wound dressings. *StatPearls*.
- Brown, J. E. et al., 2019. Injectable silk protein microparticle-based fillers: a novel material for potential use in glottic insufficiency. *Journal of Voice*, 33(5), pp. 773-780.
- Byrd, A. L., Belkaid, Y. & Segre, J. A., 2018. The human skin microbiome. *Nature reviews microbiology*, Volume 16, pp. 143-155.
- Calamak, S., Erdogdu, C., Ozalp, M. & Ulubayram, K., 2014. Silk fibroin based antibacterial bionanotextiles as wound dressing materials. *Mater Sci Eng C Mater Biol Appl.*, Volume 43, pp. 11-20.
- Canadian Agency for Drugs and Technologies in Health, 2013. *Optimal Care of Chronic, non-healing, lower extremity wounds: A review of clinical evidence and guidelines*, Ottawa, Canada: s.n.
- Cao, Y. & Wang, B., 2009. Biodegradation of Silk Biomaterials. *Int J Mol Sci*, 10(4), pp. 1514-1524.
- Carlotti, A., 2023. *A3P*. [Online]
Available at: <https://www.a3p.org/en/investigation-by-molecular-method-of-potentially->

[non-compliant-aseptic-process-simulation-media-fill-test-aps-mft-and-sterility-test/](#)
[Accessed Sep 2023].

Carter, M. J., Tingley-Kelley, K. & Warriner, R. A., 2010. Silver Treatments and silver-impregnated dressings for the healing of leg wounds and ulcers: a systematic review and meta-analysis. *J. Am. Acad. Dermatol.*, Volume 63, pp. 668-679.

Chakraborty, J. & Ghosh, S., 2020. Cellular Proliferation, Self-Assembly, and Modulation of Signalling Pathways in Silk Fibroin Gelatin-Based 3D Bioprinted Constructs. *ACS Applied Bio Materials*, pp. 8309-8320.

Chawla, S. et al., 2017. Elucidating role of silk-gelatin bioink to recapitulate articular cartilage differentiation in 3D bioprinted constructs. *Bioprinting*, Volume 7.

Chen, H. et al., 2019. An injectable self-healing coordinative hydrogel with antibacterial and angiogenic properties for diabetic skin wound repair. *NPG Asia Materials*, 11(3).

Chen, H.-z., Zhang, M., Bhandari, B. & Yang, C.-h., 2020. Novel pH-sensitive films containing curcumin and anthocyanins to monitor fish freshness. Volume 100.

Chiarini, A. et al., 2003. Silk fibroin/poly(carbonate)-urethane as a substrate for cell growth: in vitro interactions with human cells. *Biomaterials*, Volume 24, pp. 789-799.

Chirila, T. V., Suzuki, S. & Papolla, C., 2017. A comparative investigation of Bombyx mori silk fibroin hydrogels generated by chemical and enzymatic cross-linking. *Biotechnol Appl Biochem*, Volume 64, pp. 771-81.

Chouhan, D., Lohe, T.-u., Samudrala, P. K. & Mandal, B. B., 2018. In Situ Forming Injectable Silk Fibroin Hydrogel Promotes Skin Regeneration in Full Thickness Burn Wounds. *Advanced Healthcare Materials*, 7(24).

Chouhan, D. & Mandal, B. B., 2020. Silk biomaterials in wound healing and skin regeneration therapeutics: from bench to bedside. *Acta Biomaterialia*, Volume 103, pp. 24-51.

Cialdai, F., Risaliti, C. & Monici, M., 2022. Role of fibroblasts in wound healing and tissue remodeling on Earth and in space. *Front. Bioeng. Biotechnol.*, Volume 10.

Cuello, E. A. et al., 2020. Development of micropatterning polyimide films for enhanced antifouling and antibacterial properties. Volume 188.

Cullum, N. & Liu, Z., 2017. Therapeutic ultrasound for venous leg ulcers. *Cochrane Database Syst. Rev.*, Volume 5.

Cundell, T., 2015. *The role of water activity in the microbial stability of non-sterile pharmaceutical drug products*. [Online]
[Accessed February 2023].

Dai, X. et al., 2017. Nano-formulated curcumin accelerates acute wound healing through Dkk-1-mediated fibroblast mobilization and MCP-1-mediated anti-inflammation. *NPG Asia Materials*, Volume 9.

Dealey, C., 2012. *The care of wounds: A guide for nurses*. 4 ed. Oxford: Wiley-Blackwell.

- DeBari, M. K., King, C. I., Altgold, T. A. & Abbott, R. D., 2021. Silk fibroin as a green material. *7(8)*, pp. 3530-3544.
- Demidova-Rice, T. et al., 2007. low level light stimulates excisional wound healing in mice. *Lasers Surg med*, Volume 39, pp. 706-715.
- Dey, S. et al., 2021. DNA Origami. Volume 1, pp. 1-24.
- Dhanwani, R., Prajapati, A., Dimri, A. & Varmora, A., 2021. Smart Earth Technologies: a pressing need for abating pollution for a better tomorrow. *28(1)*.
- Domigan, L. et al., 2015. Carbonic anhydrase generates a pH gradient in Bombyx mori silk glands. *Insect Biochem Mol Biol*, Issue 65, pp. 100-106.
- Dong, Z., Xia, Q. & Zhao, P., 2023. Antimicrobial components in the cocoon silk of silkworm, Bombyx mori. *International Journal of Biological Macromolecules*, Volume 224, pp. 68-78.
- Donlan, R. M. & Costerton, W. J., 2002. Biofilms: Survival Mechanisms of Clinically Relevant Microorganisms. *15(2)*, pp. 167-193.
- D'Ovidio, T. J. et al., 2019. Micropattern-mediated apical guidance accelerates epithelial cell migration to improve healing around percutaneous gastrostomy tubes. *Biomedical Physics & Engineering Express*, Volume 5.
- Dowsett, C. & Newton, H., 2005. *woundsinternational*. [Online] Available at: https://www.woundsinternational.com/uploads/resources/content_9029.pdf [Accessed April 2023].
- Du, L. et al., 2020. From a body temperature-triggered reversible shape-memory material to high-sensitive bionic soft actuators. Volume 18.
- Edmonds, M., 2012. Body of Knowledge around the diabetic foot and limb salvage. *Journal of Cardiovascular Surgery*, Volume 53, pp. 605-616.
- Egan, G. et al., 2022. Impact of silk hydrogel secondary structure on hydrogel formation, silk leaching and in vitro response. *Scientific Reports*, Volume 12, p. 3729.
- Ehrig, S. et al., 2019. Surface tension determines tissue shape and growth kinetics. *Biophysics*, *5(9)*.
- Eming, S., Martin, P. & Tomic-Caric, M., 2014. Wound repair and regeneration: mechanisms, signalling and translation. *Sci Transl Med*, Volume 6, pp. 265-266.
- Emiroglu, G. et al., 2017. The effects of curcumin on wound healing in a rat model of nasal mucosal trauma. *Evidence-based complementary and alternative medicine*.
- Ennis, W., Sui, A. & Bartholomew, A., 2013. Stem cells and healing: impact on inflammation. *Adv Wound Care*, Volume 2, pp. 369-378.
- Faber, J. A., Arrieta, A. F. & Studart, A. R., 2018. Bioinspired spring origami. *359(6382)*.
- Falanga, V., 2000. Classifications for wound bed preparation and stimulation of chronic wounds. *Wound Repair Regen*, *8(5)*, pp. 347-52.

- Falanga, V., 2002. Wound bed preparation and the role of enzymes: A case for multiple actions of therapeutic agents. *Wounds: a compendium of clinical research and practice*, 14(2), pp. 47-57.
- Falanga, V., 2005. Wound healing and its impairment in the diabetic foot. *lancet*, Volume 366, pp. 1736-1743.
- Fang, H., Zhang, Y. & Wang, K. W., 2017. Origami-based earthworm-like locomotion robots. 12(6).
- Farokhi, M. et al., 2021. crosslinking strategies for silk fibroin hydrogels: promising biomedical materials. *Biomedical Materials*, 16(2), p. 022004.
- Farokhi, M. et al., 2018. Overview of Silk Fibroin Use in Wound Dressings. *Trends in Biotechnology*, 36(9), pp. 907-922.
- Fenger, J.-A. et al., 2019. The influence of acylation, metal binding and natural antioxidants on the thermal stability of red cabbage anthocyanins in neutral solution. Issue 10.
- Fernandez-Garcia, L. et al., 2016. Safety and tolerability of silk fibroin hydrogels implanted into the mouse brain. *Acta biomaterialia*, Volume 45, pp. 262-275.
- Fernandez-Garcia, L. et al., 2018. Cortical Reshaping and Functional Recovery Induced by Silk Fibroin Hydrogels-Encapsulated Stem Cells Implanted in Stroke Animals. *Front. Cell. Neurosci.*, 12(296).
- Fernandez-Marin, R., Fernandes, S. C. M., Sanchez, M. A. A. & Labidi, J., 2022. Halochromic and antioxidant capacity of smart films of chitosan/chitin nanocrystals with curcuma oil and anthocyanins. Volume 123.
- Fini, M. e. a., 2005. The healing of confined critical size cancellous defects in the presence of silk fibroin hydrogel. *biomaterials*, Volume 26, pp. 3527-3536.
- Floren, M., Migliaresi, C. & Motta, A., 2016. Processing techniques and applications of silk hydrogels in bioengineering. *J Funct Biomater*, Volume 7, p. 26.
- Forbes India, 2023. *FibroHeal Woundcare: Silken touch for healthcare*. [Online] Available at: <https://www.forbesindia.com/article/startups/fibroheal-woundcare-silken-touch-for-healthcare/83321/1> [Accessed Sep 2023].
- Francolini, I. & Donelli, G., 2010. Prevention and control of biofilm-based medical-device-related infections. 59(3), pp. 227-238.
- Freiesleben, S. H., Soelberg, J., Nyberg, N. T. & Jager, A. K., 2017. Determination of the wound healing potentials of medicinal plants historically used in Ghana. *Evid Based Complement Alternat Med*.
- Frobose, N. J., Idelevich, E. A. & Schaumburg, F., 2021. Short Incubation of Positive Blood Cultures on Solid Media for Species Identification by MALDI-TOF MS: Which Agar is the Fastest?. *Microbiol Spectr*, 9(1), pp. 00038-21.

- Frykberg, R. & Banks, J., 2015. Challenges in the treatment of chronic wounds. *Wound Healing Society*, pp. 560-582.
- Galvez, P. et al., 2014. Standard Requirement of a Microbiological Quality Control Program for the Manufacture of Human Mesenchymal Stem Cells for Clinical Use. *Stem cells dev*, 23(10), pp. 1074-1083.
- George, K. A. et al., 2013. Effect of the sterilization method on the properties of Bombyx mori silk fibroin films. *Mater Sci Eng C Mater Biol Appl.*, 33(2), pp. 668-74.
- Ge, Y. et al., 2018. A Bio-inspired homogeneous graphene oxide actuator driven by moisture gradients. Issue 25.
- Ghalei, S. & Handa, H., 2022. A review on antibacterial silk fibroin-based biomaterials: current state and prospects. *Materialstoday chemistry*, Volume 23, p. 100673.
- Ghavamian, S. et al., 2021. Three-Dimensional Micropatterning Deters Early Bacterial Adherence and Can Eliminate Colonization. 13(20), pp. 23339-23351.
- Gil, E. S. et al., 2014. Impact of sterilization on the enzymatic degradation and mechanical properties of silk biomaterials. *Macromol Biosci*, 14(2), pp. 257-69.
- Gontcharova, V. et al., 2010. A comparison of bacterial composition in diabetic ulcers and contralateral intact skin. *Open microbiol J*, Volume 4, pp. 8-19.
- Gorenkova, N. et al., 2021. The innate immune response of self-assembling silk fibroin hydrogels. *Biomater Sci*, Volume 9, pp. 7194-7204.
- Gorenkova, N., Osama, I., Seib, F. P. & Carswell, H. V., 2019. In vivo evaluation of engineered self-assembling silk fibroin hydrogels after intracerebral injection in a rat stroke model. *ACS Biomater. Sci. Eng.*, Volume 5, pp. 859-869.
- Gray, M., 2008. Is larval (maggot) debridement effective for removal of necrotic tissue from chronic wounds. *J Wound Ostomy Continence Nurs.*, 35(4), pp. 378-84.
- Greaves, N. S., Benatar, B., Baguneid, M. & Bayat, A., 2013. Single-stage application of a novel decellularized dermis for treatment-resistant lower limb ulcers: positive outcomes assessed by SIAscopy, laser perfusion, and 3D imaging, with sequential timed histological analysis. *Wound repair regen.*, 21(21), pp. 813-822.
- Guan, Y. et al., 2020. Silk fibroin hydrogel promote burn wound healing through regulating TLN1 expression and affecting cell adhesion and migration. *J Mater Sci Mater Med*, 31(5).
- Guest, J. F., Fuller, G. W. & Vowden, P., 2020. Cohort study evaluating the burden of wounds to the UK's National Health Service in 2017/2018: update from 2012/2013. *BMJ Open*, 10(12).
- Guo, C., Li, C. & Kaplan, D. L., 2020. Enzymatic Degradation of Bombyx mori Silk Materials: A Review. *Biomacromolecules*, 21(5), pp. 1678-1686.
- Guo, S. & DiPietro, L., 2010. Factors Affecting Wound Healing. *J Dent Res*, 89(3), pp. 219-229.

- Gu, X. et al., 2021. Pure-silk fibroin hydrogel with stable aligned micropattern toward peripheral nerve regeneration. *10(1)*, pp. 10-19.
- Haghighattalab, M. et al., 2022. Silk Fibroin Hydrogel Reinforced With Magnetic Nanoparticles as an Intelligent Drug Delivery System for Sustained Drug Release. *Front Bioeng Biotechnol*, Volume 10, p. 891166.
- Halasz, K. & Csoka, L., 2018. Black chokeberry (*Aronia melanocarpa*) pomace extract immobilized in chitosan for colorimetric pH indicator film application. Volume 16, pp. 185-193.
- Halim, A. S., Khoo, T. L. & Mat Saad, A. Z., 2012. Wound bed preparation from a clinical perspective. *Indian J Plast Surg*, 45(2), pp. 193-202.
- Hallsworth, J., 2022. Water is a preservative of microbes. *Microbial Biotechnology*, 15(1), pp. 191-214.
- Han, G. & Ceilley, R., 2017. Chronic wound healing: a review of current management and treatments. *Adv Ther*, Volume 34, pp. 599-610.
- Hartmann, F., Baumgartner, M. & Kaltenbrunner, M., 2020. Becoming Sustainable, The New Frontier in Soft Robotics. 33(19).
- Hashimoto, T. et al., 2020. The influence of thermal treatments on the secondary structure of silk fibroin scaffolds and their interaction with fibroblasts. Volume 2.
- Heller, E. & Fuchs, E., 2015. Tissue Patterning and cellular mechanics. *J Cell Biol*, 211(2), pp. 219-231.
- Herrick, S., Sloan, P., McGurk, M. & al, e., 1992. Sequential changes in histologic pattern and extracellular matrix deposition during the healing of chronic venous ulcers. *Am J Pathol*, Volume 141, pp. 1085-1095.
- He, S. et al., 2019. Heparinized silk fibroin hydrogels loading FGF1 promote the wound healing in rats with full-thickness skin excision. *Biomedical engineering online*, Volume 18.
- Hewlings, S. J. & Kalman, D. S., 2017. Curcumin: A Review of It's Effects on Human Health. *Foods.*, 6(10), p. 92.
- Hirabayashi, K., Ayub, Z. H. & Kume, Y., 1990. Gelation of silk fibroin. *Sen'i Gakkaishi*, 46(11), pp. 521-524.
- Hofmann, S. et al., 2014. Effect of sterilization on structural and material properties of 3-D silk fibroin scaffolds. *Acta Biomater*, 10(1), pp. 308-17.
- Holland, C., Numata, K., Rnjak-Kovacina, J. & Seib, F., 2019. The Biomedical Use of Silk: Past, Present, Future. 8(1).
- Horne, J. et al., 2020. Interfacial Phenomena of Advanced Composite Materials toward Wearable Platforms for Biological and Environmental Monitoring Sensors, Armor, and Soft Robotics. 7(4).

- Huang, E. & Reichardt, L. F., 2003. Trk receptors: roles in neuronal signal transduction. *Annu Rev Biochem*, Volume 72, pp. 609-642.
- Hu, L. et al., 2020. Direct observation of native silk fibroin conformation in silk gland of *Bombyx mori* silkworm. *ACS Biomater Sci Eng*, 6(4), pp. 1874-1879.
- Hu, X., Kaplan, D. & Cebe, P., 2006. Determining Beta-Sheet Crystallinity in Fibrous Proteins by Thermal Analysis and Infrared Spectroscopy. *Macromolecules*, 39(18), pp. 6161-6170.
- Hu, X. et al., 2011. Regulation of silk material structure by temperature-controlled water vapor annealing. 12(5).
- Iglewski, B., 1996. Medical Microbiology 4th edition. In: Galveston TX: University of Texas Medical Branch at Galveston, p. Chapter 27.
- Janani, G. et al., 2019. Insight into Silk-Based Biomaterials: From Physicochemical Attributes to Recent Biomedical Applications. *ACS Appl. Bio Mater*, 2(12), pp. 5460-5491.
- Jarvis, G. N. et al., 2001. The mechanism of carbonate killing of *Escherichia coli*. *Lett Appl Microbiol*, 33(3), pp. 196-200.
- Jeong, L. e. a., 2009. Plasma-treated silk fibroin nanofibres for skin regeneration. *int J biol Macromol*, Volume 44, pp. 222-228.
- Jewell, M., Daunch, W., Bengtson, B. & Montarino, E., 2015. The development of SERI[®] Surgical Scaffold, an engineered biological scaffold. *Annals of the new york academy of sciences*, 1358(1), pp. 44-55.
- Jia, G. et al., 2021. Flexible, biocompatible and highly conductive MXene-graphene oxide film for smart actuator and humidity sensor. Volume 346.
- Jia, L., Zheng, W. & Huang, F., 2020. Vacuum-ultraviolet photodetectors. Volume 1.
- Jin, H.-J. & Kaplan, D. L., 2003. Mechanism of silk processing in insects and spiders. *Nature*, 424(6952), pp. 1057-1061.
- Jin, H. -J. et al., 2005. Water-stable Silk Films with Reduced B-Sheet Content. 15(8).
- Ji, Z. et al., 2017. Multimaterials 3D Printing for Free Assembly Manufacturing of Magnetic Driving Soft Actuator. 4(22).
- Jones, E. M., Cochrane, C. A. & Percival, S. L., 2015. The effect of pH on the extracellular matrix and biofilms. *Adv Wound Care (New Rochelle)*, 4(7), pp. 431-439.
- Jonkman, J. E. N. et al., 2014. An introduction to the wound healing assay using live-cell microscopy. *Cell Adh Migr*, 8(5), pp. 440-451.
- Ju, H. w. et al., 2014. Silk Fibroin based Hydrogel for Regeneration of Burn Induced Wounds. *Tissue Engineering and Regenerative Medicine*, 11(3), pp. 203-210.
- Ju, H. W. et al., 2016. Wound healing effect of electrospun silk fibroin nanomatrix in burn model. *int j biol macromol*, Volume 85, pp. 29-39.

- Kampf, G. & Hollingsworth, A., 2008. Comprehensive bactericidal activity of an ethanol-based hand gel in 15 seconds. *Annals of Clinical Microbiology and Antimicrobials*, Volume 7, p. 2.
- Kang, K. B. et al., 2019. The effect of micro- and nanoscale surface topographies on silk on human corneal limbal epithelial cell differentiation. Volume 9.
- Kaplan, D. L., 1998. Fibrous proteins- silk as a model system. *Polymer Degradation and stability*, Volume 59, pp. 25-32.
- Kaur, J. et al., 2013. Facts and myths of antibacterial properties of silk. *Biopolymers*, 101(3), pp. 237-245.
- Khalifa, I. & Ladhari, N., 2012. Eco-Friendly Finishes for Textile Fabrics. *Journal of the Textile Institute*, 103(4), pp. 370-377.
- Khoo, H. E., Azlan, A., Tang, S. T. & Lim, S. M., 2017. Anthocyanidins and anthocyanins: colored pigments as food, pharmaceutical ingredients, and the potential health benefits. *Food Nutr Res*, 61(1).
- Kim, B. H. et al., 2021. Three-dimensional electronic microfliers inspired by wind-dispersed seeds. Volume 597.
- Kim, C. et al., 2017. Effects of silk fibroin in murine dry eye. Volume 7.
- Kim, H. e. a., 2016. Osteoinductive silk fibroin/titanium dioxide/hydroxyapatite hybrid scaffold for bone tissue engineering. *Int J Biol Macromol*, Volume 82, pp. 160-167.
- Kim, J.-Y. et al., 2010. Low molecular weight silk fibroin increases alkaline phosphatase and type I collagen expression in MG63 cells. *BMB Rep*, 43(1), pp. 52-6.
- Kim, J. H., Pyo, J.-B. & Kim, T.-S., 2020. Highly Mobile Levitating Soft Actuator Driven by Multistimuli-Responses. 7(21).
- Kim, U.-J. et al., 2004. Structure and properties of silk hydrogels. *Biomacromolecules*, Volume 5, pp. 786-92.
- Kojic, N. et al., 2012. Ion electrodiffusion governs silk electrogelation. *Soft matter*, 8(26), pp. 6897-6905.
- Kostakioti, M., Hadjifrangiskou, M. & Hultgren, S. J., 2013. Bacterial Biofilms: Development, Dispersal, and Therapeutic Strategies in the Dawn of the Postantibiotic Era. *Cold Spring Harb Perspect Med*, 3(4).
- Kronqvist, N. et al., 2017. Efficient protein production inspired by how spiders make silk. *Nature*, Issue 8, p. 15504.
- Kumari, A. et al., 2022. Wound-Healing Effects of Curcumin and Its Nanoformulations: A Comprehensive Review. *Pharmacautics*, 14(11).
- Kwak, H. W. et al., 2017. Sericin Promotes Fibroin Silk I Stabilization Across a Phase-Separation. *Biomacromolecules*, Issue 18, pp. 2343-2349.

Kweon, H., Ha, H. C., Um, I. C. & Park, Y. H., 2001. Physical properties of silk fibroin/chitosan blend films. *Journal of Applied Polymer Science*, Volume 80, pp. 928-934.

Lab Pro, 2021. *How does pH paper work and what does it detect?*. [Online] Available at: <https://labproinc.com/blogs/laboratory-equipment/how-does-ph-paper-work-and-what-does-it-detect> [Accessed August 2023].

Lawrence, B. D. et al., 2012. Human Corneal Limbal-Epithelial Cell Response to Varying Silk Film Geometric Topography In Vitro. 8(10), pp. 3732-3743.

Lawrence, B. D., Pan, Z. & Rosenblatt, M. I., 2012. Silk Film Topography Directs Collective Epithelial Cell Migration. 7(11).

Lawrence, B. D. et al., 2010. Effect of Hydration on Silk Film Material Properties. *Macromolecular Bioscience*, Volume 10, pp. 393-403.

Lecomte, A. et al., 2015. Silk and PEG as means to stiffen a parylene probe for insertion in the brain: toward a double time-scale tool for local drug delivery. Volume 25.

Lee, K. Y. & Mooney, D. J., 2012. Alginate: properties and biomedical applications. *Prog Polym Sci*, 37(1), pp. 106-126.

Lee, M., Seo, S. & Kim, J.-C., 2012. B-cyclodextrin, polyethyleneimine and silk fibroin hydrogel containing Centella asiatica extract and hydrocortisone acetate: releasing properties and in vivo efficacy for healing of pressure sores. *Clinical and Experimental Dermatology*, 37(7).

Lefevre, T., Rousseau, M.-E. & Pezolet, M., 2007. Protein secondary structure and orientation in silk as revealed by raman spectroscopy. *Biophys J*, 92(8), pp. 2885-2895.

Lehmann, T. et al., 2022. Silk fibroin-based therapeutics for impaired wound healing. *Pharmaceutics*, 14(3), p. 651.

Leisk, G. et al., 2010. Electrogelation for protein adhesives. *Adv Mater*, Volume 22, pp. 711-715.

Lescarbaeu, et al., 2012. In vitro model of metastasis to bone marrow mediates prostate cancer castration resistant growth through paracrine and extracellular matrix factors. *PLoS One*, Volume 7.

Lewis, K., 2008. Multidrug tolerance of biofilms and persister cells. Volume 322, pp. 107-131.

Liang, C.-C., Park, A. Y. & Guan, J.-L., 2007. In vitro scratch assay: a convenient and inexpensive method for analysis of cell migration in vitro. *Nature Protocols*, Volume 2, pp. 329-333.

Liao, C.-H. & Shollenberger, L., 2003. Survivability and long-term preservation of bacteria in water and phosphate-buffered saline. *Lett Appl Microbiol*, 37(1), pp. 45-50.

Li, B. & Wang, J. H.-C., 2011. Fibroblasts and Myofibroblasts in Wound Healing: Force Generation and Measurement. *J Tissue Viability*, 20(4), pp. 108-120.

- Li, G. & Sun, S., 2022. Silk fibroin-based biomaterials for tissue engineering applications. *Molecules*, 27(9), p. 2757.
- Li, J. et al., 2023. Micropatterned composite membrane guides oriented cell growth and vascularisation for accelerating wound healing. *Regenerative Biomaterials*, Volume 10.
- Lin, Y. et al., 2013. Tuning Chemical and Physical Cross-Links in Silk Electrodes for Morphological Analysis and Mechanical Reinforcement. *Biomacromolecules*, 14(8), pp. 2629-2635.
- Li, S. et al., 2018. Antibacterial hydrogels. *Advanced Science*, 5(5), p. 1700527.
- Li, S. et al., 2019. Architected Origami Materials: How Folding Creates Sophisticated Mechanical Properties. Volume 31.
- Li, S. et al., 2018. In vivo degradation and neovascularization of silk fibroin implants monitored by multiple modes ultrasound for surgical applications. *Biomed Eng Online*, 17(87).
- Liu, H. et al., 2023. Optimization of surface-engineered micropatterns on bacterial cellulose for guided scar-free skin wound healing. *Biomolecules*, 13(5), p. 793.
- Liu, L., Han, Y. & Lv, S., 2019. Design of Self-Healing and Electrically Conductive Silk Fibroin-Based Hydrogels. *ACS Appl Mater Interfaces*, 11(22), pp. 20394-20403.
- Liu, T.-L. et al., 2010. Cytocompatibility of regenerated silk fibroin film: a medical biomaterial applicable to wound healing. *J Zhejiang Univ Sci B*, 11(1), pp. 10-16.
- Li, Y. S. et al., 2016. Protease Inhibitors in Bombyx mori silk might participate in protecting the pupating larva from microbial infection.. *Insect Science*, 23(6), pp. 835-842.
- Li, Z. et al., 2020. Topical application of silk fibroin-based hydrogel in preventing hypertrophic scars. *Colloids Surf B Biointerfaces*, Volume 186.
- Luangbudnark, W. et al., 2012. Properties and biocompatibility of chitosan and silk fibroin blend films for application in skin tissue engineering. *Scientific World Journal*, p. 697201.
- Luchese, C. L., Sperotto, N., Spada, J. C. & Tessaro, I. C., 2017. Effect of blueberry agro-industrial waste addition to corn starch-based films for the production of a pH-indicator film. Volume 104.
- Luo, Y. et al., 2021. Silk films with nanotopography and extracellular proteins enhance corneal epithelial wound healing. Volume 11.
- Madden, P. W., Klyubin, I. & Ahearne, M. J., 2020. Silk fibroin safety in the eye: a review that highlights concern. *BMJ Open Ophthalmology*, 5(1).
- Maitz, M. F. et al., 2017. Biocompatibility assessment of silk nanoparticles: hemocompatibility and internalization by human blood cells. *Nanomedicine*, 13(8), pp. 2633-2642.
- Manna, B., Nahimiak, P. & Morrison, C. A., 2022. Wound Debridement. *StatPearls*.

- Martinez-Mora, C. et al., 2012. Fibroin and Sericin from *Bombyx mori* silk stimulate cell migration through upregulation and phosphorylation of c-Jun. *PLoS One*, 7(7).
- Mastore, M., Quadroni, S., Caramella, S. & Brivio, M. F., 2021. The Silkworm as a Source of Natural Antimicrobial Preparations: efficacy on Various Bacterial Strains. *Antibiotics (Basel)*, 10(11), p. 1339.
- Matthew, S. A. et al., 2022. Smart Silk Origami as Eco-Sensors for Environmental Pollution. *ACS Appl. Bio Mater.*, 5(8), pp. 3658-3666.
- Matthew, S. L. et al., 2020. Silk nanoparticle manufacture in semi-batch format. *ACS Biomater. Sci. Eng.*, 6(12), pp. 6748-6759.
- May, R. M. et al., 2014. Micro-Patterned surfaces reduce bacterial colonization and biofilm formation in vitro: Potential for enhancing endotracheal tube designs. 3(8).
- McCarty, S. & Percival, S., 2013. proteases and delayed wound healing. *Adv wound care*, Volume 2, pp. 438-447.
- Medina-Sanchez, M. et al., 2018. Swimming microrobots: Soft, reconfigurable, and smart. 28(25).
- Melancon, D. et al., 2021. Multistable inflatable origami structures at the metre scale. *Nature*, 592(7855).
- Mendez, A. R. et al., 2018. Micro-textured films for reducing microbial colonization in a clinical setting. 98(1), pp. 83-89.
- Meng, L. et al., 2020. Autonomous self-healing silk fibroin injectable hydrogels formed via surfactant-free hydrophobic association. *ACS Appl Mater Interfaces*, 12(1), pp. 1628-1639.
- Metris, A., George, S. M., Peck, M. W. & Baranyi, J., 2003. Distribution of turbidity detection times produced by single cell-generated bacterial populations. *Journal of Microbiological Methods*, 55(3), pp. 821-827.
- Milne, S. D. et al., 2015. A wearable wound moisture sensor as an indicator for wound dressing change: an observational study of wound moisture and status. *International Wound Journal*, 13(6), pp. 1309-1314.
- Minami, M. et al., 2004. Effect of Glycine on helicobacter pylori in vitro. *Antimicrob agents chemother.*, 48(10), pp. 3782-3788.
- Mintchev, S., Shintake, J. & Floreano, D., 2018. Bioinspired dual-stiffness origami. 3(20).
- Mohd Zubir, M. Z., Holloway, S. & Mohd Noor, N., 2020. Maggot therapy in wound healing: a systematic review. *Int. J. Environ. Res. Public Health*, Volume 17.
- Molinie, N. & Gautraeu, A., 2018. Directional Collective Migration in Wound Healing Assays. *Methods Mol Biol*, Volume 1749, pp. 11-19.
- Muller, K. et al., 2007. Effect of ultrasmall superparamagnetic iron oxide nanoparticles (Ferumoxtran-10) on human monocyte-macrophages in vitro. *Biomaterials*, 28(9), pp. 1629-1642.

- Munoz, J. & Pumera, M., 2020. Accounts in 3D-Printed Electrochemical Sensors: Towards Monitoring of Environmental Pollutants. 7(16).
- Murphy, A. R., John, P. S. & Kaplan, D. L., 2008. Modification of Silk Fibroin using diazonium coupling chemistry and the effects on hMSC proliferation and differentiation. 29(19).
- Murray, C. J. L., Ikuta, K. S., Sharara, F. & Swetschinski, L., 2022. Global burden of bacterial antimicrobial resistance in 2019: a systematic analysis. *The Lancet*, 399(10325), pp. 629-655.
- Nagarkar, S. et al., 2009. Some mechanistic insights into the gelation of regenerated silk fibroin sol. *Ind Eng Chem Res*, 48(17), pp. 8014-8023.
- Naghibi, M., Smith, R., Baltch, A. & et al, 1987. The effect of diabetes mellitus on chemotactic and bactericidal activity of human polymorphonuclear leukocytes. *diabetes res clin pract*, Volume 4, pp. 27-35.
- Nawaz, H. et al., 2021. Recent studies on cellulose-based fluorescent smart materials and their applications: A comprehensive review. Issue 267.
- Neubauer, V. J., Dobi, A. & Schneibel, T., 2021. Silk based materials for hard tissue engineering. *Materials (Basel)*, Volume 14.
- Nguyen, H. M. et al., 2023. Biomedical materials for wound dressing: recent advances and applications. *RSC Adv.*, Volume 13, pp. 5509-5528.
- Noda, K. et al., 2021. Safety of Silk-elastin Sponges in Patients with Chronic Skin Ulcers: a phase I/II, single-centre, open-label, single-arm clinical trial. *Plast Reconstr Surg Glob Open*, 9(4).
- Norman, G. et al., 2016. Antibiotics and antiseptics for surgical wounds healing by secondary intention. *Cochrane Database Syst Rev*, Volume 3.
- Norman, G. et al., 2020. Negative pressure wound therapy for surgical wounds healing by primary closure. *Cochrane Database of Systemic Reviews*, Volume 5.
- Nuchadomrong, S., Senakoon, W., Sirimungkararat, S. & Senawong, T., 2009. Antibacterial and antioxidant activities of sericin powder from eri silkworm cocoons correlating to degumming processes. *International Journal of Wild Silkworm and Silk*, Volume 13, pp. 69-78.
- Numata, K., 2014. 19- Silk hydrogels for tissue engineering and dual-drug delivery. In: *Silk biomaterials for tissue engineering and regenerative medicine*. s.l.:woodhead publishing, pp. 503-518.
- Numata, K. & Kaplan, D., 2010. Silk-based delivery systems of bioactive molecules. *Adv Drug Deliv Rev*, 62(15), pp. 1497-1508.
- Offord, C., Vollrath, F. & Holland, C., 2016. Environmental effects on the construction and physical properties of Bombyx mori cocoons. *Journal of Materials Science*, Volume 51, pp. 10863-10872.

- O'Meara, S., Cullum, N., Majid, M. & Sheldon, T., 2000. Systematic reviews of wound care management: (3) antimicrobial agents for chronic wounds. *Health technology assessment*, 4(21).
- Onder, O. C., Batool, S. R. & Nazeer, M. A., 2022. Self-assembled silk fibroin hydrogels: from preparation to biomedical applications. *Mater Adv*, Volume 3, pp. 6920-6949.
- Ongarora, B. G., 2022. Recent technological advances in the management of chronic wounds: a literature review. *Health Sci Rep*, 5(3), p. e641.
- Onida, S. et al., 2021. Study protocol for a multicentre, randomised controlled trial to compare the use of the decellularised dermis allograft in addition to standard care versus standard care alone for the treatment of venous leg ulceration: DAVE trial. *BMJ open*, 11(4).
- Osama, I. et al., 2018. In vitro studies on space-conforming self-assembling silk hydrogels as a mesenchymal stem cell-support matrix suitable for minimally invasive brain application. *Sci Rep*, Volume 8.
- Padol, A. et al., 2011. Safety evaluation of silk protein film (a novel wound healing agent) in terms of acute dermal toxicity, acute dermal irritation and skin sensitisation. *toxicol int*, Volume 18, pp. 17-21.
- Pandiarajan, J., Cathrin, B. P., Pratheep, T. & Krishnan, M., 2011. Defense role of the cocoon in the silk worm *Bombyx mori* L. *Rapid Commun Mass Spectrom*, 25(21), pp. 3203-6.
- Park, J. H. et al., 2017. Metal-Organic Framework "Swimmers" with Energy-Efficient Autonomous Motility. 11(11).
- Park, Y. R. et al., 2017. NF- κ B signalling is key in the wound healing process of silk fibroin. *Acta Biomaterialia*, Volume 67, pp. 183-195.
- Pastar, I., Stojadinovic, O., A, K. & al, e., 2010. Attenuation of the transforming growth factor B-signalling pathway in chronic venous ulcers. *Mol Med*, Volume 16, pp. 92-101.
- Peel, A. L. G., 1992. Definition of Infection. *Infection in surgical practice*, pp. 82-87.
- Peleg, M., Corradini, M. & Normand, M., 2015. On Modeling the effect of water activity on microbial growth and mortality kinetics. In: *Water Stress in Biological, Chemical, Pharmaceutical and Food Systems*. s.l.:Springer, pp. 263-278.
- Pelegrini, P. B. et al., 2008. Identification of a novel storage glycine-rich peptide from guava (*Psidium guajava*) seeds with activity against Gram-negative bacteria. *Peptides*, 29(8), pp. 1271-1279.
- Petrini, P., Parolari, C. & Tanzi, M., 2001. Silk fibroin-polyurethane scaffolds for tissue engineering. *J mater sci mater med*, Volume 17, pp. 849-853.
- PharmaState, 2023. *Quality control tests for gels*. [Online] Available at: <https://pharmastate.academy/quality-control-tests-for-gels/> [Accessed August 2023].

- Phuagkhaopong, S. et al., 2021. Silk Hydrogel Substrate Stress Relaxation Primes Mesenchymal Stem Cell Behavior in 2D. *ACS Appl. Mater. Interfaces*, 13(26), pp. 30420-30433.
- Powers, J. G., Morton, L. M. & Philips, T. J., 2013. Dressings for chronic wounds. *Dermatologic therapy*, 26(3), pp. 197-206.
- Prasad, A. S. B. et al., 2020. Pseudomonas aeruginosa virulence proteins pseudolysin and protease IV impede cutaneous wound healing. *Laboratory Investigation*, Volume 100, pp. 1532-1550.
- Pub Chem, 2023. *Phenol Red*. [Online]
Available at: <https://pubchem.ncbi.nlm.nih.gov/compound/Phenol-red>
[Accessed August 2023].
- Puca, V. et al., 2021. Microbial Species Isolated from Infected Wounds and Antimicrobial Resistance Analysis: Data Emerging from a Three-Years Retrospective Study. *Antibiotics (Basel)*, 10(10), p. 1162.
- Qi, J. et al., 2021. Energy absorption characteristics of origami-inspired honeycomb sandwich structures under low-velocity impact loading. Volume 207.
- Raeder, K., Jachan, D. E., Muller-Werdan, U. & Lahmann, N. A., 2020. Prevalence and risk factors of chronic wounds in nursing homes in Germany. *Int Wound J*, 17(5), pp. 1128-1134.
- Rajendran, R. et al., 2011. Extraction and application of natural silk protein sericin from Bombyx mori as antimicrobial finish for cotton fabrics. *The journal of the textile institute*, 103(4), pp. 458-462.
- Ranzato, E., Patrone, M., Pedrazzi, M. & Burlando, B., 2010. Hmgb1 promotes wound healing of 3T3 mouse fibroblasts via RAGE-dependent ERK1/2 activation. *Cell Biochem Biophys*, 57(1), pp. 9-17.
- Raziyeva, K. et al., 2021. Immunology of acute and chronic wound healing. *Biomolecules*, 11(5), p. 700.
- Repanas, A. e. a., 2016. The significance of electrospinning as a method to create fibrous scaffolds for biomedical engineering and drug delivery applications. *J Drug Deliv Sci Technol.*, Volume 31, pp. 137-146.
- Rice, J. et al., 2014. Burden of diabetic foot ulcers for medicare and private insurers. *Diabetes Care*, Volume 37, pp. 651-658.
- Rnjak-Kovacina, J., DesRochers, T. M., Burke, K. A. & Kaplan, D., 2015. The effect of sterilization on silk fibroin biomaterial properties. 15(6).
- Rnjak-Kovacina, J., DesRochers, T. M., Burke, K. A. & Kaplan, D., 2015. The effect of sterilization on silk fibroin biomaterial properties. 15(6), pp. 861-74.
- Rockwood, D. N. et al., 2011. Materials fabrication from bombyx mori silk fibroin. *Nat Protoc*, 6(10), pp. 1612-31.

- Rodriguez-Menocal, L., Salgado, M., Ford, D. & Van Badivas, E., 2012. Stimulation of skin and wound fibroblast migration by mesenchymal stem cells derived from normal donors and chronic wound patients. *Stem cells transl med*, Volume 1, pp. 221-229.
- Roh, D.-H. et al., 2006. Wound healing effect of silk fibroin/alginate blended sponge in full thickness skin defect of rat. *Journal of materials science: materials in medicine*, 12(6), pp. 547-552.
- Rothin, C. V., Carrera-Silva, E. A., Bosurgi, L. & Ghosh, S., 2015. TAM receptor signaling in immune homeostasis. *Annu Rev Immunol*, Volume 33, pp. 355-391.
- Roy, S., Sharma, A. & Ghosh, S., 2022. Macrophage Polarization Profiling on Native and Regenerated Silk Biomaterials. *ACS Biomater Sci Eng*, 8(2), pp. 659-671.
- Ryu, J. et al., 2020. Paper Robotics: Self-Folding, Gripping, and Locomotion. 5(4).
- Samal, S. K. et al., 2014. Silk/chitosan biohybrid hydrogels and scaffolds via green technology. *RSC Adv*, Volume 4, pp. 53547-56.
- Sarovart, S. et al., 2003. The use of sericin as an antioxidant and antimicrobial for polluted air treatment. *Rev Adv Mater Sci*, Volume 5, pp. 193-198.
- Schafer, S. et al., 2022. Silk proteins in reconstructive surgery: Do they possess an inherent antibacterial activity? A systematic review. *Wound Repair and Regeneration*, 31(1), pp. 99-110.
- Scheifer, J. L. et al., 2020. Feasibility of pure silk for the treatment of large superficial burn wounds covering 10% of the total body surface. *J Burn Care Res.*, Volume 41, pp. 131-140.
- Schiefer, J. L. et al., 2021. A clinical comparison of pure knitted silk and a complex synthetic skin substitute for the treatment of partial thickness burns. *Int Wound J*.
- Schneider, L. et al., 2010. Directional cell migration and chemotaxis in wound healing response to PDGF-AA are coordinated by the primary cilium in fibroblasts. *Cell Physiol Biochem*, 25(2-3), pp. 279-292.
- Seib, F. P. et al., 2014. Multifunctional silk-heparin biomaterials for vascular tissue engineering applications. *Biomaterials*, 35(1), pp. 83-91.
- Seib, F. P. et al., 2012. Impact of processing parameters on the haemocompatibility of Bombyx mori silk films. *Biomaterials*, 33(4), pp. 1017-23.
- Seib, P., 2018. Self-assembling hydrogels from reverse-engineered silk. *Self-assembling Biomaterials*, Issue 1, pp. 27-47.
- Seib, P. F., 2017. Silk nanoparticles- an emerging anticancer nanomedicine. *AIMS Bioengineering*, 4(2), pp. 239-258.
- Seib, P. F., 2018. Reverse-engineered silk hydrogels for cell and drug delivery. *Therapeutic Delivery*, 9(6), pp. 469-487.
- Seib, P. F. & Kaplan, D. L., 2013. Silk for drug delivery applications: opportunities and challenges. *Isr. J Chem*, 53(9-10), pp. 756-766.

- Semenza, G. L., 2002. HIF-1 and tumor progression: pathophysiology and therapeutics. *Trends Mol Med*, 8(4(suppl)), pp. S62-7.
- Setti, M. & Wiersma, D. S., 2020. Pros and Cons: Magnetic versus Optical Microrobots. 32(20).
- Seves, A., Romano, m., Maifreni, T. & Sora, S., 1998. The microbial degradation of silk: A laboratory investigation. *International Biodeterioration and Biodegradation*, 42(4), pp. 203-211.
- Shankaran, V., Brooks, M. & Mostow, E., 2013. Avdanced therapies for chronic wounds: NPTW, engineered skin, growth factors, extracellular matrices. *Dermatological therapy*, Volume 26, pp. 215-221.
- Sharma, D., Misba, L. & Khan, A. U., 2019. Antibiotics versus biofilm: an emerging battleground in microbial communities. 8(76).
- Shelenkov, A. et al., 2020. Multidrug-Resistant *Proteus mirabilis* Strain with Cointegrate Plasmid. *Microorganisms*, 8(11), p. 1775.
- Shi, C. et al., 2020. selection of appropriate wound dressing for various wounds. *Front Bioeng Biotechnol*, Volume 8, p. 00182.
- Shultz, G., Ladwig, G. & Wysocki, A., 2005. *World Wide Wounds*. [Online] Available at: <http://www.worldwidewounds.com/2005/august/Schultz/Extrace-Matric-Acute-Chronic-Wounds.html> [Accessed 2023].
- Shultz, G. S., Chin, G. A., Moldawer, L. & Diegelmann, R. F., 2011. Principles of Wound Healing. In: *Mechanisms of vascular disease: a reference book for vascular specialists*. Adelaide AU: University of Adelaide Press, p. Chapter 23.
- Shultz, G., Sibbald, R., Falanga, V. & al, e., 2003. Wound bed preparation: a systematic approach to wound management. *Wound repair regen*, pp. 1-28.
- Sibbald, G. R. & Elliott, J. A., 2017. The role of inadine in wound care: a consensus document. *Int Wound J*, 14(2), pp. 316-321.
- Sibbald, G. R. et al., 2003. Preparing the wound bed 2003: focus on infection and inflammation. *Ostomy Wound Manage.*, 49(11), pp. 24-51.
- Sibbald, R. G. et al., 2000. Preparing the wound bed- debridement, bacterial balance, and moisture balance. *Ostomy wound manage.*, 46(11), pp. 14-22, 24-8, 30-5.
- Silk Tech, 2022. *Silk tears*. [Online] Available at: <https://www.silk-tech.com/silktears> [Accessed Aug 2023].
- Simel, D. & Rennie, D., 2009. Chronic Wound Infection. In: *The rational clinical examination: Evidence-based clincial diagnosis*. s.l.:McGraw Hill.
- Singh, C. P. et al., 2014. Characterization of antiviral and antibacterial activity of Bombyx mori seroin proteins. *Cell Microbiol*, 16(9), pp. 1354-65.

- Sofregen Medical Inc, n.d. *Products in Development*. [Online]
Available at: <https://www.sofregen.com/products-in-development>
[Accessed Feb 2023].
- Sondi, I. & Salopek-Sondi, B., 2004. Silver nanoparticles as antimicrobial agent: a case study on E Coli as a model for gram-negative bacteria. *J colloid interface sci*, Volume 275, pp. 177-182.
- Stojadinovic, O., Yin, N., Lehmann, J. & et al, 2013. Increased number of langerhans cells in the epidermis of diabetic foot ulcers correlates with healing outcome. *Immunol Res*, Volume 57, pp. 222-228.
- Su, D. et al., 2017. Enhancing mechanical properties of silk fibroin hydrogel through restricting the growth of B-sheet domains. *ACS Appl Mater Interfaces*, Volume 9, pp. 17489-98.
- Sugihara, A. et al., 2000. Promotive effects of a silk film on epidermal recovery from full-thickness skin wounds.. *Proc Soc Exp Biol Med*, 225(1), pp. 58-64.
- Sultan, M. T. et al., 2018. Silk Fibroin in Wound Healing Process. *Novel Biomaterials for Regenerative Medicine*, Volume 1077, pp. 115-126.
- Sun, B., Siprashvili, Z. & Khavari, P., 2014. Advances in skin grafting and treatment of cutaneous wounds. *Science*, Volume 346, pp. 941-945.
- Sun, W. et al., 2021. Cell guidance on peptide micropatterned silk fibroin scaffolds. Volume 603, pp. 380-390.
- Suresh, A. K. e. a., 2010. Silver nanocrystallites: biofabrication using shewanella oneidensis, and an evaluation of the comparative toxicity on gram negative and gram positive bacteria. *environ. sci. technol.*, Volume 44, pp. 5210-5215.
- Suvarna, K. et al., 2018. Identification of a small-molecule ligand of B-arrestin1 as an inhibitor of stromal fibroblast cell migration accelerated by cancer cells. *Cancer Medicine*, 7(3), pp. 883-893.
- Tabei, Y. et al., 2011. Application of Insoluble Fibroin Film as Conditioning Film for Biofilm Formation. *Sensors and Materials*, 23(4), pp. 195-205.
- Takeo, M., Lee, W. & Ito, M., 2015. Wound healing and skin regeneration. *Cold Spring Harb Perspect Med.*, 5(1).
- Tanaka, K. et al., 1999. Determination of the site of disulphide linkage between heavy and light chains of silk fibroin produced by Bombyx mori. *Elsevier*, Volume 1432, pp. 92-103.
- Taylor, T. & Unakal, C., 2021. *Staphylococcus aureus*. [Online]
Available at: <https://www.ncbi.nlm.nih.gov/books/NBK441868/>
[Accessed Nov 2021].
- Telgenhoff, D. & Shroot, B., 2005. Cellular senescence mechanisms in chronic wound healing. *cell death differ*, Volume 12, pp. 695-698.

- Thakral, G. et al., 2013. Electrical stimulation to accelerate wound healing. *Diabet. foot ankle.*, 16(4).
- Thangavel, P., Ramachandran, B., Kannan, R. & Muthuvijayan, V., 2016. Biomimetic hydrogel loaded with silk and L-proline for tissue engineering and wound healing applications. *Journal of biomedical materials research part B: applied biomaterials*, 105(6).
- Thurber, A. E., Omenetto, F. G. & Kaplan, D. L., 2015. In vivo Bioresponses to Silk Proteins. *Biomaterials*, Volume 71, pp. 145-157.
- Toprakcioglu, Z. & Knowles, T. P. J., 2021. Shear-mediated sol-gel transition of regenerated silk allows the formation of Janus-like microgels. *Scientific Reports*, Volume 11, p. 6673.
- Totten, J. D., Wongpinyochit, T. & Seib, P. F., 2017. Silk nanoparticles: proof of lysosomotropic anticancer drug delivery at single-cell resolution. *J. Drug. Target*, Volume 25, pp. 865-872.
- Tran, S. H., Wilson, C. G. & Seib, F. P., 2018. A review of the emerging role of silk for the treatment of the eye. *Pharm. Res.*, 35(248).
- Tsukawaki, S., Murakami, T., Suzuki, K. & Nakazawa, Y., 2016. Studies on the potential risk of amyloidosis from exposure to silk fibroin. *Biomedical Materials*, 11(6).
- Ud-Din, S. & Bayat, A., 2014. Electrical stimulation and cutaneous wound healing: a review of clinical evidence. *Healthcare (Basel)*, Volume 2, pp. 445-467.
- Uttayarat, P. e. a., 2012. Antimicrobial electrospun silk fibroin mats with silver nanoparticles for wound dressing application. *Fiber Polym*, Volume 13, pp. 999-1006.
- Velickovic, V. M. et al., 2023. Individualized Risk Prediction for Improved Chronic Wound Management. *Advances in wound care*, 12(7).
- Ventre, M., Natale, C. F., Rianna, C. & Netti, P. A., 2014. Topographic cell instructive patterns to control cell adhesion, polarization and migration. 11(100).
- Vepari, C. & Kaplan, D. L., 2007. Silk as biomaterial. *Prog Polym Sci*, 32(8-9), pp. 991-1007.
- Vert, M. et al., 2012. Terminology for biorelated polymers and applications (IUPAC Recommendations 2012)*. *Pure Appl Chem*, 84(2), pp. 377-410.
- Vestby, L. K., Gronseth, T., Simm, R. & Nesse, L. L., 2020. Bacterial Biofilm and its Role in Pathogenesis of Disease. *Antibiotics (Basel)*, 9(2), p. 59.
- Vidya, M. & Rajagopal, S., 2021. Silk fibroin: a promising tool for wound healing and skin regeneration. *International Journal of Polymer Science*.
- Vikesland, P. J., 2018. Nanosensors for water quality monitoring. Volume 13.
- Volkov, V., Ferreira, A. & Cavaco-Paulo, A., 2015. On the routines of wild-type silk fibroin processing toward silk-inspired materials: a review. *Macromol Mater eng*, Volume 300, pp. 1199-216.
- Wall, I., Moseley, R., Baird, D. & et al, 2008. Fibroblast dysfunction is a key factor in the non-healing of chronic venous leg ulcers. *J Invest Dermatol*, Volume 128, pp. 2526-2540.

- Wang, D. et al., 2017. Influence of micropatterned silk fibroin films on human umbilical endothelial cell behaviours. *Journal of medical and biological engineering*, Volume 37, pp. 750-759.
- Wang, L. et al., 2021. Synergistic effect of highly aligned bacterial cellulose/gelatin membranes and electrical stimulation on direction cell migration for accelerated wound healing. *Chemical Engineering Journal*, Volume 424.
- Wang, S.-D., Ma, Q., Wang, K. & Chen, H.-W., 2018. Improving Antibacterial Activity and Biocompatibility of Bioinspired Electrospinning Silk Fibroin Nanofibers Modified by Graphene Oxide. *ACS Omega*, 3(1), pp. 406-413.
- Wang, X., Kluge, J. A., Leisk, G. G. & Kaplan, D. L., 2008. Sonication-induced gelation of silk fibroin for cell encapsulation. *Biomaterials*, Volume 29, pp. 1054-1064.
- Wang, Y., Deng, L., Caballero-Guzman, A. & Nowack, B., 2016. Are engineered nano iron oxide particles safe? an environmental risk assessment by probabilistic exposure, effects and risk modeling. *Nanotoxicology*, 10(10), pp. 1545-1554.
- Wang, Y. et al., 2020. Stimuli-responsive composite biopolymer actuators with selective spatial deformation behaviour. Volume 117, pp. 14602-14608.
- Wang, Y., Kim, B. J., Peng, B. & Omenetto, F. G., 2019. Controlling silk fibroin conformation for dynamic, responsive, multifunctional, micropatterned surfaces. 116(43), pp. 21361-21368.
- Wang, Y. et al., 2023. Nature-inspired micropatterns. *Nature Reviews methods primers*, 3(68).
- Wang, Z. et al., 2020. Green Gas-Mediated Cross-Linking Generates Biomolecular Hydrogels with Enhanced Strength and Excellent Hemostasis for Wound Healing. *ACS Appl. Mater. Interfaces*, 12(12), pp. 13622-13633.
- Wani, O. M., Verpaalen, R., Zeng, H. & Priimagi, A., 2019. An Artificial Nocturnal Flower via Humidity-Gated Photoactuation in Liquid Crystal Networks. 31(2).
- Wani, S. U. D. & Veerabhadrapa, G. H., 2018. Silk fibroin based drug delivery applications: promises and challenges. *Curr Drug Targets*, 19(10), pp. 1177-1190.
- Ward, A. C., Connolly, P. & Tucker, N. P., 2014. *Pseudomonas aeruginosa* Can be detected in a polymicrobial competition model using impedance spectroscopy with a novel biosensor. *PLOS One*.
- Ward, A. C. et al., 2018. Identification and characterisation of *Staphylococcus aureus* on low cost screen printed carbon electrodes using impedance spectroscopy. *Biosensors and Bioelectronics*, Volume 110, pp. 65-70.
- Wei, J. et al., 2021. Tough and Multifunctional Composite Film Actuators Based on Cellulose Nanofibers toward Smart Wearables. 13(32).
- Wei, M., Gao, Y., Li, X. & Serpe, M. J., 2017. Stimuli-responsive polymers and their applications. 8(1), pp. 127-143.

- Wiczowski, W., Szawara-Nowak, D. & Topolska, J., 2013. Red cabbage anthocyanins: Profile, isolation, identification, and antioxidant activity. 51(1).
- Wilkinson, H. N. & Hardman, M. J., 2020. Wound healing: cellular mechanisms and pathological outcomes. *Open Biology*, 10(9).
- Wilson, D., Valluzzi, R. & Kaplan, D., 2000. Conformational transitions in model silk peptides. *Biophys J*, 78(5), pp. 2690-2701.
- Wongpinyochit, T., Uhlmann, P., Urquhart, A. J. & Seib, P. F., 2015. PEGylated Silk Nanoparticles for Anticancer Drug Delivery. *Biomacromolecules*, 16(11), pp. 3712-22.
- Wounds International, 2010. A review of the applications of the hydrofiber dressing with silver (Aquacel Ag®) in wound care. *Ther Clin Risk manag*, Volume 6, pp. 21-27.
- Wounds International, 2011. *International consensus. The role of proteases in wound diagnostics. An expert working group review.* [Online]
Available at:
https://www.woundchek.com/uploads/downloads/consensus_documents/Role-of-proteases-in-wound-diagnostics-International.pdf
[Accessed April 2023].
- Wu, X. L., Mao, L., Qin, D. K. & Lu, S. Z., 2011. Impact of Sterilization Methods on the Stability of Silk Fibroin Solution. *Advanced Materials Research*, Volume 311-313, pp. 1755-1759.
- Wu, Z., Gao, W. & Bai, H., 2022. Silk-based bioinspired structural and functional materials. *iScience*, 25(3), p. 103940.
- Xiang, X., Lu, G. & You, Z., 2020. Energy absorption of origami inspired structures and materials. Volume 157.
- Xiao, L., Lu, G., Lu, Q. & Kaplan, D. L., 2016. Direct formation of silk nanoparticles for drug delivery. *ACS biomater sci eng*, 2(11), pp. 2050-2057.
- Xu, B. et al., 2017. Surface Micropattern reduces colonization and medical device-associated infections. 66(11), pp. 1692-1698.
- Xu, H.-L. et al., 2017. Liposomes with Silk Fibroin Hydrogel Core to Stabilize bFGF and Promote the Wound Healing of Mice with Deep Second-Degree Scald. *Adv Healthc Mater*, 6(19).
- Xu, L. et al., 2013. Anthocyanins from black soybean seed coat enhance wound healing. *Ann plast surg*, 71(4), pp. 415-20.
- Xu, W. et al., 2020. A droplet-based electricity generator with high instantaneous power density. Volume 578, pp. 392-396.
- Yamada, H. et al., 2004. Identification of fibroin-derived peptides enhancing the proliferation of cultured human skin fibroblasts. *Biomaterials*, Volume 25, pp. 467-472.
- Yang, D. C., Blair, K. M. & Salama, N. R., 2016. Staying in shape: the Impact of Cell Shape on Bacterial Survival in Diverse Environments. 80(1), pp. 187-203.

- Yavuz, B., Chambre, L. & Kaplan, D. L., 2020. Extended release formulations using silk proteins for controlled delivery of therapeutics. *Expert Opin Drug Deliv*, 16(7), pp. 741-756.
- Youn, Y. H. et al., 2021. Micropatterned Silk-Fibroin/Eumelanin Composite Films for Bioelectronic Applications. 7(6), pp. 2466-2474.
- Yousef, H., Alhajj, M. & Sharma, S., 2022. Anatomy, Skin (integument), Epidermis. *Statpearls*.
- Zahra, D. et al., 2023. Exploring the recent developments of alginate silk fibroin material for hydrogel wound dressing: a review. *International journal of biological macromolecules*, Volume 248.
- Zhai, Z., Wang, Y. & Jiang, H., 2018. Origami-inspired, on-demand deployable and collapsible mechanical metamaterials with tunable stiffness. 115(9).
- Zhang, H. et al., 2022. Silk fibroin hydrogels for biomedical applications. *Smart medicine*, 1(1), p. e20220011.
- Zhang, L. et al., 2017. Silk Fibroin Biomaterial Shows Safe and Effective Wound Healing in Animal Models and a Randomized Controlled Clinical Trial. *Adv Healthcare Mater*, 6(10).
- Zhang, W. et al., 2017. Silk fibroin biomaterial shows safe and effective wound healing in animal models and a randomized controlled clinical trial. *Adv Healthc Mater*, 6(10).
- Zhang, X., Cao, C., Ma, X. & Li, Y., 2012. Optimization of macroporous 3D silk fibroin scaffolds by salt leaching procedure in organic solvent-free conditions. *J Mater Sci Mater Med*, Volume 23, pp. 315-324.
- Zhao, H. et al., 2014. Decoration of silk fibroin by click chemistry for biomedical application. 186(3), pp. 420-430.
- Zhao, Y. et al., 2011. The effects of different sterilization methods on silk fibroin. 4(5).
- Zhao, Z., Hwang, Y., Yang, Y. & Cho, N.-J., 2020. Actuation and locomotion driven by moisture in paper made with natural pollen. 117(16).
- Zheng, X. et al., 2020. Microskin-Inspired Injectable MSC-Laden Hydrogels for Scarless Wound Healing with Hair Follicles. *Advanced Healthcare Materials*, 9(10).
- Zhou, C. -Z. et al., 2000. Fine organization of Bombyx mori fibroin heavy chain gene. *Nucleic Acids Res*, Volume 28, pp. 2413-2419.
- Zhou, C. et al., 2000. Fine organization of Bombyx mori fibroin heavy chain gene. *Nucleic Acids Res*, Volume 28, pp. 2413-2419.
- Zhou, J. et al., 2018. Humidity-sensitive polymer xerogel actuators prepared by biaxial pre-stretching and drying. Volume 54.
- Zhu, H. et al., 2020. Antibacterial Mechanism of Silkworm Seroins. *Polymers(Basel)*, 12(12), p. 2985.

Zhu, Y. et al., 2019. A Multifunctional Pro-Healing Zwitterionic Hydrogel for Simultaneous Optical Monitoring of pH and Glucose in Diabetic Wound Treatment. *Advanced functional materials*, 30(6), p. 1905493.